UNIVERSITY OF BAHRAIN

College of Science

Environmental and Sustainable Development Program

Development of Polymeric Hydrogel Systems as an Alternative Approach for Wastewater Treatment in the Kingdom of Bahrain

A Thesis Submitted in Partial Fulfilment of the Requirements for the Ph.D. Degree in Environmental and Sustainable Development

Submitted by
Muna AbdulAziz Aljar
ID: 19951462

Supervised by
Dr. Ahmed Abdelfattah Hussein
(Associate Professor)
University of Bahrain

Co-Supervisor: Dr. Suad Ahmed Rashdan
(Assistant Professor)
University of Bahrain

Kingdom of Bahrain
May 2023

University of Bahrain
Deanship of Graduate Studies
And scientific Research

جامعة البحرين
عمادة الدراسات العليا والبحث العلمي

Thesis Discussion Committee Decision

Student Name: **Mona Abdulaziz Aljar**	Student ID: 19951462
Department: Choose an item.	College: **Science**
Program: **PhD in Environment and Sustainable Development**	
Thesis Title: **Development of Polymeric Hydrogel Systems as an Alternative Approach for Wastewater Treatment in the Kingdom of Bahrain**	
Supervisor Name: **Dr. Ahmed Abdelfattah** Co-supervisor Name: **Dr. Suad Ahmed**	Student GPA: **3.95**

The Discussion Committee met on 15-May-2023 In Online. Upon discussing the student whose details arestated above in public, the discussion committee recommends the following:

The student is awarded a grade A in the thesis subject.

☐ Without making any changes to the thesis.

☒ After making the modifications attached with this decision.

Discussion Committee Members Approval:

Name

1. **Dr. Ahmed Abdefattah** (Supervisor)
2. **Dr. Suad Ahmed** (Co-supervisor)
3. **Dr. Wael Amer** (Internal Examiner)
4. **Prof. Amr Hussain** (External Examiner)

Approved at the University Council 6th meeting, 2013
In accordance with Decision No. 736/2013 dated 14/3/2013
Modified by University Council Decision No. 2043/2013 dated 20/11/2013.

Abstract

The aim of this study is to prepare polymeric hydrogel beads as sustainable and environmentally friendly adsorbents for the removal of organic dyes: Methylene Blue MB and Congo Red CR) and heavy metals ions (Lead (Pb), Cadmium (Cd), Cobalt (Co) and Zinc (Zn)) from aqueous solutions.

Green protocol based on physical crosslinking approach was used to fabricate various adsorbent polymeric hydrogel structures and compositions using different types of polymers (natural and synthetics) along with added nanoparticles and fillers. Two porous hydrogel beads were designed; the first one was composed of Polyvinyl alcohol, Alginate and natural Bentonite clay and was employed for the removal of organic dyes. Whereas the second hydrogel beads were consisted of Alginate, Chitosan and Cellulose and was used for the removal of heavy metals ions from aqueous solutions. The structural analysis and morphology of the prepared adsorbents were investigated by using different spectroscopic instruments such as Fourier Transform Infrared spectroscopy, Scanning Electron Microscope coupled with energy dispersive X-ray analysis and X-ray diffraction analysis. The adsorption capacity as well as kinetics and isotherms analysis of the synthesized hydrogels were then investigated for the removal of pollutants in aqueous solution. The stability and reusability of the fabricated polymeric hydrogel adsorbents as low-cost environmentally friendly systems were tested.

The results demonstrate the potential of (Polyvinyl alcohol, Alginate, and natural Bentonite) hydrogels to remove organic dyes and (Alginate, Chitosan and Cellulose) hydrogel for the removal of heavy metals ions from synthetic water systems. The experimental results indicate that the incorporation of fillers (bentonite and cellulose) in the nanocomposite formulation sustain the porous structure, preserve water uptake, and increase the removal of dyes and heavy metals compared to the control beads (hydrogels without fillers). Both adsorbents possessed high adsorption capacities and fitted well to pseudo-second-order kinetic model with a high correlation coefficient. Moreover, the designed beads had good stability and reusability as they exhibited excellent removal efficiencies (90 %) for Methylene Blue, (75 %) for Congo Red, (98.01 %) for Pb(II), (98.8 %) for Cd(II), (83.13 %) for Co(II) and (99.85 %) for Zn(II) after six consecutive adsorption-desorption cycles. The maximum adsorption capacity of the designed beads system as calculated by Langmuir isotherm for Methylene Blue,

Congo Red, Pb(II), Cd(II), Co(II) and Zn(II) were found to be 51.34, 16.193, 24, 24, 11.76, 12.5 mg/g respectively. Both semi-IPN nanocomposite Hydrogels beads demonstrated good adsorbent properties and could be potentially used for the removal of dyes and heavy metals ions from polluted water. The adsorption process was found be combination of both monolayer adsorption on homogeneous surface and multilayer adsorption on heterogeneous surface.

Publications

1. Aziz Aljar, M. A., Zulqarnain, M., Shah, A., Akhter, M. S., & Iftikhar, F. J. (2020). A review of renewable energy generation using modified titania for photocatalytic water splitting. *AIP Advances*, *10*(7). https://doi.org/10.1063/5.0006196

2. Aljar, M. A. A., Rashdan, S., & El-Fattah, A. (2021). Environmentally friendly polyvinyl alcohol− alginate/bentonite semi-interpenetrating polymer network nanocomposite hydrogel beads as an efficient adsorbent for the removal of methylene blue from aqueous solution. *Polymers*, *13*(22), 4000. https://doi.org/10.3390/polym13224000

3. Allangawi, A., Aljar, M. A. A., Ayub, K., Abd El-Fattah, A., & Mahmood, T. (2023). Removal of methylene blue by using sodium alginate-based hydrogel; validation of experimental findings via DFT calculations. *Journal of Molecular Graphics and Modelling*, *122*, 108468. https://doi.org/10.1016/j.jmgm.2023.108468

4. Aljar, M. A. A., Rashdan, S., Almutawah, A., & El-Fattah, A. A. (2023). Synthesis and Characterization of Biodegradable Poly (vinyl alcohol)-Chitosan/Cellulose Hydrogel Beads for Efficient Removal of Pb (II), Cd (II), Zn (II), and Co (II) from Water. *Gels*, *9*(4), 328. https://doi.org/10.3390/gels9040328

Dedication

This dissertation is wholeheartedly dedicated to my husband, who has been a source of support, encouragement, strength and sacrificial care for me and our children throughout the four past years.

To Sarah, Shaima, and Yousif. I hope that this achievement will motivate their future education.

To my mother, brothers, and sisters, for their advice and encouragement.

To my dear colleagues in Department of Chemistry for their support and cooperation.

To Asma, the real friend that I met during this meaningful journey.

Acknowledgements

I would like to express my deepest appreciation to all who have helped me to complete this doctoral degree.

To start, my deepest appreciation goes to my advisers Dr. Ahmed A. Fattah, Associate Professor of Inorganic Chemistry and Dr. Suad Ahmed Rashdan, Assistant Professor of Organic Chemistry, for their sincere guidance and continuous supervisions during this endeavor. Without their feedbacks and guidance this Ph.D. would not have been accomplished.

I gratefully appreciate the funding and support received for my Ph.D. from University of Bahrain and sincerely acknowledge Department of Chemistry at College of Science for providing the chemicals and facilities that helped me to finish my thesis.

I would like to express my sincere thanks to Prof. Mohamed Al-Hilo for his keen encouragement and mentorship during my study. My deepest appreciation goes also to all concerned persons in College of Science who cooperated with me during my research. Many thanks and appreciations are goes to my colleagues in Department of Chemistry for their support and encouragement.

Finally, I am grateful to my family for their support and encouragement; a special thanks goes to my husband and children for their understanding and support during this research.

TABLE OF CONTENTS

DEFENSE COMMITTEE'S APPROVAL ..... ERROR! BOOKMARK NOT DEFINED.

ABSTRACT ..... **C**

PUBLICATIONS ..... **E**

DEDICATION ..... **F**

ACKNOWLEDGEMENTS ..... **G**

LIST OF TABLES ..... **N**

LIST OF FIGURES ..... **R**

LIST OF ABBREVIATIONS ..... **AA**

CHAPTER 1: INTRODUCTION TO THE STUDY **1**

1.1. INTRODUCTION **2**

1.2. RESEARCH PROBLEM **5**

1.3. RESEARCH QUESTIONS (RQ) **6**

1.4. RESEARCH OBJECTIVES **8**

1.5. RESEARCH SIGNIFICANCE **8**

1.6. THE STUDY'S SETTING **9**

1.7. RESEARCH TERMINOLOGY **10**

CHAPTER 2: LITERATURE REVIEW **12**

2.1. WATER RESOURCES IN KINGDOM OF BAHRAIN **13**

2.2. TARGET POLLUTANTS **18**

2.2.1. TOXIC HEAVY METALS IONS (HMIS) **18**

2.2.2. ORGANIC DYES **21**

2.3. WASTEWATER TREATMENT METHODS **26**

2.3.1. ION EXCHANGE **29**

2.3.2. CHEMICAL PRECIPITATION **30**

2.3.3. REVERSE OSMOSIS (RO) **31**

2.3.4. ELECTROLYSIS 31
2.3.5. COAGULATION/ FLOCCULATION 32
2.4. ADSORPTION TECHNIQUE AS METHOD FOR WASTEWATER TREATMENT: 36
2.5. HYDROGEL SYSTEM 41
2.6. POLYSACCHARIDE-BASED COMPOSITES HYDROGEL 46
2.6.1. CHITOSAN (DEACETYLATED CHITIN). 48
2.6.2. SODIUM ALGINATE 62
2.7. SYNTHETIC BASED COMPOSITES 67
2.7.1. POLYVINYL ALCOHOL 67

CHAPTER 3: MATERIALS, METHODS, AND PHYSIO-CHEMICAL CHARACTERIZATION 71

3.1. CHEMICALS AND REAGENTS 73
3.2. APPARATUS AND MINOR INSTRUMENTS 79
3.3. PREPARATION OF THE ADSORBENT BEADS: 81
3.3.1. SYNTHESIS OF PVA-ALG-BENT COMPOSITE BEADS 82
3.3.2. SYNTHESIS OF PVA-CHTS-CLS COMPOSITE BEADS 83
3.4. ADSORBATE: DYES AND HEAVY METAL IONS 85
3.4.1. PREPARATION OF DYE SOLUTION 85
3.4.2. PREPARATION OF HMIS SOLUTIONS 86
3.5. CHARACTERIZATION OF ADSORBENTS 86
3.5.1. SCANNING ELECTRON MICROSCOPE (SEM) 86
3.5.2. ENERGY DISPERSIVE X-RAY SPECTROSCOPY (EDX) 87
3.5.3. FT-IR SPECTROMETER 87
3.5.4. X-RAY DIFFRACTION STUDIES 87
3.6. EQUILIBRIUM SWELLING TEST AT VARIOUS PH 87
3.7. PH OF POINT OF ZERO CHARGE (pH_{PZC}) 88

3.8. BATCH ADSORPTION EQUILIBRIUM STUDIES 88
3.9. ADSORPTION OPTIMIZATION 91
3.9.1. EFFECT OF CONTACT TIME 91
I. EFFECT OF CONTACT TIME ON THE REMOVAL OF MB 91
II. EFFECT OF CONTACT TIME ON THE REMOVAL OF CR 91
III. EFFECT OF CONTACT TIME ON THE REMOVAL OF HMIS 92
3.9.2. EFFECT OF INITIAL PH 92
I. EFFECT OF INITIAL PH ON THE REMOVAL OF MB 92
II. EFFECT OF INITIAL PH ON THE REMOVAL OF CR 93
III. EFFECT OF INITIAL PH ON THE REMOVAL OF HMIS 93
3.9.3. THE EFFECT OF INITIAL CONCENTRATION OF ADSORBATE 93
I. EFFECT OF INITIAL CONCENTRATION ON THE REMOVAL OF MB 93
II. EFFECT OF INITIAL CONCENTRATION ON THE REMOVAL OF CR94
III. EFFECT OF INITIAL CONCENTRATION ON THE REMOVAL OF HMIS 94
3.9.4. THE EFFECT OF ADSORBENT DOSAGE 95
I. EFFECT OF ADSORBENT DOSAGE ON THE REMOVAL OF MB 95
II. EFFECT OF ADSORBENT DOSAGE ON THE REMOVAL OF CR 95
III. EFFECT OF ADSORBENT DOSAGE ON THE REMOVAL OF HMIS... 96
3.9.5. THE EFFECT OF INITIAL TEMPERATURE 96
I. EFFECT OF INITIAL TEMPERATURE ON THE REMOVAL OF MB .. 96
II. EFFECT OF INITIAL TEMPERATURE ON THE REMOVAL OF CR... 96
III. EFFECT OF INITIAL TEMPERATURE ON THE REMOVAL OF HMIS 96
3.10. ADSORBENT REUSABILITY STUDY 96
3.12. ADSORPTION ISOTHERMS 98
3.12.1. LANGMUIR ISOTHERM MODELS (LINEAR MODEL) 99
3.11.2. FREUNDLICH ISOTHERMS 100

3.12. ADSORPTION KINETIC 102
3.12.1. PSEUDO-FIRST ORDER KINETICS (PFO) 102
3.12.2. PSEUDO-SECOND ORDER KINETICS (PSO) 103
3.13. APPLICATION OF ADSORPTION IN REAL SAMPLES: 103
CHAPTER FOUR 104
RESULTS, DISCUSSION, AND RECOMMENDATION 104
CHAPTER FOUR: RESULTS, DISCUSSION, AND RECOMMENDATION 107
4.1. REMOVAL OF DYES (METHYLENE BLUE (MB) AND CONGO RED (CR) FROM AQUEOUS SOLUTION BY POLYVINYL ALCOHOL- SODIUM ALGINATE- BENTONITE (PVA-ALG-BENT) NANOCOMPOSITE HYDROGEL BEADS 107
4.1.1. PHYSICAL AND CHEMICAL CHARACTERIZATION OF PVA-ALG-BENT 107
4.1.1.1. FOURIER TRANSFORM INFRARED SPECTROSCOPY (FTIR) 112
4.1.1.2. ENERGY-DISPERSIVE X-RAY SPECTROSCOPY (EDX) 114
4.1.1.3. SCANNING ELECTRON MICROSCOPY (SEM) 115
4.1.1.4. X-RAY DIFFRACTION STUDIES (XRD) 116
4.1.2. EQUILIBRIUM SWELLING TEST AT VARIOUS PH 117
4.1.3. POINT OF ZERO CHARGE pH_{PZC} 119
4.1.4. BATCH ADSORPTION EQUILIBRIUM STUDIES 120
4.1.4.1. EFFECT OF PH OF THE SOLUTION 120
I. EFFECT OF SOLUTION PH ON THE ADSORPTION OF MB 120
II. EFFECT OF SOLUTION PH ON THE ADSORPTION OF CR 123
4.1.4.2. EFFECT OF CONTACT TIME 125
I. EFFECT OF CONTACT TIME ON THE REMOVAL MB 125
II. EFFECT OF CONTACT TIME ON THE ADSORPTION OF CR 129
4.1.4.3. EFFECT OF INITIAL DYE CONCENTRATION 132
I. EFFECT OF INITIAL MB CONCENTRATION 132
II. EFFECT OF INITIAL CR CONCENTRATION 146

4.1.4.4. Effect of Adsorbent Dosage 155
i. Effect of Adsorbent Dosage on the removal of MB ... 156
ii. Effect of Adsorbent Dosage on the removal of CR 159
4.1.4.5. Effect of Temperature 161
i. Effect of Temperature on the removal of MB 161
ii. Effect of Temperature on the removal of CR 168
4.1.5. Adsorbent Reusability Test 170
4.1.5.1. Adsorbent Reusability Test for the removal of MB .. 170
4.1.5.2. Adsorbent Reusability Test for CR 172
4.1.6. Adsorption Isotherm studies for the removal of MB and CR 174
4.1.6. Adsorption Kinetics models for MB and CR dyes 180
4.1.7. Adsorption Mechanism of Dyes 182
4.2. Patch Adsorption Studies of Pb(II), Cd(II), Co(II) and Zn(II) ions Using Environmentally Friendly Polyvinyl Alcohol - Chitosan- nanocellulose (PVA-CHTS-CLS) 184
4.2.1. Physical and chemical characterization methods ... 184
4.2.1.1. Fourier Transform Infrared Spectroscopy (FTIR) 186
4.2.1.2. Energy-Dispersive X-ray Spectroscopy (EDX) 187
4.2.1.3. Scanning Electron Microscopy (SEM) 189
4.2.1.4. X-ray Diffraction studies (XRD) 191
4.2.2. Equilibrium Swelling Test at various pH 192
4.2.3. pH at Point of Zero Charge (pH_{PZC}) 198
4.2.4. Batch Adsorption Equilibrium Studies 199
4.2.4.1. Effect of solution pH on the removal of HMIs. 199
4.2.4.2. Effect of Contact Time on the removal of HMIs 205
4.2.4.3. Effect of Initial HMIs Concentration 211
4.2.4.4. Effect of Adsorbent Dosage on the removal of HMIs 225
4.2.4.5. Effect of Temperature on the removal of HMIs 230

4.2.5. Adsorbent Reusability Test for HMIs adsorption 241
4.2.6. Adsorption Isotherm Study for the adsorption of HMIs 246
4.2.7. Adsorption Kinetics Study for the adsorption of HMIs 252
4.2.8. Selectivity adsorption of HMIs 254
4.2.9. Adsorption Mechanism of PVA-CHTS-CLS and HMI ... 255
4.2.10. Application in real samples: 256
4.3. Conclusion 259
4.4. Recommendation: 263
5.0 References: 264
ملخص الرسالة 2

List of Tables

Chapter 2: Literature Review

Table (2.1): Major and minor wastewater treatment plants in Bahrain. Adapted from REF.: Sanitary Engineering Operation and Maintenance Directorate, Ministry of Works, 2017. 16
Table (2.2): Permissible limit of heavy metals in wastewater effluents; (mg/L). 19
Table (2. 3): Advantages and drawbacks of dyes treatments methods. Adapted from: (Sivarajasekar, 2015) 25
Table (2. 4): The advantages and disadvantages of wastewater treatment methods. (Darban et al., 2022) 33
Table (2. 5): Review articles focusing on adsorption of pollutants using low-cost adsorbent materials for wastewater remediation 39
Table (2. 6): A comparative analysis of the adsorption capacity of modified CHTS-based hydrogels for the removal of HMIs and dyes. 54
Table (2. 7): Adsorption capacity for some ALG-based hydrogels 66
Table (2. 8): Adsorption studies of PVA-based hydrogels 68

Chapter Three: Methods and procedures

Table (3. 1): Physical Characteristics of Methylene Blue and Congo Red 85
Table (3. 2): Batch adsorption parameters 90
Table (3. 3): Optimal pH for the removal of adsorbate solutions 97

Chapter Four: Results, Discussion, and Recommendation

Table (4. 1): Effect of bentonite content (0, 10, 20, 30 wt.%) on the removal percentage of MB and CR 111
Table (4. 2): Effect of initial pH on the adsorption capacity and removal percentage of MB onto the semi-IPN PVA-ALG-BENT nanocomposite hydrogel beads. Note: the optimal pH value highlighted in blue 122
Table (4. 3): Effect of initial pH on the adsorption capacity and removal percentage of CR by semi-IPN PVA-ALG-BENT nanocomposite hydrogel beads. Note: The optimal pH value highlighted in blue 124
Table (4. 4): Effect of contact time on the adsorption capacity and removal percentage of MB onto the semi-IPN PVA-ALG-BENT nanocomposite hydrogel beads 127
Table (4. 5): Effect of contact time on the adsorption capacity and removal percentage of CR onto the semi-IPN PVA-ALG-BENT nanocomposite hydrogel beads 130
Table (4. 6): Effect of initial MB concentration on the adsorption capacity and removal percentage of MB onto the semi-IPN PVA-ALG-BENT nanocomposite hydrogel beads 134
Table (4. 7): Effect of initial CR concentration on the adsorption capacity and removal percentage of CR onto the semi-IPN PVA-ALG-BENT nanocomposite hydrogel beads. 148
Table (4. 8): Effect of adsorbent dosage on the adsorption capacity and removal percentage of MB onto the semi-IPN PVA-ALG-BENT nanocomposite hydrogel beads 157
Table (4. 9): Effect of adsorbent dosage on the adsorption capacity and removal percentage of MB onto the semi-IPN PVA-ALG-BENT nanocomposite hydrogel beads 160
Table (4. 10): Effect of temperature on the adsorption capacity and removal percentage of MB onto the semi-IPN PVA-ALG-BENT nanocomposite hydrogel beads 163

Table (4. 11): Effect of temperature on the adsorption capacity and removal percentage of CR onto the semi-IPN PVA-ALG-BENT nanocomposite hydrogel beads. 169
Table (4. 12): Reusability study onto the semi-IPN PVA-ALG-BENT nanocomposite hydrogel beads for the removal of MB 171
Table (4. 13): Reusability study of the removal of CR by the semi-IPN PVA-ALG-BENT nanocomposite hydrogel beads 173
Table (4. 14): Parameters of the adsorption isotherms of MB and CR 177
Table (4. 15): Comparison of the Qe values of the designed semi-IPN PVA-ALG-BENT nanocomposite hydrogel beads and previously reported adsorbents for the removal of MB and CR dye. 178
Table (4. 16): Kinetics parameters for the adsorption of MB and CR onto hydrogel beads based on pseudo- first order and Pseudo-second order equations 182
Table (4. 17): SR of PVA–CHTS-CLS nanocomposite hydrogel beads at different pH values (3,7 and 9) 195
Table (4. 18): Effect of initial pH on the adsorption capacity and removal percentage of HMIs onto the PVA-CHTS-CLS nanocomposite hydrogel beads. 201
Table (4. 19): Effect of contact time on the adsorption capacity and removal percentage of HMIs onto the PVA-CHTS-CLS nanocomposite hydrogel beads. 207
Table (4. 20): Effect of initial concentrations on the adsorption capacity and removal percentage of HMIs onto the PVA-CHTS-CLS nanocomposite hydrogel beads. 213
Table (4. 21): Effect of adsorbent's dosage on the adsorption capacity and removal percentage of HMIs onto the PVA-CHTS-CLS nanocomposite hydrogel beads. 227

Table (4. 22): Effect of temperature on the adsorption capacity and removal percentage of HMIs onto the PVA-CHTS-CLS nanocomposite hydrogel beads. 232
Table (4. 23): Reusability study onto the PVA-CHTS-CLS nanocomposite hydrogel beads for the removal of HMIs 243
Table (4. 24): Adsorption isotherm parameters of Pb (II), Cd (II), Co (II) and Zn(II) on to PVA-CHTS-CLS..... 250
Table (4. 25): Adsorption capacity of some adsorbents for Pb (II), Cd (II), Co (II) and Zn(II) 251
Table (4. 26): Kinetics parameters for the sorption metal ions on a batch adsorption system 252
Table (4. 27): Levels of HMIs in real sample in Kingdom of Bahrain.. 257

List of Figures

Chapter 1: Introduction to the Study:

Fig.1.1: Global population rate and annual growth rate: Estimates 1950-2020 and prediction intervals (2020-2100) (UN, 2019). 2

Chapter 2- Literature Review:

Fig. 2.1: Water resources and uses in Kingdom of Bahrain in 2011, in Million cubic meters (Mm^3)..... 14

Fig. 2.2: a) Population growth (2007-2018). (Source: Bahrain Data Portal, 2018); b) Urbanization trends (Source: Bahrain Data Portal, 2018); c) Trends in total demands in the kingdom of Bahrain from 1950-2015 (Source: VNR, 2018); d) Annual per capita (1970-2010) renewable freshwater and desalination capacity in Kingdom of Bahrain. 15

Fig. 2. 3: Tubli WPCC wastewater classification in million cubic meter per year (MCM) (received, reuse, and discharge to the sea). (Data source: Sanitation Directorate, Ministry of Works). 17

Fig. 2.4: Toxic effects of HMIs on human health. (Sonone et al., 2021).19

Fig. 2. 5: a) A sites of 29 sampling stations in Bahrain (source: (Nicolaus et al., 2022); b) Sediment sampling locations during 2017 (Site: 1-14) and 2019 (Site: 1-20) (Bersuder et al., 2020). 21

Fig. 2.6: Main industries that release dyes in the environment (Samsami et al., 2020). 22

Fig. 2.7: The annual increase of textile dyes of the period 2016-2023 (A. D. fergusont & P. Taylor, 2020). 22

Fig. 2. 8: Structure of azo dye: chromophore and auxochrome (Benkhaya, M'rabet, et al., 2020). 23

Fig. 2. 9: Classification of dyes based on their ionic structure (Tan et al., 2015). 23

Fig. 2. 10: (a) Thiazine structure, (b) Azo reactive dye (Benkhaya, M'rabet, et al., 2020), (c) Chemical structure of MB dye, (d) Chemical Structure of CR dye. 24
Fig. 2. 11: Classification of Wastewater contaminants. 27
Fig. 2.12: Classification of wastewater treatment step..... 28
Fig. 2. 13: A schematic diagram of ion exchange system..... 30
Fig. 2. 14: A schematic diagram of Chemical precipitation process..... 30
Fig. 2. 15: A schematic diagram of Reverse Osmosis..... 31
Fig. 2. 16: A schematic diagram of Coagulation/ Flocculation process (Teh et al., 2016). 32
Fig. 2. 17: Schematic illustration of the adsorption process system of a surface**.** 36
Fig. 2. 18: Schematic cross section of a porous material: (1) closed pores; (2) open pores; (3) blind pores; (4) through pores; (5) roughness pores (David, 2015). 37
Fig. 2. 19: components of hydrogel (E. M. Ahmed, 2015b). 42
Fig. 2. 20: Chemical and physical properties for the classification of Hydrogel. 42
Fig. 2. 21: Graphical Illustration of homopolymer, copolymer, semi-IPNs and IPN Hydrogels (T.-C. Ho et al., 2022). 45
Fig. 2. 22: Preparation methods of hydrogels (Ali & Ahmed, 2018)..... 46
Fig. 2. 23: Structure of some polysaccharides (Lim et al., 2019). 47
Fig. 2. 24: Chemical structure of (a): Chitin and (b) CHTS (Hossain et al., 2018). 49
Fig. 2. 25: Effect of pH on the structure of CHTS (Ardean et al., 2021).50
Fig. 2. 26: Effect of DD and molecular weight on the removal efficiency of HMIs (Younis et al., 2019). 52
Fig. 2. 27: Schematics model of the modification-for CHTS (J. Wang & Zhuang, 2022). 53

Fig. 2. 28: Comparison of different adsorbent for the removal of MO dye (Khapre et al., 2021). 60
Fig. 2. 29: Structure of ALG; (a) ALG monomer; (b) Chain conformation and (c) block configuration (Sutirman et al., 2021). 63
Fig. 2. 30: Schematic representation of the "egg-box" model (Urbanova et al., 2019). 64
Fig. 2. 31: Schematic examples of Na-ALG -hydrogels combined with other polymers for the removal of HMIs and dyes (ALSamman & Sánchez, 2021). 65
Fig. 2. 32: Alkaline Hydrolysis of polyvinyl acetate to obtain PVA (Singh et al., 2021). 67
Fig. 2. 33: Effect of initial concentration on the removal of MB on to BENT, PVA-BENT, and PVA hydrogel (Sanchez et al., 2019b). 69

Chapter Three: Methods and procedures

Fig. 3. 1: Chemical structure of HNO_3 73
Fig. 3. 2: Chemical structure of PVA 74
Fig. 3. 3: Chemical structure of CHTS 74
Fig. 3. 4: Chemical structure of CLS 74
Fig. 3. 5: Chemical structure of CH_3COOH 75
Fig. 3. 6: Chemical structure of sodium ALG 75
Fig. 3. 7: Structure of BENT clay (Masindi & Africa, 2016). 76
Fig. 3. 8: SEM micrograph of BENT clay nanoparticles 76
Fig. 3. 9: components of ICP-OES (S. R. Khan et al., 2022). 81
Fig. 3. 10: Flowchart of the formation and characterization of PVA-ALG-BENT beads 83
Fig. 3. 11: Flowchart of preparation and characterization of PVA-CHTS-CLS hydrogel beads. 84

Fig. 3. 12: Langmuir Linear adsorption model. 100
Fig. 3. 13: Freundlich adsorption model 101

Chapter Four: Results, Discussion, and Recommendation

Fig. 4. 1: Gelation process of ALG. (a) SALG dropped to a $CaCl_2$ to produce hydrogel beads by cross-linking of ALG-polymers with Ca^{2+} cations. (b) Crosslinking between Ca^{2+} and ALG polymer (Paredes Juárez et al., 2014). 108
Fig. 4. 2: The color of Semi-IPN PVA-ALG-BENT nanocomposite hydrogel beads (a) before drying (inset shows the size of wet beads), (b) after 48 h air drying (inset shows the size of dried beads) 109
Fig. 4. 3: Semi-IPN PVA-ALG-BENT nanocomposite hydrogel beads (a) after adsorption of MB dye, (b) after adsorption of CR dye (inset shows the size of dyes-adsorbed beads)**.** 109
Fig. 4. 4: Effect of BENT content (0, 10, 20, 30 wt.%) on the removal percentage of Dyes, (a) MB (C_0[MB] = 200 mg/L, V = 50 mL, pH = 8, beads dosage = 1.5 g, t = 300 min, T = 30 C). (b) CR (C_0[CR] = 100 mg/L, V = 50 mL, pH = 3, beads dosage = 1.5 g, t = 300 min, T = 30 °C). 112
Fig. 4. 5: FTIR spectra of pristine BENT, semi-IPN PVA-ALG hydrogel and semi-IPN PVA-ALG-BENT nanocomposite hydrogel..... 113
Fig. 4. 6: EDX spectra of (a) pristine BENT clay (b) semi-IPN PVA-ALG control hydrogel, and (c) semi-IPN PVA-ALG-BENT nanocomposite hydrogel. The insets show the corresponding weight and atomic percentages of the elements present in the samples. 115
Fig. 4. 7: SEM micrographs of (a,b) semi-IPN PVA-ALG control hydrogel beads, and (c,d) semi-IPN PVA-ALG-BENT nanocomposite hydrogel beads. 116
Fig. 4. 8:XRD for PVA-ALG-BENT..... 117

Fig. 4. 9: Swelling behavior of the semi-IPN PVA-ALG-BENT nanocomposite hydrogel beads at different pH values: (a) Swelling ratio and (b) Schematic illustration of the swelling process at different pH.. 118
Fig. 4. 10: pH_{PZC} for PVA-ALG-BENT nanocomposite's hydrogel beads 119
Fig. 4. 11: Effect of initial pH on the adsorption capacity and removal percentage of MB onto the semi-IPN PVA-ALG-BENT nanocomposite hydrogel beads (C_0[MB] = 200 **(mg/L)**, V = 50 mL, beads dosage = 1.5 g, pH = 8, t = 300 min, T = 30 ºC). 123
Fig. 4. 12: Effect of initial pH on the adsorption capacity and removal percentage of CR onto the semi-IPN PVA-ALG-BENT nanocomposite hydrogel beads (C_0[CR] = 100 mg/L, V = 50 mL, beads dosage = 1.5 g, pH = 3-10, t = 300 min, T = 30 ºC). 125
Fig. 4. 13: Effect of contact time on the adsorption capacity and removal percentage of MB onto the semi-IPN PVA-ALG-BENT nanocomposite hydrogel beads (C_0[MB] = 200 mg/L, V = 50 mL, beads dosage = 1.5 g, pH = 8, t = 20-320 min, T = 30 ºC). 129
Fig. 4. 14: Effect of contact time on the adsorption capacity and removal percentage of CR onto the semi-IPN PVA-ALG-BENT nanocomposite hydrogel beads (C_0[CR] = 100 mg/L, V = 50 mL, beads dosage = 1.5 g, pH = 3, t = 20-320 min, T = 30 ºC). 132
Fig. 4. 15: Effect MB initial concentration on the adsorption capacity and removal percentage of MB onto the semi-IPN PVA-ALG-BENT nanocomposite hydrogel beads (C_0[MB] = 50-350 mg/L, V = 50 mL, beads dosage = 1.5 g, pH = 8, t = 350 min, T = 30 ºC). 146
Fig. 4. 16: Effect CR initial concentration on the adsorption capacity and removal percentage of CR onto the semi-IPN PVA-ALG-BENT

nanocomposite hydrogel beads (C_0[CR] = 20-100 mg/L, V = 50 mL, beads dosage = 1.5 g, pH = 3, t = 350 min, T = 30 ºC). 155
Fig. 4. 17: Effect of adsorbent dosage on the adsorption capacity and removal percentage of MB onto the semi-IPN PVA-ALG-BENT nanocomposite hydrogel beads (C0[MB] = 200 mg/L, V = 50 mL, beads dosage = 0.1-2.0 g, pH = 8, t = 350 min, T = 30 ºC). 159
Fig. 4. 18: Effect of adsorbent dosage on the adsorption capacity and removal percentage of CR onto the semi-IPN PVA-ALG-BENT nanocomposite hydrogel beads (C_0[CR] = 100 mg/L, V = 50 mL, beads dosage = 0.1-2.0 g, pH = 3, t = 300 min, T = 30 ºC). 161
Fig. 4. 19: Effect of temperature on the adsorption capacity and removal percentage of MB onto the semi-IPN PVA-ALG-BENT nanocomposite hydrogel beads (C_0[MB] = 200 mg/L, V = 50 mL, beads dosage = 1.5 g, pH = 8, t = 300 min, T = 20-50 ºC). 168
Fig. 4. 20: Effect of temperature on the adsorption capacity and removal percentage of CR onto the semi-IPN PVA-ALG-BENT nanocomposite hydrogel beads (C_0[CR] = 100 mg/L, V = 50 mL, beads dosage = 1.5 g, pH = 3, t = 300 min, T = 30-50 ºC). 169
Fig. 4. 21: Reusability study of the semi-IPN PVA-ALG-BENT nanocomposite hydrogel beads for the removal of MB for five cycles (C_0[MB] = 200 mg/L, V = 50 mL, beads dosage = 1.5 g, pH = 8, t = 300 min, T = 30 ºC). 172
Fig. 4. 22: Reusability study onto the semi-IPN PVA-ALG-BENT nanocomposite hydrogel beads for the removal of CR (C_0[CR] = 100 mg/L, V = 50 mL, beads dosage = 1.5 g, pH = 3, t = 300 min, T = 30 ºC)..... 174
Fig. 4. 23: (a) The Langmuir adsorption isotherm and (b) Freundlich adsorption isotherm, for the adsorption of the MB onto the semi-IPN PVA-ALG-BENT nanocomposite hydrogel beads. 176

Fig. 4. 24: (a) The Langmuir adsorption isotherm and (b) Freundlich adsorption isotherm, for the adsorption of the CR onto the semi-IPN PVA-ALG-BENT nanocomposite hydrogel beads. 176
Fig. 4. 25: (a) The PFO and (b) PSO kinetic models for the adsorption of the MB onto the semi-IPN PVA-ALG-BENT nanocomposite hydrogel beads. 181
Fig. 4. 26: (a) The PFO and (b) PSO kinetic models for the adsorption of the CR onto the semi-IPN PVA-ALG-BENT nanocomposite hydrogel beads. 181
Fig. 4. 27: Proposed scheme indicating the possible interaction mechanism for the removal of MB and CR onto the PVA-ALG-BENT nanocomposite hydrogel beads. 183
Fig. 4. 28: PVA–CHTS-CLS nanocomposite hydrogel beads (a) before drying (inset shows the size of wet beads), (b) after 48 hr. air drying, (c) dried beads after adsorption of Pb, (d) dried beads after adsorption of Cd, (e) dried beads after adsorption of Co, (f) dried beads after adsorption of Zn. 185
Fig. 4. 29: Effect of CLS content (0, 0.5 wt. %) on the removal percentage of HMIs (C_0[heavy metals] = 50 mg/L, V = 50 mL, pH (Pb & Cd) = 6, , pH (Pb & Cd) = 6, pH (Co & Zn) = 8, beads dosage = 0.5 g, t = 200 min, T = 30 °C). 186
Fig. 4. 30: FTIR spectra of PVA, CHTS, CLS, and PVA-CHTS-CLS nanocomposite hydrogel. 187
Fig. 4. 31: EDX spectra of (a) PVA-CHTS-CLS (b) PVA-CHTS-CLS after adsorption of Pb, (c) PVA-CHTS-CLS after adsorption of Cd, (d) PVA-CHTS-CLS after adsorption of Co and (e) PVA-CHTS-CLS after adsorption of Zn. (C_0[Heavy metals] = 50 mg/L, V = 50 mL, pH (Pb & Cd) = 6, pH (Co& Zn) = 8, beads dosage = 0.5 g, t = 200 min, T = 30 °C) (g). 189

Fig. 4. 32: SEM images of the dried hydrogel beads at higher and lower magnification for (a, b) PVA-CHTS- 0.5 wt. % CLS, (c, d) PVA-CHTS-CLS after Pb (II) adsorption, (e, f) PVA-CHTS-CLS after Cd (II) adsorption, (g,h) PVA-CHTS-CLS after Co (II) adsorption and (i, j) PVA-CHTS-CLS after Zn(II) adsorption..... 191
Fig. 4. 33: XRD patterns of PVA, CHTS, CLS and PVA-CHTS as well as PVA-CHTS-CLS composite hydrogel..... 192
Fig. 4. 34: Swelling behavior of PVA–CHTS-CLS nanocomposite hydrogel beads at different pH values (3,7 and 9): (a) swelling ratio and (b) Swelling mechanism. 194
Fig. 4. 35:PH_{PZC} study for PVA-CHTS-CLS nanocomposite hydrogel beads. 199
Fig. 4. 36: Effect of pH on the adsorption capacity and removal percentage of HMIs onto the semi-IPN PVA- CHTS-CLS nanocomposite hydrogel beads. (a) Pb(II), (b) Cd(II), (c) Co(II), and (d) Zn (II) (C_0[Metals] = 50 mg/L, V = 50 mL, beads dosage = 0.5 g, pH = 3-10, t = 200 min, T = 30 °C). 205
Fig. 4. 37: Effect of contact time on the adsorption capacity and removal percentage of HMIs onto the semi-IPN PVA- CHTS-CLS nanocomposite hydrogel beads. (a) Pb(II) (b) Cd(II), (c) Co(II) and (d) Zn(II) (C0[Metals] = 50 mg/L, V = 50 mL, beads dosage = 0.5 g, pH = 6 (Pb & Cd), 8 (Co &Zn) , t = 200 min, T = 30 °C)..... 211
Fig. 4. 38: Effect of initial HMIs concentration on the adsorption capacity and removal percentage onto the semi-IPN PVA- CHTS-CLS nanocomposite hydrogel beads. (a) Pb^{2+}, (b) Cd^{2+}, (c) Co^{2+} and (d) Zn^{2+} (C_0[Metals] = 50 mg/L, V = 50 mL, beads dosage = 0.5 g, pH = 6 (Pb and Cd), 8 (Co &Zn), t = 200 min, T = 30 °C 225
Fig. 4. 39: Effect of adsorbent dosages (PVA- CHTS-CLS nanocomposite hydrogel beads) on the adsorption capacity and removal percentage of

HMIs: (a) Pb (II), (b) Cd (II), (c) Co (II) and (d) Zn (II) (C_0[Metals] = 50 mg/L, V = 50 mL, beads dosage = 0.1-0.5 g, pH = 6 (Pb and Cd), 8 (Co &Zn), t = 200 min, T = 30 °C)..... 230
Fig. 4. 40: Effect of temperature on the adsorption capacity and removal percentage of HMIs: (a) Pb (II), (b) Cd (II), (c) Co (II) and (d) Zn (II) ((C_0[Metals] = 50 mg/L, V = 50 mL, beads dosage = 0.1-0.5 g, pH = 6 (Pb and Cd), 8 (Co &Zn), t = 200 min, T = 20-40 °C)..... 241
Fig. 4. 41: Reusability test for the removal of HMIs on PVA-CHTS-CLS (C_0[Metals] = 50 mg/L, V = 50 mL, pH = 6 (Pb &Cd) and pH = 8 (Co &Zn)), beads dosage = 0.5 g, t = 200 min, T = 30 °C)..... 246
Fig. 4. 42: (a) The Langmuir adsorption isotherm models for the adsorption of Pb (II), Cd (II), Co (II) and Zn(II) onto the semi-IPN PVA-CHTS-CLS composite hydrogel beads..... 248
Fig. 4. 43: Freundlich adsorption isotherm models for the adsorption of Pb (II), Cd (II), Co (II) and Zn(II) onto the semi-IPN PVA-CHTS-CLS composite hydrogel beads..... 249
Fig. 4. 44: (a) The (PFO) and (b) (PSO) kinetic models for the adsorption of Pb (II), Cd (II), Co (II) and Zn (II) onto the semi-IPN PVA-CHTS-CLS nanocomposite hydrogel beads..... 253
Fig. 4. 45: Adsorption selectivity of HMIs. (C_0[HMIS] = 50mg/L, V = 50 mL, pH =6, t =120 min, T = 30 ºC). 255
Fig. 4. 46: Proposed scheme indicating the possible interaction mechanism of the HMIs onto the PVA-CHTS-CLS nanocomposite hydrogel beads. Adapted from REF:(Kong et al., 2018) 256
Fig. 4. 47: Locations of samples in kingdom of Bahrain 258
Fig. 4. 48: The % removal of HMIS on the surface of PVA-CHTS-CLS in three locations of real sea water samples..... 258

List of Abbreviations

ALG	Alginate
BENT	Bentonite
BG	Brilliant green
C0	Initial concentration of adsorbate (ppm)
Ce	adsorbate concentration at equilibrium (mg/g)
CHTS	Chitosan
CLS	Cellulose
COD	Chemical Oxygen Demand
Conc.	Concentration
CR	Congo Red
C_t	Concentration of adsorbate at time t in (min)
DC	Degree of Acetylation
DD	Degree of Deacetylation
EBT	Eriochrome black T
EDX	Energy Dispersive X-ray
FTIR	Fourier Transform Infrared Spectroscopy
G	Glutaraldehyde
GO	Graphene Oxide
HMIs	Heavy Metal Ions
IPN	Interpenetrating polymer network
IWW	Industrial wastewater
K1	Rate constant of PFO(1/min)
KF	Freundlich constants [(mg/g) (L/gm)1/n)]
KL	Langmuir constant (L/mg)
MB	Methylene Blue
MCM	Million Cubic Meter

MO	Methyl Orange
Mol. Wt.	Molecular weight
n	Freundlich constants it represents the adsorption intensity
PAM	Polyacrylamide
PBV	Patent Blue V
PEI	polyethyleneimine
PEO	polyethylene oxide
PFO	Pseudo-First order
PG	polyethylene glycol
PHpzc	PH point of zero charge
PSO	Pseudo-Second order
PVA	Poly Vinyl Alcohol
Q_1	Initial adsorption capacity (mg/g)
Q_e	Adsorption capacity or amount of pollutant adsorbed at equilibrium (mg/g)
q_m	maximum monolayer adsorption capacity (mg/g)
Q_n	nth time adsorption capacity (mg/g)
qt	amount of adsorbate adsorbed on adsorbent at time t (min)
R^2	correlation coefficient
R_L	Dimensionless constant or separation factor
RO	Research Question
SD	Standard Deviation
SDGs	Sustainable Development Goals
SDGs	Sustainable Development Goals
SEM	Scanning Electron Microscope
Semi-IPN	Semi-interpenetrating polymer network

SIDS	Small Island Developing State
SR	Swelling Ratio
TSE	Treated Sewage Effluent
Tubli WPCC	Tubli Water Pollution Control enter
TWW	Treated wastewater
UN	United Nations
UNWWDR	United Nation World Water Development report
USEPA	US Environmental Protection Agency
UV-Vis	Ultravisible- Visible
V	Volume in (mL)
W	Weight of adsorbent in (g)
W_d	weight of dry hydrogel (g)
WHO	World Health Organization
WRI	World Resources Institute
WW	weight of wet hydrogel (g)
XAN	Xanthate
XRD	X-ray diffraction
λ_{max}	Maximum wavelength
% R	Percentage removal
3D	Three dimensional

Chapter 1

Introduction to the Study

1. Introduction
2. Research Problem
3. Research Questions
4. Research objectives
5. Research significance
6. The study setting
7. Research Terminology

Chapter One

Introduction to the Study

1.1. Introduction

Water, a mandatory resource for life, accounts for 71% of the earth's total surface, in which only 3.0 % of water is available as fresh water, while the residual amount of water is unreachable in many forms including ice and glaciers (Darban et al., 2022; Samsami et al., 2020). The first United Nation World Water Development Report (UNWWDR) headlined "water for people, water for life" emphasized the importance of water for human health and societies (UNWWDR, 2003). However, the ongoing expansion of population, urbanization, agriculture, and economic growth increase water consumption, impose a strain on water resources, accelerate water scarcity and emphasize the fact that the traditional water recourses are insufficient to fulfill the increasing demand of water (Morote & Hernández, 2016). According to 2019 version of World Population Prospects, estimated by United Nation Medium Population Projections, the world's population will increase from 7.7 billion in 2019 to 8.5 billion in 2050 and 10.9 billion in 2100, Fig. 1.1 (UN, 2019).

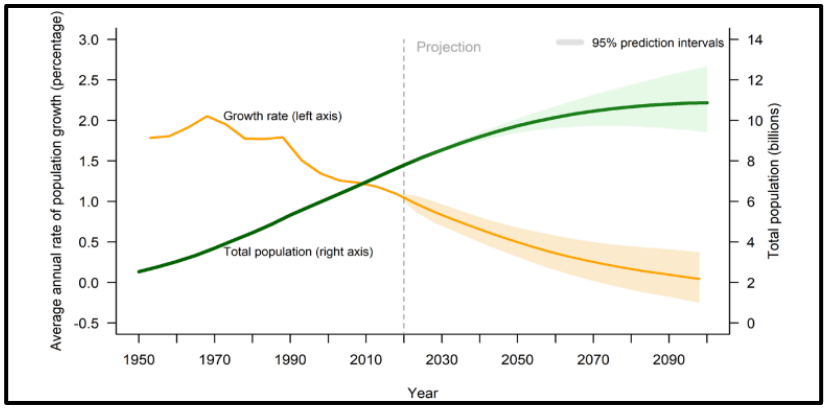


Fig.1.1: Global population rate and annual growth rate: Estimates 1950-2020 and prediction intervals (2020-2100) (UN, 2019).

In addition to water scarcity, the direct and indirect discharge of wastewater into water system in the modern society is the main threat to living species which causes the degradation of the aquatic environment. Most of these pollutants come from the industrial sector which consumes extensive amount of water and consequently discharges huge amount of wastewater (Crini, Lichtfouse, et al., 2019). Within industry and according to UNWWDR wastewater is a major contributor to environmental pollution (UNWWDR, 2003). Industrial wastewater (IWW) contains two categories of pollutants: biodegradable and non-biodegradable (AlJaberi & Mohammed, 2018). Moreover, wastewater covers a range of pollutants, including dyes (Bhatti et al., 2020) and heavy metals ions (HMIs) (Almomani et al., 2020).

Access to clean water is the first step towards good health (Ashbolt, 2004). In this sense, the United Nations (UN) regards clean water to be a fundamental priority and one of its objectives is "*By 2030, improve water quality by reducing pollution, eliminating dumping and minimizing release of hazardous chemicals and materials, halving the proportion of untreated wastewater and substantially increasing recycling and safe reuse globally*" (Bhatti et al., 2020). Accordingly, there is a global demand towards intensifying the use of wastewater treatment technique as a strategy for reducing existing water pollution and water scarcity. Wastewater treatment techniques and their cost have become crucial requirements for sustainable water management and should be handled more efficiently to increase the supply of water and guarantees safe use of treated wastewater (Fytianos et al., 2020; Gallego-Valero et al., 2021; Vázquez et al., 2015). Water reuse provides economic advantages with few environmental effects compared with other treatment techniques such as desalination (Garrido-Cardenas et

al., 2020). The current global wastewater treatment and reuse practice directly affect the quality and quantity of water resources and have two benefits: reduce the amount of effluent that is released to the aquatic system and reduce the pressure on water resources (Watkinson et al., 2007). The appropriate procedure for wastewater treatment depends on its final use. Consideration must be given to the types and amount of chemicals used in the treatment process as well as to the residual compounds produced from the process to prevent additional stressing to the environment (Garrido-Cardenas et al., 2020). On this basis, several conventional methods have been adapted for the removal of organic pollutants and heavy metals from wastewater including chemical, biological, and physical methods (M. Kumar et al., 2021). However, those methods are not efficient to remove all the pollutants with sufficient degree and limit extent. Additionally, some of these techniques cause additional challenges such as the production and disposal of sludge which discharge into water surfaces or landfills (De Carvalho Gomes et al., 2019). As a result, there is an urgent need for innovative and sustainable methods to remove pollutants from wastewater (El-sayed, 2020). Researchers have conducted many experiments to minimize the harmful effects of theses pollutants such as membrane filtration (Moreira et al., 2021; X. Zhang, 2022), chemical precipitation (Son et al., 2020; Yan et al., 2019), electrolysis(L. Zhang et al., 2020), flocculation-coagulation (Zhao et al., 2021), adsorption (Maryanti et al., 2020; L. W. Yang et al., 2021), etc. However, among these methods' adsorption process has achieved significant importance because it is efficient, ecofriendly, fast, and affordable with lots of potential for industrial applications (J. Liu et al., 2020). Accordingly, to present a recent achievement in the state of wastewater treatment for scientific and industrial applications, this study developed new, reusable, inexpansive, efficient, and environmentally friendly adsorptive hydrogel for the removal

of organic dyes (methylene blue (MB) and Congo red (CR)) and heavy meals (Pb, Cd, Co and Zn) from aqueous solution. Three polymers were used in the synthesis of the absorptive hydrogel, chitosan (CHTS), polyvinyl alcohol (PVA) and sodium alginate (ALG). Composite polymeric hydrogel was the focus of this study to benefit of polymeric crosslinking property to prepare mechanically stable hydrogel and thus overcomes the limitation of the previously studied non-composite polymeric hydrogel (Sanchez et al., 2019). CHTS is considered as one of the most effective biomaterials and has wide environmental applications due to its properties such as non-toxic, biodegradable, biocompatible, soluble in acidic solution, cationic hydrophilic in nature and natural abundant. ALG is a natural polysaccharide which displays distinctive gelation features for divalent cations in aqueous solution (W. Wang, Zhao, Bai, Zhang, & Ibarra-galvan, 2018; Zou et al., 2020a). Finally, PVA is a nontoxic polymer with excellent mechanical and thermal stability (Baigorria et al., 2020; Sanchez et al., 2019). Moreover, the addition of trace quantities of nanometric fillers such as clay and nanocellulose also consider as an effective approach to enhance the functionality of the hydrogel beads (Kausar et al., 2022; J. Liu et al., 2020; Nasrollahzadeh et al., 2021; D. Wang et al., 2018).

1.2. Research Problem

Advancement in wastewater treatment technologies have improved the water quality. However, elevated levels of toxins may still be a significant risk to ecosystem and human health. In 2015, 17 Sustainable Development Goals (SDGs) were established by the UN as part of 2030 Agenda for sustainable Development. Two goals of them are interrelated to water: SDG-6 (Clean Water and Sanitation) and SDG-14 (Life Below

Water). Hence, to achieve these goals, the problems of scarcity of water need to be solved.

Kingdom of Bahrain is a water scare country and is regarded as one of the world's highest water-stressed countries in term of freshwater resource availability (Al-Noaimi, 2005; Supreme Council For Environment, 2020). Due to the modernization development, Bahrain has experienced an increase in economic structure, population, and industrialization. This improves the standards of living but at the same time increases the demand of water, therefore there is a need to find alternative water resources. Wastewater reuse is regarded as one of the most crucial strategies to cope with water scarcity especially when there is a significant amount of wastewater (Hashem & Qi, 2021). The uncontrolled discharge of contaminated water into aquatic systems is posing serious problems to the environment. Therefore, there is an urgent need to develop more efficient, sustainable, and cost-effective methods to purify wastewater with minimal reagents that are necessary for achieving sustainable water management.

1.3. Research Questions (RQ)

This study will answer the following research questions (RQ):

RQ 1. Why adsorption method is a promising technique for pollutants remediation?

RQ 2. What is the effectiveness of using polysaccharide-based materials as adsorbents for pollutants?

RQ 3. Does the modification of polysaccharide-based polymers with fillers (bentonite and cellulose) enhances the adsorption efficiency of the adsorbents?

RQ 4. Is the adsorption efficiency of the proposed adsorbent comparable with those previously proposed in the literature?

RQ 5. What are the adsorption influences that can affect the efficiency of the proposed adsorbents for wastewater treatment?

To answer the above research questions, three studies were conducted in this research, the aims and hypothesis of each study are listed below:

Study (1): Study the removal of MB dye in aqueous solution by the synthesized polyvinyl alcohol- sodium alginate-Bentonite (PVA-ALG-BENT) composite beads (Section: 4.1).

Aim: to synthesize PVA-ALG-BENT composite and study its efficiency in the removal of MB dye from aqueous solution.

Hypothesis: BENT clay which acts as nano-filler materials can enhance the adsorption efficiency of MB dye in aqueous solutions.

Study (2): Study the removal of CR dye from aqueous solution by PVA-ALG-BENT composite beads (Section :4.1)

Aim: To study the efficiency of PVA-ALG- BENT composite in the removal of CR dyes from aqueous solutions.

Hypothesis: BENT clay which acts as nano-filler materials can enhance the adsorption efficiency of CR dye in aqueous solutions

Study (3): Synthesis of polyvinyl alcohol- Chitosan-Cellulose (PVA-CHTS-CLS) composite beads and study their efficiency in the removal of HMIs (Pb, Cu, As and Zn) from aqueous solutions (Section:4.2)

Aim: To synthesize PVA-CHTS-CLS composite and study its effectiveness in the removal of HMIs from aqueous solution.

Hypothesis: PVA-CHTS-CLS composite has enhanced adsorption efficiency of HMIs in aqueous solutions.

1.4. Research Objectives

The objectives of this study are as follow÷

1. To fabricate and characterize various polymeric-based hydrogel adsorbents by applying physical crosslinking of various polymers (natural and synthetics) along with the addition of fillers and nanoparticles.
2. To Investigate the adsorption efficiency of the synthesized hydrogels in the removal of organic dyes and heavy metals from aqueous solutions.
3. To study the effect of various operating parameters on the effectiveness of adsorption process such as contact time, adsorbent dosage, initial concentration of the adsorbate, temperature, and pH.
4. To estimate the mechanism of adsorption process of the prepared composites.
5. To evaluate the stability and reusability of the synthesized composites.

1.5. Research Significance

To the researcher's knowledge, this study is a novel in terms of the proposed composites that were used to remediate wastewater from dyes and HMIs by adsorption technique. The successful accomplishment of this research will enhance the implementation of sustainable Development Goals (SDGs), especially (goal # 6: ensure availability and sustainable management of water and sanitation for all) and (goal #14: Life below water), both focus on clean water availability to all and sustainable use of marine and ocean resources. The expected outcomes from the study can be summarized as follows:

1. Establish an environment friendly protocol for the synthesis of hydrogels adsorbents from natural polymers which are crosslinked by non-covalent interactions and thus are free of chemical contamination such as toxic crosslinkers and monomers.
2. Identify the best hydrogel composition and the appropriate reaction parameters that exhibit the maximum efficiency in the removal of wastewater pollutants.

1.6. The Study's Setting

This research involves various laboratory works which can be divided into 5 stages:

Stage 1: Synthesis of novel polymeric hydrogel adsorbents through crosslinking reaction using different precursor polymers (natural or synthetic).

Stage 2: Modification of the physicochemical properties of the prepared hydrogels such as hydrophilicity, porosity, and strength by changing the degree of crosslinking between the polymer chains through the addition of different types of nanoparticles and fillers.

Stage 3: Characterization of the prepared hydrogel by using different spectroscopic techniques such as Fourier Transform Infrared spectroscopy (FTIR), Scanning Electron Microscope coupled with energy dispersive X-ray analysis (SEM/EDX) and X-ray diffraction analysis (XRD).

Stage 4: Optimization of the optimal adsorption parameters for best adsorption efficiency including contact time, initial pH, initial concentration, adsorbent dosage, and initial temperature.

Stage 5: Investigation of the adsorption mechanism and efficiency of the prepared polymeric hydrogels in the removal of HMIs and dyes pollutants from aqueous solutions using different adsorption

isotherms and kinetic models such as the Langmuir, Freundlich, pseudo-first order and pseudo second order kinetics.
Stage 6: Testing the stability and reusability of the prepared polymeric adsorbents after several treatment cycles.

1.7. Research Terminology

According to (Pourhakkak et al., 2021)

1. Adsorption:

Adsorption is a "A reversible phenomenon based on physical or chemical attachment of adsorbate (molecules, atoms, and ions) to the adsorbent." (Pourhakkak et al., 2021)

2. Adsorbent:

"The term adsorbent or sorbent refers to usually a high porous, large specific surface area solid (also found in liquid phase), which has lattice vacancies of uniform/diverse particle size, homogenous/heterogeneous pore structure and different molecular dimensions for quick uptake of adsorbates from the system"(Pourhakkak et al., 2021).

3. Adsorbate

" The guest molecules that concentrate at the active surface of adsorbent are called adsorbate; from adsorption perspective, these substances either in the gaseous or liquid phase are the targets which should be removed from the bulk of system and collected onto adsorbent" (Pourhakkak et al., 2021).

4. Desorption

“The process of detaching the adsorbate from the surface of the adsorbent and releasing adsorbed molecules into the bulk of the fluid system (aqueous solution here) is called desorption” (Pourhakkak et al., 2021).

5. Kinetics:

“Mathematical calculation of the rate of contaminant uptake at a different time interval in which each particle moves from fluid phase to the external and internal pore of the adsorbent.”

6. Isotherms:

“Mathematical calculation of equilibrium state of loaded adsorbent against the partial pressure of the adsorbed adsorbate in the fluid phase at a fixed temperature.” (Pourhakkak et al., 2021).

Chapter 2

Literature Review

2.1. Water resources in Kingdom of Bahrain

2.2. Target pollutants

2.2.1. Toxic heavy metal ions (HMIs)

2.2.2. Organic Dyes

2.3. Wastewater treatment methods

2.3.1. Ion Exchange

2.3.2. Chemical precipitation

2.3.3. Reverse Osmosis (RO)

2.3.4. Electrolysis

2.3.5. Coagulation/Flocculation

2.4. Adsorption technique as method for wastewater treatment

2.5. Hydrogel systems

2.6. Polysaccharide- based composites hydrogel

2.6.1. Chitosan (Deacetylated chitin)

2.6.2. Sodium Alginate

2.7. Synthetic based composite hydrogel

2.7.1. Polyvinyl alcohol.

Chapter 2

Literature Review

2.1. Water resources in Kingdom of Bahrain

Kingdom of Bahrain is a small island developing state (SIDS) located in the Arabian Gulf which is one of the driest regions in the world (Al-Zubari et al., 2018a). The Arabian Gulf water surrounding Bahrain has high temperature, evaporation rate and salinity (Wabnitz, C.C., Lam, 2018). Like any arid country, Bahrain is a water scarce country, as it depends heavily on groundwater and desalinated sea water(Al-Ansari, 2013) . The World Resources Institute (WRI) have declared that by 2040, 33 countries are predicated to experience a critical water crisis in which Bahrain is among the top ten countries (Water Scarcity in Bahrain, 2022). Moreover, climate change caused high average annual temperatures, high evapotranspiration rates, rising sea levels and lack in rainfall which led in a significant decrease in the country's water level, intensify the water scarcity challenges and place additional strains on the overloaded water management system in Bahrain (W. K. Zubari & Lori, 2006). According to recent estimates, climate change is responsible for 20 % increase of water scarcity (Al-Zubari et al., 2018b; Supreme Council for Environment, 2020; UNWWDR, 2003).

The kingdom's water requirements in 2011 are displayed in Fig. 2.1, the sectoral water supply comes from three sources which are: (1) groundwater abstraction (36.5%), (2) desalination plants (54.1 %) and (3) the use of tertiary treated wastewater (9.4 %). Bahrain depends heavily on non-traditional water resources (desalinated water) and traditional water resources (groundwater relies on the Dammam aquifer) (Al-Zubari et al., 2018c). Water desalination exerts pressure on the environment in terms of

energy consumption and air pollution (VNR, 2018). The heavy reliance on groundwater resources has decreased the ground water volumes to more than twice the optimum sustainable quantity, causing decline in water level and quality and increased its salinization (W. Zubari, 2005).

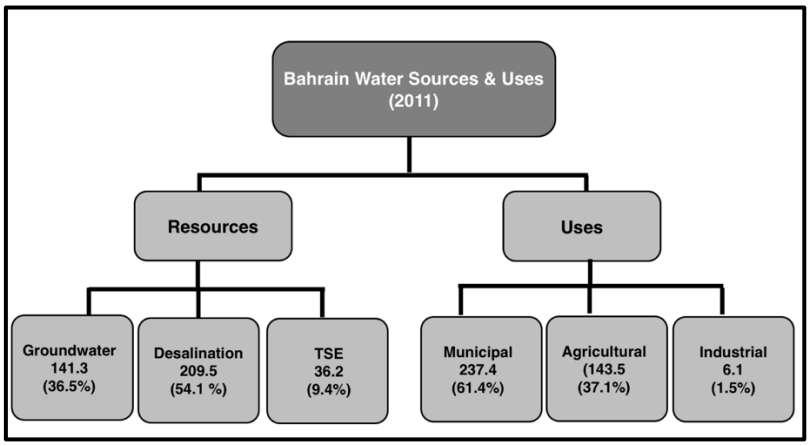


Fig. 2.1: Water resources and uses in Kingdom of Bahrain in 2011, in Million cubic meters (Mm^3).

In addition, rapid growth in population and urbanization are known to be significant concerns for small countries like Bahrain which suffers from scarce natural resources. Fig 2.2 a & b show the population increases (from 2007 to 2018) and urbanization growth (from 1960 to 2017), respectively in the kingdom of Bahrain. As a result of those changes, the total water demands increase as shown in Fig. 2.2c. With regards to the water consumption assiciated from the current population growth, Al-Zubari et al. mentioned that the percentage of per capita freshwater has been steadily decreased from 525m^3/yr. in 1970 to less than 100 m^3/yr. in 2010 as shown in Fig. 2.2 d (Al-Zubari et al., 2018a). Moreover, in 2019, the per capita water resources in Bahrain decreased from 382.6 cubic meters in 1977 to 70.7 cubic meter according to (Bahrain Renewable Water Resources per Capita, 1958-2021 - Knoema.Com, n.d.),

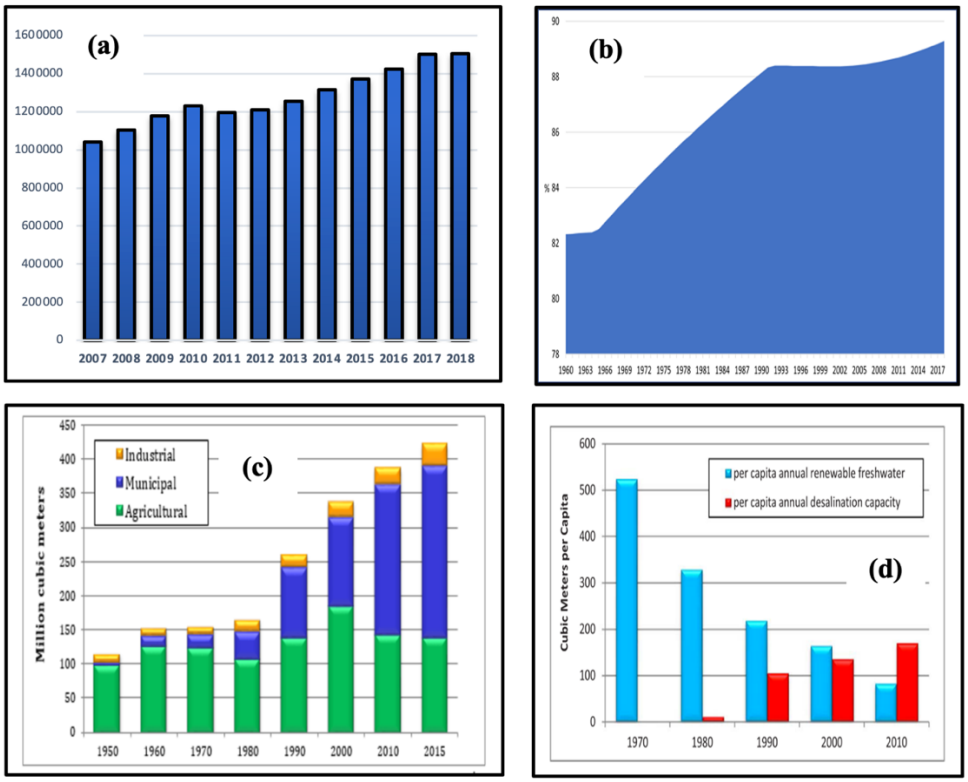


Fig. 2.2: a) Population growth (2007-2018). (Source: Bahrain Data Portal, 2018); b) Urbanization trends (Source: Bahrain Data Portal, 2018); c) Trends in total demands in the kingdom of Bahrain from 1950-2015 (Source: VNR, 2018); d) Annual per capita (1970-2010) renewable freshwater and desalination capacity in Kingdom of Bahrain.

To balance the increase of water demand and the decrease in water supply (the supply-demand gap), Bahrain's water authorities have adapted a national policy for allocating groundwater to agriculture sector and reducing groundwater dependency by relying on nonconventional sources (building additional desalination plants and expanding wastewater treatment technologies).

In Bahrain, there are 11 wastewater treatment plants with a total capacity of 352,770 m^3/day in 2017 as shown in Table (2.1). The main wastewater treatment plant with reuse transmission network is Tubli Water Pollution Control Center (Tubli WPCC). The amount of recovered, tertiary

treated, reused, and discharged wastewater in Tubli WPCC is shown in Fig 2.3. From the Fig. in the year 2015, the amount of wastewater flowed to Tubli were about 116 MCM of which 35 MCM were tertiary treated. Almost 28.5 MCM of the treated water was reused for agriculture (landscaping and irrigation) and the remaining (6.7 MCM) was used within Tubli plant. In addition, 74 MCM was treated to a secondary level and then discharged to the sea.

Table (2.1): Major and minor wastewater treatment plants in Bahrain. Adapted from REF.: Sanitary Engineering Operation and Maintenance Directorate, Ministry of Works, 2017.

Plant name	**Type of fluent**	**Level of treatment**	**Highest level of treatment**	**Design m^3/d * flow**	**Actual m^3/d* flow**
Tubli WPCC	Domestic	Tertiary	Ozone, chlorine, filtration	200,000	328,222
North Sitra	Industrial and Domestic	Tertiary	Deep gravity sand filters	16,500	13,322
Askar	Domestic	Secondary	Activated sludge	288	527
Hidd	Industrial and Domestic	Tertiary	Sand filter	2,325	1,800
Jasrah	Domestic	Tertiary	Sand filter	340	524
University of Bahrain	Domestic	Tertiary	Sand filter	504	902
Jaow	Domestic	Secondary	Activated sludge	408	942

South Alba	Industrial and Domestic	Tertiary	Chlorine	900	1,205
Al-Dur	Domestic	Tertiary	Sand filters	70	171
Hamalah	Domestic	Membrane bioreactor	Membrane bioreactor	1,100	868
Ma'ameer	Industrial and Domestic	Membrane bioreactor	Membrane bioreactor	2,250	1,931

- M^3/d; Cubic meter per day

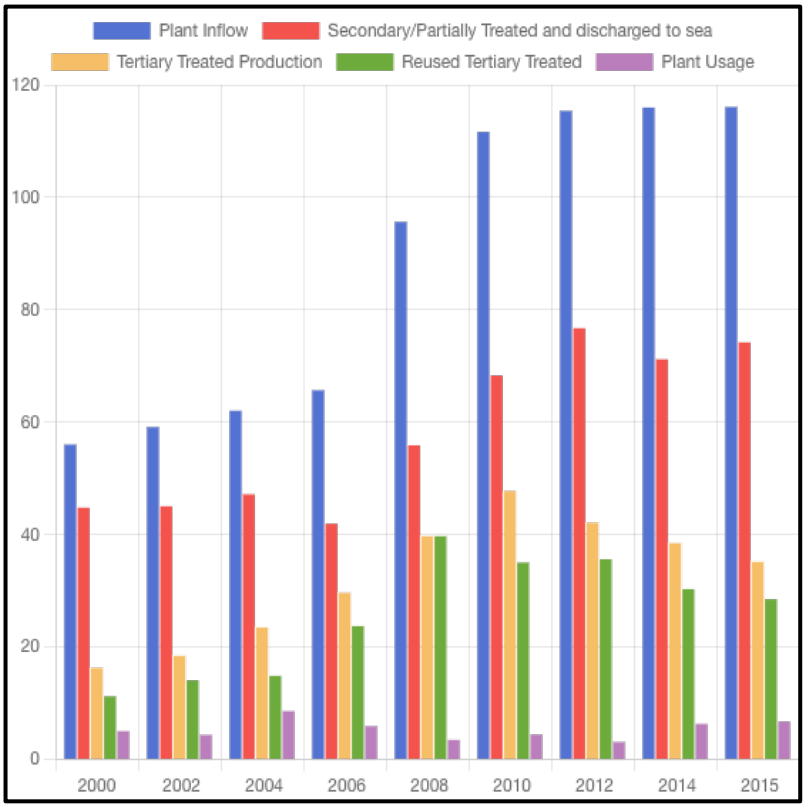


Fig. 2. 3: Tubli WPCC wastewater classification in million cubic meter per year (MCM) (received, reuse, and discharge to the sea). (Data source: Sanitation Directorate, Ministry of Works).

Reusing treated wastewater can be considered as economically and environmentally effective solution against scarcity and water pollution by

limiting the harm of the pollutant's discharged on the environment (Maquet & Christophe, 2020). Reusing treated water will also help to minimize the pressure on desalination of sea water and groundwater consumption and hence decreases their environmental effects (Aleisa & Al-Zubari, 2017). Accordingly, this study aims to develop and provide new and environmentally friendly absorbents to remove HMIs and organic dyes from wastewater.

2.2. Target pollutants

2.2.1. Toxic heavy metals ions (HMIs)

Toxic (HMIs) in particular, lead, cadmium, cobalt, zinc, copper, nickel, and chromium have been widely used in industries (Burakov et al., 2018; Soliman & Moustafa, 2020; Sonone et al., 2021). The level of metals has gradually increased in the environment, threatening both ecosystem and human health. HMIs are metallic elements which have higher density than that of water and are one of the most persistent pollutants in wastewater (Akpor, 2014; de Castro et al., 2018; Hasan et al., 2020; Kinuthia et al., 2020; Sanchez et al., 2020; D. Wang et al., 2018). Because heavy metals are non-biodegradable and extremely soluble in water, they can be absorbed directly by living organisms (Kinuthia et al., 2020).

According to Kim *et al*., HMIs have been grouped into two categories: essential and non-essential heavy metals. Essential HMIs function as nutrients in biological processes and are less toxic at low concentration such as iron, zinc, and cobalt. While the non-essential HMIs are non-biodegradable and extremely hazardous even at low concentrations such as: lead, mercury, and cadmium (J. J. Kim et al., 2019). Exposing to certain levels of HMIs could induces respiratory diseases, carcinogenicity, neurological abnormalities, skin toxicity etc. (Mitra et al.,

2022). Table (2.2) displays the permissible limit of heavy metals in wastewater effluents recommended by World Bank and World Health Organization (WHO) and their toxic effect on human health is displayed in Fig. 2.4 (Farooq et al., 2010; K. Gupta et al., 2021; Kinuthia et al., 2020; Sonone et al., 2021). From this perspective, the removal of HMIs from industrial wastewater is an urgent need for safe ecosystem (K. Gupta et al., 2021).

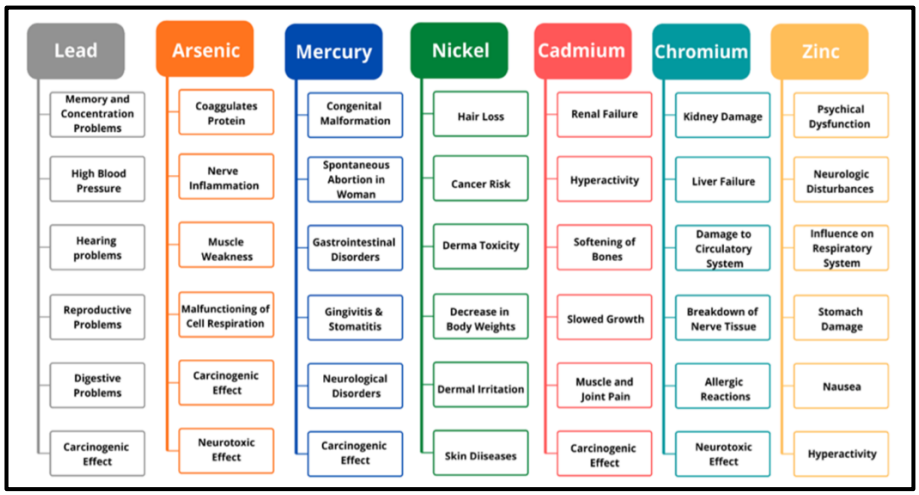
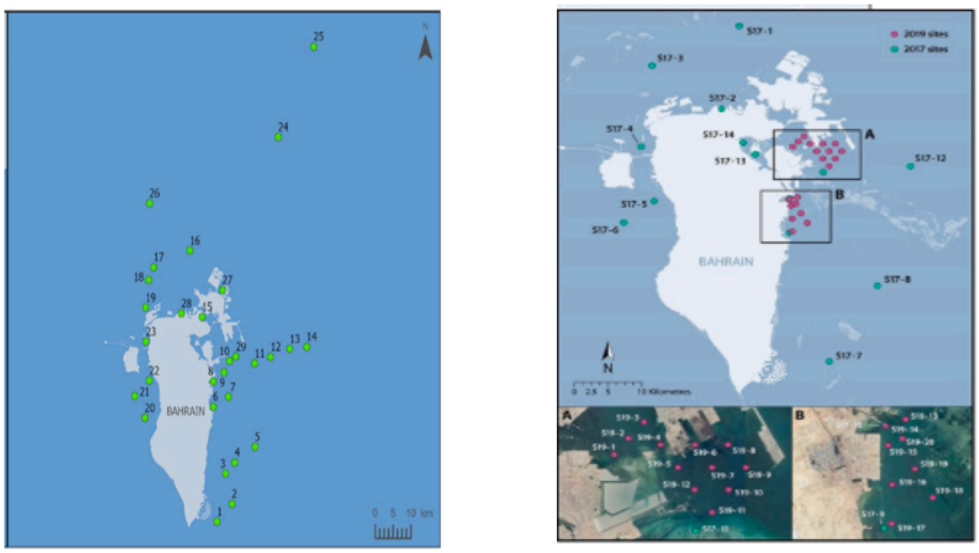


Fig. 2.4: Toxic effects of HMIs on human health. (Sonone et al., 2021).

Table (2.2): Permissible limit of heavy metals in wastewater effluents; (mg/L).

Heavy Metal	Permissible Level, (mg/L)	
	World bank	WHO
Lead	0.1	0.01
Cadmium	0.1	0.003
Mercury	0.01	0.001
Chromium (hexavalent)	0.5	0.05
Nickel	0.5	0.07

With regards to the state of Bahrain's marine systems, many studies have been conducted to evaluate the level of pollutants in Bahrain's marine sediments. In a study conducted by Nicolaus and his co-workers, 29 sediments stations (Fig. 2.5a) were monitored each year between 2007 and 2020 for the presence of (HMIs) such as: cadmium (Cd), chromium (Cr), copper (Cu), iron (Fe), manganese (Mn), nickel (Ni), lead (Pb) and zinc (Zn)). The results of the study showed that the concentration of the studied HMIs in most locations were within the permissible levels. The concentration of Zn and Ni was low, while little increase in concentration was observed for Cd, pb, and Zn in areas connected to the industrial facilities (Nicolaus et al., 2022). Moreover, a baseline survey of sediment contamination was conducted to measure the level of industrial pollutants such as HMIs. In that study, 14 costal sites of Bahrain were examined in May 2017 followed by another 20 sites in November 2019 (Fig. 2.5b). The results revealed that Bahrain's costal environment comprises low to medium levels of HMIs and consequently does not introduce any hazardous impact (Bersuder et al., 2020). However, the level of some contaminates can be increased by transferring from the neighbor countries and navigational movement in the Arabian Gulf.



(a) (b)

Fig. 2. 5: a) A sites of 29 sampling stations in Bahrain (source: (Nicolaus et al., 2022); b) Sediment sampling locations during 2017 (Site: 1-14) and 2019 (Site: 1-20) (Bersuder et al., 2020).

2.2.2. Organic Dyes

Synthetics dyes are non-biodegradable organic compounds due to their complex chemical structures (Sivarajasekar, 2015). The main sources of dye discharges are textile industry (about 54%) followed by dye industry (about 21 %), as shown in Fig. 2.6 (Samsami et al., 2020). Dyes industries consume large amount of water and consequently produced high quantity of wastewater containing hazardous dyes that possess major ecological threat to the environment (Asadi et al., 2018; Hamad & Saied, 2021a) . Many of these synthetic dyes are toxic, the extended exposure to dyes can cause respiratory issues, skin irritation, and increase the risk of cancer (Lellis et al., 2019) . In addition, according to a detailed study by Market Research Future, the global market for textile dyes increased from 2016-2022 and expected to increase more over the forecast period of 2023 (Fig. 2.7) (A. D. fergusont & P. Taylor, 2020).

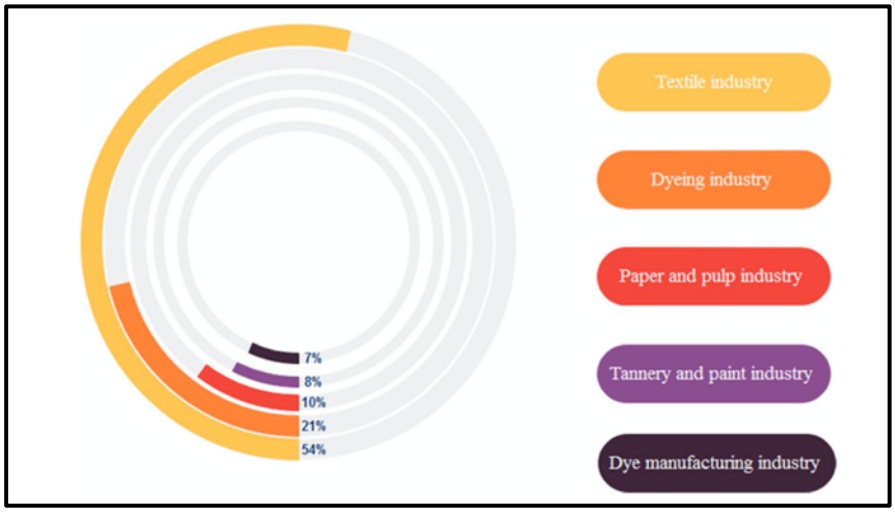


Fig. 2.6: Main industries that release dyes in the environment (Samsami et al., 2020).

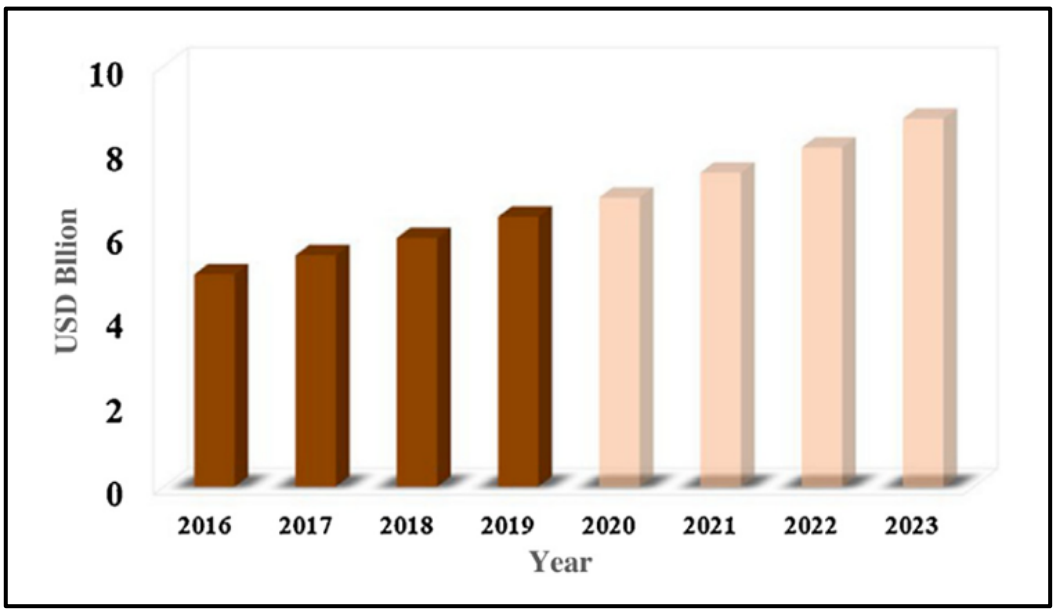


Fig. 2.7: The annual increase of textile dyes of the period 2016-2023 (A. D. fergusont & P. Taylor, 2020).

The major components of dye molecule are chromophores, auxochromes and the skeleton (Fig 2.8). Chromophore is an unsaturated group that is responsible of the color of the dye (absorbs light of UV and visible wavelengths from 200 nm to 400 nm and from 400 nm -800 nm, respectively). Examples of chromophore groups are azo (-N=N-), carbonyl (C=O), methine (-CH=), nitro ($-NO_2$) and quinoid rings. The other

component of dyes is the auxochrome, which is either electron withdrawing or donating group, and is essential to intensify the color of the chromophore. Example of auxochromes is amine (-NH_2), carboxyl (-COOH), and hydroxyl (-OH) (Benkhaya, M' rabet, et al., 2020) .

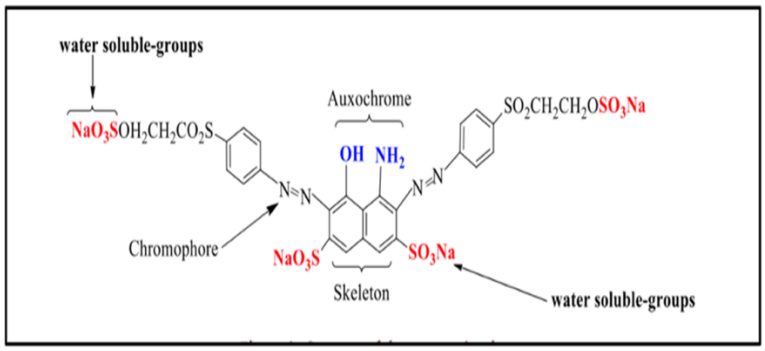


Fig. 2. 8: Structure of azo dye: chromophore and auxochrome (Benkhaya, M'rabet, et al., 2020).

Dyes can be classified into two categories based on their structure, namely ionic and nonionic dyes as shown in Fig. 2.9 (Mokhtar et al., 2020; Purkait et al., 2005; Tan et al., 2015). Ionic dyes are further classified to cationic and anionic dyes (Sivarajasekar, 2015).

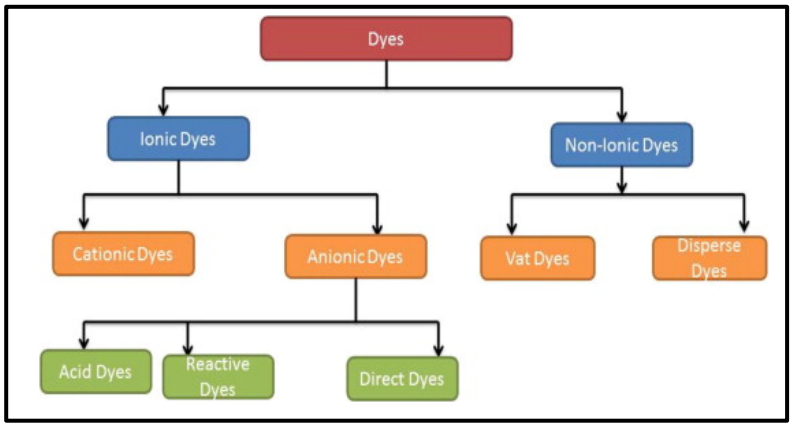


Fig. 2. 9: Classification of dyes based on their ionic structure (Tan et al., 2015).

Methylene Blue (MB) and Congo Red (CR) are the most common synthetic dyes. MB is a blue cationic thiazine dye (Fig. 2.10 a) and CR is anionic Azo dye (Fig. 2.10b). Thiazine dye is an organic compound containing a central heterocyclic ring containing S and N atoms (Baker et al., 2022). Azo dyes are distinguished by the existence of azo bond (-N=N-) and aromatic amines functional groups (W. Liu et al., 2016). Hamad and Saied mentioned that the effluent of azo dyes containing wastewater exposed hazardous characteristics resulting in serious environmental problems (Hamad & Saied, 2021b). Both MB and CR dyes have versatile industrial applications, and both are nonbiodegradable due to their complex aromatic structure (Alsamhary et al., 2021; Ansari et al., 2003; Donkadokula et al., 2020; Eltaweil et al., 2021; Jain et al., 2021; X. J. Liu et al., 2021; Olusegun et al., 2021; Shen et al., 2021; Silvestri et al., 2020).

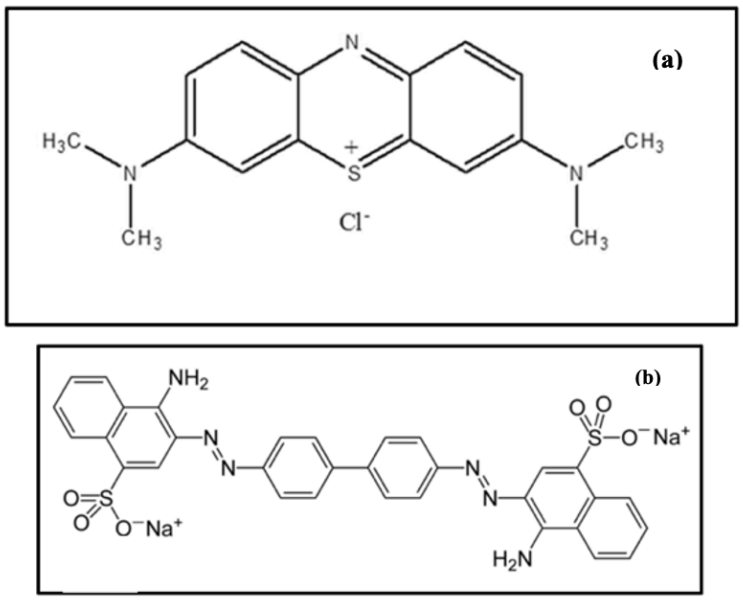


Fig. 2. 10: (a) Thiazine structure, (b) Azo reactive dye (Benkhaya, M'rabet, et al., 2020), (c) Chemical structure of MB dye, (d) Chemical Structure of CR dye.

Synthetics dyes are non-biodegradable organic compounds due to their complex chemical structure, thus the complete degradation of these dyes is very difficult (Sivarajasekar, 2015). Moreover, dyes are soluble in water and consequently their elimination using conventional techniques such as chlorination and ozonation is difficult (Lellis et al., 2019). Table 2.3 illustrates the chemical and physical methods applied the removal of dyes from wastewater effluent, as well as the advantages and drawbacks of each methods.

Table (2. 3): Advantages and drawbacks of dyes treatments methods. Adapted from: (Sivarajasekar, 2015)

Method	Advantages	Disadvantages
Chemical treatment		
Ozonation	Zero production of sludge, decrease the volume of water discharge	Ozon is instable compound, it decays rapidly and has short half-life (20 min)
Oxidation process by using H_2O_2	Easy and simple process	Requirement of oxidizing agent (H_2O_2), sludge formation
Oxidation by chlorine	Simple process, low cost	Formation of toxic by- product
Fenton`s reagent	Fenton reagent is inexpensive, easy process.	sludge formation, limited by narrow pH
Coagulation/flocculation	Simple and effective process	Toxicity of coagulants

Method	Advantages	Disadvantages
		compounds, sludge formation, difficulty of the scaling up.
Physical treatment		
Adsorption by activated carbon	High adsorption efficiency	High Cost of activated carbon
Membrane filtration	Stable at high temperature, high adsorption efficiency, suitable for all types of dyes	High cost and slow filtration speed
Ion exchange	Reusable adsorbent (regeneration)	Not suitable for all types of dyes (dispersive)

2.3. Wastewater treatment methods

United Nations World Water Report entitle "Wastewater: The untapped Resource" stated that globally over 80% of wastewater is discharged to the environment without treatment (WWAP, 2017). Wastewater is defined as the discharge of used water from residence, institutions, and industrial organization through a carefully designed network of pipes to the treatment plant (Kaur et al., 2017). Two general categories of wastewaters: domestic and industrial (Sonune & Ghate, 2004). Industrial wastewater (IWW) is declared among the most serious challenges to the environment due to its toxicity (Int & Iqbal, 2019; Mu et al., 2020b). IWW is known as any undesired solid products, liquid, or mixes released or discharged from any industrial activity (Soliman & Moustafa, 2020). IWW streams covers a

range of toxic pollutants, including dyes, high level of HMIs, radioactive materials and other toxic chemical produced from different industries as represented in Fig. 2.11 (Kemp et al., 2013). HMIs and organic dyes are regarded as major anthropogenic toxic pollutants of marine ecosystems that induce damage to the natural water and have harmful effects on human health (Ansari et al., 2003 and Bhatnagar & Sillanpää, 2009).

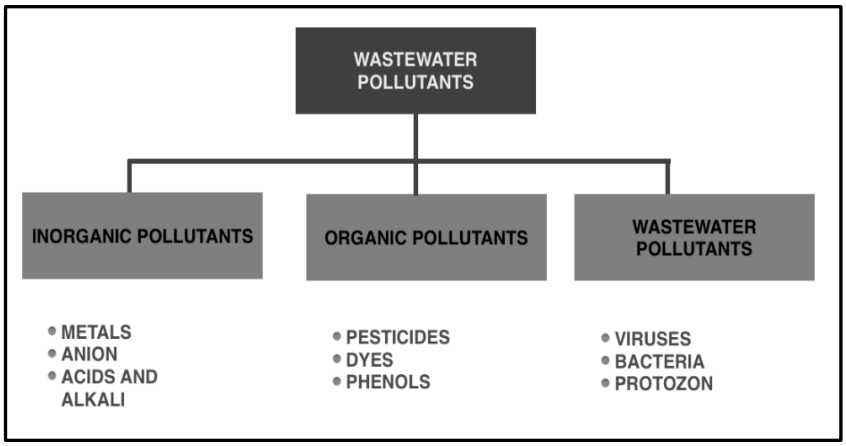


Fig. 2. 11: Classification of Wastewater contaminants.

The conventional wastewater treatment process is broadly divided into four stages, each with distinct purpose: (1) preliminary stage, (2) primary step, (3) secondary (biological) treatment and (4) tertiary treatment or advance wastewater treatment (Fig 2.12). These treatment steps involve numerous techniques depending on the nature of wastewater (Poerio et al., 2019). The purpose of preliminary step is to remove all insoluble solids and materials (plastics, papers, etc and dense solids) from the influent wastewater before they damaged the sewage system pump lines (V. K. Gupta et al., 2012). The main suspended solids and sediments are removed in primary treatment step. The dense sludge is settled in the bottom of the tanks whereas oils/greases are collected from the surface. The discharge from the primary treatment comprises biological matters that need a further treatment before discharge. The secondary stage involves the degradation

of dissolved organic matter and nutrients by using bacterial biological degradation (Shon et al., 2006). The primary and secondary steps are insufficient to reuse water. Thus, tertiary treatment step is essential to remove the majority of residual organic and inorganic solid and microorganisms mainly by using ozonation, chlorination or UV treatment (Meneses et al., 2010).

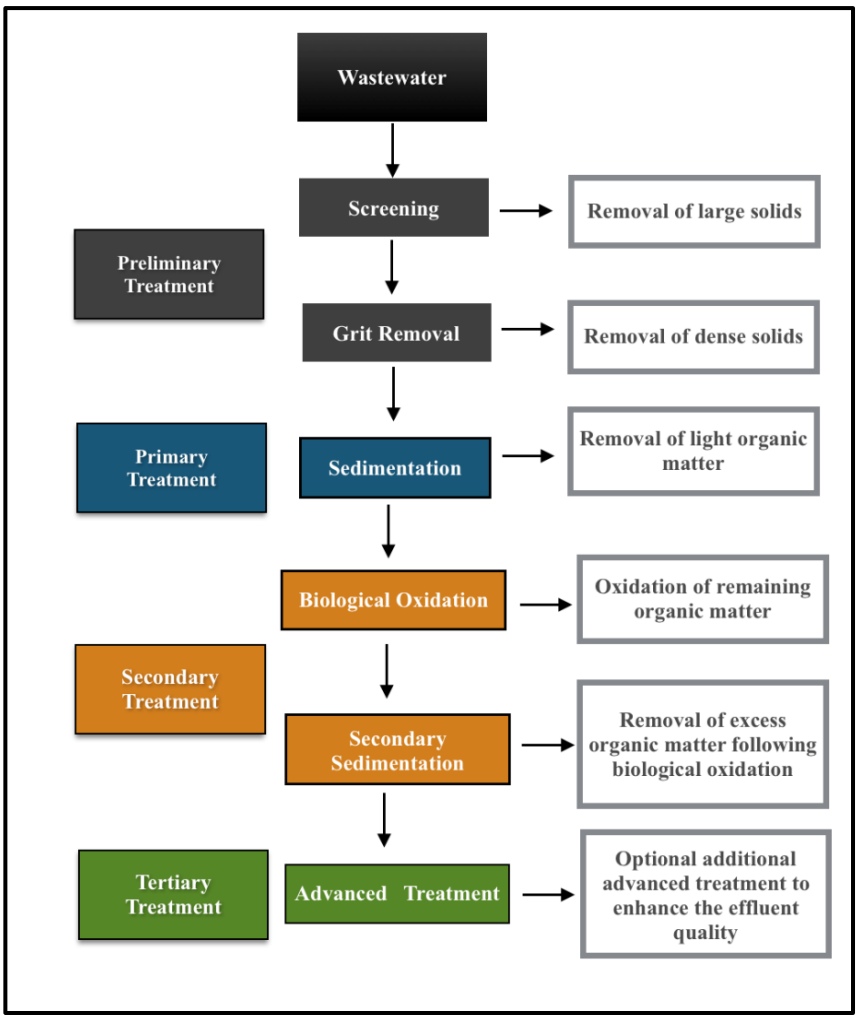


Fig. 2.12: Classification of wastewater treatment step

In tertiary treatment stage, different advanced methods are used including ion exchange method (X. Wang et al., 2018), chemical precipitation (Son et al., 2020) (Son et al., 2020; Yan et al., 2019), reverse osmosis (Vinardell et al., 2020), electrolysis (L. Zhang et al., 2020),

coagulation/ flocculation (Lau et al., 2014; Zhao et al., 2021), ultrafiltration (Goh et al., 2015), adsorption (J.Fernandes et al., 2020; Kumari et al., 2019; J. Wang & Guo, 2020b; L. W. Yang et al., 2021; Z. H. Zhang et al., 2021a); etc. Among them, adsorption is techno-economically effective method for wastewater treatment because of its cost effectiveness, easy control and simple, low energy consumption, low harmful secondary products, and reusability of adsorbents (Aljar et al., 2021; Crini et al., 2018; Crini, Lichtfouse, et al., 2019; Kang et al., 2017; Rouhani & Morsali, 2018; S. Wang et al., 2005). The next sub-sections review the most common wastewater treatment methods and Table (2.4) displays the advantages and disadvantages of these methods.

2.3.1. Ion Exchange

Ion exchange process is widely used in industry for the removal of dissolved ions from wastewater effluents (Soliman & Moustafa, 2020). This approach involves a reversible ion exchange between the solid and liquid phases. Polymer beads are placed in a resin matrix, the insoluble material (resin) absorbs the undesirable metal ions (either negatively or positively charges ions from solution) and releases the other ions of similar charge (Fig. 2.13) (Z. Liu et al., 2021). The selection of resins is based on the type of pollutants, for instant for the treatment of heavy metal ions such as cadmium and cobalt, cationic resins (Sodium or hydrogen ions) are used. Whereas, for the treatment of negatively charge ions such as chromate and cyanide, anionic resins (hydroxide ion) are selected. Over a period, an ion exchanger becomes saturated and can be regenerated using acid or base.

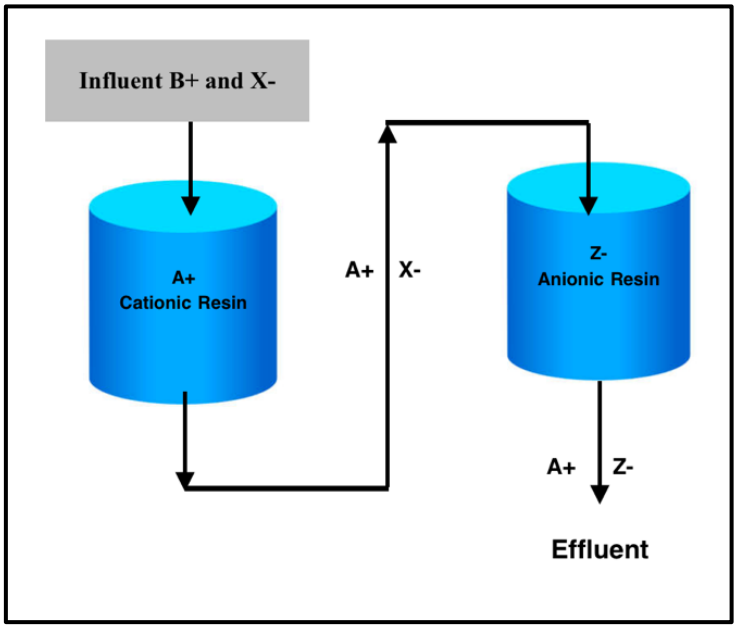


Fig. 2. 13: A schematic diagram of ion exchange system

2.3.2. Chemical precipitation

Chemical precipitation process is one of the most widely used process in industry for removing heavy metals from wastewater (Fig. 2.14) (F. Fu & Wang, 2011) (Int, 2019). In this process the HMIs and other pollutants are precipitated by adding a precipitating agent to the influent to remove the ions as insoluble materials such as hydroxide precipitates, carbonate precipitates, sulfide precipitates and metal chelating precipitates. The precipitates are then separated from the solution by filtration.

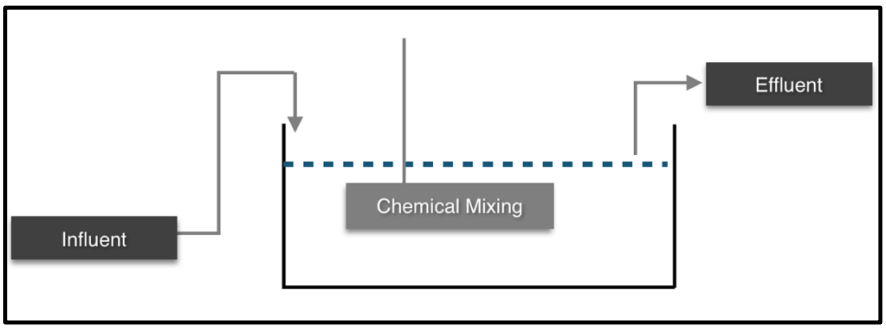


Fig. 2. 14: A schematic diagram of Chemical precipitation process

2.3.3. Reverse Osmosis (RO)

Reverse Osmosis (RO) is a well-known water purification technique that is used to remove a broad range of salts, ions, heavy metals and other contaminates by using a pressure-driven semipermeable membrane (pore size > 2 nm) (Al-Obaidi et al., 2021) (Poerio et al., 2019). Fig. 2.15 displays a schematic diagram for RO, a high pressure (10-100 bar) is used to force the feed stream (concentrated water solution) and overcome forward osmotic pressure of RO feed solution (Al-Najar et al., 2020). Herein, only water is passed through the RO semipermeable membrane leaving all other materials on the high-pressure side of the membrane (Poerio et al., 2019).

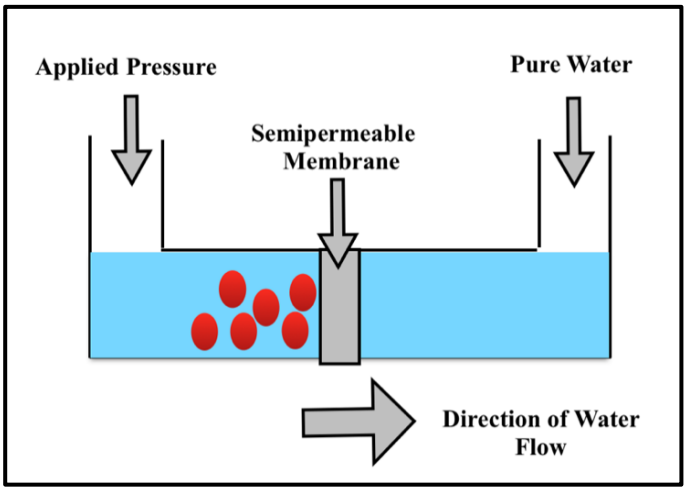


Fig. 2. 15: A schematic diagram of Reverse Osmosis process

2.3.4. Electrolysis

Electrolysis is an electrochemical wastewater treatment technique that can remove a wide range of undesired chemicals from wastewater (Chopra et al., 2011). During the process, an electric current is applied in an electrolyte solution that allows ions to move between two electrodes system (anode and cathode) (W. Y. Kim et al., 2017). The positive ions are oxidized at the cathode and negative ions are reduced at anode.

2.3.5. Coagulation/ Flocculation

It's one of the most essential methods that is used to separate the suspended solids from the wastewater. Suspended particles in water are negatively charged that repel each other, thus remain in suspension without settle out unless adequate coagulation and flocculation are applied. Coagulation is a chemical process which involves the addition of chemical reagents called coagulant (with charge opposite to the suspended solids) to neutralizes the negatively charged particles (destabilization). Whereas flocculation is a physical method that allows the aggregation of the destabilized particles, thus are easy to be separated from the solution as depicted in Fig. 2.16 (Beyene et al., 2016).

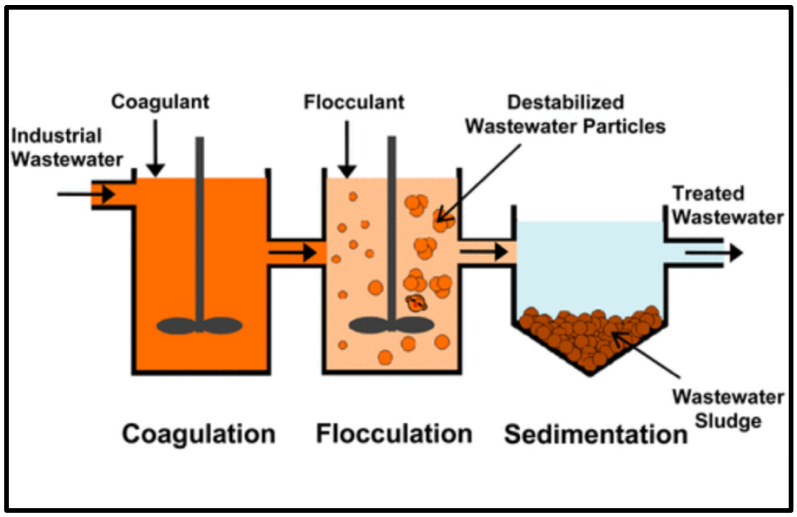


Fig. 2. 16: A schematic diagram of Coagulation/ Flocculation process (Teh et al., 2016).

Table (2. 4): The advantages and disadvantages of wastewater treatment methods. (Darban et al., 2022)

Technique	Advantage	Disadvantages	References
Ion Exchange	• Ease recovery of ion exchange metal and regeneration of beds. • Selective removal of ions (depends on the type of ion exchanger used). • Effective removal for cations and anions. • Simple to generate resin. • Release less amount of sludge.	• The formation of secondary pollution from regeneration process. • Expensive process, particularly when used to treat huge amount of wastewater. • Limited availability of resins for all types of heavy metals	(Darban et al., 2022)
Chemical precipitation	• Simple and safe method • Inexpensive to operate.	• Need addition of chemicals to reduce heavy metals in solution to a level that is	(Int, 2019)

Technique	Advantage	Disadvantages	References
		acceptable or disposal. • Formation of hazardous sludge. • Time consuming. • Expensive process when using large amount of wastewater. • Ineffective for treating low concentrations of heavy metals ions	
Reverse Osmosis	• Safe and environmentally friendly technique. • low cost	• Requires proper pretreatment and maintenance for the membrane because membrane can be clogged with solids.	

Technique	Advantage	Disadvantages	References
		• High power is needed for constant pressure flow.	
Electrolysis	• It can remove several pollutants in one time (heavy metals, organic matter, colloidal solids • Low sludge formation • Low maintenance cost • Easy system	• Energy consumption. • Not tested in full scale application	(Chopra et al., 2011)
coagulation/ flocculation	• Easy to operate • Low cost and low energy process	• Produce large amount of sludge.	
Adsorption	• Easy and efficient method • No waste production • Low cost	• Low selectivity • Formation of waste products	(Hasanpour & Hatami, 2020)

Technique	Advantage	Disadvantages	References
	• Applicable for a wide range of pH		

2.4. Adsorption technique as method for wastewater treatment:

Adsorption process is a surface deposition method in which the adsorbate molecular species (gas, liquid, or solids) is accumulated at the surface of the active sites of the adsorbent (Alasadi et al., 2019; Velasco-Garduño et al., 2020). This method is mostly applied in industrial applications for example water remediation. The concept of adsorption is described through the interaction of three components, i.e., the wastewater, the adsorbate, and the adsorbent as illustrated in Fig. 2.17 (Crini, 2005).

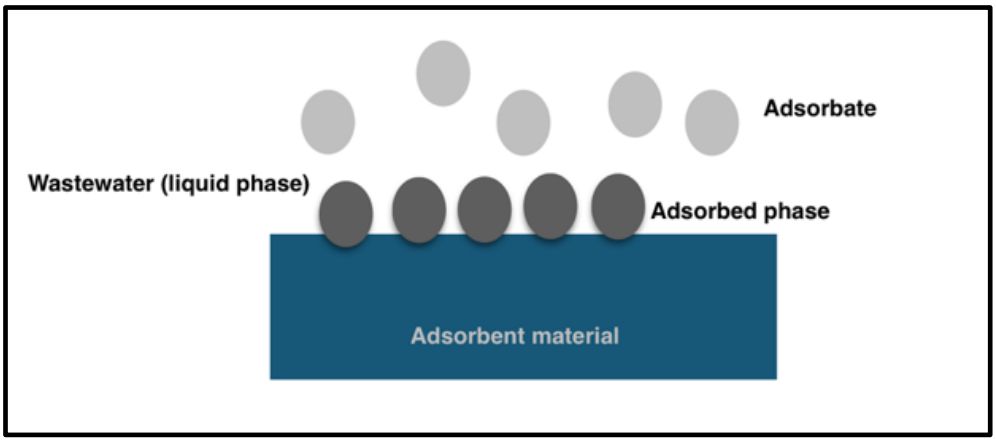


Fig. 2. 17: Schematic illustration of the adsorption process system of a surface.

The efficiency of adsorption depends on the type of adsorbents; a porous adsorbent material with high surface area, high physical strength, cost-effective, abundant, and have appropriate mechanical properties are

important (Kluczka et al., 2018). A porous material is a solid with a structural geometry that creates pores and channels within the materials (David, 2015). Porosity offers significant properties to a material such as large surface area and low density.

David *et al*. mentioned that the porous structure can be classified into five types: (1) closed holes which are completely separated; (2) open holes which contain channels to the external system; (3) blind holes (one side open); (4) through holes (two sides open); (5) rough holes which are not classified as real holes unless contain deeper irregularities**,** as shown in Fig. 2.18:

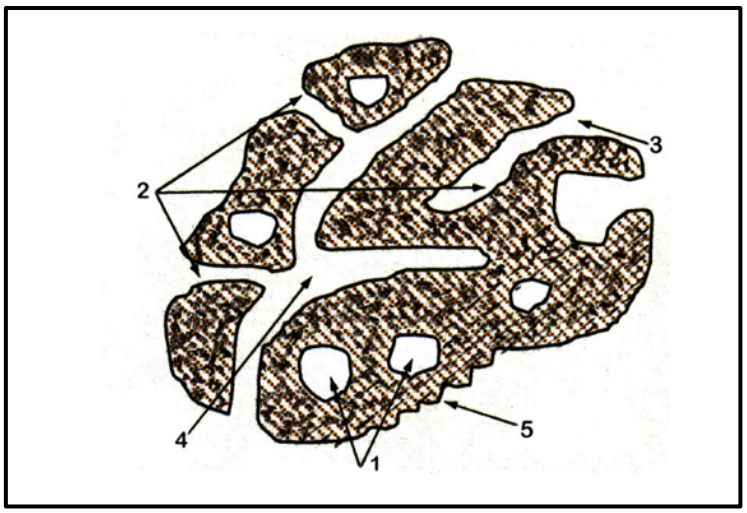


Fig. 2. 18: Schematic cross section of a porous material: (1) closed pores; (2) open pores; (3) blind pores; (4) through pores; (5) roughness pores (David, 2015).

The functionality of adsorption process depends on the physiochemical properties of adsorbents. In general, most solids have adsorbent capacities depending on their functional groups (Sazali et al., 2020). Many porous adsorbents have been developed to remove contaminants from the aquatic environment ranging from natural

adsorbents to advanced nano adsorbents (Sazali et al., 2020). The most well-known adsorbents are zeolite, activated carbon, porous organic polymers, metal organic frameworks and covalent organic frameworks (W. Wang, Zhao, Bai, Zhang, Ibarra-Galvan, et al., 2018a). However, most of these adsorbent's materials have high production cost especially for large scale application (Darban et al., 2022). In fact, cost is a crucial factor when considering developing different adsorbent materials. A sorbent can be termed as low-cost material if its abundant in nature, requires low treatment and it is a by-product produced from industry (Crini, 2005).

Recently, attention has focused in using natural materials as adsorbents for wastewater treatment, several reviews are summarized in Table 2.5. Polysaccharide is a broad category of carbohydrate polymers derived from natural origin and have made a remarkable influence on the application of wastewater treatment (Qi et al., 2021). These biopolymers exhibit ~~a~~ compelling and interesting adsorption properties due to their unique structure (porous structure), physio-chemical properties, chemical reactivity, high water absorption capacity, cost-effective, renewability, biodegradability, and biocompatibility (Barclay et al., 2019; Mohammadzadeh Pakdel & Peighambardoust, 2018a). The adaption of polysaccharide-based materials for the preparation of new adsorbent beads and enhancing the existing wastewater remediation techniques is one of the main goals of the current research in academia and industry.

Table (2. 5): Review articles focusing on adsorption of pollutants using low-cost adsorbent materials for wastewater remediation

No.	References	Objective	Adsorbent	pollutants
1	(Dutta et al., 2021)	Examine the adsorption effectiveness of several adsorbents for dye remediation.	Activated carbon, metal oxide-based, carbon-based, metal-organic framework, and polymer-based adsorbents	Dyes
2	(Upadhyay et al., 2021)	Test the efficiency of some CHTS-based adsorbents for the removal of HMIs.	CHTS-based adsorbent	HMIs
3	(Qi et al., 2021)	Use polysaccharide-based adsorbents in wastewater remediation and investigate the adsorption parameters that affect the efficiency of the adsorption process	Polysaccharide- based adsorbent	HMIs and dyes

No.	References	Objective	Adsorbent	pollutants
4	(M. J. Ahmed et al., 2020)	Prepare and apply CHTS /Chitin carbonaceous composites materials for the adsorption of water pollutants.	CHTS /Chitin carbonaceous composites materials, such as carboncaeus: activated carbon, biochar, carbon nanotubes and GO	HMIs and Dyes
5	(Y. Liu et al., 2019)	Investigate the efficiency of CHTS and Glucose towards the adsorption of Co (II)	CHTS/Glucose hydrogel	Cobalt (II)
6	(Jawad et al., 2020)	Evaluate the performance of CHTS /charcoal adsorbents for the removal of cationic dyes from wastewater	CHTS/Charcoal	Thionine Cationic dye
7	(da Silva Alves et al., 2021)	Study the performance of CHTS-based adsorbents for the removal of several pollutants from aqueous solutions.	CHTS-based	Cr(VI), Pb(II), Cd(II), Cu(II), and different cationic and anionic dyes

2.5. Hydrogel system

Hydrogel is a hydrophilic polymeric material which has the tendency to absorb large quantity of solution, causing enlargement of the hydrogel size without dissolving in the solution (Fennell & Huyghe, 2019; Gyles et al., 2017). When the fluid is water than the gel is defined as hydrogel (Jing et al., 2013). The solid structure of a Hydrogel is a matrix of three dimensional (3D) (Frachini & Petri, 2019; Varaprasad et al., 2022). The three main parts involved in preparation of hydrogel are monomer, initiator, and crosslinker (Fig. 2.19) (Ullah et al., 2015; Wallmersperger et al., 2004). Polar monomers are typically used to create hydrogels, according to the starting materials, they can be classified into synthetic, natural or the combination between the two classes. The crosslinker agent is used to provide highly crosslinked polymer network (E. M. Ahmed, 2015b). It increases the viscosity of the hydrogel by joining and fixing the functional monomers to each other and increases the molecular weight of the hydrogel (Belyadi et al., 2019). The crosslinking agent controls the shape, morphology, and mechanical stability of the polymer matrix. Excessive amount of crosslinking agent has a negative impact on the structure of hydrogel since it results in a very dense polymer structure, reduces the hydrophilic characteristics and the pores will be too deep and difficult to access. While, low level of crosslinking agent affect the flexible structure of polymer, the pores will easily collapse leading to lose to the structure of polymers (Deng et al., 2018) .

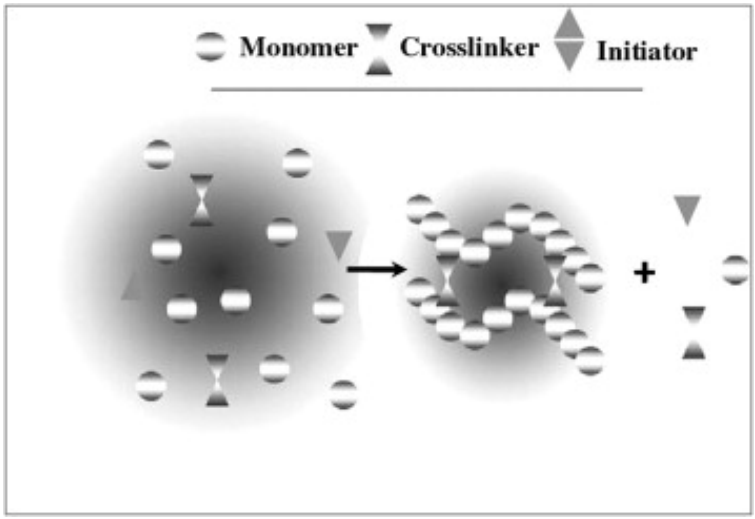


Fig. 2. 19: components of hydrogel (E. M. Ahmed, 2015b).

Hydrogels are categorized based on several parameters such as source, composition, preparation methods, ionic charge, and types of crosslinking. Fig. 2.20 represents some chemical and physical properties for each type of hydrogel.

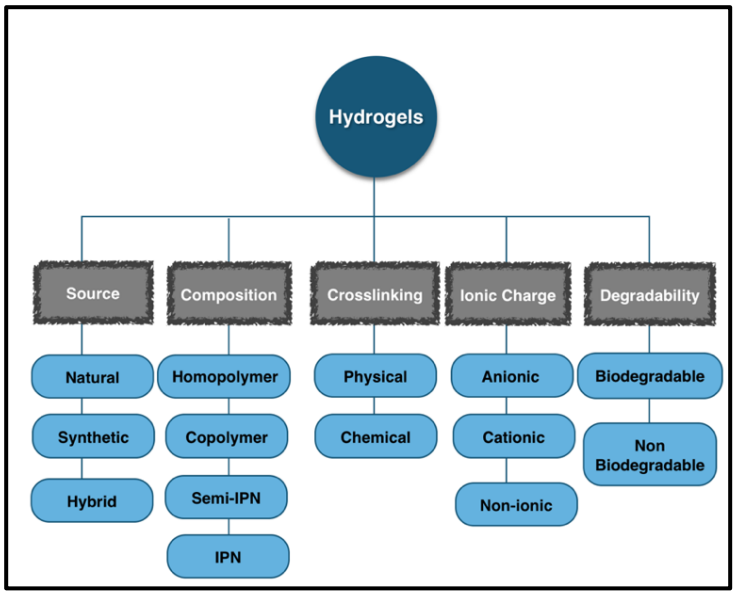


Fig. 2. 20: Chemical and physical properties for the classification of Hydrogel.

According to the polymer source, hydrogel polymers can be classified as natural (biopolymer) polymers, synthetic macromolecule, and hybrid polymers (Gyles et al., 2017; Mu et al., 2020b) . The natural polymers have gradually replaced by synthetic or hybrid polymers to increase the strength and water absorptivity of the gel (Garnica-Palafox & Sánchez-Arévalo, 2016).

A. **Natural polymers and their derivatives:** natural hydrophilic polymers have low production cost, high solubility, high biocompatibility but suffer from low mechanical strength. Examples of natural polymers are Polysaccharides (e.g., chitosan, dextran, alginate, and pullulan) and protein (e.g., albumin, gelatin, lectin, legumine, collagen and viciline) (Zou et al., 2020a).
B. **Synthetic polymers:** are hydrophobic polymers prepared from synthetic polymers. They are chemically stable and mechanically stronger than natural polymers. The hydrophilic region or part of the synthetic polymers is due to the presence of special hydrophilic functional groups such as –OH, –COOH, –CONH, –$CONH_2$, SO_3H, amines, R_4N^+, and ether (Dragan, 2014; Gyles et al., 2017).
C. **Hybrid hydrogels:** are combination of natural and synthetic polymers. They are widely used as they merge the advantages of both natural and synthetic polymers.

Most of the hydrogel in the market are prepared from synthetic polymers because of their superior mechanical, chemical and physical properties, but these hydrogels are non-renewable, have a high manufacturing cost, not ecofriendly and non-biodegradation (Tanan et al., 2019). To overcome these drawbacks, a combination of natural and

synthetic polymers is considered to create a new material with better physical properties (Jayakumar et al., 2021; Qin, 2016).

Moreover, hydrogels are formed by crosslinking of monomers in the presence of suitable initiator (polymerization) (Vinchhi et al., 2021). Based on hydrogel's polymeric composition, Hydrogels can be classified into three groups as shown in Fig. 2.21:

(1) Homopolymer Hydrogels which are originated from one type of monomeric units.

(2) Copolymer Hydrogels which are formed from two or more different monomers with at least one hydrophilic monomer, the hydrophilic constituent is essential to maximize the swelling of the hydrogel (L. Yang et al., 2002).

(3) Interpenetrating polymer network (IPN) Hydrogels which can further group as semi-IPN and IPN Hydrogels. IPN Hydrogels are multipolymer frameworks of two or more crosslinked polymers connected in a network (Dragan, 2014).

Semi-IPN hydrogen is formed when linear polymer is non-chemically or physically bonded to another crosslinked polymer network. (Aljar et al., 2021). For example, considering two polymers' chains named as A and B. In full IPN, there is no crosslinking among polymer A and B; chains of polymer A are self-crosslinked, and chains of polymer B are also self-crosslinked. Whereas in semi-IPN, polymer A chains are linked with each other, while chains of polymer B are physically entrapped (Frachini & Petri, 2019). IPN-based Hydrogels exhibit a variety of advantages such as high mechanical strength and stability (Zou et al., 2020a).

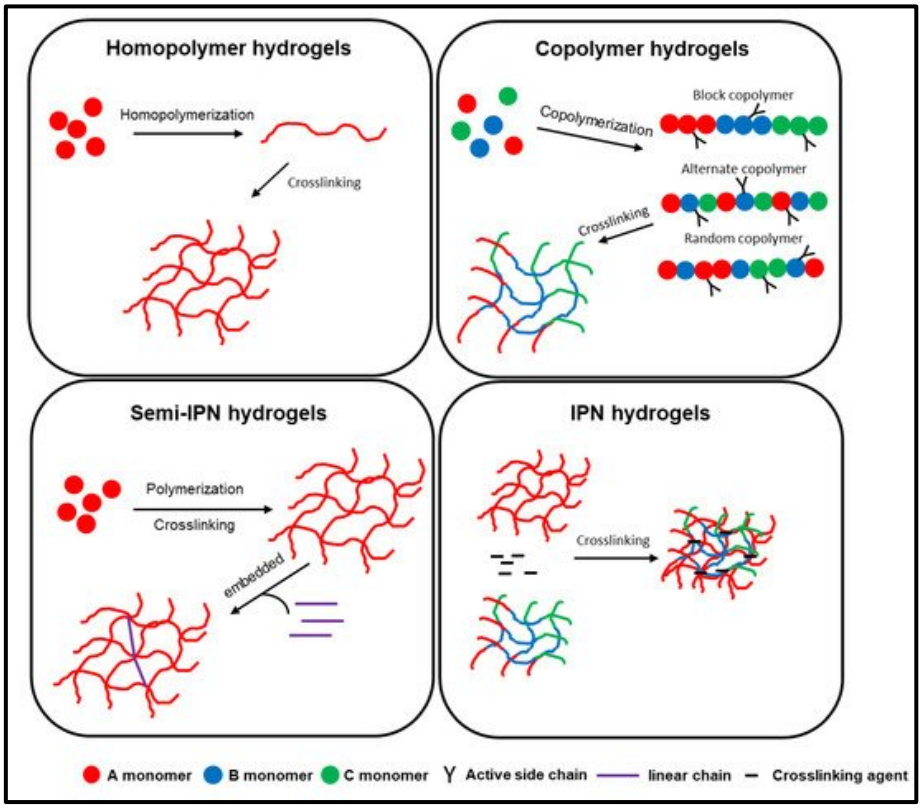


Fig. 2. 21: Graphical Illustration of homopolymer, copolymer, semi-IPNs and IPN Hydrogels (T.-C. Ho et al., 2022).

The structural properties of hydrogels can be optimized by carefully controlled methods (Patel & Thareja, 2022). Generally, hydrogels are prepared from natural polymers (hydrophilic monomers) and synthetic polymers (hydrophobic monomers which are more chemically stable than natural polymers) (E. M. Ahmed, 2015a).

The crosslinking of polymer chains can be of physical or chemical nature (T.-C. Ho et al., 2022). In physical (reversible) crosslinking, the polymer chains are linked together by physical forces (i.e. weak van der Waals forces, hydrogen bonds, polarity, dipole-dipole interaction, hydrophobic interactions, etc.) (El-Naas & Alhaija, 2013; Mu et al., 2020b). Whereas chemical (permanent or irreversible) crosslinking occurs through the formation of covalent bonds between polymers (Koumanova & Allen, 2005). It's important to mention that chemical hydrogels have a high level

of stability than physical hydrogels. Fig. 2.22 depicts a schematic illustration of several preparation procedures of hydrogel.

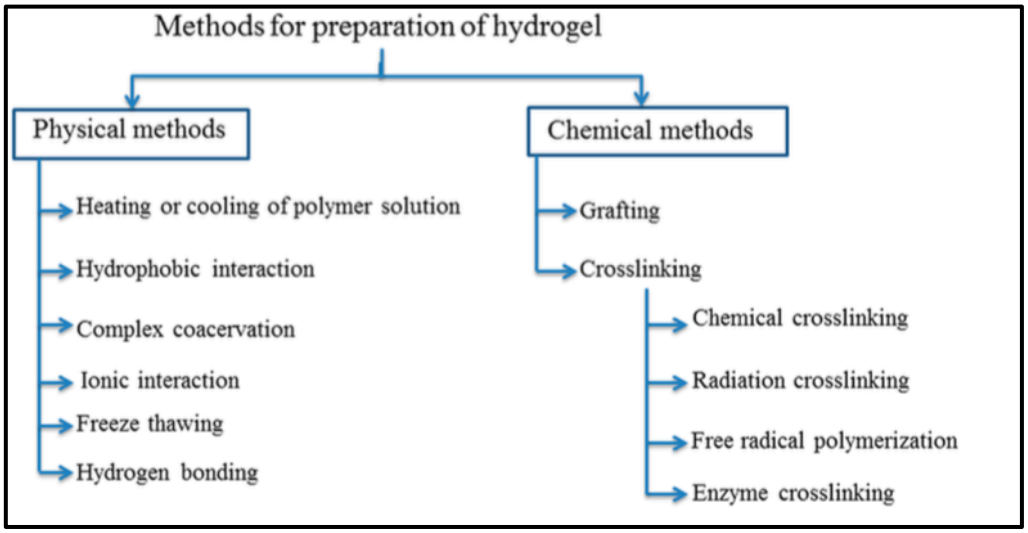


Fig. 2. 22: Preparation methods of hydrogels (Ali & Ahmed, 2018).

2.6. Polysaccharide-based composites hydrogel

Natural biopolymers are polymeric organic compounds constructed from natural sources such as (plants, animal, and algae) (Nasrollahzadeh et al., 2021). Polysaccharides are among various biomaterials that can be used to fabricate adsorbents, because as natural materials they are: (i) inexpensive and renewable; (ii) abundant at large scale; (iii) biocompatible and biodegradable (Barclay et al., 2019; Mohammadzadeh Pakdel & Peighambardoust, 2018c; Su et al., 2019). Polysaccharides are a class of carbohydrates with long repeat units of monosaccharide sugars (between 100 to1000 monosaccharide units) linked together by glycosidic bonds (which are responsible for holding monomers together to produce polymers) (Afrin & Karim, 2021). Carbohydrate includes numerous hydroxyl groups, ketones, and aldehyde groups. The empirical formula of carbohydrate is $[(C_n(H_2O)_n]_m$, where n is the number of atoms and m is the number of units (Gomez-Maldonado et al., 2019).

Polysaccharides are the most abundant natural polymer on earth, examples of polysaccharide are cellulose, chitin/chitosan, alginate, hyaluronic acid, starch, gum, and pectin. They all are considered as natural and sustainable compounds that compete the potential of the conventional material (Lim et al., 2019). The structure of some polysaccharides is illustrated in Fig. 2.23.

Depending on their structure, polysaccharides are classified to two major groups: (1) Homo-polysaccharide and (2) hetero-polysaccharide. The homo-polysaccharide are composed of a single type of monosaccharide such as glucose in cellulose and N-acetyl glucosamine in chitin. While Hetero polysaccharides are made up of two or more types of monosaccharides (Valdés et al., 2016).

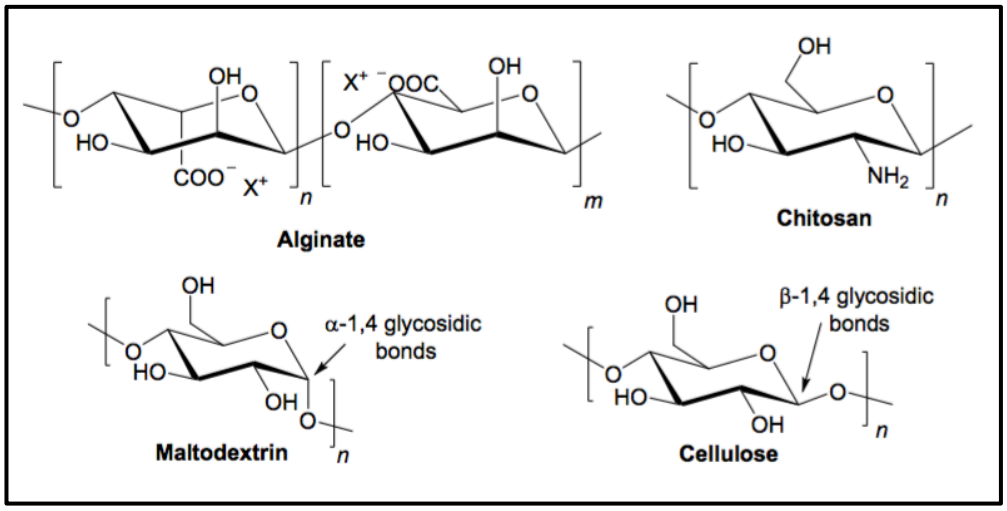


Fig. 2. 23: Structure of some polysaccharides (Lim et al., 2019).

Nowadays, polysaccharides are raw materials which have distinctive properties such as: abundant natural polymers (refers as biopolymers), nontoxic, biodegradable, biocompatible, hydrophilic biopolymers, inexpensive and have high adsorption capacity (Mohammadzadeh Pakdel & Peighambardoust, 2018b). According to (Crini, 2005), the remarkable

adsorption efficiency of polysaccharides is related to: (1) strong hydrophilicity of the polymer because of the hydroxyl groups; (2) the existence of a high number of functional groups (primary amino, acetamido and hydroxyl groups). (3) strong chemical reactivity; and (4) the flexibility of the polymer chain.

The manufacture of adsorbents based on polysaccharides has been the subject of many investigations in the literature. In this study, we restricted our study on two types of polysaccharides which are CHTS and ALG. After a brief review on the structure of each polymer, their performance and application in wastewater purification are reviewed.

2.6.1. Chitosan (Deacetylated chitin).

Chitin is a natural polysaccharide that is considered the second most abundant (Jiménez-Gómez & Cecilia, 2020b). From a chemical viewpoint, the structure of chitin is composed of repeated β-(1-4)-*N*-acetyl-D-glucosamine units linked by β-(1,4) glyosidic bonds as shown in Fig. 2.24 (Das et al., 2020; Gomez-Maldonado et al., 2019; J. Hou et al., 2021)).

Although, chitin is considered as abundant material with remarkable advantages such as, biocompatibility, biodegradability, and has high mechanical strength, it has limited applications because of its poor solubility. Chitin is insoluble in majority of common solvents such as water, organic solvents and slightly basic or acidic solution because of the intermolecular hydrogen bond interactions between the acetyl groups in the polymer chains (Achparaki et al., 2012; J. Hou et al., 2021; Jiménez-Gómez & Cecilia, 2020a). The low solubility of chitin limits its application and therefore the attention was focused to CHTS (chitin derivative) as an alternative because CHTS has better solubility in dilute acidic aqueous solution (PH <6.5) (Gomez-Maldonado et al., 2019).

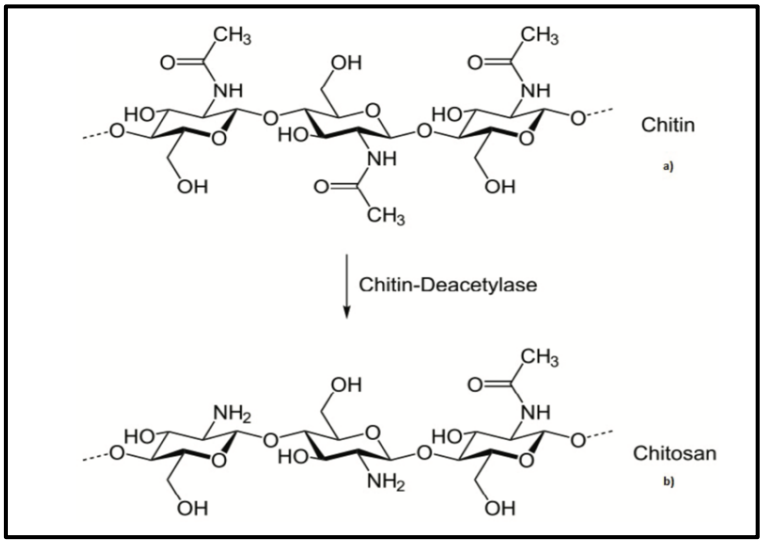


Fig. 2. 24: Chemical structure of (a): Chitin and (b) CHTS (Hossain et al., 2018).

CHTS is a linear hydrophilic polysaccharide obtained from deacetylation of chitin in alkaline medium (deacetylated chitin with ≥ 70 % deacetylation degree). It is defined as a copolymer of D-glucosamine (deacetylated unit) and N-acetyl-D-glucosamine (acetylated unit) linked by β-(1,4) glyosidic bonds (Das et al., 2020; Gomez-Maldonado et al., 2019). Recently, CHTS-based materials have received considerable interest as ecofriendly adsorbents for wastewater treatment due to their distinctive properties such as low cost, renewable, nontoxic, hydrophilicity and biodegradability. The chemical structure of CHTS comprises of many reactive groups such as amino groups (-NH_2) and hydroxyl groups (-OH) (Nechita, 2017). The ortho positions between NH_2 and OH groups in CHTS molecules enable the coordination with divalent heavy metal and consequently enhance the adsorption process of heavy metals (J. Zhang et al., 2012). In addition, CHTS are polyelectrolytes at acidic pH because of the positive surface charge generated on the amine and acetyl amine functional groups that can neutralize the anionic particles (Crini, Torri, et

al., 2019). Fig. 2.25 explains the effect of pH on the solubility of CHTS. Solubilization of CHTS occurs at lower pH because the amino groups in CHTS backbone are totally protonated ($-NH_3^+$), giving the polymers polycationic characterization (positive charge to the polymer). However, at higher pH (above 6.3), CHTS's amine groups are deprotonated, and their reactivity is increased. In addition, Crini et al. pointed that the protonation reaction changes the configuration of CHTS to gels (because of crosslinking), membrane, fibers, and films (Crini, Torri, et al., 2019) .

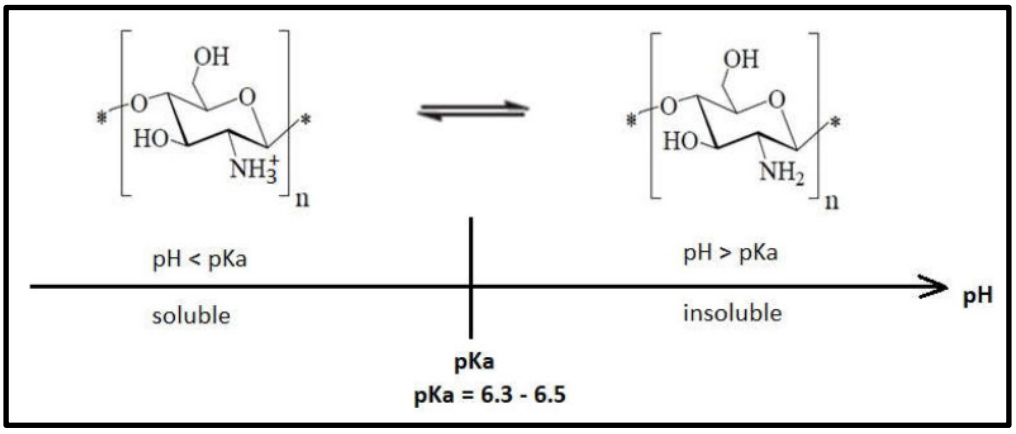


Fig. 2. 25: Effect of pH on the structure of CHTS (Ardean et al., 2021).

Deacetylation of chitin involves the removal of acetyl groups (-CH_3CO) on *N*-acetylglucosamine monomer of chitin to produce amino groups (-NH_2) and forming glucosamine monomer of CHTS (Hossain et al., 2018) as shown in Fig. 2.24. The two primarily differences between chitin and CHTS are the number of glucosamine groups and the degree of deacetylation (amino group content). The ratio of *N*-amino-D-glucosamine units to *N*-acetyl-D-glucosamine is refereed to Degree of Deacetylation (DD). While the degree of acetylation (DA) is calculated as the difference between 100 and the DD (i.e. 100-DD) (Achparaki et al., 2012). DD is an indicator for the number of amino groups in the structure of CHTS as a crucial chemical characteristic that affects the physiochemical properties

of CHTS (Annaduzzaman, 2015). The *N*-acetyl-D-glucosamine is insoluble in water because of the hydrogen-bond interactions between the acetyl groups in the polymer chains, while *N*-amino-D-glucosamine is a hydrophilic and has cationic nature in acidic media (Achparaki et al., 2012). CHTS is insoluble in water and organic solvents (Nechita, 2017). However, CHTS is soluble in dilute acidic solution when DD reaches about ≥ 50% (Hamedi et al., 2018) (Hasan et al., 2020).

Depending on the value of DD, it is possible to produce partially deacetylated chitin-CHTS compounds (J. Hou et al., 2021). When DD is in the range of 60-90 %, CHTS compound is produced (Achparaki et al., 2012). Low deacetylated CHTS is obtained when DD range is of 55-70 %, in this case CHTS is completely insoluble in water. At DD between 70 to 80 %, CHTS is partially dissolved in water and CHTS becomes very soluble when DD is in the range of 85-95 % (Lv, 2016). Therefore, to get good solubility quality CHTS, DD value should be at least 85% (Annaduzzaman, 2015).

The effects of DD values and molecular weights of CHTS on the removal of toxic HMIs (Zn (II), Cd (II), Pb (II) and Cu (II)) were investigated by Younis and coworkers and displayed in Fig. 2.26 (Younis et al., 2019). According to the study, three types of CHTS were examined (types 1-3), type 1 of CHTS had lower molecular weight and higher DD, type 2 had the middle molecular weight, and type 3 had the highest molecular weight and lowest DD. The range of DD of CHTS ranged between 77% to 82 %, the results showed that the removal efficiency of all metal ions increased in type 1 of CHTS sample compared to type 2 and 3. This is can be linked to the increase in the number of functional groups ((-NH_2) and (-OH)) on CHTS chain that functions as adsorption sites and increases the adsorption capacity of the adsorbent (Lone et al., 2019).

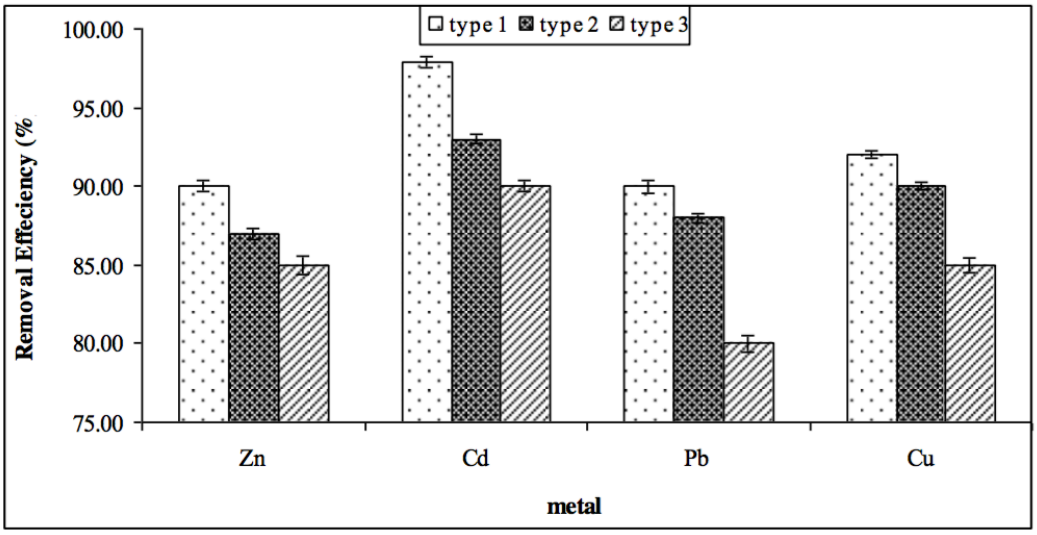


Fig. 2. 26: Effect of DD and molecular weight on the removal efficiency of HMIs (Younis et al., 2019).

However, CHTS have certain chemical and mechanical constraints that limit its application such as low surface area, pH sensitivity, weak stability, acid solubility, low mechanical strength, slow adsorption rate and thermal resistance, low adsorption capacity after certain run, and swelling (M. J. Ahmed et al., 2020; Habiba, Siddique, et al., 2017a; Y. Li et al., 2013; Tanhaei et al., 2015). Therefore, physical, chemical, and biological modification are required to improve CHTS adsorption capability. Fig. 2.27 illustrates a schematic model of the possible modification for CHTS, and Table - 2.6 displays a comparative analysis of the adsorption capacity of modified CHTS-based hydrogels for the removal of HMIs and dyes.

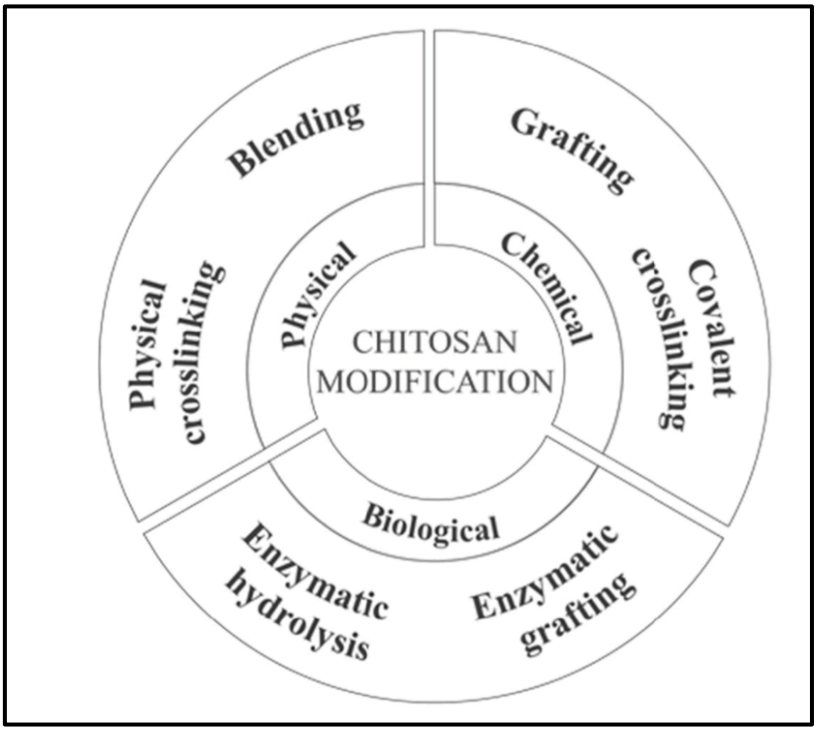


Fig. 2. 27: Schematics model of the modification-for CHTS (J. Wang & Zhuang, 2022).

Table (2. 6): A comparative analysis of the adsorption capacity of modified CHTS-based hydrogels for the removal of HMIs and dyes.

Adsorbate	Type of adsorbent	Dose of adsorbent (g/L)	Initial Concentration of HMIs (mg/L)	Optimum pH	Adsorption capacity (mg/g)	References
CR	CHTS/CuO	0.01	50	7	119.70	(Srivastava & Choubey, 2021)
Hg(II)	CHTS/Fe_3O_4	0.1	25	7	0.4	(Rahmi et al., 2019)
Cd(II)				7	3.04	
Cu (II)	CHTS beads	-	40	5	52.6	(Igberase et al., 2014)
	polyaniline graft CHTS beads	-	40	5	100	(Igberase et al., 2014)
	CHTS/AgNPs/clay	0.3	55	7	181.5	(Azzam et al., 2016)

Adsorbate	Type of adsorbent	Dose of adsorbent (g/L)	Initial Concentration of HMIs (mg/L)	Optimum pH	Adsorption capacity (mg/g)	References
	CHTS/Clay	0.3	55	7	134.5	(Azzam et al., 2016)
	CHTS/AuNPs/ Clay	0.3	55	7	174.1	(Azzam et al., 2016)
	CHTS/organic rectorite-Fe_3O_4 composite (CHTS/OREC-Fe_3O_4)	2	10	5	61.01	(Xie et al., 2015)
	(lignosulfonate and CHTS)	0.03	100	-	283	(Mu et al., 2020a)
Cr(VI)	CHTS/PVA/Zeolite	5	250	-	450	(Habiba, Siddique, et al., 2017b)

Adsorbate	Type of adsorbent	Dose of adsorbent (g/L)	Initial Concentration of HMIs (mg/L)	Optimum pH	Adsorption capacity (mg/g)	References
	(CHTS-DEO-SP) Di epoxy octane (DEO) and spermine (SP)	1.5	1.5	2	358.1	(Vakili et al., 2019)
Cd(II)	Crosslinked CHTS/PVA blend beads	0.5	50	6	73.75	(M. Kumar et al., 2009)
	CHTS/ Fe_3O_4 composite	2	10	5	28.74	Xie et al., 2015)
Pb (II)	CS/magnetite nanocomposite beads	-	-	6	63.3	(H. V. Tran et al., 2010)
Ni (II)	CS/magnetite nanocomposite beads	-	-	6	52.55	(H. V. Tran et al., 2010)

Adsorbate	Type of adsorbent	Dose of adsorbent (g/L)	Initial Concentration of HMIs (mg/L)	Optimum pH	Adsorption capacity (mg/g)	References
Co	lignosulfonate and CHTS	0.03	100	-	386	(Mu et al., 2020a)
Ag^{+}	CHTS/montmorillonite composite beads	5		4	43.48	(Jintakosol & Nitayaphat, 2016)

The physical modification on CHTS structure which particularly covers the blending process and crosslinking as the most convenient and effective modification methods (J. Wang & Zhuang, 2022). The Low mechanical characteristics (strength and toughness) of CHTS hydrogels are the main concerns for their usage as adsorbent. This problem can be solved by blending CHTS with another synthetic polymer (Mohammadzadeh Pakdel & Peighambardoust, 2018d). Blending process includes the merging of two or more materials into CHTS structure to form CHTS-based composites with a wide range of properties. There are many blended materials reported for CHTS such as polymers (range from synthetics polymers: polyvinyl alcohol (PVA), polyethylene oxide (PEO), polyethylene glycol (PG) to biopolymer such as cellulose and alginate), metal nanoparticles, carbon-based materials, magnetic materials, etc. (J. Wang & Zhuang, 2022).

CHTS/polymer blends (sometimes referred to as composites) have been extensively used for water purification, according to the literary works, solution blending is most used to prepare CHTS/polymer composites since it is appropriate for designing variety of blends (beads, films, and fibers). In this method, CHTS is dissolved in suitable solvent (often diluted acetic acid) under constant stirring at room temperature with suitable solvent (often diluted acetic acid). Then the dissolved CHTS combines with different polymer. The CHTS/polymer blended solution is crosslinked with crosslinking agent to enhance the mechanical strengths. The choice of the polymers depends on the desired feature to be enhanced. For instance, mixing PVA with CHTS modifies the hydrophilic characteristic of CHTS (El-Hefian et al., 2014). Additionally, mixing PEO with CHTS can adjust the interaction between the hydrophilic and hydrophobic structure of the separate solutions and increase the viscosity

of the blended polymers, as compared to the separate solution (Lemma et al., 2016).

CHTS's amino groups are essential for the synthesis of chemically and physically crosslinked hydrogels (Pita-López et al., 2021). Several publications study the physical crosslinked of CHTS. Tang et al. studied the physical crosslinked of CHTS/ALG /calcium ion hydrogel and was employed for the removal of heavy metals (Pb (II), Cu (II), and Cd (II)). The porous structure of the prepared hydrogels provides large surface areas and adsorption sites for the HMIs adsorption. The adsorption capacities of the HMIs were found to be 176.50 mgg^{-1} for Pb (II), 70.83 mgg^{-1} for Cu (II), and 81.25 mgg^{-1} for Cd (II) (Tang et al., 2020a).

In another study carboxylic acid functionalized carbon nanotubes (CNTs-COOH) were incorporated into CHTS structure to add COOH functional group to the matrix of CHTS without blocking the adsorption sites. A significant removal of Co (II), Ni (II), Cu (II), Cd (II), and Pb (II) was observed (Refaat Alawady et al., 2020).

Habiba and co-workers was able to strengthen CHTS structure by loading both PVA and zeolite. PVA forms hydrogen bonds with the amino group in CHTS molecules and thus creates more active sites for adsorption. In the other hand, zeolite prevents swelling of CHTS and improves CHTS reusability owing to the porous aluminosilicate structure of zeolite (Habiba, Siddique, et al., 2017b).

Additionally, a micro porous composite of CHTS and ALG using glutaraldehyde as a cross linker have been synthesized and was tested as an adsorbent for three dyes namely methyl orange (MO), Patent Blue V (PBV) and brilliant green (BG). The maximum adsorption capacity was

198.09 mgg^{-1} for MO (at pH 6.0), 117.34 mgg^{-1} for PBV (at pH 3.0) and 235.82 $mgg^{-1}$for BG (at pH 8.0) (Khapre et al., 2021).

It was reported that crosslinking of ALG with CHTS beads improves the mechanical strength and the stability of CHTS (Vakili et al., 2014). A study showed that the unmodified CHTS and ALG have low dye adsorption capacities. However, as shown in Fig 2.28, the structural modification of each biopolymer enhances their–adsorption efficiency towards MO dye.

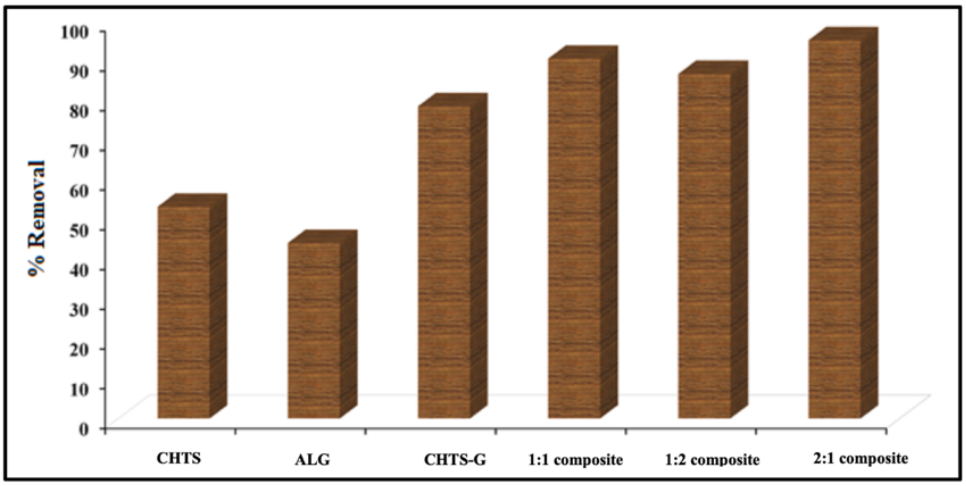


Fig. 2. 28: Comparison of different adsorbent for the removal of MO dye (Khapre et al., 2021).

Moreover, CHTS can be blended with inorganic nanomaterials such as nano clay (bentonite, montmorillonite, graphene oxide, etc.) and metal nanoparticles. These compounds typically have potential properties such as high adsorption capacity, large surface area, strong biocompatibility, and low cost. Nano clay can significantly enhance the mechanical strength and loading capabilities of CHTS beads (Lewandowska et al., 2014). Natural clay was used as an adsorbent to remove pollutants from aqueous solution for example, Elanchezhiyan and his coworker have immobilized

CHTS beads with magnetic kaolinite and tested for the adsorption of Pb (II) and Cd (II) from wastewater. The results revealed that the adsorption of Pb (II) and Cd (II) increased as the loading amount of kaolinite increased from 0%-4.0 % and was attributed to the presence of more functional groups. Moreover, increase the loading of kaolin to 5 % decreases the adsorption capacity of metal ions due to the aggregation of CHTS and magnetic kaolinite (Elanchezhiyan et al., 2021). Recently, CHTS have been modified with graphene oxide (GO) and polyethyleneimine (PEI) to remove HMIs (As and Hg) as well as CR and amaranth (anionic azo dyes) from aqueous solution. The study indicated that there were large number of active sites on the surface of the CHTS/GO-PEI with maximum adsorption capacities of As, Hg, CR, and amaranth of about 220.26, 124,84, 162.84, and 92.81 mgg^{-1}, respectively. (Y. Li et al., 2021). In addition, blending metal and metal oxide with polymeric hydrogel increases the adsorption capacity towards the pollutant's removal because the free amino groups of CHTS can form complexes with metal and metal oxides (Liang et al., 2019). Srivastava & Choubey investigated the adsorption of organic dyes (CR and Eriochrome black T (EBT)) in wastewater by using CHTS/CuO nanocomposites beads. The results specified that adding CuO nanoparticles improved the removal efficiencies and the adsorption capacity of the two dyes as compared to the pure CHTS beads with maximum adsorption capacity of 119.70 and 235.70 mgg^{-1} for CR and EBT, respectively. The increase in the percentage removal of dyes was due to the increase on the surface area of adsorbent (Srivastava & Choubey, 2021).

In addition, to improve the stability of CHTS in acid media, CHTS was blended with Fe_3O_4 extracted from Aceh iron sand. The adsorption capacity of the prepared beads for Hg (II) and Cd (II) was 0.4 and 3.04

mgg^{-1}, respectively, which is higher than that of unmodified CHTS beads (Rahmi et al., 2019).

2.6.2.Sodium Alginate

One of the natural most prevalent polysaccharides is Alginate (ALG) (Sutirman et al., 2021). ALG is a hydrophilic biopolymer with significant properties such as nontoxicity, biocompatibility, biodegradability and biostability (A. Kumar et al., 2022). It is obtained from seaweed (microalgae sources e.g., green, red, and brown). When compared all seaweed sources, the brown kind is the main source of alginic acid (an insoluble salt) (Mallakpour et al., 2021). Alginic acid, also called alginate is the major component of ALG, whereas sodium alginate (Na-ALG) is the water-soluble salt of alginic acid (Sutirman et al., 2021). On a molecular level, ALG is composed of a linear anionic polysaccharide with β -D-mannuronic acid (M-blocks) and α-L-guluronic acid (G-blocks) linked by 1-4 glycoside bonds (A. Kumar et al., 2022; Sutirman et al., 2021). ALG is arranged in a pattern of blocks, and there are three main compositions of ALG as reported by (A. Haug, 1966) . Two are consisted of homopolymeric structure of M-block and G-block (Fig. 2.29 a& b), whereas the third composition contains a heteropolymeric sequence of MG-blocks (Fig. 2.29 c).

ALGs are characterized by their ability to create gel-network, the viscoelasticity of gel network is related to the ratio of originated blocks. A. Kumar et al., 2022 mentioned that the higher content of G block in ALG structure forms more brittle and strong gels network. While the higher content of M block gives more flexibility and shrinkage properties to the gel structure.

In ALG structure, two hydroxyl groups (C2-OH and C3-OH) and C6-COOH can be chemically modified for composite formation. In the presence of divalent charged cations (such as Ca (II), Cu (II), Ba (II) ions), inotropic ALG gels are produced (ionic gelation) in which the cations act as crosslinkers and the monovalent ions (sodium ion in case of sodium alginate) are replaced by the divalent ions (Petrova et al., 2019). The most common cation used for alginate gel is Ca (II), the gelation mechanism is known as "egg-box" in which Ca (II) ions are linked with G blocks to produce 3D structure as shown in Fig. (2.30) (Urbanova et al., 2019).

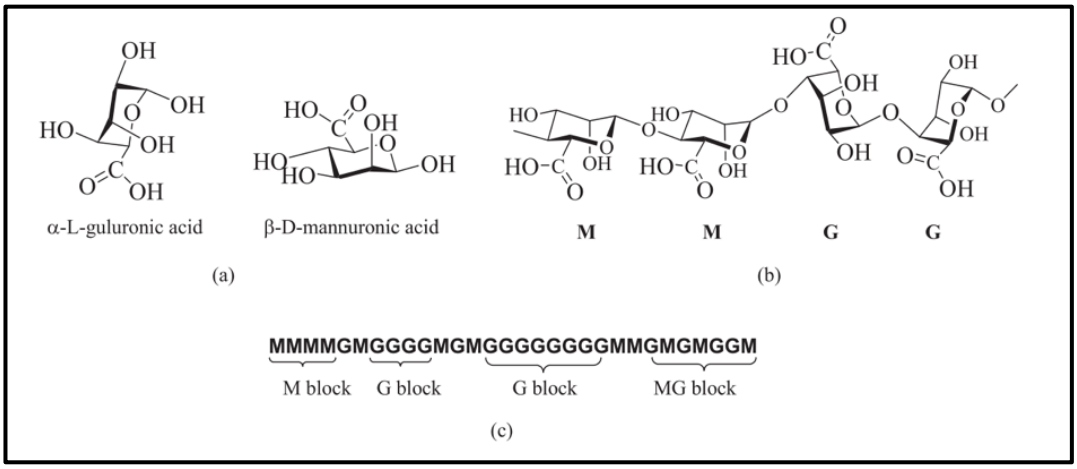


Fig. 2. 29: Structure of ALG; (a) ALG monomer; (b) Chain conformation and (c) block configuration (Sutirman et al., 2021).

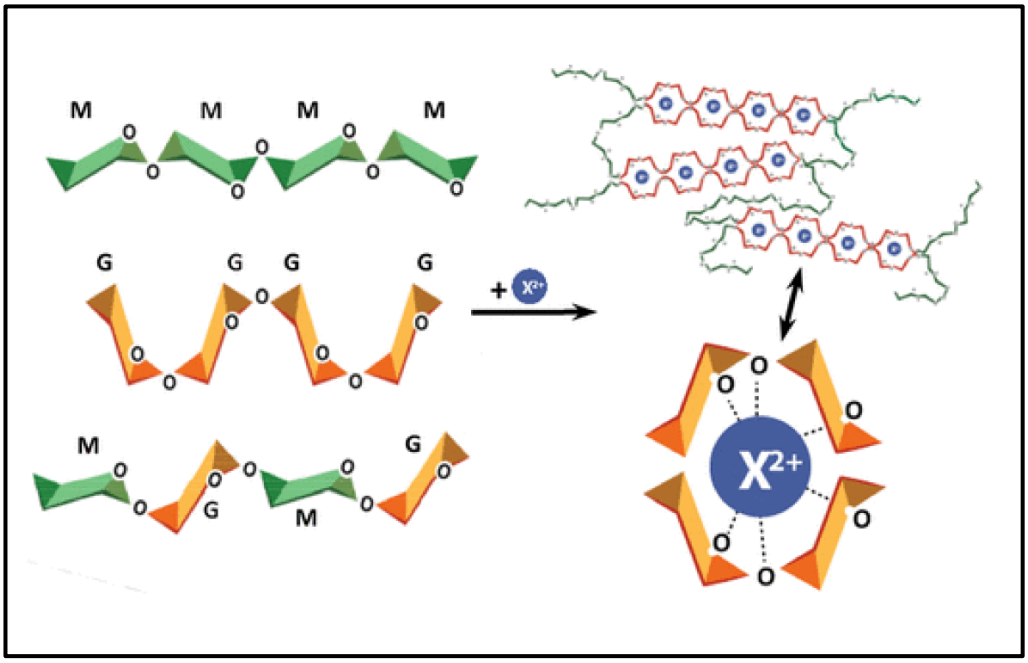


Fig. 2. 30: Schematic representation of the "egg-box" model (Urbanova et al., 2019).

Although ALG has excellent gel-forming features and remarkable encapsulation potential, it also has several drawbacks. One critical problem of crosslinked alginate is its low stability. These gels can breakdown and dissolve due to the release of divalent ions into surrounding media because of exchange interactions with monovalent cations.(A. Kumar et al., 2022; Lee & Mooney, 2012). Moreover, in an acidic solution, ALG gels shrink, which reduces their ability to encapsulate water soluble materials and causes a noticeable release of soluble molecules from the Ca^{2+}-ALG crosslinked network (Østberg et al., 1994). In addition, during ALG-gel fabrication, and because of electrostatic interaction between Ca^{2+} and the COO^- groups, syneresis (shrinkage of gels due to liquid release) is occurred. To overcome these drawbacks and improve the structural properties and the mechanical stability of ALG, additional polymers and particles can be added.

Many Na-ALG based hydrogels have been prepared through copolymerization with a variety of natural and synthetic materials. These hydrogels have natural characteristics, good mechanical performance, and capable to operate under basic and acidic mediums (ALSamman & Sánchez, 2021). Fig. 2.31 represents the different types of Na-ALG based hydrogels and their adsorption performance is recorded in Table (2.7). In the following subsections, only three ALG-based hydrogels will be reviewed.

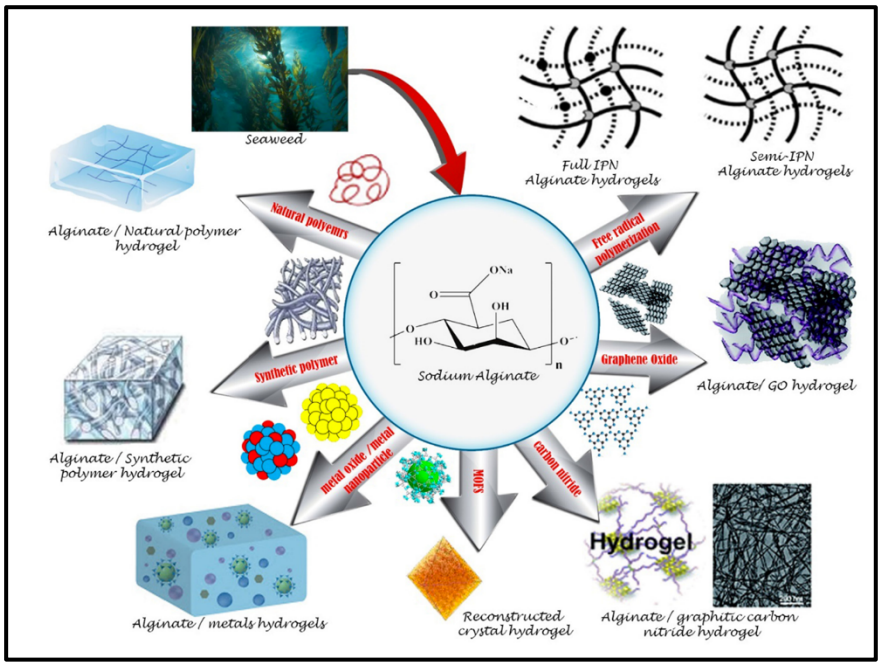


Fig. 2. 31: Schematic examples of Na-ALG -hydrogels combined with other polymers for the removal of HMIs and dyes (ALSamman & Sánchez, 2021).

Table (2. 7): Adsorption capacity for some ALG-based hydrogels

Adsorbent	Adsorbate	Adsorption capacity (mg/g)	References
CHTS/Na-ALG/calcium ion	Pb^{2+}	176.50	(Tang et al., 2020b)
	Cu^{2+}	70.83	
	Cd^{2+}	81.25	
CLS/Na-ALG/clay	MB	-	
Montmorillonite nanosheet/poly (acrylamide-co-acrylic acid)/Na-ALG	MB	530.7	(W. Wang et al., 2022)
Na-ALG/PVA/GO	Cu^{2+}	247.16	(Yi et al., 2018)
	U(VI)	403.78	
PAM/PVA/Na-ALG	Cu^{2+}	79.5	W. Zhang et al., 2018

(Tang et al., 2020b) have successfully prepared physically crosslinked double-network hydrogel of CHTS/Na-ALG/calcium. The prepared hydrogels exhibited a porous structure with additional surface areas and binding sites for HMIs adsorption. The adsorption capacities of Pb^{2+}, Cu^{2+} and Cd^{2+} were found to be 176.50, 176.50, 81.25 mg/g, respectively. Furthermore, Kausar and his collaborators have designed cellulose-ALG-clay composites which showed adsorption capacity of 90%

for MB. The surface of the clay contains exchangeable anions and cations that can be employed for the removal of pollutants through ion exchange mechanisms (Kausar et al., 2022).

Na-ALG/PVA/ GO which was prepared by Xiaofeng Yi and his team, removed Cu (II) and U (VI) from aqueous solution with maximum adsorption capacities of 247.16 and 403.78 mg/g, respectively. PVA was added to enhance the flexibility and the stability of the prepared hydrogel whereas GO was incorporated as filler to harden the structure of ALG-PVA hydrogel (Yi et al., 2018).

In addition, Zhang et al accompanied the benefit of both synthetic and natural polymers by preparing PAM/PVA/ALG hydrogel which removed Cu(II) from an aqueous solution with adsorption capacity of 79.5 mg/g (W. Zhang et al., 2018a).

2.7. Synthetic based composites

2.7.1.Polyvinyl alcohol

Polyvinyl alcohol (PVA) is a hydrophilic synthetic polymer prepared from polyvinyl acetate through alkaline hydrolysis as represented in Fig. 2.32 (Dhall & Alam, 2020; Kaur et al., 2022).

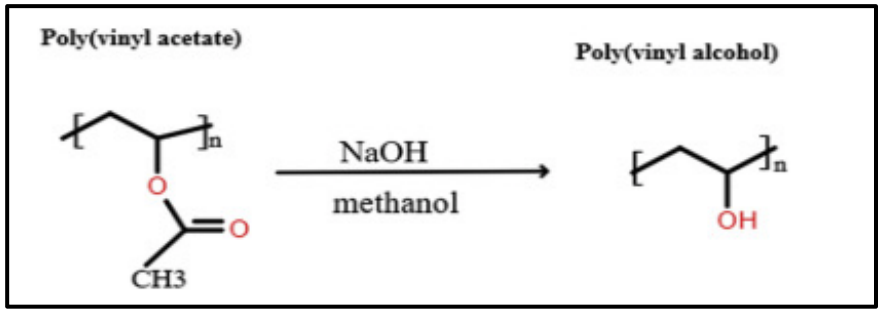


Fig. 2. 32: Alkaline Hydrolysis of polyvinyl acetate to obtain PVA (Singh et al., 2021).

PVA has been used as an adsorbent for HMIs and dyes due to the abundance of free hydroxyl (-OH) groups, ability to hold water (high water content), low toxicity, good biocompatibility, and excellent mechanical properties (Bavya et al., 2021; Mallakpour & Rashidimoghadam, 2017; Radoor et al., 2020; Sanchez et al., 2019; W. Wang, Zhao, Bai, Zhang, Ibarra-Galvan, et al., 2018a). PVA has been widely used to prepare polymer composites with CHTS, ALG, CLS, clay and others. Table 2.8 summarizes the adsorption efficiency of some PVP based composites.

Table (2. 8): Adsorption studies of PVA-based hydrogels

Adsorbents	Adsorbate	Maximum adsorption capacity(mg/g)	Reference
PVA	MB	13.80	(Umoren et al., 2013)
PVA-BENT	MB	26.3	(Sanchez et al., 2019b)
XAN/PVA/CHTS	Pb (II)	67	(S. Wang et al., 2022)
	Cd (II)	100	
	Cu (II)	307	
PVA-ALG-PAM	Cu (II)	79.5	(W. Zhang et al., 2018b)

Umoren et. al. has shown that the unmodified PVA exhibited an adsorption capacity of 13.80 mg/g at 303 k towards the removal of MB

from wastewater and the adsorption data showed strong correlations with the Langmuir, Freundlich and Temkin adsorption isotherm models (Umoren et al., 2013). Sanchez et al evaluated the performance of PVA/3 wt % BENT hydrogel composite. The results showed that, in comparison to pure PVA hydrogel, the adsorption capacity of the examined composites increased towards a wide range of MB concentrations as shown in Fig. 2.33 (Sanchez et al., 2019b)

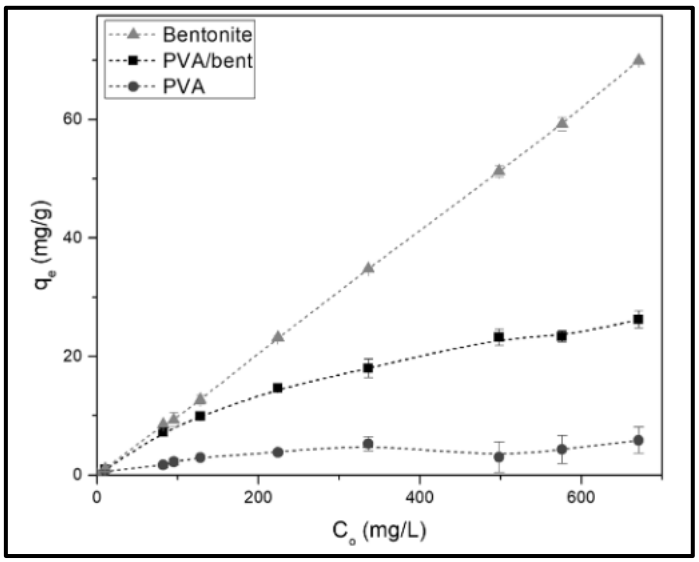


Fig. 2. 33: Effect of initial concentration on the removal of MB on to BENT, PVA-BENT, and PVA hydrogel (Sanchez et al., 2019b).

A composite of PVA and other polymers and crosslinkers have satisfactory chemical and mechanical characteristics (Mok et al., 2020). Wang et al. have used xanthate (XAN) to prepare XAN/PVA/CHTS hydrogel beads for the removal of Pb (II), Cd (II), and Cu (II) from aqueous solutions. The maximum adsorption capacity of Pb (II), Cd (II), and Cu (II) ions were 67 mg/g, 100 mg/g, and 307 mg/g, respectively. The adsorbent exhibited good magnetic properties and was stable below 150 ^{o}C. XAN was used to enhance the binding between the CHTS and HMIs (S. Wang et al., 2022). The removal of Cu (II) from wastewater was investigated by

using PAM-PVA-ALG composite. The results showed that the adsorption of Cu (II) was well fitted with the Freundlich model and PSO in batch system. The maximum adsorption capacity of the prepared hydrogel was 79.5mg/g (W. Zhang et al., 2018b).

Chapter 3

Materials, Methods, and physio-chemical Characterization

3.1. Chemical and Reagents

3.2. Apparatus and minor instruments

3.3. Preparation of adsorbent beads

i. Synthesis of PVA-ALG-BENT composites beads

ii. Synthesis of PVA-CHTS-CLS composites beads

3.4. Preparation of Adsorbates

i. Preparation of Dyes solution

ii. Preparation of Heavy Metals Ions and calibration curves

3.5. Characterization of adsorbents

i. Scanning Electron Microscope

ii. Energy Dispersive X-ray Spectroscopy

iii. FT-IR Spectrometer

iv. X-ray Diffraction Studies

3.6. Equilibrium Swelling Test at various pH

3.7. PH of point of Zero Charge (pH_{PZC})

3.8. Adsorbent Reusability Study

3.9. Batch Adsorption Equilibrium Studies

3.10. Adsorption optimization

3.10.1. Effect of contact time

i. Effect of contact time on the removal of MB.

ii. Effect of contact time on the removal of CR.

iii. Effect of contact time on the removal of HMIs.

3.10.2. Effect of initial pH

i. Effect of initial pH on the removal of MB.

ii. Effect of initial pH on the removal of CR.

iii. Effect of initial pH on the removal of HMIs.

3.10.3. Effect of initial concentration

i. Effect of initial concentration on the removal of MB.

ii. Effect of initial concentration on the removal of CR.

iii. Effect of initial concentration on the removal of HMIs.

3.10.4. Effect of Adsorbent dosage

i. Effect of adsorbent dosage on the removal of MB.

ii. Effect of adsorbent dosage on the removal of CR.

iii. Effect of the adsorbent dosage on the removal of HMIs.

3.10.5. Effect of initial temperature

i. Effect of initial temperature on the removal of MB.

ii. Effect of initial temperature on the removal of CR.

iii. Effect of initial temperature on the removal of HMIs.

3.11. Adsorption isotherms models

3.11.1. Langmuir isotherm model.

3.11.2. Freundlich isotherm model.

3.12. Adsorption Kinetics

3.12.1. Pseudo-first order kinetics.

3.12.2. Pseudo-second order kinetics.

3.13. Application of adsorption in real samples

Chapter 3

Materials, Methods, and physio-chemical Characterization

3.1. Chemicals and reagents

In this section, all the chemicals that were used during the adsorption process were described. All the reagents were purchased from Sigma Aldrich and were used without further purification.

i. Nitric acid (HNO_3)

The chemical structure of nitric acid (HNO_3) is displayed in Fig. 3.1 and has a Mol. Wt. of 63.01 g/mol. 2.0% (w/w) HNO_3 was used for the preparation of the (HMIs) stock and standard solutions.

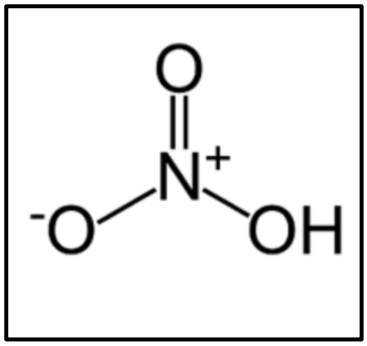


Fig. 3. 1: Chemical structure of HNO_3

ii. Polyvinyl alcohol (PVA)

The chemical structure of (PVA) is displayed in Fig 3.2 and its Mol. Wt. is 13,000-23,000 g/mol. A round 4.0 g of (PVA) was dissolved in 40.0 mL deionized water and was used for the preparation of (PVA-CHTS-CLS) Hydrogel beads composites and 2.0 g of (PVA) was dissolved in 100 mL deionized water for the preparation of (PVA-ALG-BENT) hydrogel beads composites.

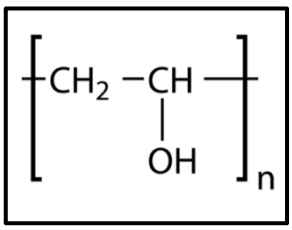


Fig. 3. 2: Chemical structure of PVA

iii. Chitosan ($C_{56}H_{103}N_9O_{39}$)

The chemical structure of CHTS (93% degree of deacetylation) is displayed in Fig. 3.3 and its Mol. Wt. = 200,000 g/mol. 2.0 g of CHTS was dissolved in 100 mL of 2.0% (v/v) acetic acid for the preparation of PVA-CHTS-CLS hydrogel beads composites.

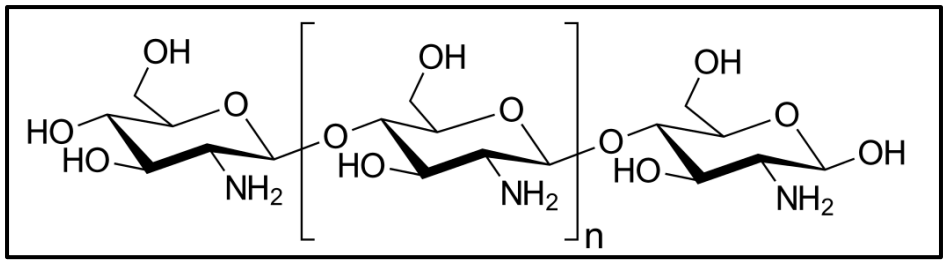


Fig. 3. 3: Chemical structure of CHTS

iv. Cellulose (CLS)

The structure of the microcrystalline powered CLS $(C_6H_{10}O_5)_n$ is displayed in Fig. 3.4. 0.50 %(w/w) of CLS was used for the preparation of PVA-CHTS-CLS hydrogel beads composites.

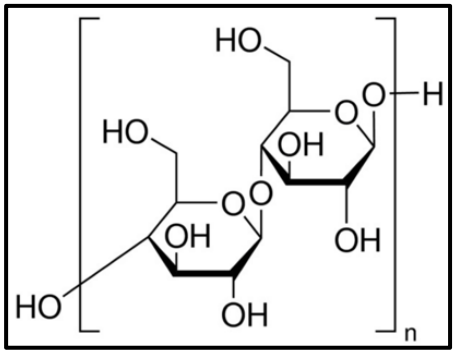


Fig. 3. 4: Chemical structure of CLS

v. Acetic Acid (CH_3COOH)

The structure of Acetic acid CH_3COOH is displayed in Fig. 3.5 and its Mol. Wt. = 60.052 g/mol. 100.0 mL of 2.0 % (v/v) acetic acid was used to dissolve 2.0 g of CHTS for the preparation of PVA-CHTS-CLS hydrogel beads composites.

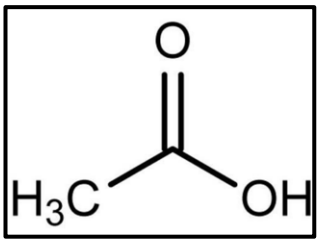


Fig. 3. 5: Chemical structure of CH_3COOH

vi. Sodium Hydroxide (NaOH)

The Mol. Wt. of NaOH is 40.0 g/mol. 10 % NaOH (30.0 g NaOH was dissolved in 270 mL water) for the preparation of PVA-CHTS-CLS hydrogel beads composites.

vii. Sodium Alginate ($C_6H_9NaO_7$)

The structure of Sodium ALG is displayed in Fig. 3.6. Approximately 2.0 g of Sodium ALG was used for the preparation of PVA-ALG-BENT hydrogel beads composites.

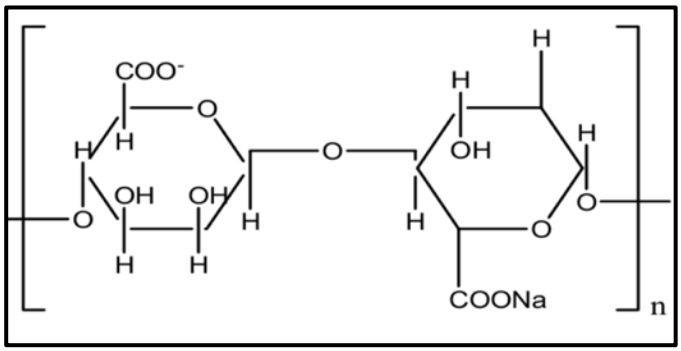


Fig. 3. 6: Chemical structure of sodium ALG

viii. Bentonite clay ($Al_2H_2Na_2O_{13}Si_4$)

The molecular structure of Bentonite (BENT) is displayed in Fig. 3.7. About 1.2 g of BENT clay was used for the preparation of PVA-ALG-BENT hydrogel beads composites. As shown in Fig. 3.8, the SEM image of BENT clay revealed a spherical nanosized particle with average particle size of 26 ± 1.43 nm and narrow size distribution ranging from 18 ± 1.72 nm to 37 ± 53 nm as determined by SEM image analysis software.

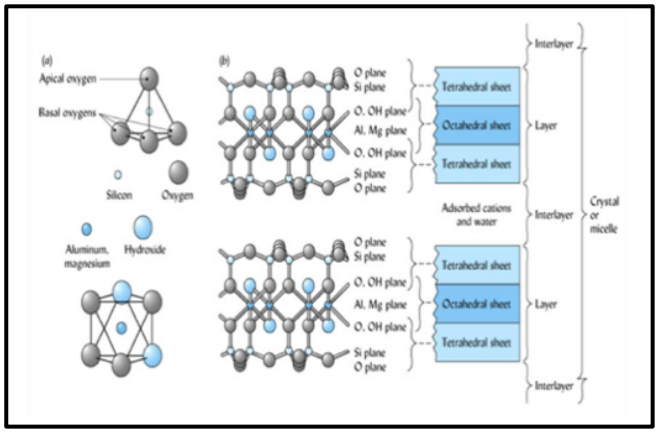


Fig. 3. 7: Structure of BENT clay (Masindi & Africa, 2016).

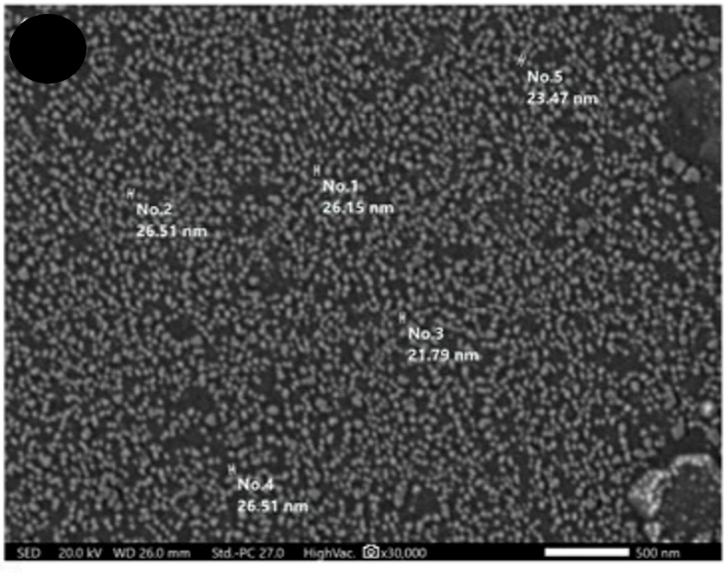


Fig. 3. 8: SEM micrograph of BENT clay nanoparticles

ix. Calcium chloride $CaCl_2$

The Mol. Wt. of $CaCl_2$ is 110.98 g/mol. Around 300 mL of (2.5 %) $CaCl_2$ solution (7.5 g $CaCl_2$ in 292.5 mL deionized water) was used for the preparation of PVA-ALG-BENT hydrogel beads composites.

x. Hydrochloric acid 1.0 M HCl

The Mol. Wt. of hydrochloric acid (HCl) is 36.458 g/mol. About 0.1 M of HCl was used for pH adjustment in acidic range.

xi. Sodium Hydroxide 1.0 M NaOH

The Mol. Wt. of sodium hydroxide (NaOH) is 40.0 g/mol. (0.1 M) of NaOH was used for pH adjustment in basic medium. Around 0.4 g of NaOH was dissolved in 100.0 mL deionized water to prepare 0.1 M NaOH solution.

xii. Adsorbate solution

The synthetic wastewater used in the adsorption process was prepared in the laboratory. The following are the lists of pollutants investigated in the adsorption process:

1. Methylene Blue $C_{16}H_{18}ClN_3S$

The structure of Methylene Blue (MB) is displayed in Table (3.1) and its Mol. Wt. is 319.85 g/mol. A Stock solution of MB (500.0 mg/L) was prepared by dissolving (0.5 g) of MB in (1000.0 mL) deionized water. Further dilutions of MB solutions were prepared from the stock solution.

2. Congo Red $C_{32}H_{22}N_6Na_2O_6S_2$

The structure of Congo Red (CR) is displayed in Table 3.1 and its Mol. Wt. is 696.665 g/mol. A stock solution of CR (100.0 mg/L) was prepared by dissolving 0.1 g of CR in 1000.0 mL deionized water. Further dilutions of CR solutions were prepared from the stock solution.

3. Lead (II) Nitrate Pb $(NO_3)_2$

The Molecular mass of $Pb(NO_3)_2$ is 63.01 g/mol. Approximately 50 mg/L solution of Pb $(NO_3)_2$ was prepared by diluting 5.0 mL of 1000 mg/L stock solution of $Pb(NO_3)_2$ in 100.0 mL of (2 % w/w) HNO_3. A series of Pb (II) standard solutions (1.0 mg/L, 2.0 mg/L, 3.0 mg/L, 4.0 mg/L, and 5.0 mg/L) were prepared from the 50 mg/L $Pb(NO_3)_2$ solution and diluted by 2.0 % w/w HNO_3.

4. Cadmium (II) Nitrate Cd $(NO_3)_2$

The Molecular mass of $Cd(NO_3)_2$ is 236.42 g/mol. 50 mg/L solution of Cd $(NO_3)_2$ was prepared by diluting 5.0 mL of 1000 mg/L stock solution of $Cd(NO_3)_2$ in 100.0 mL of (2 % w/w) HNO_3. A series of Cd (II) standard solutions (1.0 mg/L, 2.0 mg/L, 3.0 mg/L, 4.0 mg/L, and 5.0 mg/L) were prepared from the 50 mg/L $Cd(NO_3)_2$ solution and diluted by (2.0 % w/w) HNO_3.

5. Cobalt (II) Nitrate Co $(NO_3)_2$

The Molecular mass of Co $(NO_3)_2$ is 182.943 $gmol^{-1}$. A 50 mg/L solution of Co $(NO_3)_2$ was prepared by diluting 5.0 mL of 1000 mg/L stock solution of Co $(NO_3)_2$ in 100.0 mL of (2 % w/w) HNO_3. A series of Co (II) standard solutions (1.0 mg/L, 2.0 mg/L, 3.0 mg/L, 4.0 mg/L, and 5.0 mg/L)

were prepared from the 50 mg/L Co $(NO_3)_2$ solution and diluted by (2.0 % w/w) HNO_3.

6. Zinc (II) Nitrate Zn $(NO_3)_2$

The molecular mass of Zn $(NO_3)_2$ is 189.36 g/mol. (50 mg/L) solution of Zn $(NO_3)_2$ was prepared by diluting 5.0 mL of 1000 mg/L stock solution of Zn $(NO_3)_2$ in 100.0 mL of (2 % w/w) HNO_3. A series of Zn (II) standard solutions (1.0 mg/L, 2.0 mg/L, 3.0 mg/L, 4.0 mg/L, and 5.0 mg/L) were prepared from 50 mg/L Zn $(NO_3)_2$ solution and diluted by (2.0 % w/w) HNO_3.

3.2. Apparatus and minor instruments

This section provides the apparatus used during the batch adsorption experiments:

i. Electronic Balance

(A&D) electronic balance was used for weighing purposes. The smallest balancing count is 0.0001 mg.

ii. Filter paper

After adsorption process, the solution was filtered by using Whatman filter paper (Grade 1, size = 2.1cm, pore size =11 μm).

iii. Cuvette

Quartz cuvettes are used for measuring the absorbance of dye solution.

iv. Hot plate and stirrer

Hot plate model (Medline Scientific Limited MS 300HS) was used for heating and stirrer purposes.

v. Round bottom flask

vi. pH -meter

pH meter (EUTECH digital pH meter) was used for measuring and adjusting the pH of the solutions before and after the adsorption process and for calculating the pH at point of zero charge (pH_{PZC}). The pH meter is calibrated before analysis using buffer solutions at pH 4.00, 7.00, and 10.00

vii. Oven

Oven was used for drying purposes

viii. Ultra pre water purification system:

Ultra pre water purification system is used to obtain de-ionized water (DIW).

ix. Thermostatic water bath shaker

Thermostatic water bath shaker was used to incubate and shake the samples in water at constant temperature and adjustable shaking speed (unit Revolutions per minute: rmp).

x. UV-Vis double beam spectrophotometer

UV-Visible spectrophotometer is a quantitative technique used to verify the characteristic absorption spectrum of the material and to find the amount of the light absorbed by the materials (Jiménez-Miramontes et al., 2017). Herein, a computer-based UV-Vis double beam spectrophotometer (ORION AquaMATE 8000) was used to determine the concentrations of organic dyes (MB and CR) after the adsorption experiments.

xi. Inductive Coupled Plasma-Optical Emission Spectrometry (ICP-OES):

HMIs in water samples were analyzed by (ICP-OES, Perkin Elmer Avio 220, USA) spectrophotometer. ICP-OES is applied to quantify the concentration of specific elements in a sample. The fundamental parts of ICP-OES are the sample input system, the excitation part (plasma), the wavelength sets and the detector (S. R. Khan et al., 2022), as displayed in Fig. 3.9. In ICP-OES the samples (in acid solution form) are introduced and nebulized to produce a fine spray that is carried into the plasma where it undergoes vaporization to molecular gases and ionization from ground state to excited state at specific wavelength (de la Guardia & Armenta, 2011).

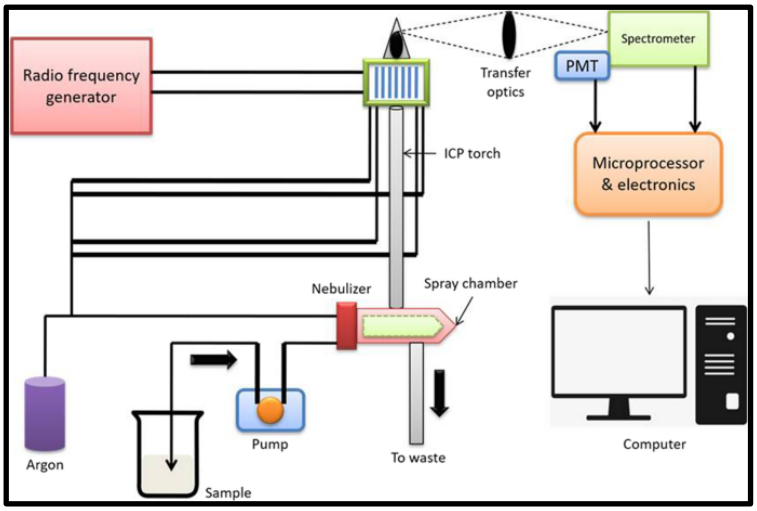


Fig. 3. 9: components of ICP-OES (S. R. Khan et al., 2022).

3.3. Preparation of the adsorbent beads:

The preparation of uniform, polymeric beads is experimentally crucial initial step of adsorbent's synthesis. The physical and chemical properties of the adsorbents are influenced by the preparation method (Bläker et al., 2019). The formation of the pore systems and the availability of the functional groups on the inner structure of the adsorbents strongly

improve the performance of the adsorption process (Marcos-Hernández & Villagrán, 2018). The following section describes the preparation methods of PVA-ALG-BENT and PVA-CHTS-CLS hydrogel nanocomposite beads.

3.3.1. Synthesis of PVA-ALG-BENT composite beads

Semi-interpenetrating polymer network (semi-IPN) nanocomposite hydrogel of PVA-ALG-BENT is composed of polyvinyl alcohol (PVA), sodium (ALG) and natural BENT clay. Approximately 2.0 g of PVA and 2.0 g of ALG were dissolved in 100 ml of deionized water and refluxed at 90 °C under constant stirring of 350 rmp for 2 hours to achieve homogenous solution. After complete dissolution, the solution was cooled at room temperature. Then, a predetermined content of the BENT powder (10, 20 and 30 wt% in relation to the mass of polymers) was dispersed in aqueous PVA- ALG solution via sonication at 40 °C for 30 min then the mixture was vigorously stirred for 1 h in a shaker. The obtained suspension was slowly added dropwise by a syringe into a stirring 3% (*w*/*v*) $CaCl_2$ solution to form semi-IPN nanocomposite hydrogel beads. To complete the gelation reaction, the beads were kept in the $CaCl_2$ solution for overnight. Finally, the beads were filtered, washed three times with deionized water to remove any unreacted $CaCl_2$, dried for 48 hr at room temperature, and stored in a clean glass bottle for further characterization and adsorption study. Hydrogel beads without BENT clay were also prepared using the same previous steps. Fig. 3.10 illustrates a flow chart of the synthesis and the characterization of PVA-ALG-30% BENT beads.

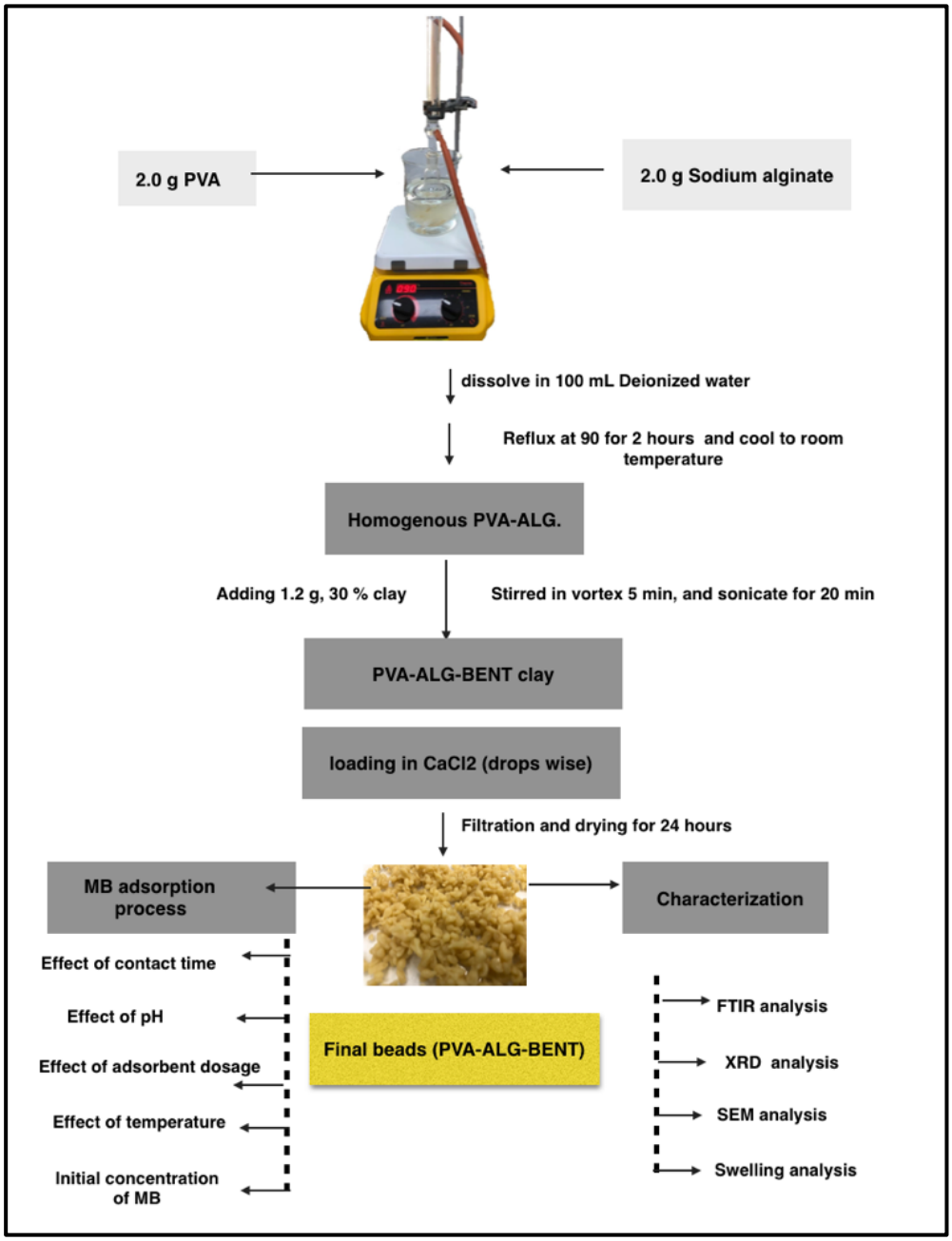


Fig. 3. 10: Flowchart of the formation and characterization of PVA-ALG-BENT beads

3.3.2. Synthesis of PVA-CHTS-CLS composite beads

PVA-CHTS-CLS composite hydrogel was prepared in four steps: (1) *preparation of PVA solution*: 10 % PVA solution was prepared by dissolving 4 g of PVA powder in 36 mL of deionized water at 90°C and continuous stirring for 1 hr to form homogenous and viscous solution. (2)

*the preparation of CHTS solution:*2.0 % CHTS solution was prepared by dissolving 2.0 g of CHTS powder in 98 mL of (2.0 % v/v) acetic acid solution at room temperature. (3) *addition of CLS: (0.5 % w/w)* CLS powder was added to PVA-CHTS polymeric solution followed by heating at 70°C and stirring for 2 hr. (4) the polymeric solution was then introduced to NaOH solution (10%, 300 mL) to form hydrogel beads and was kept for overnight. The composites beads were collected by filtration, washed with deionized water, and dried at room temperature. Fig 3.11 represents the flowchart of the preparation steps of PVA-CHTS-CLS hydrogel beads.

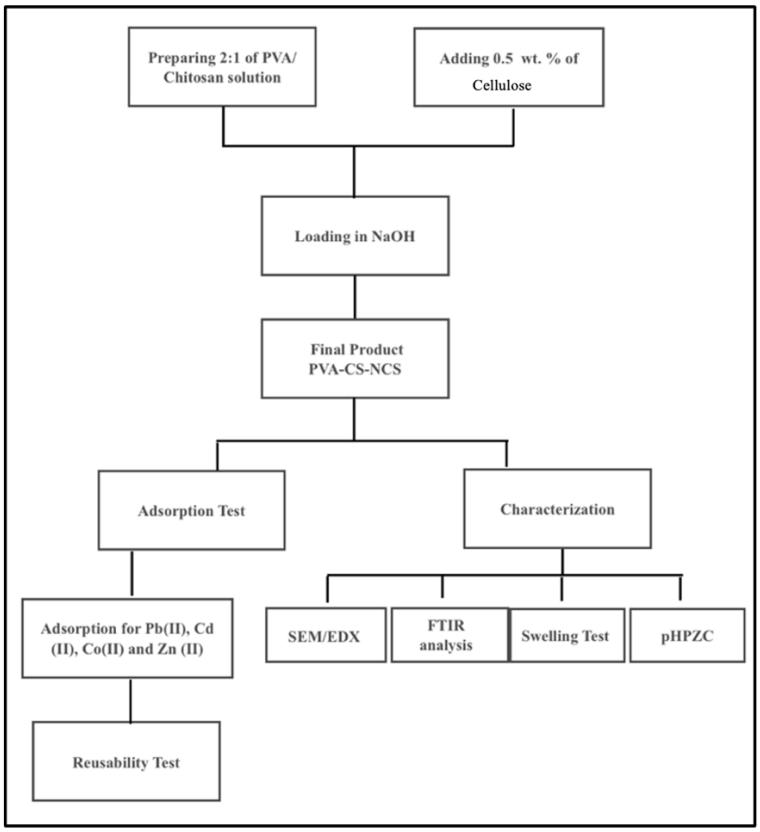


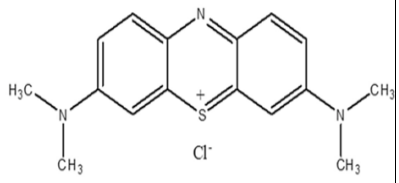
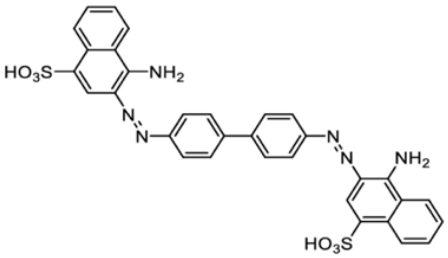
Fig. 3. 11: Flowchart of preparation and characterization of PVA-CHTS-CLS hydrogel beads.

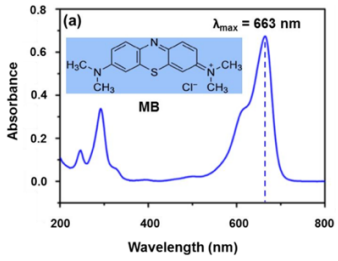
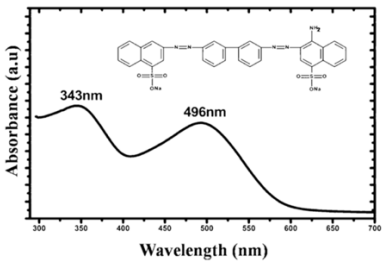
3.4. Adsorbate: Dyes and Heavy Metal Ions

3.4.1. Preparation of Dye solution

Two dyes: MB and CR were used as adsorbates for PVA-ALG-BENT nanocomposites hydrogel beads. Stock solutions (500 mg/L) of MB and (100 mg/L) of CR were prepared by dissolving the required quantity of dyes into 1000 mL deionized water. Double beam UV/Vis spectrometer was used to measure the amount of dyes adsorbed on adsorbent's surface. The structure and the characteristics properties of MB and CR are represented in Table (3.1).

Table (3. 1): Physical Characteristics of Methylene Blue and Congo Red

Dye	Methylene blue	Congo red
Structure		
IUPAC name	[7-(dimethylamino)phenothiazin-3-ylidene]-dimethylazanium;chloride	disodium 4-amino-3-[4-[4-(1-amino-4-sulfonato-naphthalen-2-yl)diazenylphenyl]phenyl]diazenyl-naphthalene-1-sulfonate
Color	Blue	Brownish red

Mol. Wt.	319.85 $gmol^{-1}$	696.66 $gmol^{-1}$
Molecular Formula and maximum wavelength (λmax)	665 nm 	496 nm 

3.4.2. Preparation of HMIs solutions

Four HMIs (Pb(II), Cd(II), Co(II), and Zn(II)) were used to evaluate the adsorption performance of PVA-CHTS-CLS towards these HMIs in aqueous solution. 50.0 m/gL of Pb(II), Cd(II), Co(II), and Zn(II) were prepared from stock solution (1000 mg/L) of each element and diluted to a final volume of 100 mL by 2.0% (w/w) HNO_3.

3.5. Characterization of adsorbents

3.5.1. Scanning Electron Microscope (SEM)

Scanning Electron Microscope (SEM) is an electron microscope that used to produce three-dimensional images with high resolution for surface's morphology before and after the adsorption of the adsorbate (Aljar et al., 2021). SEM images of the prepared adsorbents were obtained by using JSM-5300 instrument (JEOL, Tokyo, Japan) functioned at (20 kV).

3.5.2. Energy dispersive X-ray spectroscopy (EDX)

Elemental composition of the polymer present in the matrix of the adsorbents was determined using an energy dispersive X-ray (EDX) micro-analysis attached on the SEM system. The analysis was performed on uncoated samples at 15 kV for 60 second.

3.5.3. FT-IR Spectrometer

Fourier Transform Infrared Spectroscopy (FTIR) is an analytical technique used to determine the main functional groups of organic and inorganic materials. IR Prestuge-21 Shimadzu scanning from 4000 to 400 cm^{-1} was used and the sample was prepared by mixing the beads with KBr powder and pressed to plate.

3.5.4. X-ray diffraction studies

X-ray diffraction analysis (XRD) was performed to determine the patterns and the crystallinity of the bead composites using Cu-alpha radiation as source at 40 kV and 40 mA over the range (2 θ of 20°-100°).

3.6. Equilibrium Swelling test at various pH

Swelling behavior of the adsorbent's hydrogel nanocomposites was studied at various pH-varying (acidic, neutral, and basic) solutions. About 0.5 g of dried hydrogel beads was immersed in 100.0 mL deionized water adjusted at three different pH values (3.0, 7.0 and 9.0) at room temperature to allow the beads reach equilibrium. Over regular specific period (20 min), beads were removed, wiped with tissue paper to remove any residual of solution then the mass of hydrogel was measured. The experiment was repeated until the swelling ratio reached equilibrium (around five–six

times). Equation (1) was used to calculate the degree of swelling (Das et al., 2020).

$$\textbf{Swelling ratio (\%)} = \left[\frac{W_w - W_d}{W_d}\right] x\ 100 \qquad (1)$$

Where, W_w and W_d are the weight of wet and dry hydrogel in gram (g), respectively.

3.7. pH of point of Zero Charge (pH_{PZC})

The pH of the point of zero charge (pH_{PZC}) of the adsorbent was determined by placing 0.05 g of adsorbent in 50 mL of 0.01 M NaCl solution. The pH values of the solutions were adjusted by using 0.1 M HCl/NaOH to form a range of different pH solutions (1 to 10). The flasks were kept for 48 hr and the final pH of the solution was recorded. The ΔH ($H_{initial} - H_{Final}$) values vs $pH_{Initial}$ were plotted to determine the pH_{PZC} of the adsorbent.

3.8. Batch adsorption Equilibrium studies

This section evaluates the adsorption process of the prepared polymeric hydrogels beads. Table (3.2) contains the specific amount used in each batch experiment, each experiment was repeated three times. For example, in trail (1) of the adsorption experiments, 50.0 mL of 200 mg/L adsorbate solution and 1.5g of adsorbent were placed in 100.0 mL stoppered flask. Then shacked at 25°C in a temperature controlled orbital mechanical shaker at 170 rpm for 300 minutes. Aliquot samples were withdrawn at certain time intervals (every 20 minutes), filtered to remove any remaining suspended particles. The filtered solution was then analyzed for the concentration of the residual pollutant by using UV-Vis spectrometer at wavelength of maximum absorption (λ_{max}) for dyes analysis and ICP for HMIs. The quantity amount of pollutant adsorbed Q_e

(mg/g) and the percentage removal (% Removal) were calculated by using equations (3) and (4) below, respectively.

$$\mathbf{Qe} = \frac{(C_0 - C_t)\,V}{W} \qquad \mathbf{(3)}$$

$$\boldsymbol{\%\ Removal} = \frac{C_0 - C_t}{C_0}\,\boldsymbol{x\ 100\%} \qquad \mathbf{(4)}$$

Where: C_0, C_t in (mg/L) are the concentrations of adsorbate at initial and after time t (min) respectively, V is the volume of the solution in L containing the pollutant, and W is the weight in gram (g) of the adsorbent.

Table (3. 2): Batch adsorption parameters

Adsorbent hydrogel beads	Adsorbate solution	Adsorbate Initial concentration (ppm)	Adsorbate's Volume (mL)	Adsorbent's dosage (g)	Initial pH	Temp. (º C)	Adsorption Time (min)	Wave length (nm)
PVA-ALG-BENT	MB	200	50	1.5	8	25	300	665.000
	CR	100	50	1.5	3	30	300	496.000
PVA-CHTS-CLS	Pb(II)	50	50	0.5	6	30	120	220.353
	Cd(II)	50	50	0.5	6	30	120	228.802
	Co(II)	50	50	0.5	8	30	120	228.610
	Zn(II)	50	50	0.5	8	30	129	206.200

3.9. Adsorption optimization

Batch adsorption optimization method was used to select or indicate the appropriate adsorption parameters that give the highest adsorption capacity. The following subsections lists all tested parameters including contact time, initial pH, initial adsorbate concentration, temperature, adsorbent dosage, and particle fillers.

3.9.1. Effect of contact time

i. Effect of contact time on the removal of MB

A dried sample of PVA-ALG-BENT composite (1.5 g) was mixed with 50.0 mL of an aqueous solution of MB which has an initial concentration of 200.0 mg/L at pH of 8.5. The adsorption experiment was carried out at room temperature with constant shaking speed of 150.0 rmp, and period ranging from 20-320 min. After each time interval, about 5.0 mL aliquots were removed from the solution and the absorbance was measured using UV-Vis double beam spectrophotometer at 665 nm.

The results were expressed as % removal efficiency and adsorption capacity (mg/g) at time t using (Eq. (3) and (4)) mentioned in section 3.9.

ii. Effect of contact time on the removal of CR

A dried sample of PVA-ALG-BENT composite (1.5 g) was shaked with 50 mL of an aqueous solution of CR which has an initial concentration of 100 mg/L at pH ~~of~~ 3.0. The adsorption experiment was carried out at 30 ºC with constant shaking speed of 170.0 rmp. The mixture was shaked at time interval ranging from 20-300 min. After each time interval (20 min), about 5.0 mL aliquot was removed, and the absorbance was measured using UV-Vis double beam spectrophotometer at 496 nm. The results were expressed

as % removal efficiency and adsorption capacity (mg/g) at time t using (Eq. (3) and (4)) mentioned in section 3.9.

iii. Effect of contact time on the removal of HMIs

A dried sample of PVA-CHTS-CLS composite (0.5 g) was mixed with 50.0 mL of HMI aqueous solution (Pb(II), Cd(II), Co(II), and Zn(II)) with initial concentration of 50.0 ppm at pH of 6.0 for (Pb(II) and Cd(II)) and pH of 8.0 for (Co(II), and Zn(II)). The adsorption experiments were carried out at 30 ºC with constant shaking speed of 170.0 rmp for time ranging from 20-120 min. After each time interval (20 min), a 5.0 mL aliquot was removed from the solution and the concentration of the HMI present was measured using ICP spectrophotometer. The results were expressed as % removal efficiency and adsorption capacity (mg/g) at time t using (Eq. (3) and (4)) mentioned in section 3.9.

3.9.2. Effect of initial pH

i. Effect of initial pH on the removal of MB

About 1.5 g of PVA-ALG-BENT dry composite was added to a 50 mL of an aqueous solution of MB having an initial concentration of 200 mg/L. The solution was mixed for a constant time of 300 min and constant stirring speed of 150 rmp at 25 °C. This experiment was done at different initial pH ranging from 1-10 by using 0.1M HCl and 0.1M NaOH. After each time interval (20 min), about 5.0 mL aliquots were removed from the solution and the absorbance was measured using UV-Vis double beam spectrophotometer at 665 nm. The adsorbed amount of MB at different pH were expressed as % removal efficiency and adsorption capacity (mg/g) at time t using (Eq. (3) and (4)) mentioned in section 3.9.

ii. Effect of initial pH on the removal of CR

About 1.5 g of dry composite of PVA-ALG-BENT was added to a 50 mL of aqueous solution of CR having an initial concentration of 100 mg/L. The solution was mixed for a constant time of 300 min and constant stirring speed of 170 rmp at-30 °C. This experiment was repeated at different initial pH ranging from 2-10. After each time interval (20 min), about 5.0 mL aliquots were removed from the solution and the absorbance was measured using UV-Vis double beam spectrophotometer at 496 nm. The adsorbed amount of CR at different pH were expressed as % removal efficiency and adsorption capacity (mg/g) at time t using (Eq. (3) and (4)) mentioned in section 3.9.

iii. Effect of initial pH on the removal of HMIs

About 0.5 g of dry composite of PVA-CHTS-CLS were added to a 50 mL of HMIs aqueous solution having an initial concentration of 50 mg/L. The solution was mixed for a constant time of 120 min and constant stirring speed of 170 rmp at 30 °C. This experiment was repeated at different initial pH ranging from 3-9 After each time interval, about 5.0 mL aliquots were removed from the solution and the concentrations of the HMIs were measured using ICP instrument. The amount of HMIS at different pH were expressed as % removal efficiency and adsorption capacity (mg/g) at time t using (Eq. (3) and (4)) mentioned in section 3.9.

3.9.3. The effect of initial concentration of adsorbate

i. Effect of initial concentration on the removal of MB

Approximately 1.5 g of PVA-ALG-BENT composite beads was added to 50 mL of MB dye solution. Different concentrations of dye solution were tested (50, 100, 150, 200, 250, 300, 350 mg/L) and all experiments were

performed at constant time of 300 min, constant stirring speed of 150 rmp, pH of 8.5 and at room temperature (22 °C). After each time interval (20 min), about 5.0 mL aliquots were removed from the solution and the absorbance was measured using UV-Vis double beam spectrophotometer at 665 nm. The adsorbed amount of MB at different initial concentrations were expressed as % removal efficiency and adsorption capacity (mg/g) at time t using (Eq. (3) and (4)) mentioned in section 3.9.

ii. Effect of initial concentration on the removal of CR

About 1.5 g of PVA-ALG-BENT composite beads was added to 50 mL of CR dye solution. Different concentrations of dye solution were tested (20-100 mg/L) and all experiments were performed at constant time of 300 min, constant stirring speed of 170 rmp, pH of 3.0 and at 30 °C. After each time interval (20 min) , about 5.0 mL aliquots were removed from the solution and the absorbance was measured using UV-Vis double beam spectrophotometer at 496 nm. The adsorbed amount of CR at different initial concentrations were expressed as % removal efficiency and adsorption capacity (mg/g) at time t using (Eq. (3) and (4)) mentioned in section 3.9.

iii. Effect of initial concentration on the removal of HMIs

A 0.5 g of PVA-CHTS-CLS composite beads was added to 50 mL of (Pb^{2+}, Cd^{2+}, Co^{2+}, and Zn^{2+}) solutions. Different concentrations of HMIs solutions were tested (50-200 ppm) and all experiments were performed at constant time of 120 min, constant stirring speed of 170 rmp and pH of 6.0 for (Pb^{2+} and Cd^{2+}) and pH of 8.0 for (Co^{2+}, and Zn^{2+}) at 30 °C. The amount adsorbed of HMIs at different initial concentrations was

expressed as % removal efficiency and adsorption capacity (mg/g) at time t using (Eq. (3) and (4)) mentioned in section 3.9.

3.9.4. The effect of adsorbent dosage

i. Effect of adsorbent dosage on the removal of MB

Different dosages (0.10-2.0 g) of PVA-ALG-BENT composite beads were mixed separately with 50 ml of MB aqueous solution which has an initial concentration of 200 ppm. All experiments were carried out at room temperature (22 °C) and constant speed of 150 rmp, constant time of 300 min and pH of 8.5. After each time interval (20 min), about 5.0 mL aliquots were removed from the solution and the absorbance was measured using UV-Vis double beam spectrophotometer at 665 nm. The adsorbed amount of MB at adsorbent dosages were expressed as % removal efficiency and adsorption capacity (mg/g) at time t using (Eq. (3) and (4)) mentioned in section 3.9.

ii. Effect of adsorbent dosage on the removal of CR

Different dosages of PVA-ALG-BENT composite beads (0.2-2.0 g) was mixed separately with 50 ml of CR aqueous solution which has an initial concentration of 100 ppm. All experiments were carried out at 30 °C and constant speed of 170 rmp, constant time of 300 min and pH of 3.0. After each time interval (20 min), about 5.0 mL aliquots were removed from the solution and the absorbance was measured using UV-Vis double beam spectrophotometer at 496 nm. The adsorbed amount of CR at adsorbent dosages were expressed as % removal efficiency and adsorption capacity (mg/g) at time t using (Eq. (3) and (4)) mentioned in section 3.9.

iii. Effect of adsorbent dosage on the removal of HMIs

Different dosages of PVA-CHTS-CLS composite beads (0.1-0.5 g) were mixed with 50 ml of HMIs aqueous solution which has an initial concentration of 50 mg/L. All experiments were carried out at 30 °C and constant speed of 170 rmp, constant time of 120 min and pH of 6.0 for (Pb(II) and Cd(II)) and pH of 8.0 for (Co(II), and Zn(II)). The adsorbed amount of HMIS at adsorbent dosages were expressed as % removal efficiency and adsorption capacity (mg/g) at time t using (Eq. (3) and (4)) mentioned in section 3.9.

3.9.5. The effect of initial temperature

i. Effect of initial temperature on the removal of MB

This experiment was carried out following the same procedure as in section 3.10.1. (i) at different temperatures of 20, 30, 40 and 50 °C.

ii. Effect of initial temperature on the removal of CR

This experiment was carried out following the same procedure in section 3.10.1. (ii) at different temperatures of 20, 30, 40 and 50 °C.

iii. Effect of initial temperature on the removal of HMIs

This experiment was carried out following the same procedure in section 3.10.1. (iii) at different temperatures of 20, 30, 40 and 50 °C.

3.10.Adsorbent Reusability Study

The recovering of the hydrogel beads was evaluated through repeated sorption-desorption cycles. About 0.5 g of Hydrogel beads was added to the adsorbate solutions (50 mg/L, 50 mL in case of HMIs), (200 mg/L, 50 mL in case of MB solution) and (100 mg/L, 50 mL in case of CR solution) at specific optimal pH as represented in Table (3.3) and determined earlier

in sec 3.9.2. The solutions were shaken in water bath shaker for specific equilibrium time (320 min in case of MB), (200 min in case of CR) and (120 min in case of HMI solutions) at 30 ºC. The saturated loaded beads were collected, washed with deionized water, and dried for 48 hr at room temperature. For desorption process, the dried hydrogel beads were added to HCl solution (0.1 M, 50 mL) and shaken at 170 rpm for 30 min, then filtered, rinsed several times with deionized water and dried for 48 hr at room temperature. The desorption process was repeated consecutive times. The reuse efficiency of the adsorbent beads was calculated according to Equation (2) (Sun et al., 2021):

$$\textbf{Reuse efficiency (\%)} = \frac{Q_n}{Q_1} X100\% \qquad (2)$$

Where, Q_1 and Q_n (mg/g) represent the initial and the n^{th} time adsorption capacities of the adsorbate solution by reused composites beads; respectively.

Table (3. 3): Optimal pH for the removal of adsorbate solutions

	Dyes		HMIs			
Adsorbate solution	MB	CR	Pb (II)	Cd(II)	Co(II)	Zn(II)
Optimal pH	8	3	6	6	8	8

3.11.Selectivity of HMIs

Three batch adsorption experiments were conducted to quantify the selectivity and adsorption affinity of HMIs on PVA-CHTS-CLS hydrogel beads. For each experiment, 0.5 g of dried beads was added to 100 mL flask containing HMIs solution (50 mL) with 50 ppm initial concentration

of (Cd, Zn, Co, and Pb). The solution was adjusted at pH (6) and placed in a mechanical water bath shaker at 30 °C for 120 min. The removal percentage (%) as well as the equilibrium adsorption capacity, Qe, (mg/g) of HMIs onto adsorbent beads were calculated from Eq. (3) and (4).

3.12.Adsorption isotherms

As previously mentioned, adsorption is a surface mechanism in which the adsorbates adsorbed on adsorbent's surface and then removed from the solution. The affinity of the adsorbate for the adsorbent is quantified by adsorption isotherms. Modeling the adsorption isotherm can provide information about the adsorbent capacity and the adsorption mechanism(Ragadhita & Nandiyanto, 2021). Adsorption isotherm is a mathematical expression that displays the relationship between the adsorbed material (adsorbate bonded on the adsorbent's surface) and the non-adsorbed amounts (concentration of the remaining adsorbate presents in the solution when equilibrium is reached) at constant temperature (Abin-Bazaine et al., 2022; J. Wang & Guo, 2020a; Weijiang et al., 2017a).

Experiments of the removal of dyes (MB and CR) on PVA-ALG-BENT and HMIs on PVA-CHTS-CLS hydrogel beads were carried out in 50 mL flask. Operating parameters for the adsorption experiments were the same as mentioned in Table (3.3). First, 50 mL of the initial concentration solution was transferred in the adsorption flask and adjusted to its optimal pH. Then, certain dosage (1.5 g) of the respective hydrogel beads was added to the solution, and the solution was shaked in a selected temperature-controlled water bath set at 170 rmp until equilibrium was reached. At the end of the adsorption experiment, the adsorbate solution was collected, filtered and analyzed to calculate the adsorption capacities at equilibrium time (Q_e), using Eq(2) as mentioned in sec 3.9.

Several adsorption isotherms have been studied for the adsorption process; however, the most common isotherms are the Langmuir and Freundlich models because they are simple and can reflect the experimental data at wide range of concentrations (Azizian & Eris, 2021).

3.12.1. Langmuir isotherm models (Linear model)

Linear model of Langmuir adsorption isotherm is based on monolayer of adsorbate on the adsorbent's surface (homogenous adsorption) (Maryanti et al., 2020). There are four assumptions in Langmuir isotherms:

1. The adsorbate molecules are adsorbed on the surface of adsorbent's active sites.
2. Each adsorption site can accommodate one adsorbate molecule. Once the adsorbent's active site is occupied with the adsorbate molecule no further adsorption occurred at this site.
3. Every site has the same energy level.
4. There is no connection between the molecules that have been adsorbed and the nearby sits.

Schematic presentation of monolayer adsorption is presented in Fig. 3.12. The linearized form of Langmuir isotherm adsorption equation is illustrated in equation (5) (Langmuir, 1917):

$$\frac{C_e}{q_e} = \frac{1}{K_L q_m} + \frac{C_e}{q_m} \qquad (5)$$

Where C_e is the adsorbate concentration at equilibrium in mg/L, q_e is the adsorption capacity of adsorbents at equilibrium (amount of adsorbed adsorbate per gram of adsorbent) in mg/g, q_m is the maximum monolayer adsorption capacity in mg/g and K_L is the Langmuir constant related to the affinity of the binding sites in L/mg. The intercept and slop of the linear plot of C_e/q_e versus C_e can be used to determine the constants q_m and K_L

(Çınar et al., 2017). Further, the ‘‘dimensionless constant” or ‘‘separation factor’’ (R_L) is important factor in Langmuir isotherm. R_L is defined in equation (7) and used to predict the favorability of adsorption process (Ragadhita & Nandiyanto, 2021).

$$R_L = \frac{1}{1+K_L\, C_0} \qquad (6)$$

Where, C_0 is the initial concentration of the adsorbate in mg/L. R_L is separation factor constant, and has the following values:

1. $R_L > 1$, the unfavorable adsorption, mostly desorption.
2. $R_L = 1$, linear adsorption process.
3. $R_L = 0$, irreversible adsorption process (strong adsorption)
4. $(1 > R_L > 0)$ favorable normal adsorption process.

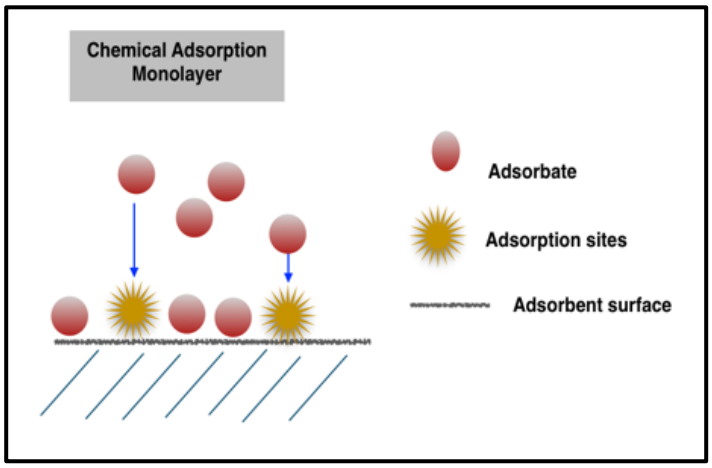


Fig. 3. 12: Langmuir Linear adsorption model.

3.11.2.Freundlich isotherms

Freundlich isotherm represents a form of adsorption in which the adsorption follows a multilayer deposition with interaction between the adsorbed molecules (J. Zhang et al., 2012). The adsorption mechanism of

this isotherm assumes heterogenous surface mechanism as shown in Fig. 3.12. The linear adsorption form of Freundlich isotherm can be expressed by equation (8) (Nemr et al., 2009)

$$ln\ q_e = ln\ K_F + \frac{1}{n}\ lnC_e \qquad (8)$$

Where: K_F [(mg/g) $(L/mg)^{1/n}$)] and n are the Freundlich constants, which represent the adsorption capacity (mg/g) and adsorption intensity, respectively. The intercept and slop of the linearized form of Freundlich model can be used to determine the values of K_F and 1/n (Malik, 2003).

The value of n is defined as follows:

1. n=1, linear adsorption
2. n<1, Chemisorption (adsorption by chemical interaction)
3. n >1, Physisorption (adsorption by physical interaction)
4. 0 < 1/n < 1value between 0 and 1, for favorable adsorption
5. 1/n > 1, cooperative adsorption.

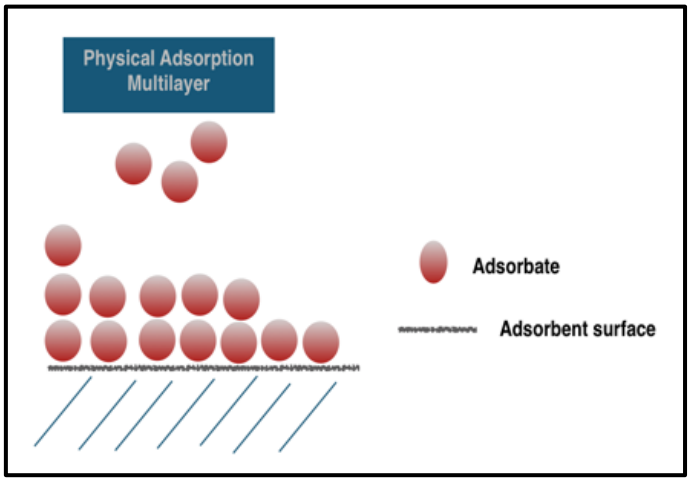


Fig. 3. 13: Freundlich adsorption model

3.12. Adsorption kinetic

The most important factor to be considered when designing an adsorption system is adsorption kinetics. Adsorption kinetics can be obtained by examining the adsorptive removal of adsorbate from the aqueous solution at specific time intervals. There are several kinetic models that explain the adsorbent-adsorbate interaction. The most widely applied models are pseudo-first and pseudo-second order kinetic models. Experimentally, the kinetic models can be calculated by performing the adsorption process described in sec (3.9.1). The applicability of any model depends on the correlation coefficient (R^2). The linear form has been used to examine the adsorption kinetics.

3.12.1.Pseudo-first order kinetics (PFO)

In PFO, the differences in the amount of adsorbed molecules on adsorbent's surface at equilibrium and at a specified time is described the adsorption process (Pooresmaeil & Namazi, 2019). Equation (9) is used to describe the adsorption process in accordance to PFO model

$$\ln(q_e - q_t) = lnq_e - K_1 t \qquad (9)$$

Where, q_t is the amount of adsorbate adsorbed on adsorbent in mg/g at time t (min), q_e is equilibrium adsorption capacity in mg/g. K_1 is the rate constant of PFO in 1/min. The plot of ln (q_e-q_t) vs time produces a straight line, in which the parameters of the models can be obtained from the slop(k_1) and intercept (q_e).

3.12.2.Pseudo-second order kinetics (PSO)

According to PSO model, the rate of adsorption is related to the number of adsorption sites on the adsorbent's surface (Azizian & Eris, 2021). Equation (10) shows the equation of PSO

$$\frac{t}{q_t} = \frac{1}{K_2 q_e^2} + \frac{1}{q_e} t \qquad (10)$$

Where K_2 is the PSO rate constant kinetics in g/mg.min. The plot of t/q_t vs time produces a linear relation which gives the value of K_2 (from the intercept) and q_e (from the slop).

3.13. Application of adsorption in real samples:

Real sea samples for the analysis of HMIs were collected from three spots in marine industrial spots. Preservation of samples during storage was done by adding Nitric acid (5%). Analysis of HMIs by ICP spectrometer were done before adding the adsorbents to quantity the original concentrations of HMIs. Adsorption batch analyses were then performed as described in sec 3.9.

Chapter Four

Results, Discussion, and Recommendation

4.1. Removal of Methylene Blue and Congo Red from Aqueous Solution using Environmentally Friendly Polyvinyl Alcohol-Sodium Alginate-Bentonite Semi-Interpenetrating Polymer Network Nanocomposite Hydrogel Beads.

4.1.1. Physical and chemical characterization of PVA-ALG-BENT

4.1.1.1. Fourier Transform Infrared Spectroscopy (FTIR).

4.1.1.2. Energy-Dispersive X-ray Spectroscopy (EDX).

4.1.1.3. Scanning Electron Microscopy (SEM).

4.1.2. Equilibrium Swelling Test at various pH

4.1.3. PH of point of zero charge (pH_{PZC})

4.1.4. Batch Adsorption Equilibrium Studies

4.1.4.1. Effect of solution pH

i. Effect of solution pH on MB

ii. Effect of solution pH on CR

4.1.4.2. Effect of Contact Time

i. Effect of Contact Time on MB

ii. Effect of Contact Time on CR

4.1.4.3. Effect of Initial Dye Concentration

i. Effect of Initial MB Concentration

ii. Effect of Initial CR Concentration

4.1.4.4. Effect of Adsorbent Dosage

i. Effect of Adsorbent Dosage on MB Removal

ii. Effect of Adsorbent Dosage on CR Removal

4.1.4.5. Effect of Temperature

i. Effect of Temperature on MB Removal

ii. Effect of Temperature on CR Removal

4.1.5. Adsorbent Reusability Test

i. Adsorbent Reusability Test for MB

ii. Adsorbent Reusability Test for CR

4.1.6. Adsorption Isotherm study

i. Adsorption Isotherm study for MB

ii. Adsorption Isotherm study for CR

4.1.7. Adsorption Kinetic studies for MB and CR.

4.1.8. Adsorption Mechanism of Dyes

4.2. Removal of Heavy Metal Ions from Aqueous Solution using Environmentally Friendly Polyvinyl Alcohol -Chitosan-nanocellulose Semi-Interpenetrating Polymer Network Nanocomposite Hydrogel Beads as An Efficient Adsorbent.

4.2.1. Physical and chemical characterization methods

4.2.1.1. Fourier Transform Infrared Spectroscopy (FTIR).

4.2.1.2. Energy-Dispersive X-ray Spectroscopy (EDX).

4.2.1.3. Scanning Electron Microscopy (SEM).

4.2.2. Equilibrium Swelling Test at various pH

4.2.3. pH of point of zero charge (pH_{PZC}).

4.2.4. Batch Adsorption Equilibrium Studies

4.2.4.1. Effect of solution pH on the removal of HMIs

4.2.4.2. Effect of Contact Time on the removal of HMIs

4.2.4.3. Effect of Initial HMI Concentration on the removal of HMIs
4.2.4.4. Effect of Adsorbent Dosage on the removal of HMIs
4.2.4.5. Effect of Temperature on the removal of HMIs
4.2.5. Adsorbent Reusability Test for HMIs adsorption
4.2.6. Adsorption Isotherm studies for HMIs adsorption
4.2.7. Adsorption Kinetic studies for HMIs Adsorption
4.2.8. Selectivity adsorption of HMIs.
4.2.9. Adsorption Mechanism of for HMIs Adsorption
4.2.10. Application in real samples
4.3. Conclusion.
4.4. Recommendation
4.5. References

Chapter Four

Results, Discussion, and Recommendation

4.1. Removal of Dyes (Methylene Blue (MB) and Congo Red (CR) from Aqueous Solution by Polyvinyl Alcohol- Sodium Alginate- Bentonite (PVA-ALG-BENT) Nanocomposite Hydrogel Beads

4.1.1. Physical and chemical characterization of PVA-ALG-BENT

The semi-IPN PVA-ALG-BENT nanocomposite hydrogel beads were successfully prepared by using ionic gelation method with Ca^{2+} ions as crosslinkers (Asadi et al., 2018; Baigorria et al., 2020b). The gelation of ALG is demonstrated in Fig. 4.1 and it's occurred because of the exchanging of sodium ions of the ALG salt with multivalent cations (Ca^{2+}). The carboxylic acid groups in ALG's chain produce negative charges and thus help to crosslink easily with positively charged cation especially divalent cations such as Ca^{2+} to form gels (Chuang et al., 2017; Mandal & Ray, 2013; Paredes Juárez et al., 2014).

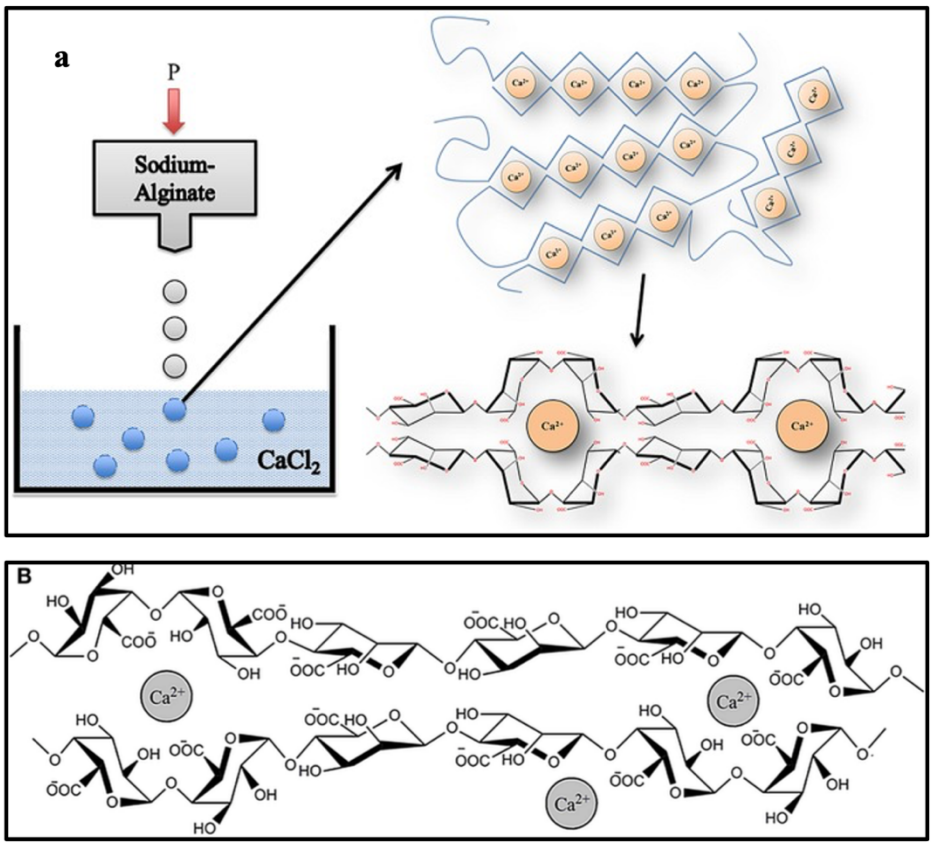


Fig. 4. 1: Gelation process of ALG. (a) SALG dropped to a $CaCl_2$ to produce hydrogel beads by cross-linking of ALG-polymers with Ca^{2+} cations. (b) Crosslinking between Ca^{2+} and ALG polymer (Paredes Juárez et al., 2014).

The digital images of the wet and dry beads before adsorption of dyes are displayed in Fig. 4.2. As shown in Fig. 4.2a, the incorporation of BENT nanoparticles into the hydrogel beads was confirmed by the formation of beige color beads, before the addition of BENT the color of the beads was colorless. The wet beads exhibited uniform spherical shapes with a smooth surface and a size of approximately 4.0 mm. However, after air drying, the-spherical shape of the beads was slightly changed, resulting in a rough surface morphology without ~~a~~ noticeable collapse on the surface, indicating an improved mechanical stability (Fig. 4.2b). Indeed, the deformation in shape is inevitable when the wet hydrogel beads are dried,

causing volume shrinkage of hydrogel beads (Merakchi et al., 2019). Fig. 4.3a and Fig. 4.3b show black and orange color indicating the encapsulation of MB and CR in PVA-ALG-BENT beads, respectively.

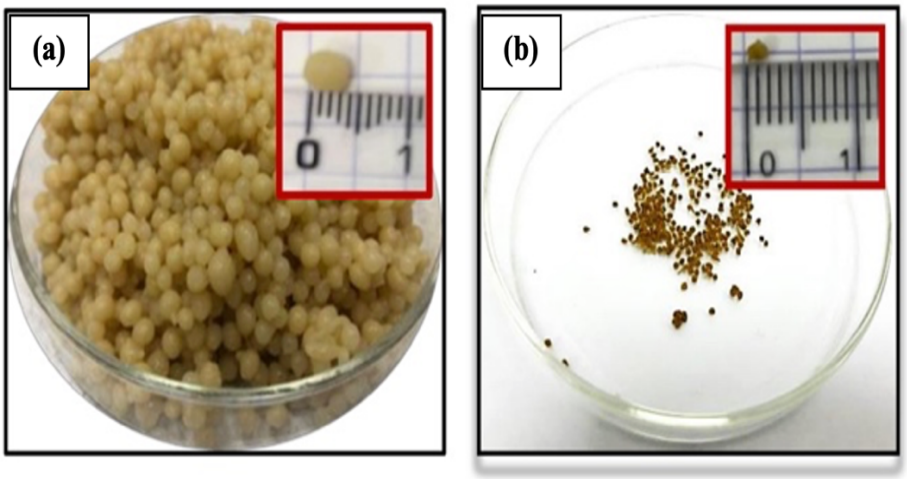


Fig. 4. 2: The color of Semi-IPN PVA-ALG-BENT nanocomposite hydrogel beads (a) before drying (inset shows the size of wet beads), (b) after 48 h air drying (inset shows the size of dried beads)

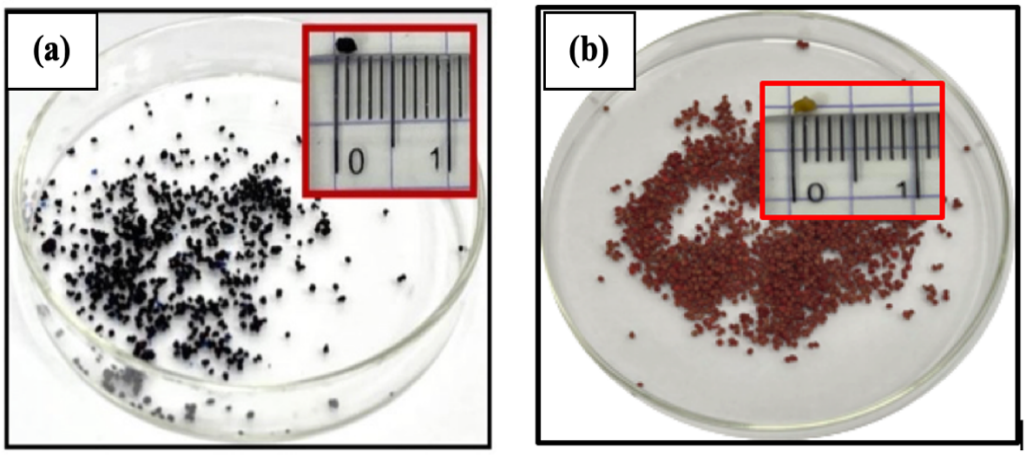


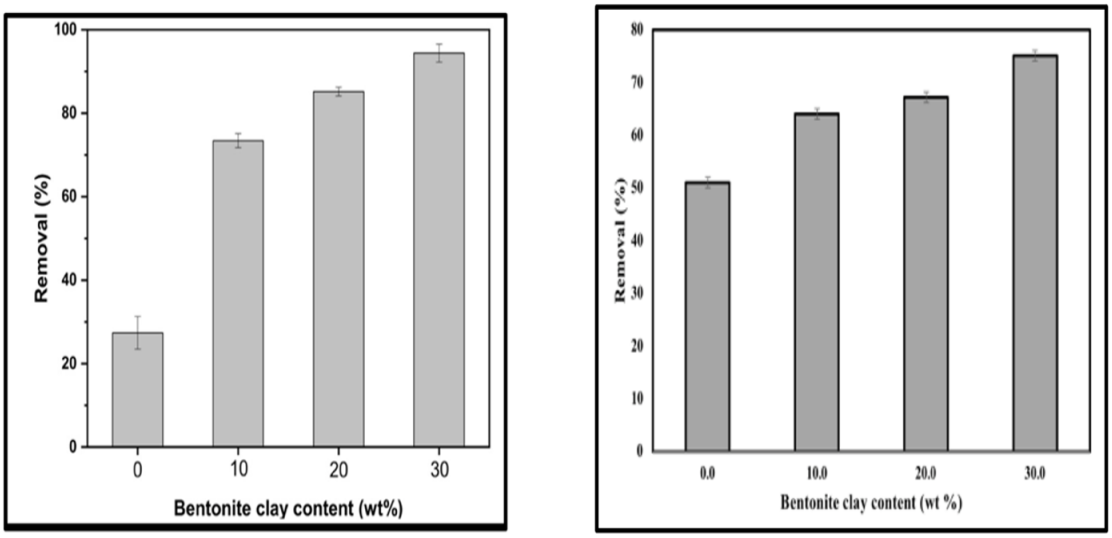
Fig. 4. 3: Semi-IPN PVA-ALG-BENT nanocomposite hydrogel beads (a) after adsorption of MB dye, (b) after adsorption of CR dye (inset shows the size of dyes-adsorbed beads).

To study the adsorption ability of the designed nanocomposite hydrogel beads, preliminary adsorption tests were performed. Hydrogel beads (PVA-ALG) was prepared as a control, other tested adsorbents were prepared by varying BENT content (10.0 %, 20.0 % and 30.0 %). As shown in Table (4.1) and Fig. 4.4, the control hydrogel beads (PVA-ALG) had limited removal rate of 27.4% for MB and 51.08 % for CR. Nevertheless, the removal rate of MB and CR were significantly improved by increasing the content of Bent nanoparticles in the hydrogel beads. For instant the incorporation of 10.0 wt.%, 20.0 wt.%, and 30.0 wt.% of BENT in the hydrogel beads increased the removal rate of MB dye by 165%, 190%, and 230%, respectively. In the other hands, incorporation of 10.0 wt.%, 20.0 wt.%, and 30.0 wt.% of BENT in the hydrogel beads increased the removal efficiency of CR by 25.0%, 31.0% and 74.05%, respectively. BENT content exceeding 30% was not used due to the aggregation of BENT nanoparticles, which in turn may deteriorate the overall mechanical stability and beads strength (Oussalah & Boukerroui, 2020; W. Wang, Zhao, Bai, Zhang, Ibarra-Galvan, et al., 2018b, Baigorria et al., 2020a)).

Therefore, in this work, the PVA: ALG weight ratio and the content of BENT nanoparticles were fixed at (1:1) and 30% (w/w), respectively and all the adsorption studies were performed on this nanocomposite hydrogel.

Table (4. 1): Effect of bentonite content (0, 10, 20, 30 wt.%) on the removal percentage of MB and CR

DYES	BENT Content	MB Concentration after adsorption in ppm			MB Concentration in ppm	% Removal	$Q_e \pm SD$ (mg/g)
		Trial 1	Trial 2	Trail 3			
MB	0.0 %	137	153	145	145	27.4±4.0	1.83±0.3
	10%	55.3	54.8	49.2	53.1	73.4±1.7	4.89±0.1
	20%	23.8	25.7	21.4	23.6	88.2±1.0	5.88±0.07
	30 %	20.2	9.62	3.83	11.2	94.4±4.0	6.29±0.3
CR	0%	41.7	43.7	61.3	48.9	51.1±10	1.70±0.4
	10%	39.7	37.5	30.9	36.0	63.9±4.6	2.13±0.2
	20%	33.7	34.2	30.4	32.8	67.2±2.0	2.24±0.07
	30 %	20.6	23.6	30.6	24.9	75.0±5.0	2.50±0.2



(a) (b)

Fig. 4. 4: Effect of BENT content (0, 10, 20, 30 wt.%) on the removal percentage of Dyes, (a) MB (C_0[MB] = 200 mg/L, V = 50 mL, pH = 8, beads dosage = 1.5 g, t = 300 min, T = 30 C). (b) CR (C_0[CR] = 100 mg/L, V = 50 mL, pH = 3, beads dosage = 1.5 g, t = 300 min, T = 30 °C).

4.1.1.1. Fourier Transform Infrared Spectroscopy (FTIR)

Fig. (4.5) displays the FTIR spectra of the pristine BENT, semi-IPN PVA-ALG control hydrogel, and semi-IPN PVA-ALG-BENT nanocomposite hydrogel. BENT exhibits characteristic peaks at 3674, 1054, 950 and 835 cm^{-1}. The peak at 3674 cm^{-1} is attributed to (O-H) stretching bands. The peak at 1054 cm^{-1} is related to the stretching vibrations of (Si-O-Si) group, whereas the peak at 950 cm^{-1} is related to (Al-OH) bending vibrations (Oussalah & Boukerroui, 2020; RAVI & Pandey, 2019). Besides, the weak band at 835 cm^{-1} is related to (Si-O) stretching vibrations of silanol group of BENT. The spectrum of the PVA-

ALG hydrogel shows a broad overlapped absorption bands in the region of 3300-3400 cm^{-1} which are corresponding to the stretching vibration of (O-H) of both PVA and ALG (Asadi et al., 2018; Baigorria et al., 2020b). Absorption peaks at 1635 cm^{-1} and 1428 cm^{-1} are due to asymmetric and symmetrical stretching vibrations of (-COO) of ALG (Baigorria et al., 2020a; Wu et al., 2019). The peak appeared at 2947 cm^{-1} was the typical stretching vibration for (C-H) in PVA. In addition, the small shift of the band near 1300 cm^{-1} would be related to the presence of hydrogen bonds between (O-H) groups of PVA and ALG or with (Si-O) groups of BENT (Baigorria et al., 2020a; Oussalah & Boukerroui, 2020; Wu et al., 2019). These results suggested that the BENT clay had successfully incorporated in the PVA-ALG hydrogel polymer matrix.

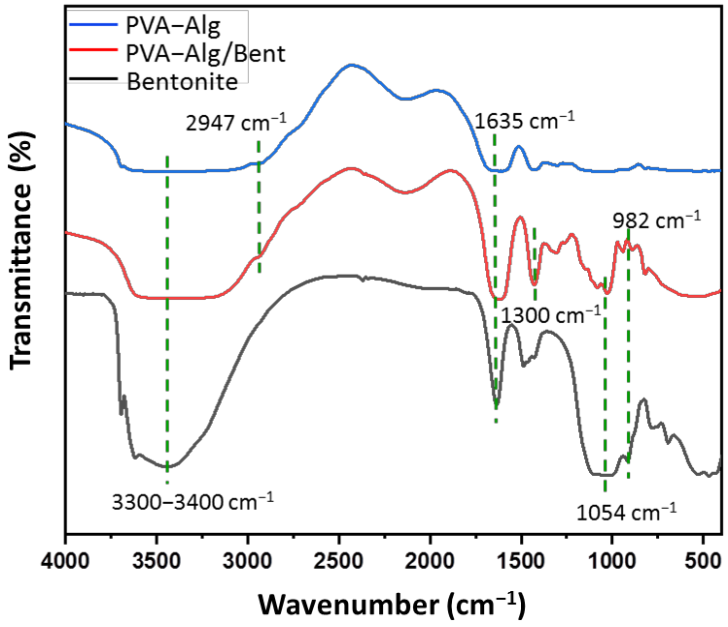
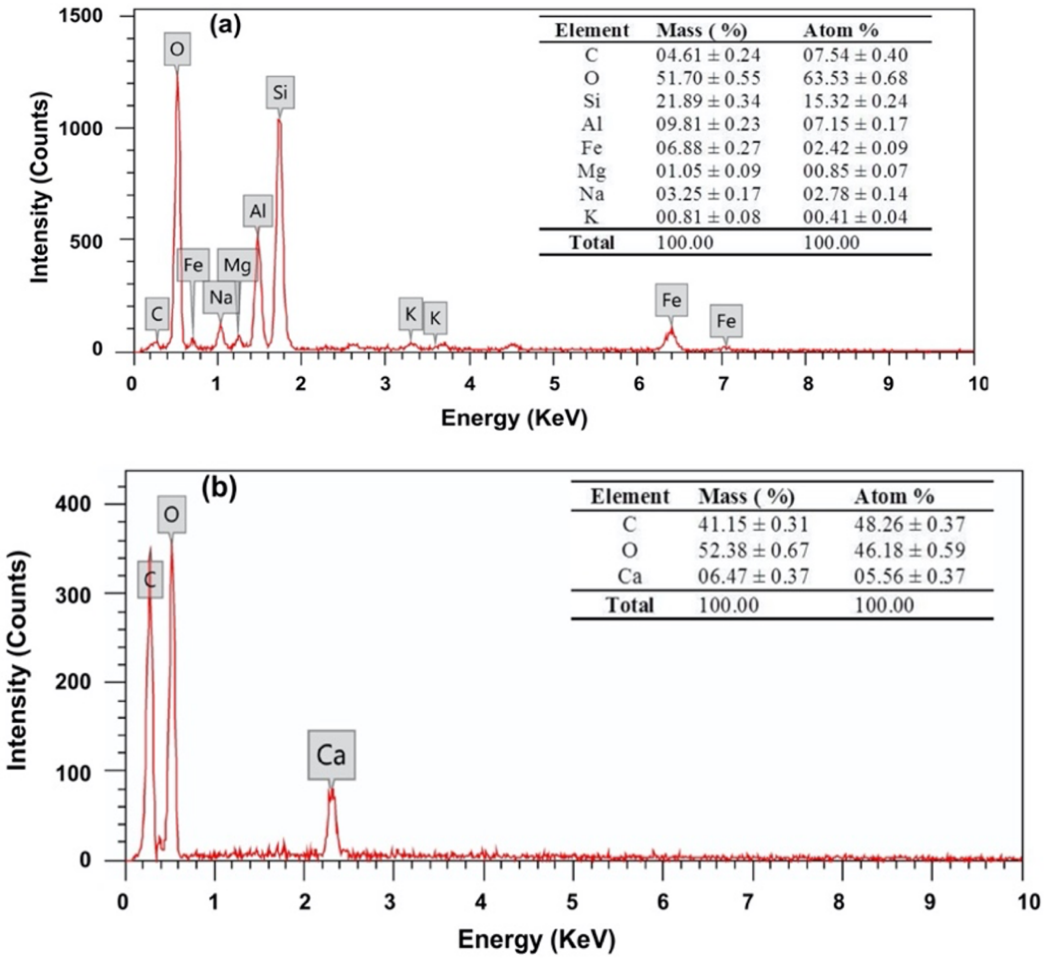


Fig. 4. 5: FTIR spectra of pristine BENT, semi-IPN PVA-ALG hydrogel and semi-IPN PVA-ALG-BENT nanocomposite hydrogel.

4.1.1.2. Energy-Dispersive X-ray Spectroscopy (EDX)

The presence of BENT nanoparticles that are successfully added in the hydrogel matrix was further confirmed by EDX elemental analysis as shown in Fig. (4.6). Fig. (4.6a) confirmed the presence of BENT main constituents such as O (51.70%), Si (21.89%), Al (9.81%), Fe (6.88%), and C (4.61%). The obtained results are in agreement with literature results (Fernandes et al., 2018; RAVI & Pandey, 2019). The main characteristic elements such as C (40.95%) and O (52.19%) were detected for PVA-ALG hydrogel (Fig. (4.6b)). The peaks of Si, Al and Fe elements were clearly observed in the EDX spectrum Fig. (4.6c) of PVA-ALG-BENT nanocomposite hydrogel, indicated the successful incorporation of BENT nanoparticles on the hydrogel.



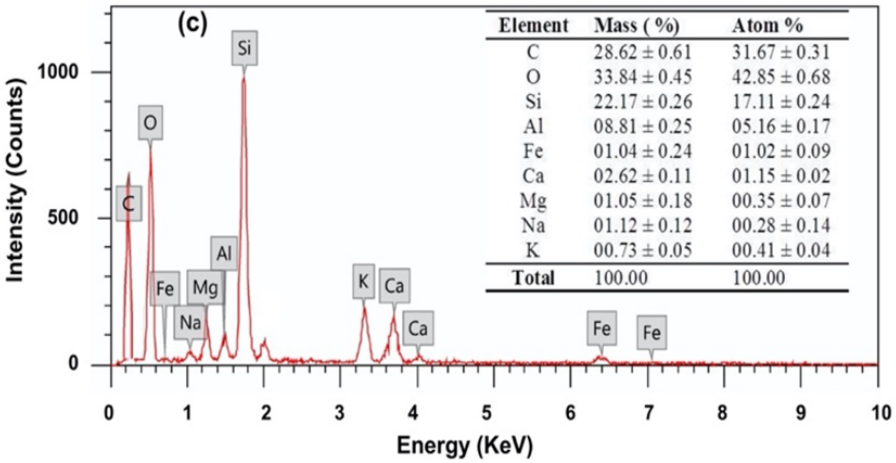


Fig. 4. 6: EDX spectra of (a) pristine BENT clay (b) semi-IPN PVA-ALG control hydrogel, and (c) semi-IPN PVA-ALG-BENT nanocomposite hydrogel. The insets show the corresponding weight and atomic percentages of the elements present in the samples.

4.1.1.3. Scanning Electron Microscopy (SEM)

The SEM micrographs and the surfaces of dried PVA-ALG and PVA-ALG-BENT hydrogels are shown in Fig 4.7. SEM micrographs revealed a slight increase in the size of the PVA-ALG-BENT nanocomposite bead (Fig. 4.7a) compared to the PVA-ALG bead (Fig. 4.7c). Besides, PVA-ALG (unfilled) beads exhibited an irregulargully that shape with some cracks and pores on their surfaces. However, as expected the incorporation of BENT (30 wt.%) resulted in a clear decrease in the size of the pores and the thickness of the cracks as displayed in Fig. 4.7 b & d. Furthermore, the PVA-ALG-BENT nanocomposite hydrogel showed uniform dispersion of the clay nanoparticles within the polymer matrix, leaving a relatively rough surface (Fig. 4.7d). This structure would provide more contact sites and convenient diffusion channels, which may enhance

or improve dye's adsorption (Baigorria et al., 2020b; Fernandes et al., 2018; Merakchi et al., 2019).

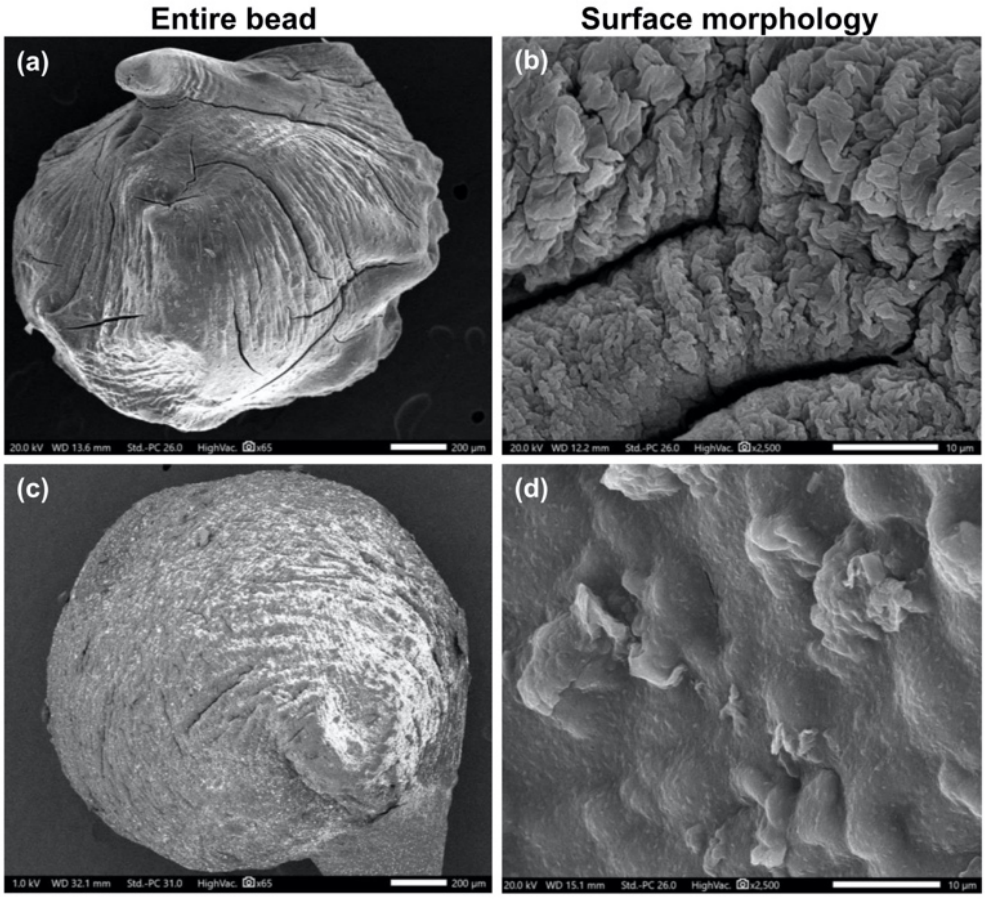


Fig. 4. 7: SEM micrographs of (a,b) semi-IPN PVA-ALG control hydrogel beads, and (c,d) semi-IPN PVA-ALG-BENT nanocomposite hydrogel beads.

4.1.1.4. X-ray Diffraction Studies (XRD)

Fig. 4.8 reflects the XRD patterns of the PVA-ALG-BENT adsorbent. The major characteristics peaks of the composite were not observed, this finding suggests that the three components of the composites became amorphous in the hydrogel matrix. The crystallization of the polymers is limited and weak because of the strong interaction between the PVA, ALG, and BENT. Similar observation of lowering the intensities of the peaks was observed and reported by (Habiba, Siddique, et al., 2017a).

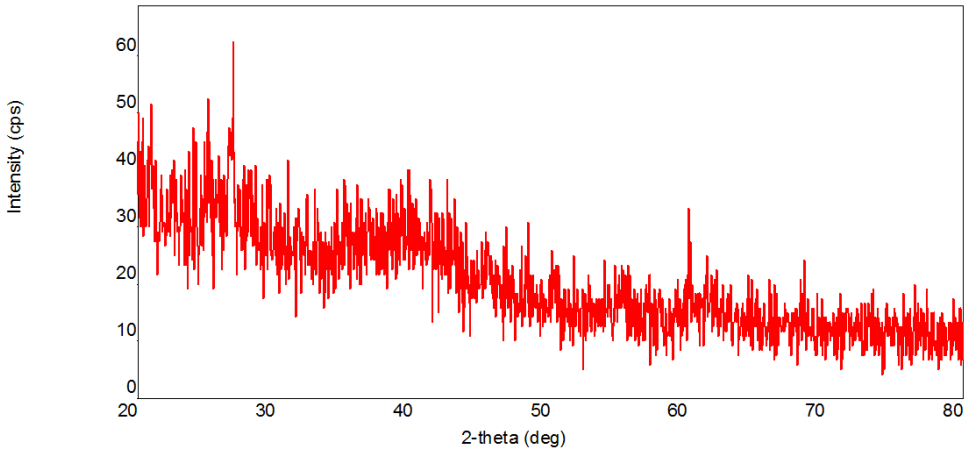


Fig. 4. 8:XRD for PVA-ALG-BENT.

4.1.2. Equilibrium Swelling Test at various pH

The swelling behavior of the semi-IPN PVA-ALG-BENT nanocomposite hydrogel beads in aqueous solution at different pH values is depicted in Fig. 4.9. All beads showed a similar tendency with different degrees of hydration. As can be seen in Fig. 4.9a, the swelling ratio enhanced slightly at 20-150 min, and then slow until reach a plateau at150-320 min. This observation can be attributed to the attraction between (–OH) groups on both the polymer chains and clay surfaces and water molecules from the soaking medium, promoting their penetration into the gel-network, and elevating water uptake ability of the nanocomposite (Fernandes et al., 2018; Hu et al., 2018). Moreover, hydrogel beads exhibited pH-dependent swelling behavior, where the water uptake of the beads increased significantly with increasing pH of the solution. More specifically, at 150 min, the swelling rate increased within pH 3-7 (from 25.5-30.2%) and increased significantly in the pH range of 7-9 (from 30.2-40.6%) indicating a structural change of the cross-linked hydrogel at different pH values (Figure 4.9b). The low swelling capacity in acidic solution (pH 3) can be due to the protonation of (-COO^- to -COOH) groups of the hydrogel matrix.

Consequently, the beads will shrink via the hydrophobic interaction, leading to more rigid gel-networks structure, which restricts crossing of water molecules (Baigorria et al., 2020a; Qi et al., 2018). In neutral and alkaline solution some of the (-COOH) groups in the hydrogel ionize to ($-COO^-$), causing repulsions between the negatively charged chains, facilitating the expansion of hydrogel, and thus enhancing the swelling rate (Hu et al., 2018; Qi et al., 2018).

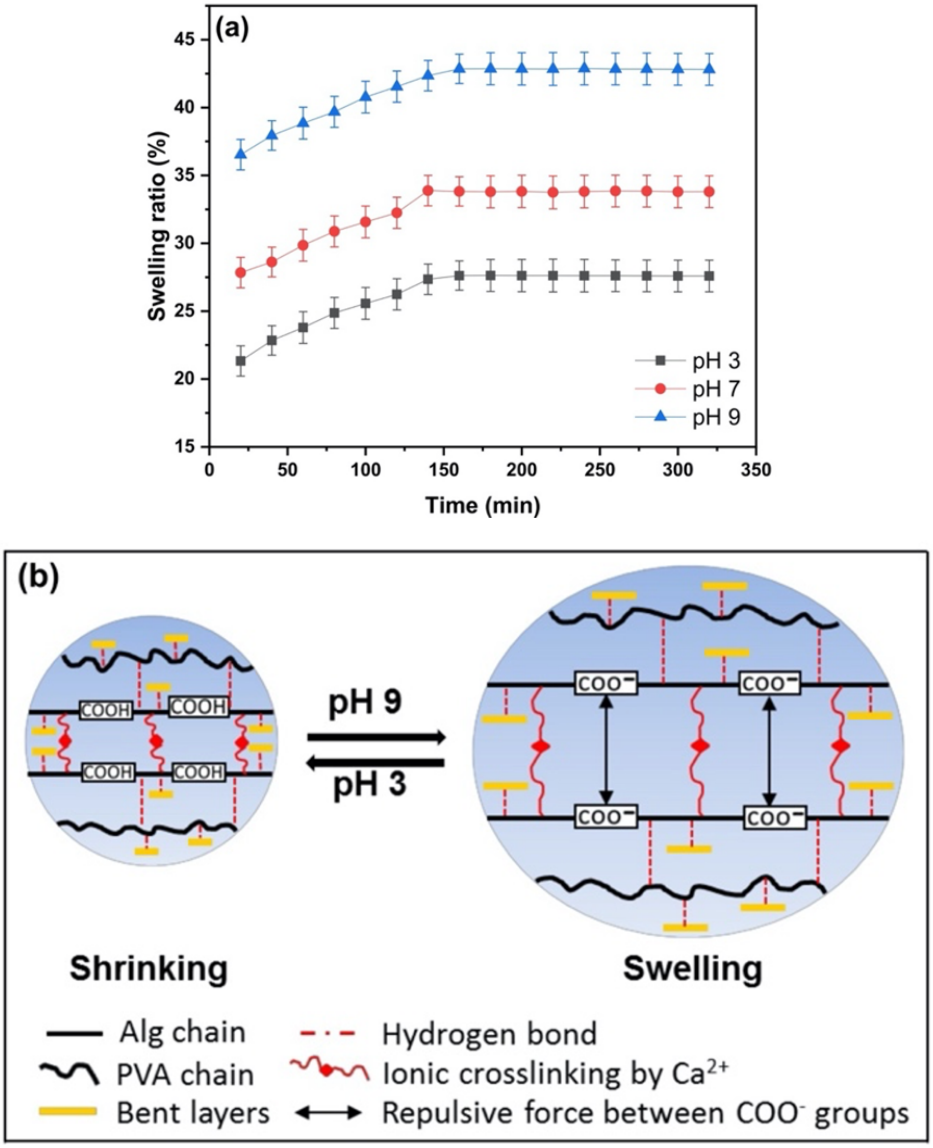


Fig. 4. 9: Swelling behavior of the semi-IPN PVA-ALG-BENT nanocomposite hydrogel beads at different pH values: (a) Swelling ratio and (b) Schematic illustration of the swelling process at different pH

4.1.3. Point of Zero Charge pH_{PZC}

Point of zero charge pH_{PZC} is an important parameter to understand the adsorption mechanism of adsorbate on the adsorbent, and it is defined as the pH at which the net charge of total particle surface (i.e. absorbent's surface) is equal to zero. The pH_{PZC} of PVA-ALG-BENT was found to be 4.00 as shown in Fig. (4.10). At a pH lower than pH_{PZC}, the active sites of the beads are positively charged which favors the adsorption of CR (anionic dyes). Whereas, at pH above pH_{PZC} MB (cationic dye) adsorption is more favorable because the surface of the beads is negatively charged (Litefti et al., 2019a; Vidal & Moraes, 2019). Therefore, it's expected that the removal of CR is favored at pH 3 whereas the removal of MB is favored at pH 8.

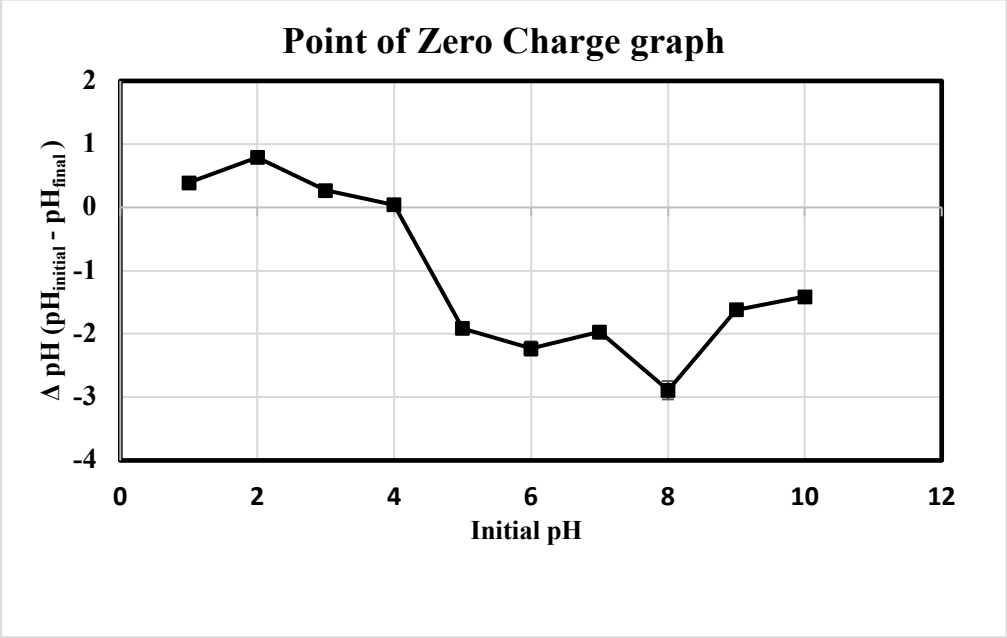


Fig. 4. 10: pH_{PZC} for PVA-ALG-BENT nanocomposite's hydrogel beads

4.1.4. Batch Adsorption Equilibrium Studies

To study the suitability of the designed semi-IPN PVA-ALG-BENT nanocomposite hydrogel beads as adsorbent for dyes, adsorption experiments were conducted utilizing a batch experimental setup. The influences of various parameters on the adsorption behaviors of the beads, such as pH, contact time, initial dye concentration, beads dosage and temperature, were explored.

4.1.4.1. Effect of pH of the solution

The pH of dye solution is the most vital parameter controlling the efficiency of dye adsorption (Hu et al., 2018).

i. Effect of solution pH on the adsorption of MB

The effect of the solution pH on the adsorption capacity and removal percentage of MB dye by PVA-ALG-BENT nanocomposite hydrogel beads is illustrated in Table (4.2) and Fig. (4.11). Low adsorption capacity was observed when the pH increased from 2 to 5, and the adsorption capacity was significantly increased at pH range from 5 to 8 and then decreased when the pH vale greater than 8. The maximum percentage of dye removal (94.64%) was achieved at pH 8. As mentioned above, the pH of dye solution may affect the ionization of the functional groups on the nanocomposite hydrogel adsorbent, which act as the active sites of the hydrogel adsorbent, in turn, governing the electrostatic attraction between the anionic sites on the hydrogel matrix and the cationic sites on the MB dye (N. Hou et al., 2020a; Oussalah & Boukerroui, 2020; Qi et al., 2018). At acid conditions, the negative surface charges of the nanocomposite hydrogel adsorbent were reduced as a result of protonation of the negative sites, hence undesirable for the removal of positively charged MB dye. At

pH 8, the surface negative charges of the hydrogel increased due to deprotonation of COOH group. Therefore, favorable for the removal of MB due to the enhanced electrostatic attraction to the positively charged MB. Above pH 8, the surface of the hydrogel is fully or mostly negatively charged causing anionic repulsion on the surface of the gel, thus lessening the electrostatic attraction between MB and the hydrogel and consequently causing smaller removal values (N. Hou et al., 2020a; Wu et al., 2019).

Table (4. 2): Effect of initial pH on the adsorption capacity and removal percentage of MB onto the semi-IPN PVA-ALG-BENT nanocomposite hydrogel beads. Note: the optimal pH value highlighted in blue

MB Removal (V = 50 mL; initial concentration = 200 (mg/L); pH= 2-10; beads dosage =1.5 g; temp= 30 ºC; time = 300 min, wavelength = 663 nm)						
pH	**MB Concentrations (mg/L) after 300 min**			**MB Average Concentration (mg/L)**	**MB % Removal**	**Q_e ± SD (mg/g)**
	Trail 1	**Trail 2**	**Trail 3**			
2	32.3	29.2	22.9	28.1	85.9±2.0	5.73±0.1
3	36.7	26.9	24.3	29.4	85.3±3.0	5.69±0.2
4	33.8	26.6	25.8	28.7	85.6±2.0	5.71±0.1
5	25.7	24.6	35.0	28.4	85.8±3.0	5.72±0.2
6	25.2	16.9	11.4	17.9	91.1±3.0	6.07±0.2
7	25.1	14.0	9.43	16.2	91.9±4.0	6.13±0.3
8	20.2	9.484	3.83	11.2	94.4±4.14	6.29±0.27
9	29.2	16.9	11.6	19.2	90.38±4.0	6.03±0.3
10	35.3	39.9	15.10	30.1	84.9±6.0	5.66±0.4

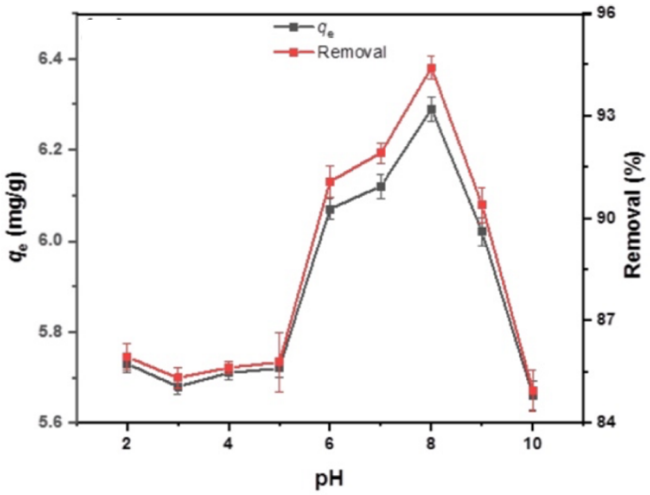


Fig. 4. 11: Effect of initial pH on the adsorption capacity and removal percentage of MB onto the semi-IPN PVA-ALG-BENT nanocomposite hydrogel beads (C_0[MB] = 200 **(mg/L)**, V = 50 mL, beads dosage = 1.5 g, pH = 8, t = 300 min, T = 30 ºC).

ii. Effect of solution pH on the adsorption of CR

The effect of pH on the CR adsorption was studied by changing the pH from 3-10. As shown in Table (4.3) and Fig. (4.12), both the adsorption capacity and removal efficiency of CR were decreased as the pH increased from 3 to 10 and the maximum percentage adsorption of CR (75.05%) was obtained at pH 3. Under acidic conditions, the negatively charged (COO^-) groups are converted to (COOH), thus the hydrogen bond interaction between the carboxyl acid groups increased. In addition, the high electrostatic force that appears between the negative charge of CR and the positively charged surface of the adsorbent increases the dye uptake. When the pH value increased, the active sites of the adsorbents become negative and therefore unsuitable for anionic dye uptake, (Purkait et al., 2007). In addition, at high pH, the OH^- ions compete with the dye ions resulting in a decrease in adsorption of dye from aqueous solution (Banerjee & Chattopadhyaya, 2017b; Zou et al., 2020b)

Table (4. 3): Effect of initial pH on the adsorption capacity and removal percentage of CR by semi-IPN PVA-ALG-BENT nanocomposite hydrogel beads. Note: The optimal pH value highlighted in blue

CR Removal (V = 50 mL; initial concentration = 100 (mg/L); pH= 2-10; beads dosage =1.5 g; temp= 30 ºC; time = 300 min, wavelength = 446 nm)						
PH	**CR Concentrations (mg/L)**			**CR Average Concentration (mg/L)**	**CR % Removal**	**Q_e ± SD (mg/g)**
	Trail 1	**Trail 2**	**Trail 3**			
3	20.6	23.6	30.6	24.9	75.05±5.12	2.50±0.17
4	28.2	29.8	24.1	27.4	72.6±3.0	2.42±0.1
5	26.0	29.9	26.1	27.4	72.6±2.0	2.42±0.07
6	28.2	30.8	24.6	27.9	72.1±3.0	2.40±0.1
7	27.5	30.3	26.2	28.0	72.0±2.0	2.40±0.07
8	25.5	29.8	31.6	29.0	71.0±3.0	2.37±0.1
9	28.7	30.2	30.0	29.7	70.3±0.8	2.34±0.03
10	31.1	31.8	30.4	31.2	68.8±0.7	2.30±0.02

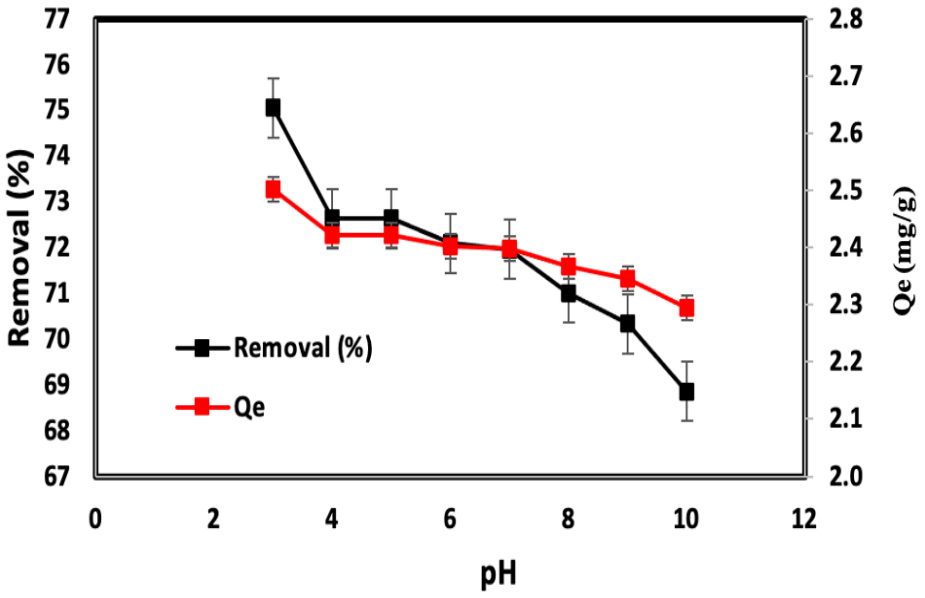


Fig. 4. 12: Effect of initial pH on the adsorption capacity and removal percentage of CR onto the semi-IPN PVA-ALG-BENT nanocomposite hydrogel beads (C_0[CR] = 100 mg/L, V = 50 mL, beads dosage = 1.5 g, pH = 3-10, t = 300 min, T = 30 ºC).

4.1.4.2. Effect of Contact Time

Contact time is important factor of adsorption because it indicates the availability of active sites during the adsorption process till it reaches an equilibrium state (Munagapati & Kim, 2017; Wu et al., 2019).

i. Effect of Contact Time on the Removal MB

The variation of removal rate of MB and the adsorption capacity of the hydrogel beads over contact time were shown in Table (4.4) and Fig. (4.13). It was noticed that the adsorption capacity and the removal percentage were improved with increasing immersion contact time. A fast adsorption over the initial 60 min was observed which relatively became slower after 60 min till 5 hr. At the same time, the color of the hydrogels became dark gradually, whereas the MB solution turned from an initial blue to

completely transparent as shown in the inset of Fig. (4.13). These observations may be attributed to the fully occupation of the adsorbent surface binding sites and the diffusion of the MB molecules into the pores of the hydrogel beads. At the starting of adsorption process, plentiful active sites are available on the surface of the beads, which could combine with the MB molecules (N. Hou et al., 2020a; Hu et al., 2018). Moreover, the high concentration of MB in the solution is a driving force for MB adsorption supported by concentration gradient. In the later stage of the adsorption process, the concentration of MB decreases and the adsorption sites of the beads are saturated. Therefore, the diffusion and adsorption of MB molecules were reduced and hence the adsorption rate decreased (Belhouchat et al., 2017a).

Table (4. 4): Effect of contact time on the adsorption capacity and removal percentage of MB onto the semi-IPN PVA-ALG-BENT nanocomposite hydrogel beads

MB Removal (V = 50 mL; initial concentration = 200 (mg/L); pH= 8; beads dosage =1.5 g; temp= 30 ºC; time = 20-320 min, wavelength = 663 nm)						
Time (min)	**MB Concentrations (mg/L)**			**MB Average Concentration (mg/L)**	**MB % Removal**	**Q_e ± SD (mg/g)**
	Trail 1	**Trail 2**	**Trail 3**			
20	128	140	154	141.2	29.4±6.0	1.96±0.4
40	125	120	120	122	38.9±1.0	2.60±0.09
60	92.5	102	92.9	95.7	52.1±2.0	3.48±0.1
80	87.8	80.1	73.8	80.6	59.7±3.0	3.98±0.2
100	80.1	64.6	51.9	65.7	67.2±7.0	4.48±0.4
120	61.5	58.4	44.7	54.9	72.6±4.0	4.84±0.3
140	58.4	55.3	23.9	45.9	77.0±9.0	5.14±0.6

MB Removal (V = 50 mL; initial concentration = 200 (mg/L); pH= 8; beads dosage =1.5 g; temp= 30 ºC; time = 20-320 min, wavelength = 663 nm)						
Time (min)	**MB Concentrations (mg/L)**			**MB Average Concentration (mg/L)**	**MB % Removal**	**Q_e ± SD (mg/g)**
	Trail 1	**Trail 2**	**Trail 3**			
160	47.6	42.9	25.8	38.8	80.6±5.0	5.37±0.4
180	31.2	33.7	28.7	31.2	84.4±1.0	5.63±0.08
200	23.0	21.5	28.3	24.3	87.9±2.0	5.86±0.1
220	21.5	18.4	19.5	19.8	90.1±0.8	6.00±0.05
240	19.2	16.8	13.9	16.7	91.7±1.0	6.11±0.09
260	16.1	13.7	10.9	13.6	93.2±1.0	6.21±0.09
280	13.7	12.2	8.09	11.3	94.3±1.0	6.29±0.1
300	12.7	10.6	6.54	9.95	95.0±1.0	6.34±0.1
320	11.4	9.87	4.14	8.48	95.8±2.0	6.38±0.1

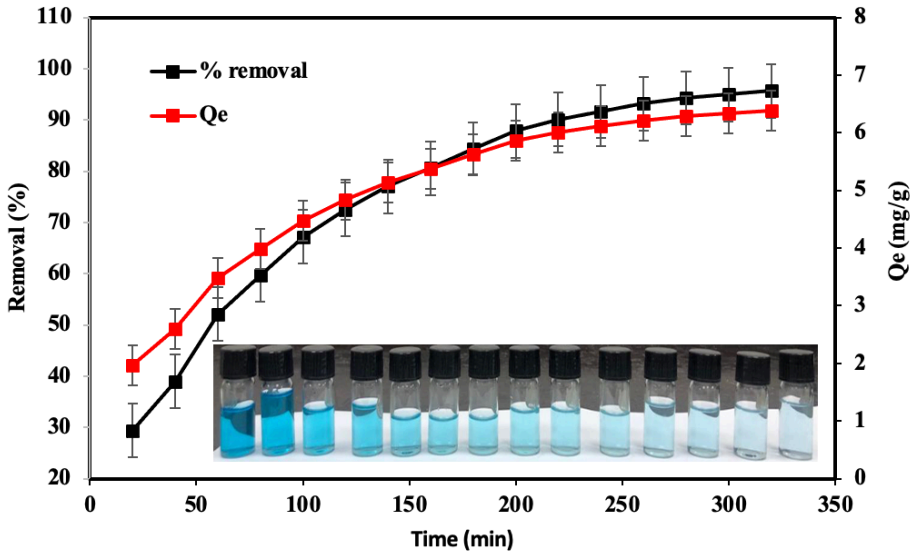


Fig. 4. 13: Effect of contact time on the adsorption capacity and removal percentage of MB onto the semi-IPN PVA-ALG-BENT nanocomposite hydrogel beads (C_0[MB] = 200 mg/L, V = 50 mL, beads dosage = 1.5 g, pH = 8, t = 20-320 min, T = 30 ºC).

ii. Effect of Contact Time on the adsorption of CR

The time duration curve versus removal % is shown in Table (4.5) and Fig. (4.14). The results implied that both the adsorption capacity of the nanocomposite beads and the adsorption efficiency of CR were increased when increasing agitation time. The initial sorption rate was occurred rapidly in early stage, this study showed that up to 60 % of CR was removed in the first 60 min. While at higher contact times the sorption rate decreased steadily as it reached the equilibrium at 300 min. This occurred due to the availability of active site during the early stage of the adsorption, and the repulsion force between the CR molecule adsorbed on the hydrogel surface and those in the aqueous bulk solution (Shojaeipoor et al., 2019). Moreover, the steady data implied that once equilibrium is reached the adsorption process did not improve.

Table (4. 5): Effect of contact time on the adsorption capacity and removal percentage of CR onto the semi-IPN PVA-ALG-BENT nanocomposite hydrogel beads

CR Removal (V = 50 mL; initial concentration = 200 (mg/L); pH= 3; beads dosage =1.5 g; temp= 30 ºC; time = 20-320 min, wavelength = 446 nm)						
Time (min)	**CR Concentrations (mg/L)**			**CR Average Concentration (mg/L)**	**CR % Removal**	**Q_e ± SD (mg/g)**
	Trail 1	**Trail 2**	**Trail 3**			
20	55.9	51.2	50.4	52.4	47.5±3.0	1.59±0.1
40	51.3	48.9	43.2	47.8	52.2±4.0	1.74±0.1
60	45.5	43.7	37.0	42.1	57.9±4.0	1.93±0.1
80	44.8	42.8	36.5	41.4	58.6±4.0	1.95±0.1
100	42.1	40.45	33.3	38.6	61.4±4.0	2.05±0.2
120	39.5	37.7	29.6	35.6	64.4±5.0	2.15±0.2
140	39.8	37.5	29.6	35.6	64.4±5.0	2.15±0.2
160	37.5	34.7	27.1	33.1	66.9±5.0	2.23±0.2

CR Removal (V = 50 mL; initial concentration = 200 (mg/L); pH= 3; beads dosage =1.5 g; temp= 30 ºC; time = 20-320 min, wavelength = 446 nm)						
Time (min)	**CR Concentrations (mg/L)**			**CR Average Concentration (mg/L)**	**CR % Removal**	**Q_e ± SD (mg/g)**
	Trail 1	**Trail 2**	**Trail 3**			
180	36.3	33.5	25.9	31.9	68.1±5.0	2.27±0.2
200	35.8	33.3	25.94	31.7	68.3±5.0	2.28±0.2
220	35.6	33.3	26.2	31.7	68.3±5.0	2.28±0.1
240	34.7	32.9	25.5	31.0	69.0±4.0	2.30±0.1
260	33.8	32.2	25.0	30.3	69.7±4.0	2.32±0.1
280	32.8	31.7	23.6	29.4	70.60±5.0	2.3±0.2
300	31.7	30.6	19.0	27.1	72.90±7.0	2.430±0.2
320	20.6	23.6	30.6	25.0	75.05±5.0	2.50±0.2

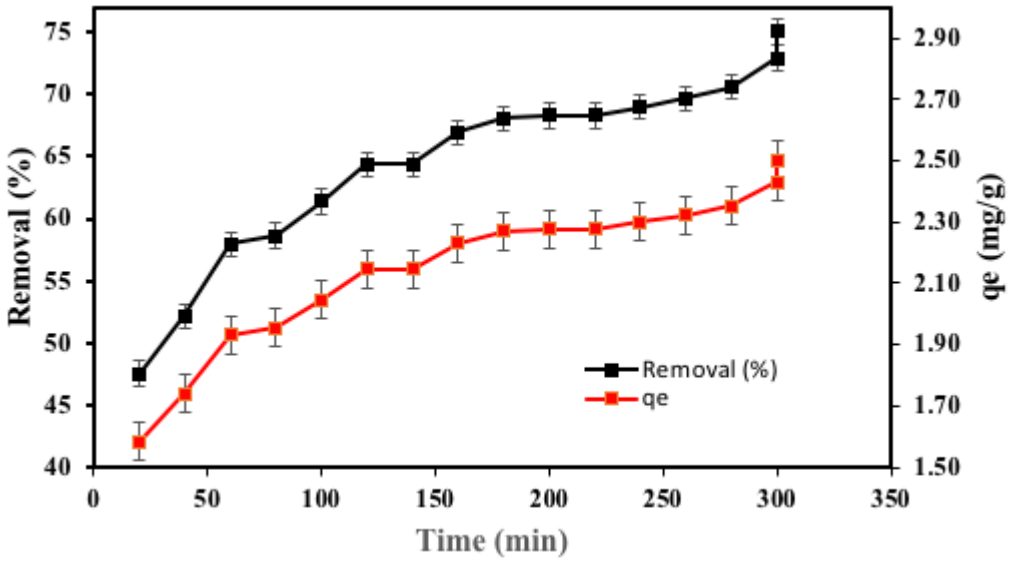


Fig. 4. 14: Effect of contact time on the adsorption capacity and removal percentage of CR onto the semi-IPN PVA-ALG-BENT nanocomposite hydrogel beads (C_0[CR] = 100 mg/L, V = 50 mL, beads dosage = 1.5 g, pH = 3, t = 20-320 min, T = 30 ºC).

4.1.4.3. Effect of Initial Dye Concentration

In batch adsorption, the initial concentration of the adsorbate molecules is the main driving force offsetting the mass diffusion resistance force (Fernandes et al., 2018)

i. Effect of Initial MB Concentration

The influence of the initial concentration of MB on adsorption capacity and removal percentage of MB is shown in Table (4.6) and Fig. (4.15). It was noticed that with increasing the initial MB concentration, the dye adsorption capacity increased while the removal percentage declined. For instance, when the initial concentration of MB was 50, 200 and 300 mg/L, the removal rate of beads was about 97, 85 and 69%, respectively. This indicated that at low concentration of MB, nanocomposite hydrogel beads

had an abundance of adsorption active sites leading to a high adsorption for most MB molecules (Su et al., 2019). Saturation of adsorption sites would be reached by further increases in the MB concentration, and thus adsorption become difficult because of the repulsion between MB molecules attached to the surface of the beads and the free MB molecules in the solution (Belhouchat et al., 2017b; N. Hou et al., 2020a; Su et al., 2019).

Table (4. 6): Effect of initial MB concentration on the adsorption capacity and removal percentage of MB onto the semi-IPN PVA-ALG-BENT nanocomposite hydrogel beads

MB Removal (V = 50 mL; initial concentration = 50-350 mg/L; pH= 8; beads dosage =1.5 g; temp= 30 ºC; time = 300 min, wavelength = 663 nm)						
MB initial Concentration = 50 (mg/L)						
Time (min)	**MB Concentrations (mg/L)**			**MB Average Concentration (mg/L)**	**MB % Removal**	**Q_e ± SD (mg/g)**
	Trail 1	**Trail 2**	**Trail 3**			
20	31.3	31.3	29.9	31.	36.9±3.0	0.615±0.05
40	26.7	26.7	16.9	22.7	54.5±10.0	0.900±0.2
60	18.8	18.8	10.2	15.7	68.5±9.0	1.14±0.2
80	8.33	8.33	6.28	7.40	85.2±2.0	1.42±0.03
100	6.59	6.59	4.37	5.73	88.5±2.0	1.48±0.04

120	5.23	5.23	2.18	3.87	92.3±3.0	1.54±0.05
140	3.16	3.16	1.59	2.54	94.9±1.0	1.58±0.03
160	2.06	2.06	1.37	1.79	96.4±0.7	1.61±0.01
180	1.68	1.68	1.17	1.48	97.0±0.5	1.62±0.009
200	1.45	1.45	0.795	1.19	97.6±0.7	1.63±0.01
220	1.19	1.19	0.738	1.02	97.9±0.5	1.63±0.008
240	1.04	1.04	0.715	0.939	98.1±0.4	1.63±0.006
260	0.9900	0.990	0.695	0.884	98.2±0.3	1.64±0.005
280	0.910	0.910	0.654	0.805	98.4±0.3	1.64±0.004
300	0.870	0.870	0.606	0.775	98.4±0.3	1.64±0.005
MB initial Concentration = 100 (mg/L)						
Time (min)	**MB Concentrations (mg/L)**			**MB Average Concentration (mg/L)**	**MB % Removal**	**Q_e ± SD (mg/g)**

	Trail 1	Trail 2	Trail 3			
20	78.9	71.2	68.4	72.8	27.2±5.0	0.905±0.2
40	51.8	51.9	48.6	50.8	49.2±2.0	1.64±0.06
60	43.9	39.0	30.1	37.7	62.1±7.0	2.08±0.2
80	31.6	31.1	28.4	30.4	69.6±2.0	2.32±0.06
100	33.01	24.9	19.1	25.8	74.3±7.0	2.48±0.2
120	19.5	16.9	19.2	18.5	81.5±1.0	2.72±0.05
140	12.8	16.2	10.0	13.0	86.9±3.0	2.89±0.1
160	12.3	8.12	10.0	10.2	89.8±2.0	2.99±0.07
180	7.08	7.72	9.64	8.15	91.0±1.0	3.06±0.04
200	6.53	6.81	6.17	6.50	93.5±0.3	3.12±0.01
220	5.96	5.29	5.70	5.65	94.34±0.3	3.14±0.01

240	5.89	3.10	2.27	3.75	96.2±2.0	3.21±0.06
260	3.337	3.36	2.57	3.09	96.9±0.4	3.23±0.01
280	2.55	2.70	2.61	2.62	97.4±0.07	3.25±0.003
300	2.49	2.52	2.18	2.39	97.6±0.2	3.25±0.006
MB initial Concentration = 150 mg/L						
Time (min)	**MB Concentrations (mg/L)**			**MB Average Concentration (mg/L)**	**MB % Removal**	**Q_e ± SD (mg/g)**
	Trail 1	**Trail 2**	**Trail 3**			
20	119	110	120	117	21.9±3.0	1.09±0.2
40	93.9	94.3	86.2	91.5	39.0±3.0	1.95±0.2
60	73.8	70.3	72.4	72.1	51.9±1.0	2.59±0.06
80	57.9	53.9	50.1	53.9	64.0±2.0	3.20±0.1
100	48.7	48.2	43.6	46.8	68.8±2.0	3.438±0.09

120	39.6	41.3	33.7	38.2	74.6±2.0	3.728±0.1
140	28.6	29.2	31.2	29.6	80.2±0.9	4.012±0.05
160	17.9	17.3	19.7	18.3	87.8±0.8	4.39±0.04
180	15.1	14.7	15.1	14.9	90.0±0.2	4.50±0.01
200	12.5	11.7	14.3	12.8	91.4±0.9	4.57±0.04
220	10.1	10.4	10.8	10.4	93.0±0.2	4.65±0.01
240	9.00	9.18	8.63	8.94	94.0±0.2	4.70±0.01
260	6.67	7.73	5.43	6.61	95.6±0.8	4.78±0.04
280	6.55	7.48	5.15	6.39	95.7±0.7	4.79±0.04
300	4.03	4.34	4.06	4.14	97.2±0.1	4.86±0.01
MB initial Concentration = 200 mg/L						
Time (min)	**MB Concentrations (mg/L)**			**MB Average Concentration (mg/L)**	**MB % Removal**	**Q_e ± SD (mg/g)**

	Trail 1	Trail 2	Trail 3			
20	128	140	154	141	29.4±6.39	1.96±0.4
40	125	120	121	122	38.9±1.28	2.60±0.09
60	92.5	102	92.9	95.7	52.1±2.62	3.48±0.1
80	87.9	80.1	73.8	80.6	59.7±3.0	3.98±0.2
100	80.1	64.6	51.9	65.6	67.2±7.0	4.40±0.4
120	61.5	58.4	44.7	54.9	72.6±4.0	4.84±0.3
140	58.44	55.34	23.2	45.9	77.0±10.0	5.14±0.6
160	47.6	42.9	25.8	38.8	80.0±6.0	5.37±0.4
180	31.2	33.8	28.7	31.2	84.4±1.0	5.6±0.08
200	23.0	21.5	28.3	24.3	87.9±2.0	5.86±0.1
220	21.5	18.38	19.5	19.8	90.1±0.8	6.01±0.05

240	19.2	16.9	13.9	16.7	91.7±1.0	6.11±0.09
260	16.1	13.7	10.9	13.6	93.2±1.0	6.21±0.09
280	13.7	12.2	8.09	11.3	94.3±1.0	6.29±0.1
300	12.6	10.6	6.54	9.95	95.0±1.0	6.34±0.1
320	11.4	9.87	4.14	8.48	95.8±2.0	6.38±0.1
MB initial Concentration = 250 mg/L						
Time (min)	**MB Concentrations (mg/L)**			**MB Average Concentration (mg/L)**	**MB % Removal**	**Q_e ± SD (mg/g)**
	Trail 1	**Trail 2**	**Trail 3**			
20	235	244	215	231	7.46±6.0	0.622±0.5
40	179	180	191	183	26.8±2.0	2.23±0.2
60	147	139.0	163	149	40.1±5.0	3.35±0.4
80	124	128	135	129	48.51±2.0	4.04±0.2

100	119	109	109	112	55.1±2.0	4.59±0.2
120	98.7	103	94.9	98.9	60.4±1.0	5.03±0.1
140	88.1	86.8	79.1	84.7	66.1±1.9	5.51±0.2
160	70.0	67.9	68.2	68.7	72.5±0.4	6.04±0.03
180	62.7	63.6	67.	64.5	74.2±0.9	6.18±0.08
200	56.3	55.7	56.0	56.0	77.6±0.1	6.47±0.01
220	47.8	45.0	49.6	47.5	81.0±0.90	6.75±0.08
240	45.8	44.7	42.7	44.4	82.2±0.60	6.85±0.05
260	39.7	39.0	41.4	40.0	84.0±0.5	6.99±0.04
280	36.0	36.5	42.5	38.3	84.7±1.0	7.06±0.1
300	32.6	32.6	34.4	33.2	86.7±0.4	7.23±0.04
MB initial Concentration = 300 mg/L						
	MB Concentrations				**MB**	**Q_e ± SD**

Time (min)	(mg/L)			MB Average Concentration (mg/L)	% Removal	(mg/g)
	Trail 1	Trail 2	Trail 3			
20	266	260	240	255	15.0±4.0	1.50±0.4
40	237	229	210	22	24.8±4.6	2.48±0.4
60	207	197	168	191	36.4±6.8	3.64±0.6
80	185	175	144	168	44.1±7.0	4.41±0.7
100	156	150	117	141	52.9±6.0	5.29±0.7
120	154	146	115	138	53.9±6.0	5.39±0.7
140	137	133	94.8	122	59.5±7.0	5.95±0.8
160	127	124	88.5	11	62.2±7.0	6.22±0.7
180	117	115	69.6	100	66.5±9.0	6.65±0.9
200	105	112	70.5	95.7	68.1±7.0	6.81±0.7

220	95.7	93.8	79.7	89.7	70.1±2.0	7.01±0.3
240	83.1	81.	77.5	80.6	73.1±0.9	7.31±0.09
260	69.9	72.42	73.0	71.8	76.1±0.5	7.62±0.06
280	65.2	66.4	65.8	65.8	78.1±0.2	7.81±0.02
300	54.8	51.0	52.9	52.9	82.4±0.6	8.24±0.06
320	54.2	54.2	57.0	55.1	81.6±0.5	8.16±0.05
340	52.3	52.0	55.4	53.2	82.3±0.6	8.23±0.06
360	50.4	50.7	47.2	49.4	83.5±0.6	8.32±0.06
MB initial Concentration = 350 mg/L						
Time (min)	**MB Concentrations (mg/L)**			**MB Average Concentration (mg/L)**	**MB % Removal**	**Q_e ± SD (mg/g)**
	Trail 1	**Trail 2**	**Trail 3**			
20	318	309	298	308	11.8±2.0	1.37±0.3

40	272	265	250	263	24.9±3.0	2.91±0.3
60	217	207	236	220	37.0±4.0	4.32±0.5
80	197	198	198	198	43.4±0.3	5.06±0.03
100	192	176	195	188	46.3±2.0	5.40±0.3
120	168	162	160	164	53.2±1.0	6.21±0.1
140	156	147	139	147	57.9±2.0	6.76±0.2
160	148	139	122	137	60.9±3.0	7.11±0.4
180	134	126	108	122	65.0±3.0	7.58±0.4
200	127	118	110	118	66.2±2.0	7.72±0.2
220	114	107	94.7	105	69.9±2.0	8.16±0.3
240	106	98.9	95.1	100	71.3±1.0	8.32±0.1
260	101	94.5	83.8	93.2	73.4±2.0	8.56±0.2
280	90.9	84.7	74.6	83.4	76.2±2.0	8.89±0.2

300	80.6	79.0	73.7	77.7	77.8±1.0	9.07±0.1
320	78.1	69.6	69.6	72.4	79.3±1.0	9.25±0.1
340	69.6	64.5	57.6	63.9	81.7±1.0	9.54±0.2
360	64.6	63.9	66.1	64.9	81.5±0.3	9.50±0.03

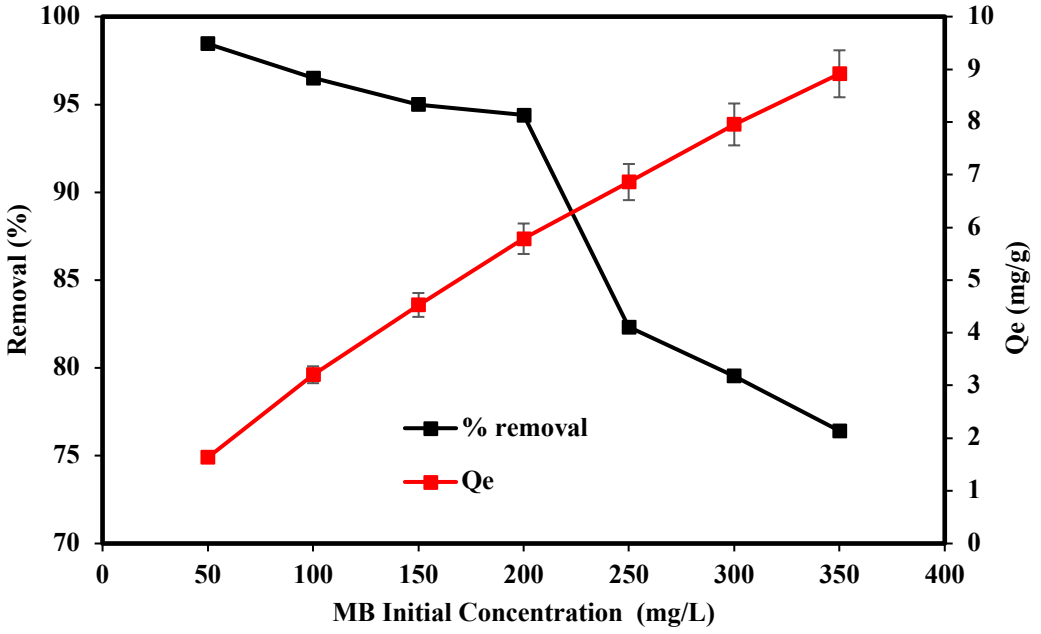


Fig. 4. 15: Effect MB initial concentration on the adsorption capacity and removal percentage of MB onto the semi-IPN PVA-ALG-BENT nanocomposite hydrogel beads (C_0[MB] = 50-350 mg/L, V = 50 mL, beads dosage = 1.5 g, pH = 8, t = 350 min, T = 30 ºC).

ii. Effect of Initial CR Concentration

Initial concentration of CR plays an important role in adsorption process and mass diffusion resistance force. Fig. 4.16 and Table (4.7) show the effect of initial concentration of CR on adsorption capacity of PVA-ALG-BENT composite and % removal of CR. Increasing the concentration of CR from 20 to 100 ppm, increased the adsorption capacity of PVA-ALG-BENT composite from 0.590 mg/g to 2.430 mg/g, respectively. The adsorption capacity of a given mass of adsorbent can adsorb a fixed concentration of adsorbate molecules and the removal rate of the adsorbate is influenced by the flow of adsorbate molecule from the aqueous adsorption system to the interior site of the adsorbent (A. Ahmad et al., 2009). Therefore, at higher concentration

of CR (before the saturation of adsorbent active site) more CR molecule adsorbed on the surface of adsorbent (Banerjee & Chattopadhyaya, 2017a). However, increasing the initial concentration of CR from 20 to 100 ppm decreased the removal efficiency, this can be explained due to the saturation of the available active sites of the adsorbent (Mahmoud et al., 2012).

Table (4. 7): Effect of initial CR concentration on the adsorption capacity and removal percentage of CR onto the semi-IPN PVA-ALG-BENT nanocomposite hydrogel beads.

CR Removal (V = 50 mL; initial concentration = 100 mg/L; pH= 3; beads dosage =1.5 g; temp= 30 ºC; time = 300 min, wavelength = 446 nm)						
CR initial Concentration = 20 mg/L						
Time (min)	**CR Concentrations (mg/L)**			**CR Average Concentration (mg/L)**	**CR % Removal**	**Q_e ± SD (mg/g)**
	Trail 1	**Trail 2**	**Trail 3**			
20	11.69	12.85	12.27	12.27	38.7±2.0	0.260±0.02
40	9.65	10.52	10.52	10.23	48.8±2.0	0.330±0.02
60	9.35	9.81	9.58	9.58	52.1±1.0	0.350±0.01
80	8.65	9.35	9.35	9.12	54.4±2.0	0.360±0.01
100	8.19	8.88	8.19	8.42	57.9±2.0	0.390±0.01
120	5.16	5.86	5.16	5.40	73.0±2.0	0.490±0.01

140	5.14	4.91	5.37	5.14	74.3±1.0	0.500±0.01
160	4.56	4.67	5.14	4.79	76.1±1.0	0.510±0.01
180	3.51	3.63	4.09	3.74	81.3±1.0	0.540±0.01
200	3.16	3.40	3.98	3.51	82.4±2.1	0.550±0.01
220	2.81	3.05	3.63	3.16	84.2±2.1	0.56±0.01
240	2.74	3.03	3.15	2.98	85.1±1.0	0.570±0.01
260	2.80	2.91	2.85	2.85	85.7±0.2	0.570±0.0
280	2.74	2.86	2.98	2.86	85.7±0.5	0.570±0.0
300	2.24	2.21	2.47	2.31	88.5±0.7	0.590±0.0
CR initial Concentration = 40 mg/L						
Time (min)	**CR Concentrations (mg/L)**			**CR Average Concentration (mg/L)**	**CR % Removal**	**Q_e ± SD (mg/g)**
	Trail 1	**Trail 2**	**Trail 3**			
20	21.1	19.9	20.1	20.4	49.1±1.0	0.650±0.02
40	19.2	17.8	18.5	18.5	53.8±1.0	0.720±0.02
60	18.0	16.6	18.0	17.5	56.2±2.0	0.750±0.03

80	14.9	15.2	16.1	15.4	61.5±1.0	0.820±0.02
100	14.9	14.5	15.4	14.9	62.6±1.0	0.840±0.02
120	12.8	13.5	14.9	13.8	65.6±2.0	0.870±0.04
140	11.6	12.4	13.8	12.6	68.5±2.0	0.910±0.04
160	10.7	11.4	12.8	11.65	70.9±2.0	0.950±0.04
180	10.0	10.7	12.1	10.9	72.6±2.0	0.970±0.04
200	10.2	11.2	11.4	10.9	72.±1.0	0.970±0.03
220	9.53	10.47	11.4	10.5	73.82±2.0	0.980±0.03
240	8.82	8.35	10.7	9.29	76.8±3.0	1.02±0.04
260	8.59	7.65	6.00	7.41	81.5±3.0	1.09±0.04
280	5.59	5.82	6.06	5.82	85.4±0.5	1.14±0.01
300	6.06	5.82	4.88	5.59	86.0±1.0	1.15±0.02
CR initial Concentration = 60 mg/L						
Time (min)	**CR Concentrations (mg/L)**			**CR Average Concentration (m/gL)**	**CR % Removal**	**Q_e ± SD (mg/g)**
	Trail 1	**Trail 2**	**Trail 3**			

20	32.6	32.1	30.9	31.9	46.9±1.0	0.940±0.03
40	29.1	29.1	26.9	28.4	52.8±2.0	1.05±0.04
60	27.2	26.7	24.1	26.00	56.7±2.0	1.13±0.05
80	24.8	24.6	20.1	23.2	61.4±4.0	1.23±0.09
100	24.8	23.6	19.7	22.7	62.2±4.0	1.24±0.09
120	24.1	22.5	18.7	21.8	63.7±4.0	1.27±0.09
140	22.5	22.7	18.7	21.3	64.5±3.0	1.29±0.07
160	23.7	21.8	18.5	21.3	64.5±4.0	1.29±0.09
180	21.29	19.6	15.9	18.9	68.4±4.0	1.37±0.09
200	21.1	20.1	13.5	18.2	69.6±6.0	1.39±0.1
220	20.4	21.1	12.6	18.0	70.0±7.0	1.40±0.2
240	14.	15.7	17.76	16.1	73.1±2.0	1.46±0.05
260	14.00	13.3	9.06	12.1	79.8±4.0	1.60±0.09
280	9.76	11.7	11.4	10.9	81.8±1.0	1.64±0.03
300	10.0	12.1	8.59	10.2	82.9±3.0	1.66±0.06
CR initial Concentration =80 mg/L						

Time (min)	CR Concentrations (mg/L)			CR Average Concentration (mg/L)	CR % Removal	Q_e ± SD (mg/g)
	Trail 1	Trail 2	Trail 3			
20	48.8	47.6	44.4	46.9	41.4±3.0	1.10±0.08
40	41.8	40.7	37.5	40.0	50.0±3.0	1.33±0.08
60	33.8	32.6	29.4	31.9	60.1±3.0	1.60±0.08
80	31.7	31.5	29.2	30.8	61.5±2.0	1.64±0.05
100	29.4	27.1	29.6	28.7	64.1±2.0	1.71±0.05
120	28.9	28.0	27.8	28.2	64.7±0.7	1.73±0.02
140	27.3	27.8	24.8	26.6	66.7±2.0	1.78±0.05
160	26.4	26.6	24.8	25.9	67.6±1.0	1.80±0.03
180	30.5	25.9	20.7	25.7	67.9±6.0	1.81±0.1
200	25.9	26.4	22.0	24.8	69.0±3.0	1.84±0.08
220	23.6	24.33	25.7	24.6	69.3±1.0	1.85±0.04
240	23.4	23.2	23.0	23.2	71.0±0.2	1.89±0.01
260	21.8	21.1	13.5	18.8	76.5±5.0	2.04±0.1

280	20.4	19.5	15.1	18.3	77.1±3.0	2.06±0.09
300	20.4	19.5	10.9	17.0	78.8±6.0	2.10±0.1
CR initial Concentration = 100 mg/L						
Time (min)	**CR Concentrations (mg/L)**			**CR Average Concentration (mg/L)**	**CR % Removal**	**Q_e ± SD (mg/g)**
	Trail 1	**Trail 2**	**Trail 3**			
20	55.9	51.1	50.4	52.4	47.6±3.0	1.59±0.1
40	51.3	49.0	43.2	47.8	52.2±4.0	1.74±0.1
60	45.5	43.7	37.0	42.1	57.9±4.0	1.93±0.1
80	44.8	42.8	36.5	41.4	58.6±4.0	1.95±0.1
100	42.1	40.5	33.3	38.6	61.4±4.0	2.05±0.1
120	39.5	37.7	29.6	35.6	64.4±5.0	2.15±0.2
140	39.8	37.5	29.6	35.6	64.4±5.0	2.15±0.2
160	37.5	34.7	27.1	33.1	66.9±5.0	2.23±0.2
180	36.3	33.6	25.9	31.9	68.1±5.0	2.27±0.2
200	35.9	33.3	25.9	31.7	68.3±5.0	2.28±0.2

220	35.6	33.3	26.2	31.7	68.3±5.0	2.28±0.2
240	34.7	32.9	25.5	31.0	69.0±5.0	2.30±0.2
260	33.8	32.2	25.0	30.3	69.7±5.0	2.32±0.1
280	32.9	31.7	23.6	29.4	70.6±7.0	2.35±0.2
300	31.7	30.6	19.0	27.1	72.9±5.0	2.43±0.2

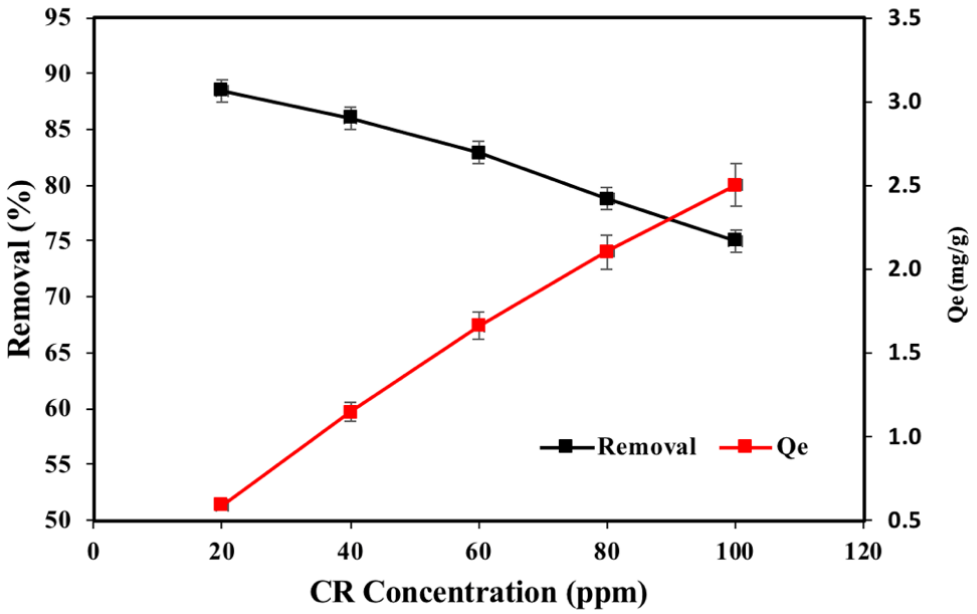


Fig. 4. 16: Effect CR initial concentration on the adsorption capacity and removal percentage of CR onto the semi-IPN PVA-ALG-BENT nanocomposite hydrogel beads (C_0[CR] = 20-100 mg/L, V = 50 mL, beads dosage = 1.5 g, pH = 3, t = 350 min, T = 30 ºC).

4.1.4.4. Effect of Adsorbent Dosage

Adsorbent dosage optimization is another important parameter in dye adsorption system to minimize the use of excess adsorbent's dosage and ensure the maximum adsorption efficiency (Su et al., 2019). Herein, dosage optimization is done by changing the mass of adsorbent from 0.1-2.0 g for MB at pH 8.0 and 200 ppm MB concentration and temperature at 30 °C. While for CR the dosages of adsorbent were varied from 0.1-1.0 g, at pH 3.0, 100 ppm initial CR concentration and temperature at 30°C (Su et al., 2019). In both dyes' cases, it was observed that the % removal increases as the adsorbent dosage increases. With further increase in dose, no effect of adsorption rate was found. The enhancement in % removal may be because of the increase in the available adsorption sites at the

surface of the adsorbent, which increases the adsorption of dye molecules. The corresponding findings with each dye are presented below:

i. Effect of Adsorbent Dosage on the removal of MB

Table (4.8) and Fig. 4.17 illustrate the effects of adsorbent dosage on the adsorption capacity and removal percentage of the nanocomposite beads towards MB. The adsorption capacity of and the removal % of the hydrogel nanocomposites toward MB were 50.0 mg/g, and 54.0 %, respectively. When increasing beads dosage above 0.10 g, the adsorption capacity decreased and the dye removal % increased. The equilibrium is reached at bead dosage of 1.50 g with maximum removal of 94.64%. This is because at higher adsorbent dosage and constant MB initial concentration , more available active sites of adsorbents are remained unsaturated during the adsorption of MB molecules , resulting in a decrease in the amount of dye adsorbed per unit surface area (Belhouchat et al., 2017b; Su et al., 2019). Accordingly, the optimal beads dosage for MB removal was set as 1.5 g.

Table (4. 8): Effect of adsorbent dosage on the adsorption capacity and removal percentage of MB onto the semi-IPN PVA-ALG-BENT nanocomposite hydrogel beads

MB Removal (V = 50 mL; initial concentration = 200 mg/L; pH= 8; beads dosage =0.1-2.0 g; temp= 30 ºC; time = 300 min, wavelength = 663 nm)						
Adsorbent Dosage (g)	**MB Concentrations (m/gL)**			**MB Average Concentration (m/gL)**	**MB % Removal**	**Q_e ± SD (mg/g)**
	Trail 1	**Trail 2**	**Trail 3**			
0.1010	90.3	103	96.4	96.4	51.8±3.0	51.3±3.0
0.2030	87.4	99.5	95.1	94.0	53.0±3.0	26.0±1.0
0.3030	75.6	87.6	87.8	83.6	58.2±3.0	19.2±1.0
0.4020	67.1	80.9	82.9	76.9	61.5±4.0	15.3±1.0
0.5050	64.8	74.4	81.2	73.4	63.3±4.0	12.5±0.8
0.6020	63.2	69.0	74.4	68.9	65.6±2.0	10.9±0.4
0.7030	55.6	57.9	57.9	57.2	71.4±0.6	10.2±0.09
0.8050	51.7	50.9	51.5	51.4	74.3±0.2	9.23±0.03

0.9030	44.5	44.8	43.76	44.4	77.8±0.2	8.62±0.03
1.004	36.4	36.8	35.69	36.3	81.8±0.2	8.15±0.03
1.100	24.8	25.4	25.1	25.1	87.5±0.1	7.95±0.01
1.200	23.5	21.4	21.6	22.2	88.9±0.6	7.41±0.05
1.300	20.3	19.9	16.66	19.0	90.5±1.0	6.96±0.07
1.400	15.29	14.8	11.6	13.9	93.0±1.0	6.65±0.08
1.500	12.84	11.8	8.87	11.2	94.4±1.0	6.29±0.07
1.600	11.5	11.2	9.03	10.6	94.7±0.6	5.92±0.04
1.700	11.2	10.6	12.2	11.3	94.3±0.4	5.55±0.03
1.800	9.18	8.57	9.79	9.18	95.4±0.3	5.30±0.02
1.900	7.96	7.80	17.3	11.0	94.5±2.0	4.97±0.1
2.000	8.41	6.58	8.87	7.90	96.0±0.6	4.80±0.0

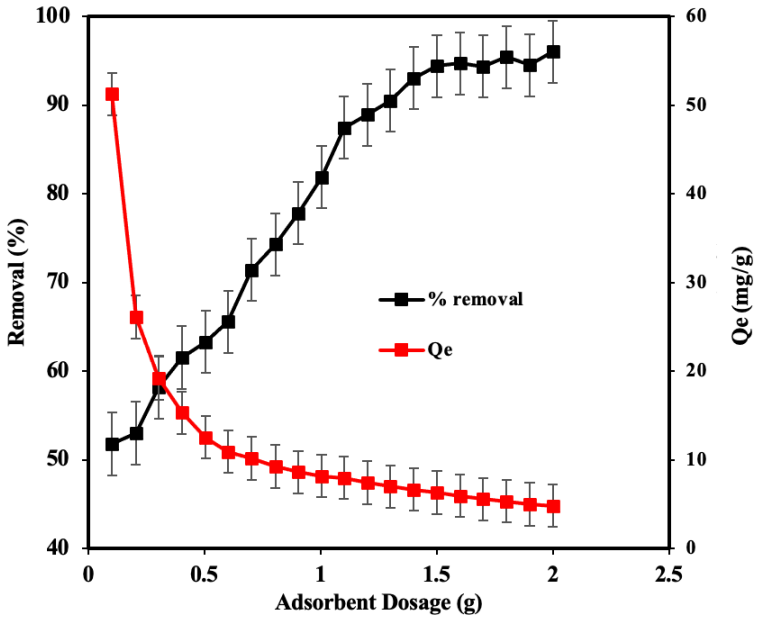


Fig. 4. 17: Effect of adsorbent dosage on the adsorption capacity and removal percentage of MB onto the semi-IPN PVA-ALG-BENT nanocomposite hydrogel beads (C0[MB] = 200 mg/L, V = 50 mL, beads dosage = 0.1-2.0 g, pH = 8, t = 350 min, T = 30 ºC).

ii. Effect of Adsorbent Dosage on the removal of CR

Table (4.9) and Fig. 4.18 reveal the effect of adsorbent dosage on CR adsorption. An increase in adsorbent dosage from 0.2 to 2.0 g resulted in an increase in % removal of CR from 64.77% to 80.517%, implying that the large dose of the adsorbent could adsorbed more dye molecules due to the existence of more active sites on adsorbents' surface (Sumanjit et al., 2015). Therefore, 1.5 g/L was chosen as the optimum adsorbent dosage for adsorption experiments. Contrarily, the equilibrium capacity—of the adsorbent decreased as the adsorbent mass increased from 0.2 to 2.0 g, which is due to the increasing of the active sites as the dosage of adsorbent is increased (Dutta et al., 2021).

Table (4. 9): Effect of adsorbent dosage on the adsorption capacity and removal percentage of MB onto the semi-IPN PVA-ALG-BENT nanocomposite hydrogel beads

CR Removal (V = 50 mL; initial concentration = 100 mg/L; pH= 3; beads dosage =0.2-2.0 g; temp= 30 ºC; time = 300 min, wavelength = 446 nm)						
Adsorbent Dosage (g)	**CR Concentrations(mg/L)**			**CR Average Concentration (mg/L)**	**CR % Removal**	**Q_e ± SD (mg/g)**
	Trail 1	**Trail 2**	**Trail 3**			
0.2	36.7	31.8	37.2	35.2	64.8±3.0	16.2±0.7
0.4	34.2	30.3	35.3	33.3	66.7±2.0	8.34±0.3
0.6	33.2	29.9	36.0	33.0	66.9±3.0	5.58±0.3
0.8	31.8	29.0	32.1	30.9	69.0±1.7	4.31±0.1
1	31.3	28.7	31.2	30.4	69.6±1.0	3.48±0.07
1.2	28.8	27.1	26.7	27.5	72.5±1.0	3.02±0.05
1.5	20.6	23.6	30.6	24.9	75.1±5.0	2.50±0.1
1.6	19.5	18.1	23.3	20.3	79.7±2.0	2.49±0.08
1.8	18.9	17.5	22.9	19.8	80.2±3.0	2.23±0.08
2	18.7	17.4	22.4	19.5	80.5±2.0	2.01±0.08

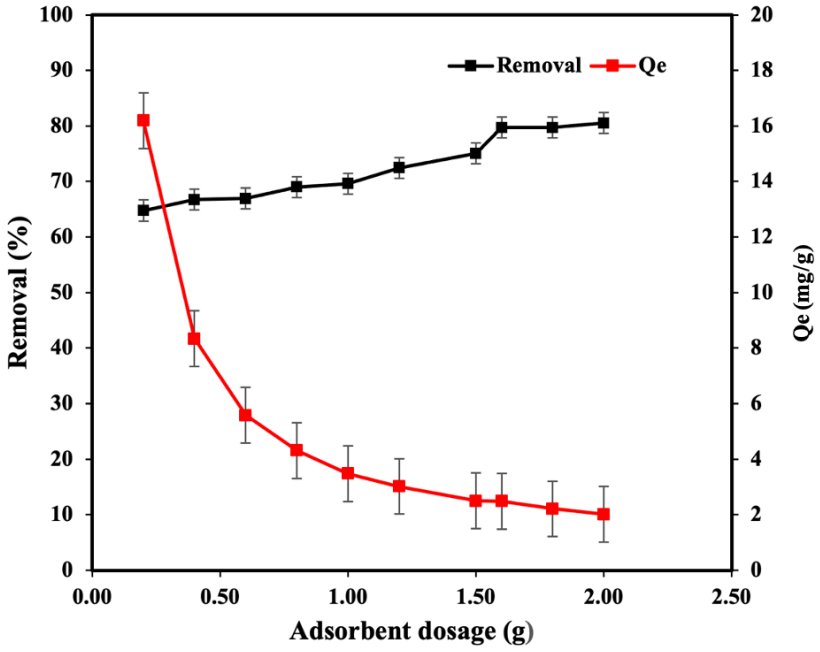


Fig. 4. 18: Effect of adsorbent dosage on the adsorption capacity and removal percentage of CR onto the semi-IPN PVA-ALG-BENT nanocomposite hydrogel beads (C_0[CR] = 100 mg/L, V = 50 mL, beads dosage = 0.1-2.0 g, pH = 3, t = 300 min, T = 30 ºC).

4.1.4.5. Effect of Temperature

The influence of temperature on the removal rate is an important factor to investigate dye adsorption in industrial wastewater at different temperatures (N. Hou et al., 2020a; Wu et al., 2019).

i. Effect of Temperature on the removal of MB

The removal percentage of MB by the nanocomposites at different temperatures ranging from 20-50 °C was investigated and the results are presented in Table (4.10) and Fig. 4.19. The results revealed that the removal percentage increased as the temperature increased from 20 to 30 ºC and reached 95.0 % after 200 min at 30 ºC, while it reached 90.0 % at 20 ºC after 300 min. However, the removal percentages of MB at 40 ºC and 50 ºC were unsignificant compared with that at 30 ºC. This finding was

attributed to the increased mobility of the MB molecules at high temperature, which enhanced the penetration of MB molecules to the interior of hydrogel beads and hence improve the removal percentage (Hu et al., 2018; Z. H. Zhang et al., 2021a). This observation confirmed the endothermic nature of the adsorption of dyes process (Z. H. Zhang et al., 2021a) . Hence, 30 ºC was chosen as the optimum solution temperature.

Table (4. 10): Effect of temperature on the adsorption capacity and removal percentage of MB onto the semi-IPN PVA-ALG-BENT nanocomposite hydrogel beads

MB Removal (V = 50 mL; initial concentration = 200 mg/L; pH= 8; beads dosage =1.5 g; temp= 20-50 ºC; time = 320 min, wavelength = 663 nm)						
Temperature 20 ºC						
Time (min)	**MB Concentrations (mg/L)**			**MB Average Concentration (mg/L)**	**MB % Removal**	**Q_e ± SD (mg/g)**
	Trail 1	**Trail 2**	**Trail 3**			
20	150	136	137	141	29.4±3.9	1.96±0.260
40	139	129	97.4	122	38.9±10.9	2.59±0.727
60	101	98.8	86.4	95.7	52.1±4.09	3.48±0.273
80	93.7	82.1	65.9	80.6	59.1±6.98	3.98±0.467
100	78.7	77.3	40.6	65.5	67.2±10.8	4.48±0.720
120	61.8	64.6	38.2	54.9	72.6±7.27	4.84±0.485
140	53.9	52.5	31.2	45.9	77.0±6.37	5.14±0.425

160	42.5	42.9	30.9	38.8	80.6±3.0	5.37±0.2
180	39.9	31.0	22.7	31.2	84.4±4.0	5.63±0.3
200	26.5	23.9	22.3	24.3	87.9±1.0	5.85±0.07
220	22.1	19.7	17.5	19.8	90.1±1.0	6.01±0.07
240	17.1	17.8	15.1	16.7	91.6±0.7	6.11±0.04
260	14.4	13.5	12.9	13.6	93.2±0.4	6.21±0.02
280	12.6	11.8	9.64	11.3	94.3±0.8	6.29±0.05
300	10.1	10.5	9.25	9.95	95.0±0.3	6.33±0.02
320	10.0	10.2	5.14	8.4	95.8±1.0	6.38±0.09
Temperature 30 ºC						
Time (min)	**MB Concentrations (mg/L)**			**MB Average Concentration (mg/L)**	**MB % Removal**	**Q_e ± SD (mg/g)**
	Trail 1	**Trail 2**	**Trail 3**			
20	116	138	101	118	40.7±9.0	2.71±0.6
40	78.4	83.1	69.7	77.1	61.4±3.0	4.09±0.2
60	55.8	51.1	51.4	52.8	73.6±1.0	4.91±0.08

80	44.3	43.4	38.1	41.9	79.0±1.0	5.27±0.1
100	35.8	34.4	24.5	31.6	84.2±3.0	5.61±0.2
120	26.2	25.4	15.6	22.4	88.8±3.0	5.92±0.2
140	19.2	15.9	13.0	16.0	91.9±1.0	6.13±0.1
160	12.9	11.6	13.7	12.7	93.6±0.5	6.24±0.03
180	11.1	10.5	9.73	10.4	94.8±0.3	6.32±0.02
200	9.29	8.04	8.58	8.64	95.7±0.3	6.38±0.02
220	6.86	5.96	6.86	6.56	96.7±0.3	6.45±0.02
240	6.26	5.19	5.69	5.72	97.1±0.3	6.48±0.02
260	5.22	5.03	4.84	5.03	97.4±0.09	6.49±0.006
280	5.00	4.68	3.85	4.51	97.7±0.3	6.51±0.02
300	4.71	4.11	3.64	4.16	97.9±0.3	6.53±0.02
Temperature 40 ºC						
Time (min)	**MB Concentrations (mg/L)**			**MB Average Concentration (mg/L)**	**% Removal**	**Q_e ± SD (mg/g)**
	Trail 1	**Trail 2**	**Trail 3**			
20	0.41	0.38	0.445	107.75	46.1±4.0	3.08±0.3

40	0.243	0.289	0.242	65.88	67.0±3.0	4.47±0.2
60	0.341	0.321	0.352	43.81	78.0±1.0	5.21±0.07
80	0.247	0.256	0.271	32.94	83.5±0.8	5.57±0.05
100	0.871	0.814	0.895	22.96	88.5±0.6	5.90±0.04
120	0.789	0.778	0.593	19.15	90.4±1.0	6.03±0.1
140	0.615	0.541	0.446	14.09	92.9±1.0	6.20±0.07
160	0.421	0.452	0.426	11.35	94.3±0.2	6.29±0.01
180	0.367	0.383	0.246	8.60	95.7±1.0	6.38±0.07
200	0.321	0.356	0.226	7.76	96.1±0.9	6.41±0.06
220	0.278	0.256	0.207	6.29	96.8±0.4	6.46±0.03
240	0.216	0.232	0.185	5.31	97.3±0.3	6.49±0.02
260	0.781	0.762	0.686	3.95	98.0±0.1	6.53±0.009
280	0.659	0.612	0.628	3.36	98.3±0.06	6.55±0.004
300	0.638	0.611	0.557	3.19	98.4±0.1	6.56±0.007
Temperature 50 ºC						
Time (min)	**MB Concentrations. (mg/L)**			**MB Average Concentration**	**MB**	**Q_e ± SD**

	Trail 1	Trail 2	Trail 3	(mg/L)	% Removal	(mg/g)
20	119	108.6	113	113	43.2±2.0	2.88±0.2
40	70.8	60.4	60.9	64.1	68.0±2.0	4.53±0.2
60	39.6	39.0	31.7	36.8	81.6±2.0	5.44±0.1
80	27.7	26.9	24.58	26.4	86.8±0.8	5.79±0.05
100	18.5	19.9	18.4	18.9	90.5±0.4	6.04±0.02
120	12.7	13.0	12.0	12.6	93.7±0.2	6.25±0.01
140	9.5	9.17	11.9	10.2	94.9±0.7	6.33±0.05
160	9.1	8.01	8.75	8.63	95.7±0.2	6.38±0.02
180	7.1	6.10	6.89	6.69	96.7±0.2	6.44±0.02
200	6.0	6.15	5.08	5.76	97.1±0.2	6.47±0.02
220	5.2	5.87	4.38	5.14	97.4±0.3	6.50±0.02
240	4.3	3.90	4.27	4.15	97.9±0.1	6.53±0.007
260	3.9	3.92	3.57	3.79	98.1±0.09	6.54±0.006
280	3.5	3.78	3.53	3.62	98.2±0.07	6.55±0.005
300	3.3	3.41	3.06	3.26	98.4±0.09	6.56±0.006

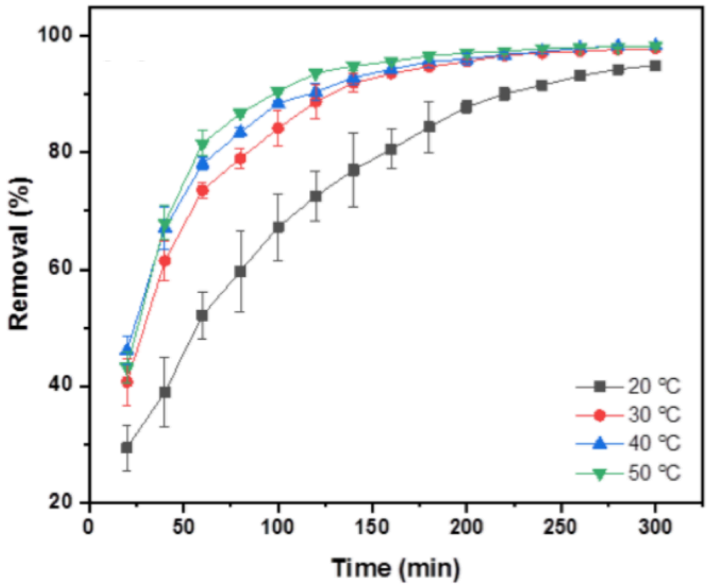


Fig. 4. 19: Effect of temperature on the adsorption capacity and removal percentage of MB onto the semi-IPN PVA-ALG-BENT nanocomposite hydrogel beads (C_0[MB] = 200 mg/L, V = 50 mL, beads dosage = 1.5 g, pH = 8, t = 300 min, T = 20-50 ºC).

ii. Effect of Temperature on the removal of CR

The effect of temperature on the adsorption of CR was studied at different temperatures ranging from 30 to 50 °C (Table (4.11) and Fig. 4.20). The results showed that as the temperature increased both the adsorption capacity of PVA-ALG-BENT hydrogel and removal efficiency of CR were increased. The removal efficiency reached 76% after 300 min at 50 °C, while at 20 °C and 300 min the removal efficiency reached 72.9 %. The obtained trend suggests the endothermic nature of the adsorption system and increasing the temperature increases the mobility of CR molecule and thus increases the interaction with the active sites of adsorbent's surface (Jain et al., 2021; Mahmoud et al., 2012).

Table (4. 11): Effect of temperature on the adsorption capacity and removal percentage of CR onto the semi-IPN PVA-ALG-BENT nanocomposite hydrogel beads.

CR Removal (V = 50 mL; initial concentration = 100 mg/L; pH= 3; beads dosage =1.5 g; temp= 30-50 ºC; time = 300 min, wavelength = 446 nm)						
Temp. (Cº)	**CR Conc. (mg/L)**			**CR Average Conc. (mg/L)**	**CR % Removal**	**Q_e ± SD (mg/g)**
	Trail 1	**Trail 2**	**Trail 3**			
30	20.6	23.6	30.6	24.9	75.0±5.0	2.50±0.1
40	19.4	22.6	24.3	22.1	77.9±2.0	2.60±0.08
50	18.9	22.1	20.5	20.5	79.5±1.0	2.65±0.05

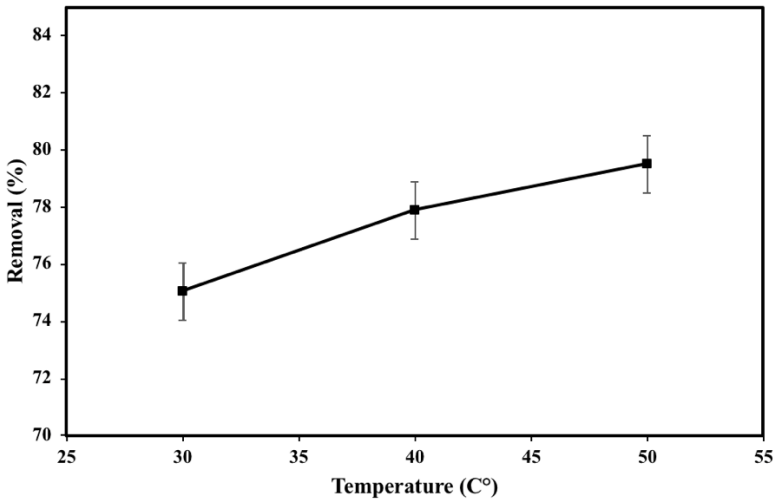


Fig. 4. 20: Effect of temperature on the adsorption capacity and removal percentage of CR onto the semi-IPN PVA-ALG-BENT nanocomposite hydrogel beads (C_0[CR] = 100 mg/L, V = 50 mL, beads dosage = 1.5 g, pH = 3, t = 300 min, T = 30-50 ºC).

4.1.5. Adsorbent Reusability Test

For a designed system to be accepted at industrial scale, the system should be economically feasible and reusable (Hong et al., 2021; Yadav et al., 2020). The prepared semi-IPN PVA-ALG-BENT nanocomposite beads can be easily separated from solution by simple separation technology, which provides the possibility for subsequent desorption and reuse.

4.1.5.1. Adsorbent Reusability Test for the removal of MB

The nanocomposite beads for the dyes were reused for six cycles, after washing with 0.1 M HCl solution. The reutilization was determined by the sorption-desorption cycles of the beads. As shown in Table (4.12) and Fig. 4.21, the beads had good adsorption effect on MB after one cycle, with a removal percentage of 94.32%. After number of cycles the removal percentage maintained at a steady value of about 90%, and the reuse efficiency (%) was found to be 77.86 % indicating that the adsorbent shows good structural stability and good application prospects because of the good adsorption performance, efficient reusability, and low cost. (RAVI & Pandey, 2019). Hence, the results obtained above indicate the possibility of using the semi-IPN PVA-ALG-BENT nanocomposites hydrogel beads at an industrial scale for the removal of MB from industrial wastewaters.

Table (4. 12): Reusability study onto the semi-IPN PVA-ALG-BENT nanocomposite hydrogel beads for the removal of MB

MB Removal (V = 50 mL; initial concentration = 200 mg/L; pH= 8; beads dosage =1.5 g; temp= 30 ºC; time = 320 min, wavelength = 663 nm)						
Number of cycles	**MB Conc. (mg/L)**			**MB Average Conc. (mg/L)**	**MB % Removal**	**Q_e ± SD (mg/g)**
	Trail 1	**Trail 2**	**Trail 3**			
1	20.2	9.62	3.83	11.2	94.4±4.0	6.23±0.2
2	9.68	9.41	7.86	8.98	95.5±0.4	6.37±0.03
3	49.0	47.0	84.92	60.	69.8±10.0	4.66±0.7
4	49.9	47.6	89.2	62.21	68.9±11.0	4.59±0.8
5	46.8	44.9	82.2	57.9	71.0±10.0	4.73±0.7
6	43.2	41.2	74.6	52.9	73.5±9.0	4.90±0.6

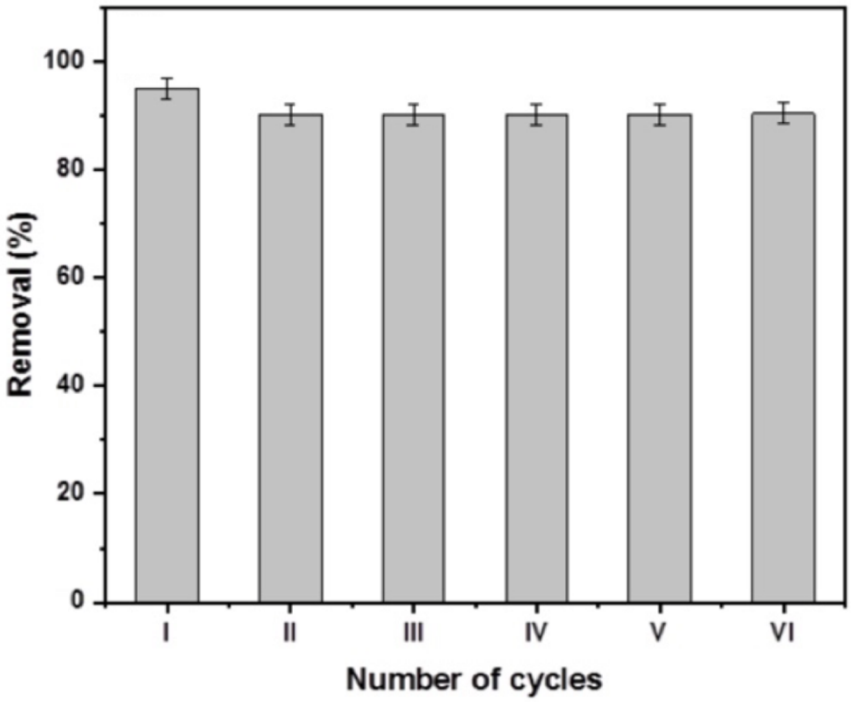


Fig. 4. 21: Reusability study of the semi-IPN PVA-ALG-BENT nanocomposite hydrogel beads for the removal of MB for five cycles (C_0[MB] = 200 mg/L, V = 50 mL, beads dosage = 1.5 g, pH = 8, t = 300 min, T = 30 ºC).

4.1.5.2. Adsorbent Reusability Test for CR

The reusability experiments showed the ability of the nanocomposite for the removal of CR dye up to five cycles. In the first cycle, about 75.0 % of the dye was removed in 300 min. During the five cycles, the % removal of dye decreased to 70.0 % and the reuse efficiency reached 95.0 % as shown in Table (4.13) and Fig. (4.22).

Table (4. 13): Reusability study of the removal of CR by the semi-IPN PVA-ALG-BENT nanocomposite hydrogel beads

CR Removal (V = 50 mL; initial concentration = 100 mg/L; pH= 3; beads dosage =1.5 g; temp= 30 ºC; time = 300 min, wavelength = 446 nm)						
Number of cycles	**Cr Concentrations (mg/L)**			**CR Average Concentration (mg/L)**	**CR % Removal**	**Q_e ± SD (mg/g)**
	Trail 1	**Trail 2**	**Trail 3**			
1	20.6	23.6	30.6	24.9	75.0±5.0	2.50±0.2
2	22.6	25.3	29.8	24.9	75.0±3.0	2.50±0.1
3	24.5	27.2	27.5	25.0	74.1±1.0	2.47±0.05
4	27.4	33.2	25.2	26.4	73.6±4.0	2.45±0.1
5	31.7	28.4	29.8	28.6	71.4±2.0	2.38±0.05

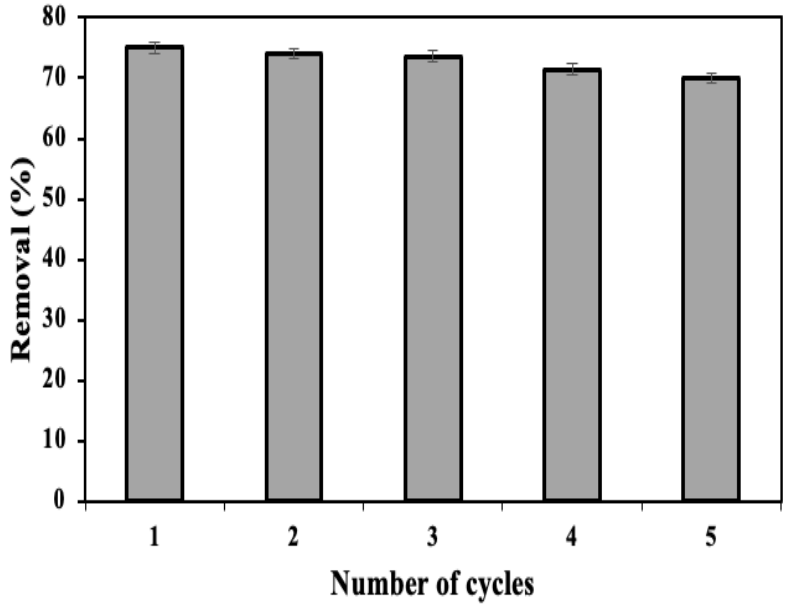


Fig. 4. 22: Reusability study onto the semi-IPN PVA-ALG-BENT nanocomposite hydrogel beads for the removal of CR (C_0[CR] = 100 mg/L, V = 50 mL, beads dosage = 1.5 g, pH = 3, t = 300 min, T = 30 ºC).

4.1.6. Adsorption Isotherm studies for the removal of MB and CR

Adsorption isotherm analysis is performed to understand the adsorption mechanism, the distribution behavior of adsorbate molecules over the adsorbent surface and to estimate the adsorption capacity of an adsorbent at equilibrium (Zahir et al., 2017). In this study, two isotherm models namely, Langmuir and Freundlich models were employed to get more insights of the removal process of MB and CR dyes by semi-IPN PVA-ALG-BENT nanocomposite hydrogel beads. Both Figures 4.23 and 4.24 show the Langmuir and Freundlich fit models for MB and CR dyes, respectively. The plot of Ce/qe vs Ce gives a straight line with high correlation coefficients (R^2 = 0.994 for MB) and (R^2 = 0.998 for CR). Accordingly, the adsorptions of both dyes were likely to comprise monolayer adsorption on homogeneous surface. The adsorption

parameters for both models are illustrated in Table 4.14. The Langmuir constants q_m and K_L are obtained from the slop and the intercept of the linear plot. For MB dye the results showed that, R_L values lay between 0.0033 to 0.011 ($0 < R_L < 1$), while for CR the R_L values were found in the range of 0.11 to 0.38 ($0 < R_L < 1$), which represent a favorable adsorption based on monolayer coverage of dyes molecules over a homogenous surface of adsorbent. This indicates that the adsorption sites of the adsorbent have equal adsorption energies and the whole process can be explained via chemisorption mechanism (Luo, Fu, et al., 2021; Luo, Yu, et al., 2021)..

Moreover, the Freundlich liner form was also used to analyze the equilibrium data by plotting ln qe vs ln Ce. The correlation coefficients (R^2) are listed in table 4.14. The Freundlich equation and the experimental results of dyes removal on PVA-ALG-BENT are in agreement, as evidenced by the high correlation coefficients (R^2 for MB =0.99) and (R^2 for Cr =0.986). The Freundlich isotherm proposes a heterogenous adsorption with multi layers adsorption via physisorption mechanism. The calculated n values were about 2.19 for MB and 1.65 for CR which are more than 1, assuming that the adsorption of dyes on the surface of adsorbent were favorable. A comparison of q_m value for the removal of MB and CR by PVA-ALG-BENT nanocomposite hydrogel beads and other adsorbents is listed in Table (4.15), which indicated the significant adsorption capacity of the designed beads.

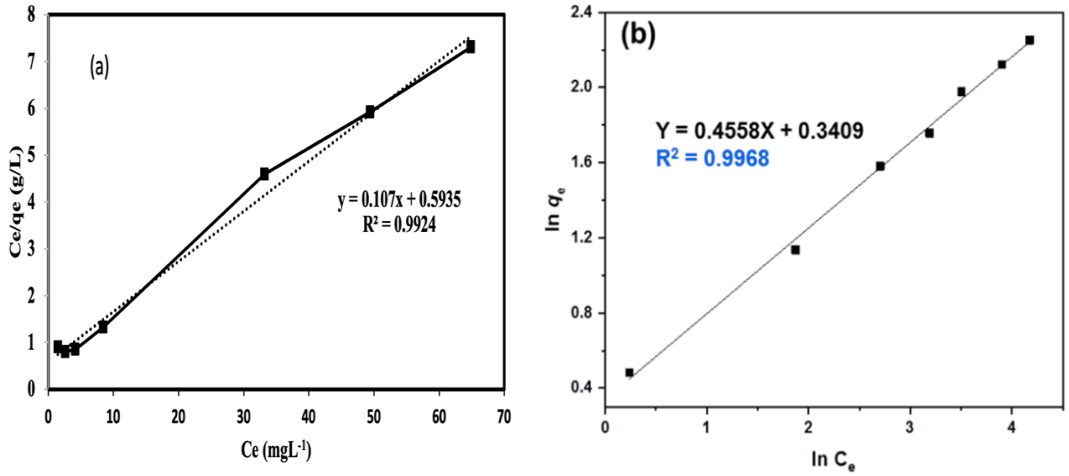


Fig. 4. 23: (a) The Langmuir adsorption isotherm and (b) Freundlich adsorption isotherm, for the adsorption of the MB onto the semi-IPN PVA-ALG-BENT nanocomposite hydrogel beads.

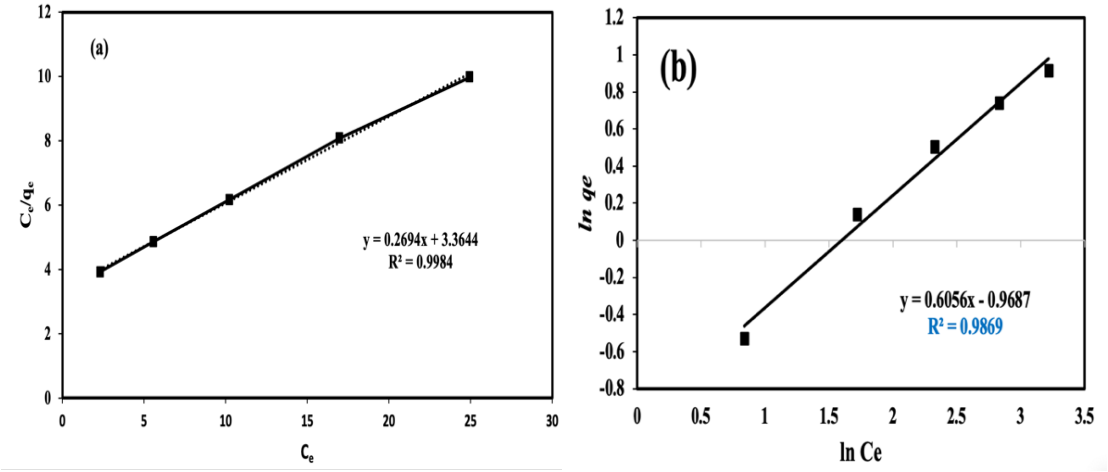


Fig. 4. 24: (a) The Langmuir adsorption isotherm and (b) Freundlich adsorption isotherm, for the adsorption of the CR onto the semi-IPN PVA-ALG-BENT nanocomposite hydrogel beads.

Table (4. 14): Parameters of the adsorption isotherms of MB and CR

Dyes	Models	Isotherms constants			
MB	Langmuir	q_m (mg/g)	K_L (L/mg)	R_L	R^2
		9.34	0.180	0.0033-0.015	0.9924
	Freundlich	1/n	KF	-	R^2
		0.4558	1.41	-	0.99
CR	Langmuir	q_m (mg/g)	K_L (L/mg)	R_L	R^2
		3.711	0.0801	0.11<RL<0.38	0.9984
	Freundlich	1/n	KF	-	R^2
		0.605	0.379		0.989

Table (4. 15): Comparison of the Qe values of the designed semi-IPN PVA-ALG-BENT nanocomposite hydrogel beads and previously reported adsorbents for the removal of MB and CR dye.

Adsorbent	Dyes	Qe (mg/g)	References
Activated charcoal/ cyclodextrin/ALG hydrogel beads	MB	10.6	(Yadav et al., 2020)
PVA/cyclodextrin-modified poly (acrylic acid) hydrogel	MB	23.0	(N. Hou et al., 2020b)
Carboxymethyl cellulose (CMC)-based hydrogel	MB	25.0	(Capanema et al., 2018)
CMC/k-carrageenan/montmorillonite (MMT) beads	MB	12.5	(C. Liu et al., 2018)
Graphene oxide (GO)/Fe_3O_4/chitosan nanocomposite	MB	30.1	(H. v. Tran et al., 2017)
PVA/CMC/halloysite nanoclay membrane	MB	40.6	(Radoor et al., 2020b)
Corn stalk/MMT composite hydrogel	MB	49.0	(Ma et al., 2017)
GO/Fe_3O_4/ALG nanocomposite	MB	37.0	(Song et al., 2015)

Chitosan/sepiolite composite	MB	40.9	(Marrakchi et al., 2016)
PVA/BENT hydrogel	MB	27.9	(Sanchez et al., 2019)
PVA-ALG-BENT nanocomposite hydrogel beads	MB	51.4	This study
Glauconite (Gl): natural clay	CR	11.9	(Salah et al., 2022)
PVA/SA/ZSM-5 zeolite membrane	CR	5.33	(Radoor et al., 2020)
silica mesoporous materials	CR	17.4	(Laaz et al., 2016)
Kalion	CR	5.6	(Vimonses et al., 2009)
Pinus pinaster bark	Cr	1.16	(Litefti et al., 2019b)
PVA-ALG-BENT nanocomposite hydrogel beads	CR	16.193	This study

4.1.6. Adsorption Kinetics models for MB and CR dyes

The kinetics of adsorption are important index in defining the efficiency of adsorption (N. Hou et al., 2020c). In this study, the kinetic models of MB and CR adsorption onto the beads were investigated using both the pseudo-first order (PFO) and pseudo-second order (PSO) kinetic models. Linearized plots of PFO and PSO are obtained by plotting *ln* (*qe- qt*) vs time and *t*/*qt* versus time, respectively as shown in Fig. 4.25 a&b for MB adsorption and Fig. 4.26 a&b for CR adsorption. The parameters of the models k_1, K_2, q_e, and correlation coefficient (R^2) values are calculated from the slope and the intercept of the best fit model and tabulated in Table 4.16 for both dyes.

For MB adsorption the R^2 value (0.9974) obtained by PSO kinetic model was higher than that obtained by PFO kinetic model (0.9615). Moreover, the q_e calculated value obtained from PSO model is closer to the q_e experimental than PFO, which indicates that PSO kinetic model is more appropriate for describing the adsorption behavior of MB onto the bead and the dominant adsorption process of MB dye was by a chemisorption mechanism.

Furthermore, CR adsorption was also examined for the best kinetic models, the corresponding R^2 values of PSO kinetic model (0.9981) was more suited to express the adsorption of CR on the designed beads than the Pseudo- first order kinetic model (R^2=0.9827). The linearity of ln(qe-qt) plot vs time (Fig. 4.25 a and Fig. 4.26 a) suggests that the MB and CR adsorption did not follow the PFO. This result agrees with the result obtained by previous studies on dye adsorption using polysaccharide-based adsorbent (Hamad & Saied, 2021a; Yu et al., 2019). The priority of PSO was explaine by Ho and Mckay (1999), who suggested that PSO can be

applied across a whole period of time, whereas PFO is only relevant at the beginning stage of the adsorption(Y. S. Ho & McKay, 1999)

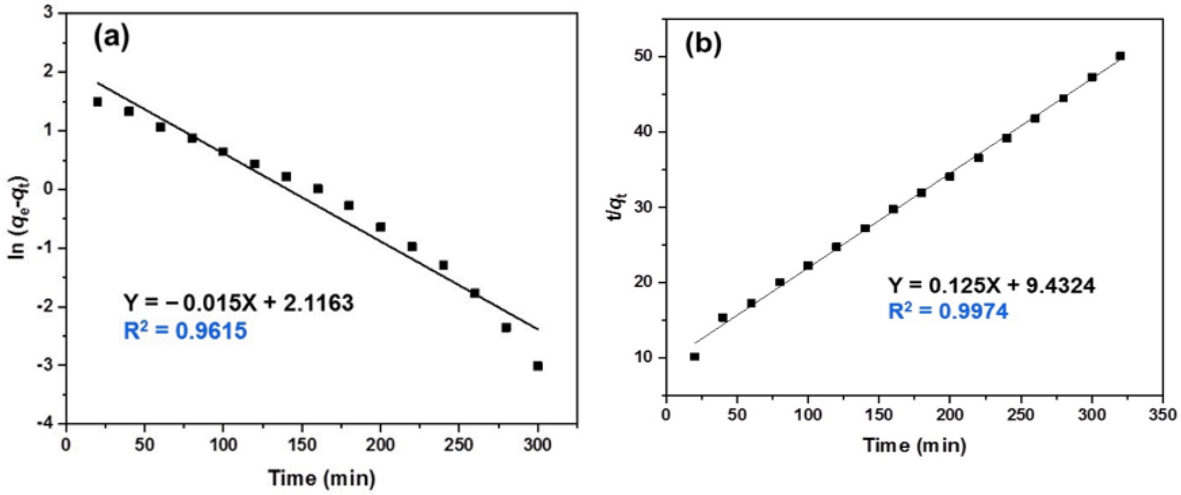


Fig. 4. 25: (a) The PFO and (b) PSO kinetic models for the adsorption of the MB onto the semi-IPN PVA-ALG-BENT nanocomposite hydrogel beads.

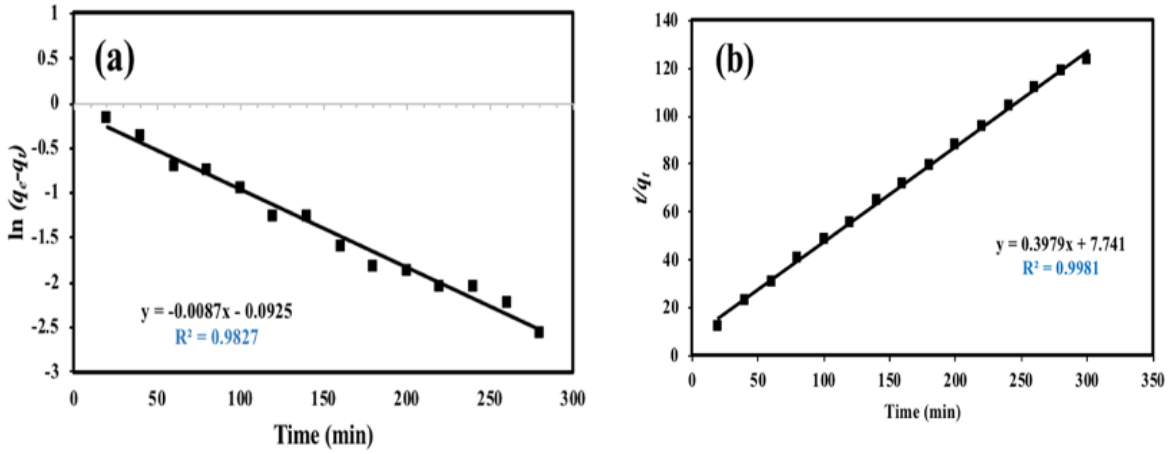


Fig. 4. 26: (a) The PFO and (b) PSO kinetic models for the adsorption of the CR onto the semi-IPN PVA-ALG-BENT nanocomposite hydrogel beads.

Table (4. 16): Kinetics parameters for the adsorption of MB and CR onto hydrogel beads based on pseudo- first order and Pseudo-second order equations

Dyes	Kinetic models	q_{exp} (mg/g)	q_e (mg/g)	K	R^2
MB	PFO	6.38	8.30	K_1= 0.015 (1/min)	0.961
	PSO	6.38	8.00	K_2= 0.0016 (g/mg.min)	0.997
CR	PFO	2.50	0.991	K_1= 0.0087 (1/min)	0.982
	PSO	2.50	2.51	K_2= 0.021 g/mg.min	0.998

4.1.7. Adsorption Mechanism of Dyes

Fig. (4.27) displays an illustrative scheme for the proposed adsorption mechanism for MB and CR on the surface of PVA-ALG-BENT. As mentioned before, when pH is above the pH_{PZC}, the negative surface charge of the PVA-ALG-BENT composite hydrogel gel adsorbent is increased due to the ionization of (-COOH) and (-SiOH) groups into ($-COO^-$) and ($-SiO^-$), respectively. Thus, the removal of MB by the designed adsorbent is due to the electrostatic interactions between the positive charges on the (=N+) present in the MB dye molecules and the abundant negative charges of the nanocomposite adsorbent. In addition, hydrogen bonding occurs between the (-OH) groups present in the adsorbent surface and nitrogen atom of MB (Jana et al., 2019; Z. H. Zhang et al., 2021b). While at pH below the pH_{PZC} the positive surface charge of the PVA-ALG-BENT nanocomposite hydrogel gel adsorbent is increased due to the

protonation of ($-COO^-$), ($-SiO^-$) and (OH) groups into ($-COOH_2^+$) and ($-SiOH_2^+$), and (OH_2^+) respectively. Thus, the removal of CR by the designed adsorbent is due to the electrostatic interactions between the negative charges on the sulfonate group (SO_3^-) present in the CR dye molecules and the abundant positive charges of the nanocomposite adsorbent. In addition, hydrogen bonding occurs between the (-OH) groups present in the adsorbent surface and nitrogen atom of CR (Jana et al., 2019; Z. H. Zhang et al., 2021b).

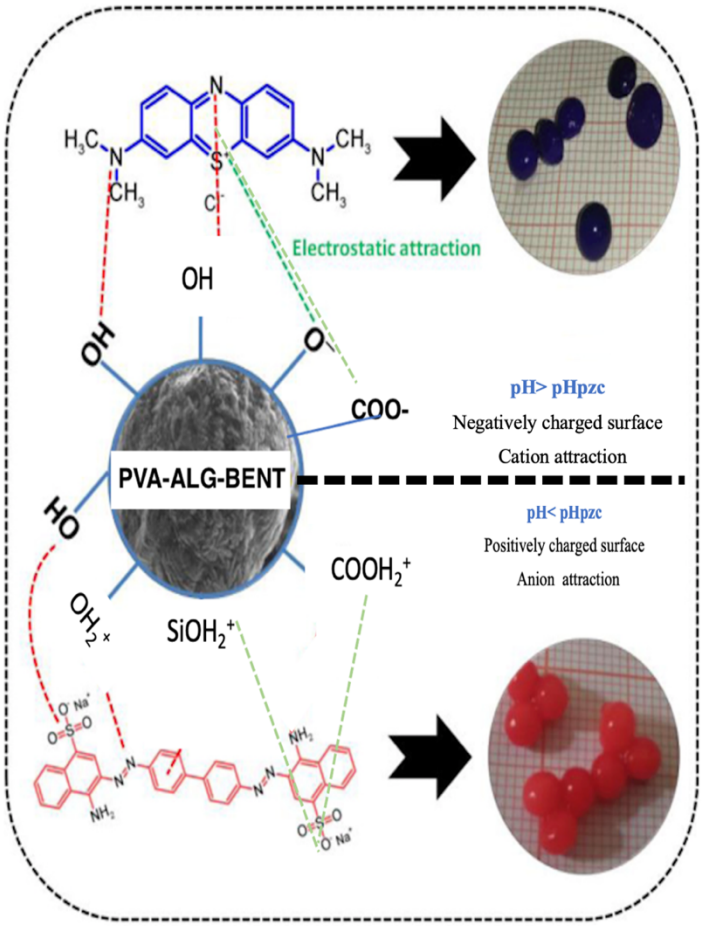


Fig. 4. 27: Proposed scheme indicating the possible interaction mechanism for the removal of MB and CR onto the PVA-ALG-BENT nanocomposite hydrogel beads.

4.2. Patch Adsorption Studies of Pb(II), Cd(II), Co(II) and Zn(II) ions Using Environmentally Friendly Polyvinyl Alcohol -Chitosan-nanocellulose (PVA-CHTS-CLS)

4.2.1. Physical and chemical characterization methods

PVA-CHTS-CLS nanocomposites hydrogel beads were successfully prepared, Fig. 4.28 a-f show the images of wet and dry hydrogel beads before and after adsorption of the heavy metals Pb(II), Cd(II), Co(II), and Zn(II), respectively. The adsorption of metal ions into the hydrogel beads was confirmed by the apparent of light yellow and pink colors (Figs. 4.28 c-f). The average size of wet beads was approximately 4.0 mm in diameter and had consistently spherical structure with smooth surface as shown in Fig. 4.28a. After air dry, the spherical beads slightly shrank and the size of the beads decreased, this is consistent with other previous studies (H. Li et al., 2021). Moreover, the surface structure was slightly rough without significant collapse of the porous structure, revealing enhanced mechanical strength.

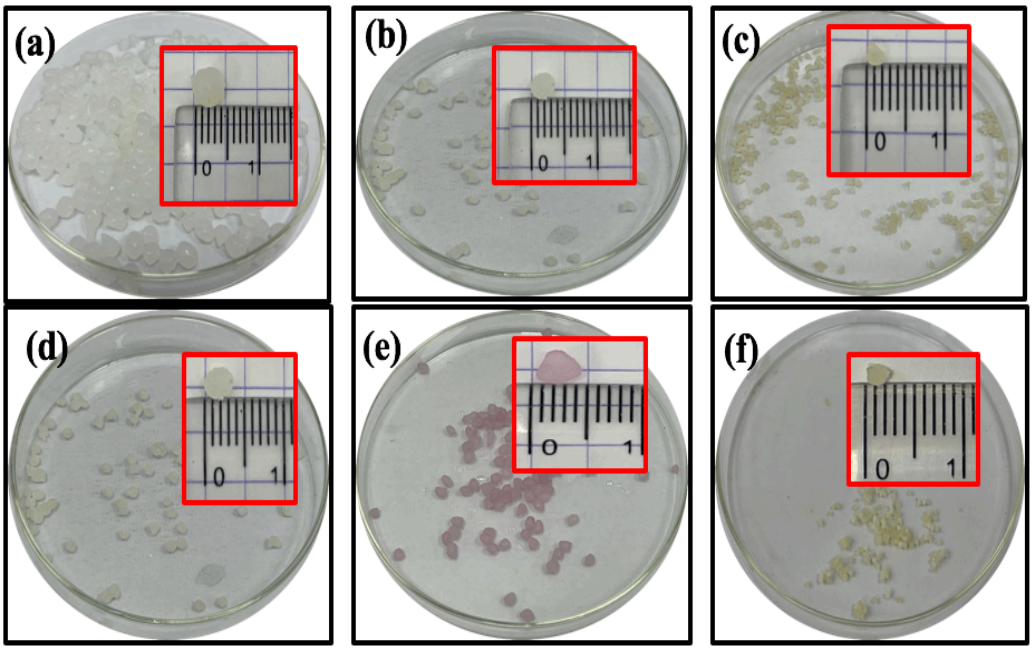


Fig. 4. 28: PVA–CHTS-CLS nanocomposite hydrogel beads (a) before drying (inset shows the size of wet beads), (b) after 48 hr. air drying, (c) dried beads after adsorption of Pb, (d) dried beads after adsorption of Cd, (e) dried beads after adsorption of Co, (f) dried beads after adsorption of Zn.

In this study, the percentage of CLS fillers was fixed to be 0.5 % and the ratio of the PVA and CHTS was specified to be 1:1. These settings were chosen because they provide stability of the nanocomposites and best adsorption conditions for the removal of HMIs as stated by H. Li et al., 2021. Fig. 4.29 compares the % removal of HMIs using two adsorbent beads, PVA-CHTS as control hydrogel beads and PVA-CHTS-CLS as modified polymer hydrogel. The results revealed that PVA-CHTS-CLS had higher removal efficiency compared to the unmodified PVA-CHTS beads. This result highlighted a significant correlation between incorporation of CLS and the efficiency of the removal of HMIs. Using CLS as a filler in the structure of PVA-CHTS polymer can enhance both

the adsorption capacity and the stability of the adsorbent because the adsorbent will have high porosity and interconnected porous structure (Abdul Khalil et al., 2016). Moreover, T. Liu et al., 2013 reported that the incorporation of CLS to CHTS structure produced highly dense and mechanically stronger hydrogel beads. Considering the enhancement in the results, PVA-CHTS-CLS hydrogel with 0.5 wt % CLS was chosen for further adsorption study.

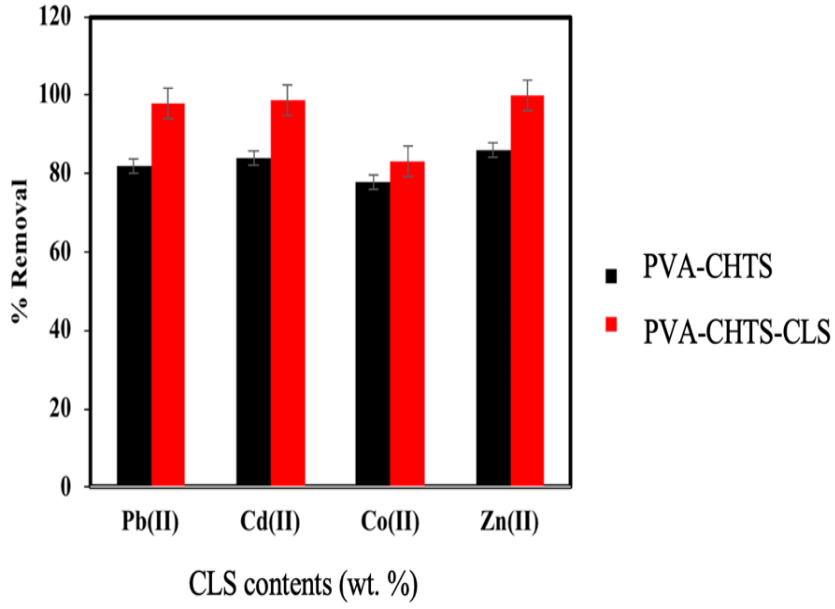


Fig. 4. 29: Effect of CLS content (0, 0.5 wt. %) on the removal percentage of HMIs (C_0[heavy metals] = 50 mg/L, V = 50 mL, pH (Pb & Cd) = 6, , pH (Pb & Cd) = 6, pH (Co & Zn) = 8, beads dosage = 0.5 g, t = 200 min, T = 30 °C).

4.2.1.1. Fourier Transform Infrared Spectroscopy (FTIR)

Surface functional groups of PVA, CHTS, CLS and PVA-CHTS-CLS were detected by using FTIR spectroscopy and the spectra is shown in Fig. 4.30. The broad band in the range of 3649-3170 cm^{-1} was related to

the (-OH) and (-NH) units of both CHTS and PVA (Das et al., 2020; D. Wang et al., 2018). The peak at 2938 cm^{-1} was corresponding to the vibration stretching of $-CH_2$. A peak at 1652 cm^{-1} was related to stretching peak of C=N, which was due to the reaction of NH_2 of CHTS and OH of PVA. The peak at 1590 cm^{-1} was associated to stretching vibration of NH_2 in CHTS (Atta et al., 2015; Das et al., 2020) and the peak at 1458 cm^{-1} was related to CH_2 vibration of the crosslinked PVA.

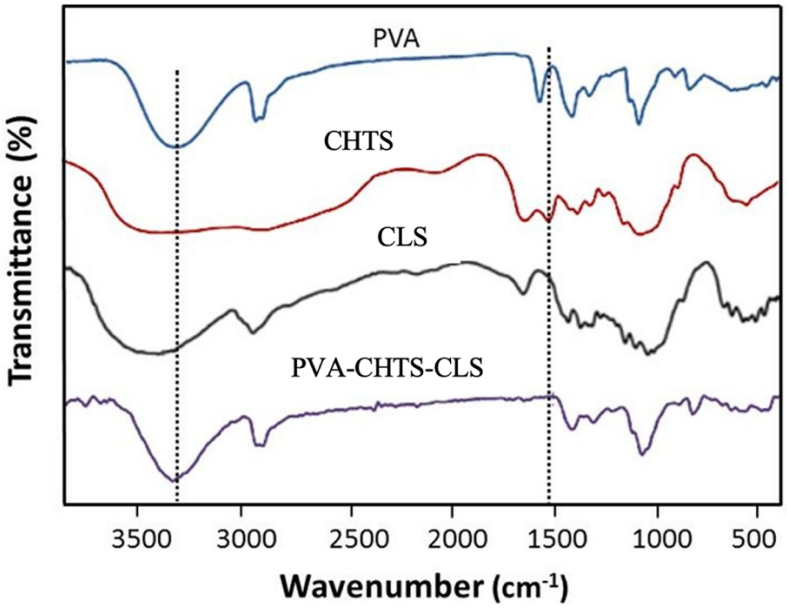
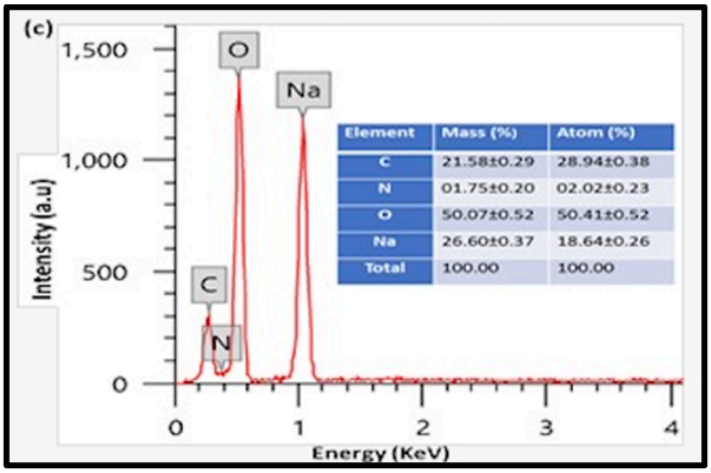


Fig. 4. 30: FTIR spectra of PVA, CHTS, CLS, and PVA-CHTS-CLS nanocomposite hydrogel.

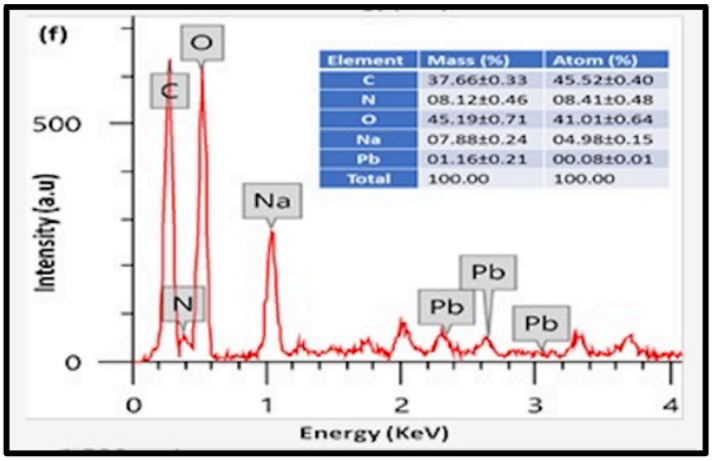
4.2.1.2. Energy-Dispersive X-ray Spectroscopy (EDX)

The adsorption of heavy metal ions by PVA-CHTS-CLS polymer was confirmed by EDX elemental analysis as shown in Fig. 4.31. EDX measured the elemental composition of PVA-CHTS-CLs beads before and after uptake metal ions. Before uptake metal ions, the EDX spectrum for the intact PVA-CHTS-CLS hydrogel did not show the characteristic peaks of heavy metal ions, however, the spectrum exhibited the mainly

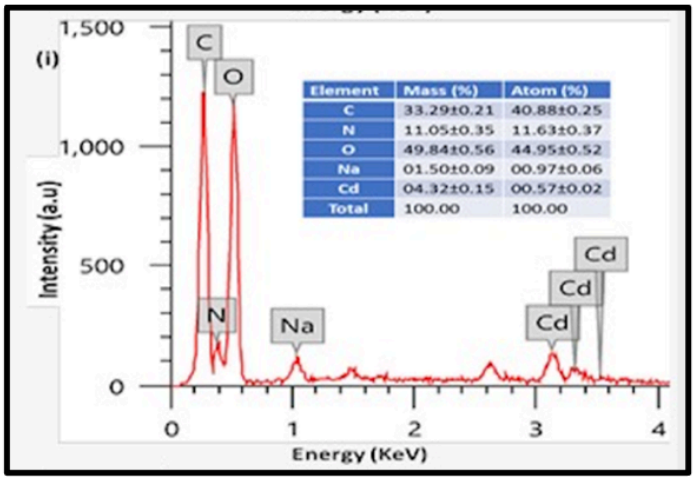
emergence of carbon, oxygen, nitrogen, and sodium(Abdul Khalil et al., 2016; T. Liu et al., 2013) . After loaded with heavy metal ions, the EDX spectra showed clearly the presence of Pb (II), Cd(II), Co(II), and Zn(II) in PVA-CHTS/CLS beads, which indicates the PVA-CHTS-CLS beads being coated with the heavy metal ions successfully



(a)



(b)



(c)

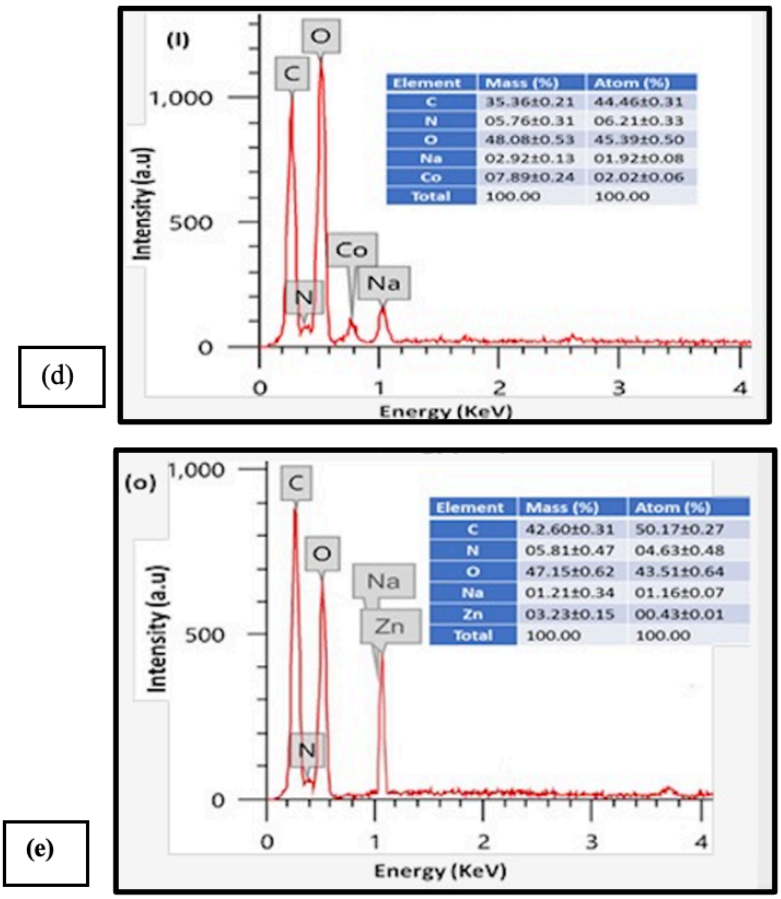
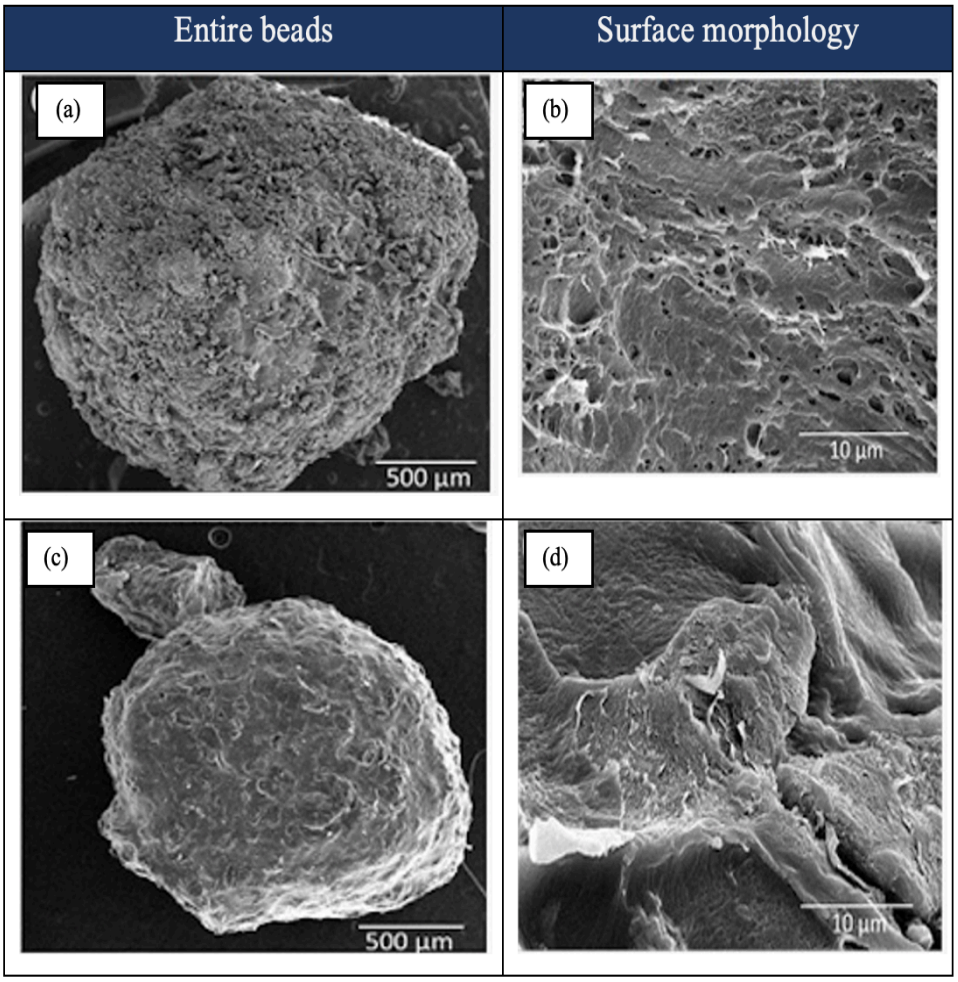


Fig. 4. 31: EDX spectra of (a) PVA-CHTS-CLS (b) PVA-CHTS-CLS after adsorption of Pb, (c) PVA-CHTS-CLS after adsorption of Cd, (d) PVA-CHTS-CLS after adsorption of Co and (e) PVA-CHTS-CLS after adsorption of Zn. (C_0[Heavy metals] = 50 mg/L, V = 50 mL, pH (Pb & Cd) = 6, pH (Co& Zn) = 8, beads dosage = 0.5 g, t = 200 min, T = 30 °C) (g).

4.2.1.3. Scanning Electron Microscopy (SEM)

The morphologies of PVA-CHTS-CLS beads before and after adsorbing heavy metal ions were characterized through SEM, as illustrated in Fig. 4.32. In all cases, SEM micrographs revealed spherical beads with robust compact surface and well-defined porous structure in a typical three-dimensional network. It can be observed that the CLS is homogeneously

distributed in the PVA-CHTS matrix without the presence of macroscopic aggregates. Studies have shown that a porous network is clearer for a low concentration of CLS (H. Li et al., 2021). This fact along with the roughness of the pore walls, provide more contact sites and allow water to act as a transport channel for heavy metal ions from water media into the interior of adsorbent network via the abundant pores structure (Al-Ghouti & Al-Degs, 2011). After loaded with heavy metal ions, it is clearly noted that the surface structure remains three-dimensional network, however, the channels became compact, and a reduction of hydrogel pores is significant.



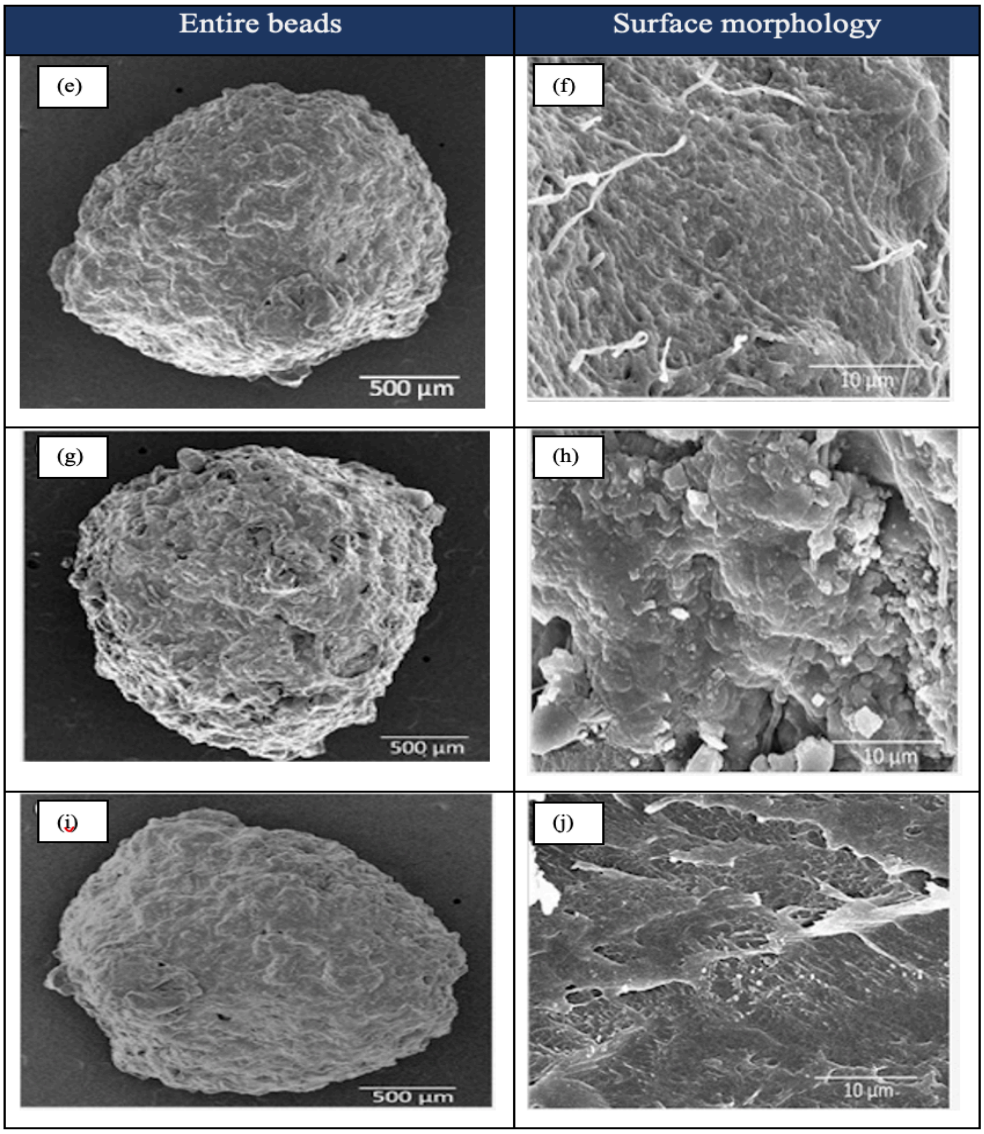


Fig. 4. 32: SEM images of the dried hydrogel beads at higher and lower magnification for (a, b) PVA-CHTS- 0.5 wt. % CLS, (c, d) PVA-CHTS-CLS after Pb (II) adsorption, (e, f) PVA-CHTS-CLS after Cd (II) adsorption, (g,h) PVA-CHTS-CLS after Co (II) adsorption and (i, j) PVA-CHTS-CLS after Zn(II) adsorption.

4.2.1.4. X-ray Diffraction studies (XRD)

Fig. 4.33 presents XRD patterns of PVA, CHTS, CLS and PVA-CHTS as well as PVA-CHTS-CLS composite hydrogel. The pure PVA

exhibited the diffraction peak at 2θ = 19.5°, corresponding to the (101) crystal plane in PVA while CHTS presented a broad peak at 2θ around 21° because of its amorphous structure (Weijiang et al., 2017b). The XRD pattern of CLS exhibited two well distinct diffraction peaks, at 2θ = 16.4° and 22.8° due to the refection from the different crystal planes of CLS such as (010) and (002)(H. Li et al., 2021; Weijiang et al., 2017b). It was observed that the characteristic peak of PVA was slightly shifted toward low θ with the incorporation of CHTS and CLS in the composite formulation. Moreover, all peaks of CLS disappeared in PVA-CHTS-CLS composite hydrogel because the content of CLS was too low. This evidence concluded that intermolecular interactions between PVA and CHTS are formed, which decreased the crystallinity of the PVA-CHTS-CLS composite hydrogel.

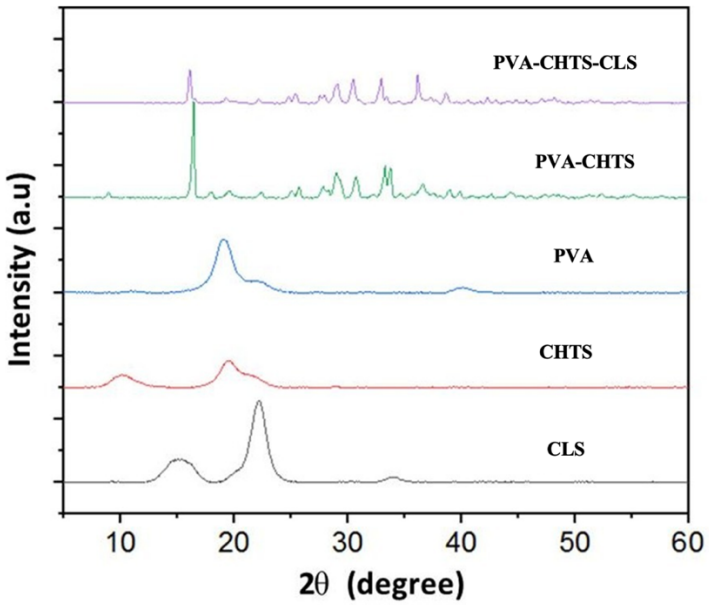


Fig. 4. 33: XRD patterns of PVA, CHTS, CLS and PVA-CHTS as well as PVA-CHTS-CLS composite hydrogel.

4.2.2. Equilibrium Swelling Test at various pH

The Swelling Ratio (SR) of the polymer is influenced by several factors such as the existence of hydrophilic groups, the characteristics of

the solution, elasticity of the polymer network, and pore distribution and size (Amri et al., 2019). Hydrophilic polymers such as CHTS and PVA which contain large number of hydroxyl (OH) and amino (NH_2) groups attract water molecules and enhance the SR of the polymers. These groups in the crosslinked hydrogel structure are pH sensitive and can change the polymer properties such as swelling behavior of the polymers (Nisar et al., 2020). CHTS based gels are recognized for having porous structure which results in a higher swelling ratio and fast equilibrium time. Table 4.17 and Fig. 4.34 a & b depicts the swelling behavior and mechanisms of PVA-CHTS-CLS hydrogel nanocomposites which have been soaked at different pH (3, 7, and 9) as a function of time. The results showed that the SR increased with decreasing pH which due to the protonation of amino and hydroxyl groups on the backbone of the PVA and CHTS and consequently the polymer beads expand and enhance the diffusion of water molecules into the hydrogel's matrix.

On the other hand, at acidic condition and below 100 min the hydrogel demonstrated a sudden decreased in SR and began to degrade and burst. Evidently, CHTS is soluble in acidic solution and cannot retain its structure because of the protonation of free amino group into ammonium group (NH_3^+) as shown in Fig. 4.34. Consequently, the repulsive interactions in the polymer structure causing the hydrogel to collapse and that explained the decrease in the SR value after 100 min. However, at neutral and basic conditions (pH =7 & 9), the SR of the hydrogel increased steadily and remained constant over longer duration time (200 min) due to the balance between the protonation and deprotonation of the hydrophilic groups and that helps to achieve high adsorption of water molecules. The obtained results are consistent with the results published by Nisar et. al. using a based polysaccharide adsorbent (CHTS) (Nisar et al., 2020). Swelling mechanism at basic media is shown in Fig. 4.34b, the ammonium groups

are deprotonated and hence the repulsive interaction is lowered and thus hydrogen bonds between the amino groups of CHTS and the hydroxyl groups of the PVA are formed, as a result the inter-intra chain hydrogen bond increased, the size of the pores decreased resulting in a reduction in the SD (Habiba, Joo, et al., 2017).

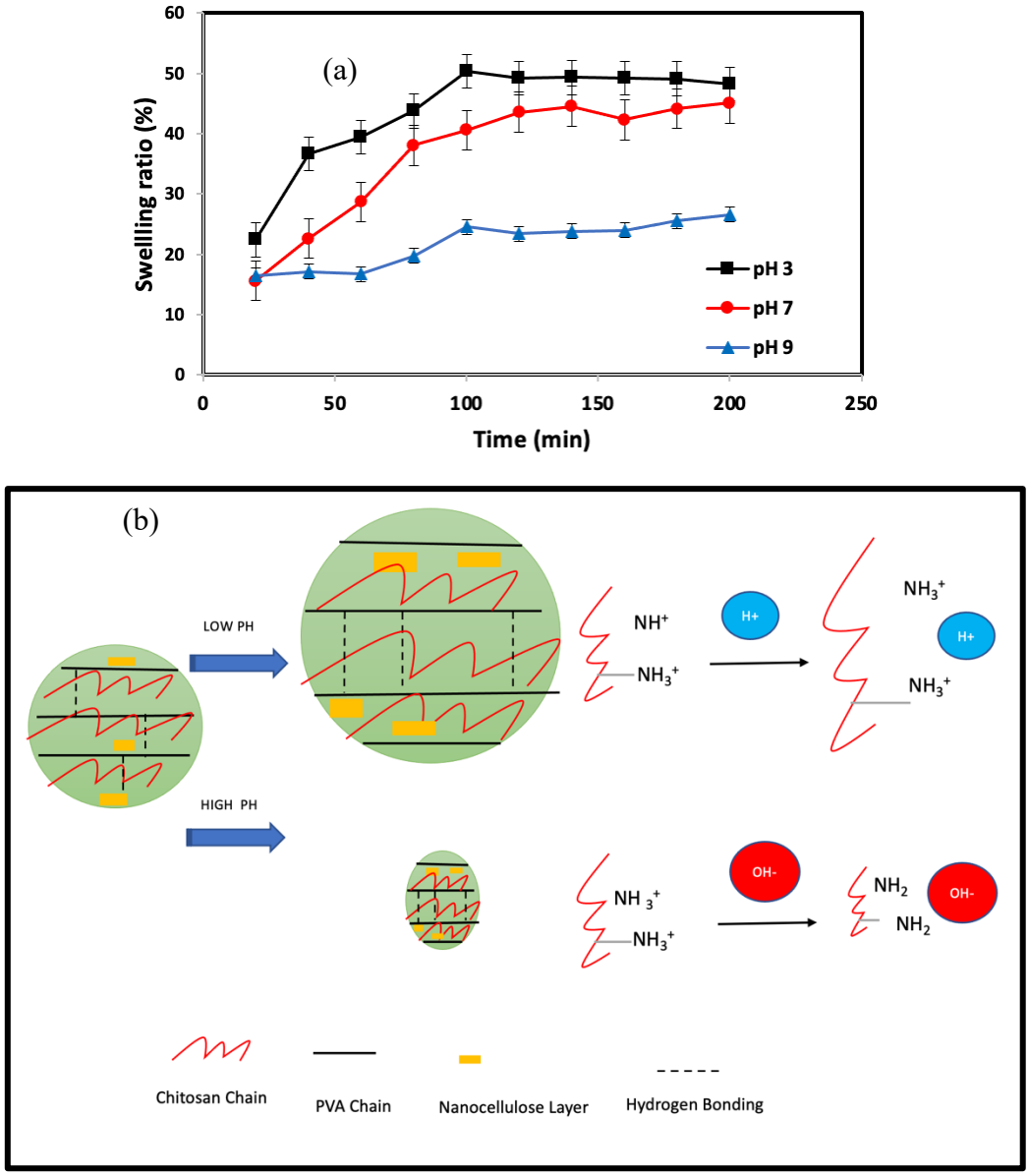


Fig. 4. 34: Swelling behavior of PVA–CHTS-CLS nanocomposite hydrogel beads at different pH values (3,7 and 9): (a) swelling ratio and (b) Swelling mechanism.

Table (4. 17): SR of PVA–CHTS-CLS nanocomposite hydrogel beads at different pH values (3,7 and 9)

pH 3										
Time (min)	Trail 1			Trail 2			Trail 3			% SR±SD
	W_{Dry} (g)	W_{wet} (g)	% SR	W_{Dry} (g)	W_{wet} (g)	% SR	W_{Dry} (g)	W_{wet} (g)	% SR	
20	0.500	0.671	33.9	0.500	0.685	37.0	0.500	0.589	17.8	35.4±10.0
40		0.676	34.9		0.675	35.0		0.615	23.0	29.2±6.0
60		0.765	52.7		0.713	42.6		0.647	29.4	39.4±11.0
80		0.79	57.7		0.721	44.2		0.691	38.2	43.7±9.0
100		0.81	61.7		0.756	51.2		0.731	46.2	50.3±7.0
120		0.751	49.9		0.757	51.4		0.700	40.0	49.1±6.0
140		0.741	47.9		0.759	51.8		0.632	26.4	46.5±13.0
160		0.741	47.9		0.717	43.4		0.613	22.6	39.2±13.0
180		0.722	44.1		0.651	30.2		0.634	26.8	32.3±9.0
200		0.671	33.9		0.621	24.2		0.633	26.6	28.1±5.0

pH 7										
Time (min)	**Trail 1**			**Trail 2**			Trail 3			**% SR±SD Average**
	W_{Dry} (g)	**W_{wet} (g)**	**% SR**	**W_{Dry} (g)**	**W_{wet} (g)**	**% SR**	**W_{Dry} (g)**	**W_{wet} (g)**	**% SR**	
20	0.501	0.541	7.6	0.500	0.627	23.7	0.500	0.563	11.5	15.6±8.0
40		0.612	21.7		0.683	34.7		0.612	21.2	22.6±7.0
60		0.628	24.9		0.71	40.0		0.661	30.9	28.7±7.0
80		0.702	39.6		0.729	43.8		0.679	34.5	38.1±4.0
100		0.714	41.9		0.737	45.4		0.721	42.8	40.6±2.0
120		0.718	42.7		0.736	45.2		0.723	43.2	43.6±1.0
140		0.726	44.3		0.741	46.2		0.723	43.2	44.6±1.0
160		0.715	42.1		0.718	41.6		0.741	46.7	42.3±3.0
180		0.711	41.4		0.732	44.4		0.756	49.7	44.2±4.0
200		0.711	41.4		0.731	44.2		0.756	49.7	45.1±4.0
pH 9										
Time (min)	**Trail 1**			**Trail 2**			**Trail 3**			**% SD±SR**

	W_{Dry} (g)	W_{wet} (g)	% SR	W_{Dry} (g)	W_{wet} (g)	% SR	W_{Dry} (g)	W_{wet} (g)	% SR	
20	0.505	0.564	11.7	0.506	0.614	21.3	0.502	0.561	11.8	16.5±5.0
40		0.567	12.3		0.644	27.3		0.571	13.7	17.1±8.0
60		0.583	15.4		0.612	20.9		0.592	17.9	16.7±3.0
80		0.602	19.2		0.618	22.1		0.637	26.9	19.8±4.0
100		0.606	20.0		0.641	26.7		0.621	23.7	24.5±3.0
120		0.605	19.8		0.641	26.7		0.623	24.1	23.4±3.0
140		0.608	20.4		0.642	26.9		0.623	24.1	23.8±3.0
160		0.608	20.4		0.645	27.5		0.641	27.7	24.0±4.0
180		0.611	21.0		0.647	27.9		0.656	30.7	25.5±5.0
200		0.611	21.0		0.648	28.1		0.656	30.7	26.6±5.0

4.2.3. pH at Point of Zero Charge (pH_{PZC})

The overall charge on the surface of the hydrogel beads is affected by the functional groups on their surface and their reactivity towards H^+ and OH^- ions. Specifically, a net surface charge is shifted from net positive at low pH to net negative at high pH (Rey et al., 2017). This point is not the neutral point (pH =7), rather it's the point in which the number of positive and negative ions is equal. PH_{PZC} is controlled by the kind and number of functional groups present on the hydrogel surface.

Fig. 4.35 shows the surface charge density of the PVA-CHTS-CLS composites beads as a function of pH. The intersection of the curve with x-axis at Δ pH ($pH_{initial}$-pH_{final}) equal zero indicates the value of pH_{pzc}. The pH_{pzc} of the PVA-CHTS-CLS was 5. When the pH is greater than 5, the surface of the adsorbent is negatively charged and if the pH is lower than 5 than the surface would have a positive charge. A net positive charge is obtained below the pH_{pzc} indicating that the adsorbent has the capacity to adsorb the negative charged ions via electrostatic force. In contrast, above pH_{pzc} the net surface charge of the adsorbent is negative suggesting interaction with positive ions (Al-Ghouti & Al-Degs, 2011).

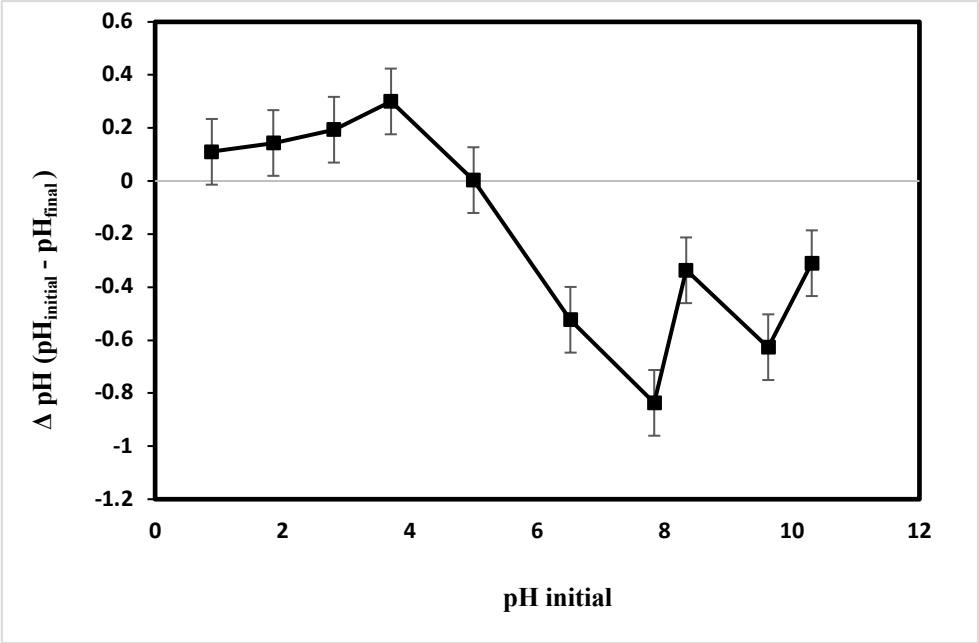


Fig. 4. 35:PH_{PZC} study for PVA-CHTS-CLS nanocomposite hydrogel beads.

4.2.4. Batch Adsorption Equilibrium Studies

4.2.4.1. Effect of solution pH on the removal of HMIs.

The pH is an important factor for regulating the adsorption process because proton concentration effects metal solubility and may affect the ionization of the functional groups on the hydrogel beads and the interface with the adsorbent (Demey et al., 2018; Naseeruteen et al., 2018). Based on pH, metal ions can be presented as cationic species or metal hydroxides (Esrafili et al., 2019). HMIs occur in different oxidation states and most HMIs precipitate as hydroxide in basic solution (F. S. A. Khan et al., 2020; Sheth et al., 2021). In the acidic medium, protonation of the electron rich group like amino (NH_2) and hydroxyl group (OH), etc is occurred. As a result, the positive charge on adsorbent surface will increase. Nevertheless, in basic media the presence of negatively charged hydroxyl group (OH^-) creates a negative surface on the adsorbent surface, OH will be

deprotonated to give O^- ion (F. S. A. Khan et al., 2020). The adsorption of Pb(II), Cd(II) , Co (II) and Zn (II) ions on PVA-CHTS-CLS nanocomposite hydrogel were measured at different pH values (3-9) and the results were recorded in Table 4.18 and presented in Fig. 4.36. The results showed that the removal of Pb (II) and Cd (II) was increased with increasing the initial pH of the solution from 3.0 to 6.0, and the maximum removal of Pb (II) and Cd (II) ions was observed at pH 6.0. On the other hand, the maximum removal of Co (II) and Zn (II) ions on PVA-CHTS-CLS nanocomposites hydrogel were achieved at pH 8.0. Since the pH_{pzc} of PVA-CHTS-CLS nanocomposites is equal to 5.0, therefore the removal efficiency of Pb (II), Cd (II), Co (II) and Zn (II) ions increased when the pH was higher than 5.0. Moreover, the low adsorption of metal at acidic media (pH <7) can be attributed to the competition of H^+ ions with the metal cations onto the adsorption sites. Importantly, at low pH an electrostatic repulsion is occurred due to the presence of cationic metal ions and the positive surface of the nanocomposite which reduce the removal efficiency of the metal (Esrafili et al., 2019; Sobhanardakani et al., 2013). The effect of pH in this study was agreed with that reported by (Esrafili et al., 2019; Karim et al., 2019)

Table (4. 18): Effect of initial pH on the adsorption capacity and removal percentage of HMIs onto the PVA-CHTS-CLS nanocomposite hydrogel beads.

Removal of Pb(II) (V = 50 mL, initial concentration = 50 mg/L, pH =3-10, beads dosage= 0.5 g, temp. =30 ºC, time = 200 min, wavelength = 220.353 nm*)*						
pH	**Pb(II) Concentrations (mg/L)**			**Pb(II) Average Concentration (mg/L)**	**% Removal ± SD**	**Q_e ± SD (mg/g)**
	Trail 1	**Trail 2**	**Trail 3**			
3	2.90	2.80	2.70	2.80	94.4±0.2	4.72±0.01
4	2.10	1.19	3.32	2.21	95.6±2.0	4.78±0.1
5	2.10	1.19	2.90	2.07	95.9±2.0	4.79±0.08
6	1.12	0.711	1.16	1.00	98.0±0.5	4.90±0.02
7	1.23	2.65	2.60	2.16	95.7±1.0	4.78±0.08
8	2.93	2.63	2.31	2.62	94.8±0.6	4.74±0.03
9	2.10	3.20	3.32	2.87	94.2±1.0	4.70±0.07
10	3.55	3.36	3.10	3.33	93.3±0.4	4.67±0.02

Removal of Cd(II) (V = 50 mL, initial concentration = 50 (mg/L), pH =3-10, beads dosage= 0.5 g, temp. =30 ºC, time = 200 min, wavelength = 228.802 nm*)*						
pH	**Cd(II) Concentrations (mg/L)**			**Cd(II)Average Concentration (mg/L)**	**Cd(II) % Removal**	**Q_e ± SD (mg/g)**
	Trail 1	**Trail 2**	**Trail 3**			
3	43.1	34.2	36.0	38.0	24.0±1.0	1.20±0.4
4	9.00	11.0	25.0	15.0	70.0±3.0	3.50±0.8
5	3.23	3.28	3.18	3.232	93.5±5.0	4.67±0.005
6	0.660	0.529	0.605	0.598	98.8±5.0	4.94±0.007
7	0.316	0.306	0.317	0.313	99.3±5.0	4.96±0.001
8	0.228	0.202	0.184	0.205	99.0±5.0	4.98±0.002
9	0.0120	0.148	0.110	0.0900	99.8±5.0	4.99±0.007
Removal of Co(II) (V = 50 mL, initial concentration = 50 mg/L, pH =3-10, beads dosage= 0.5 g, temp. =30 ºC, time = 200 min, wavelength = 228.61nm)						
pH	**Co(II) Concentrations (mg/L)**			**Co(II) Average Concentration (mg/L)**	**% Removal ±**	**Q_e ± SD (mg/g)**

	Trail 1	Trail 2	Trail 3		SD	
3	41.9	43.8	42.7	42.8	14.3±2.0	0.719±0.09
4	38.3	40.5	39.2	39.3	21.3±2.0	1.06±0.1
5	41.3	32.6	34.9	36.2	27.4±9.0	1.37±0.4
6	27.8	28.1	28.8	28.2	43.5±1.0	2.18±0.05
7	13.6	22.7	19.5	18.6	62.8±9.0	3.14±0.5
8	8.08	9.31	7.92	8.44	83.1±1.0	4.10±0.07
9	6.08	7.24	10.7	7.99	84.0±5.0	4.20±0.2
10	7.16	8.13	7.45	7.58	84.8±1.0	4.24±0.05
Removal of Zn(II) (V = 50 mL, initial concentration = 50 mg/L, pH =3-9, beads dosage= 0.5 g, temp. =30 ºC, time = 200 min, wavelength = 206.200 nm)						
pH	**Zn(II) Concentrations (mg/L)**			**Zn(II) Average Concentration (mg/L)**	**% Removal ± SD**	**Q_e ± SD (mg/g)**
	Trail 1	**Trail 2**	**Trail 3**			

3	37.4	37.6	36.9	37.3	25.5±0.653	1.27±0.03
4	32.3	33.8	32.6	32.9	34.3±1.0	1.71±0.08
5	30.5	31.2	31.4	31.02	37.9±0.8	1.89±0.01
6	25.6	26.6	25.1	25.8	48.4±1.0	2.42±0.07
7	3.96	4.92	4.26	4.38	91.2±0.9	4.56±0.04
8	0.101	0.0950	0.0960	0.100	99.8±0.006	4.99±0.0003
9	0.0840	0.0630	0.0710	0.0700	99.9±0.02	4.99±0.001

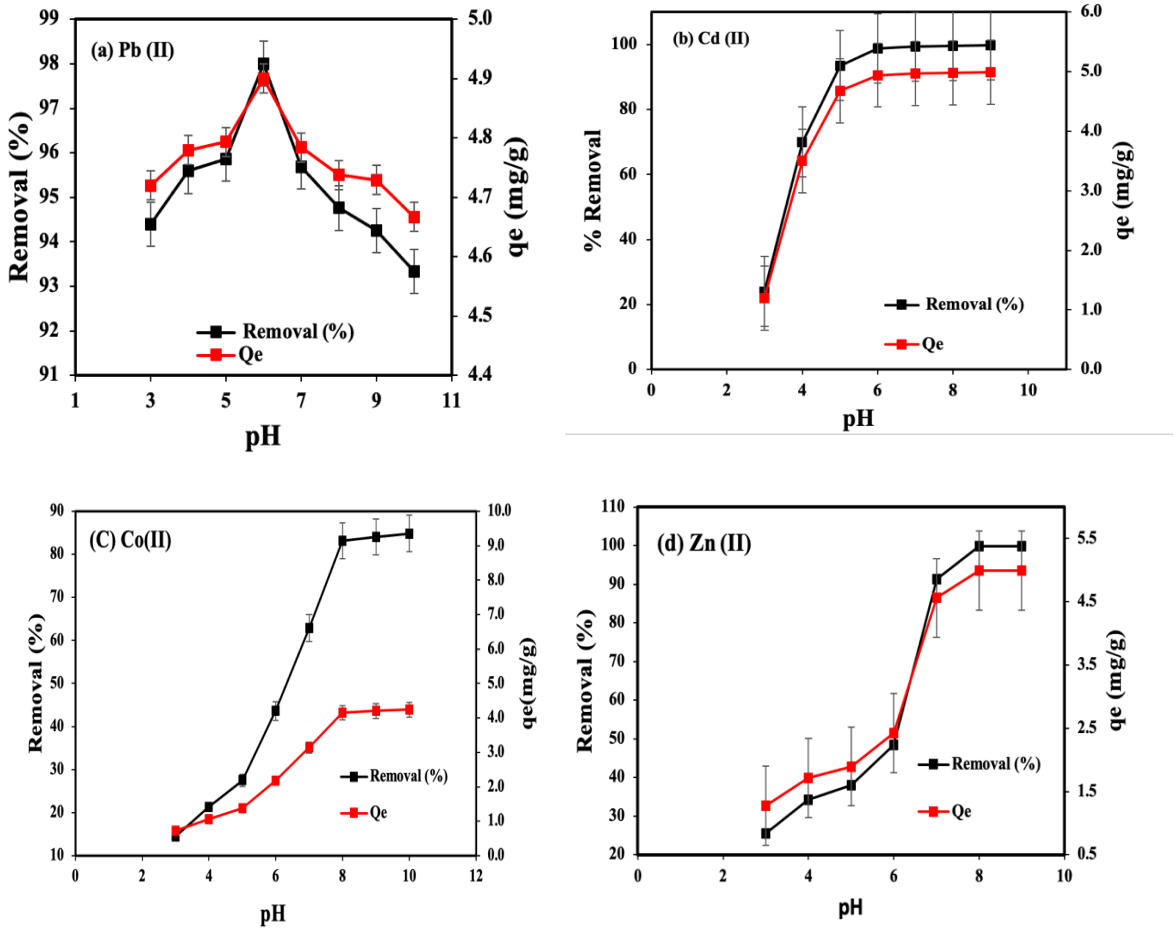


Fig. 4. 36: Effect of pH on the adsorption capacity and removal percentage of HMIs onto the semi-IPN PVA- CHTS-CLS nanocomposite hydrogel beads. (a) Pb(II), (b) Cd(II), (c) Co(II), and (d) Zn (II) (C_0[Metals] = 50 mg/L, V = 50 mL, beads dosage = 0.5 g, pH = 3-10, t = 200 min, T = 30 °C).

4.2.4.2. Effect of Contact Time on the removal of HMIs

The effects of contact time on the removal of Pb (II), Cd (II), Co (II) and Zn(II) by PVA-CHTS-CLS nanocomposites hydrogel were studied at different time periods ranging from 20 to 200 min and the results are shown in Table 4.19 and Fig. 4.37. The adsorption process undergoes multi-step sorption mechanism, the first step is corresponded to surface diffusion. The second step is related to sorption process of the metal ions and the

adsorbent beads. The last step is the equilibrium step (Wintgens et al., 2013).

The figure shows that the removal of the residual metals ions increased with increasing contact time. The adsorption equilibrium was achieved within 40 min of contact time in case of Pb (II), Cd (II) and Zn (II), whereas for Co (II) the equilibrium time attained at 200 min. The rapid removal of the metallic ions on the adsorbent surface at the initial stage of the process is attributed to the availability of more active adsorption sites at the beginning of the adsorption process which permits fast accumulation of metallic ions on the adsorption sites. As the process progresses, the active sites get filled, the accessibility of the metal ions to the active sites gradually decreased due to the saturation of the active sites and eventually the adsorption process approaches the equilibrium at certain time (P. et al., 2017; Zulfiqar et al., 2020). The maximum percent removal of Pb (II), Cd(II), Co (II) and Zn (II) were 98.0 %, 99.8 %, 83.0 % and 99.8% respectively.

Table (4. 19): Effect of contact time on the adsorption capacity and removal percentage of HMIs onto the PVA-CHTS-CLS nanocomposite hydrogel beads.

Removal of Pb(II) (V = 50 mL, initial concentration = 50 mg/L, pH =6, beads dosage= 0.5 g, temp. =30 ºC, time = 200 min, wavelength = 220.353 nm)						
Time (min)	**Pb(II) Concentrations (mg/L)**			**Pb(II) Average Concentration (mg/L)**	**% Removal ± SD**	**Q_e ± SD (mg/g)**
	Trail 1	**Trail 2**	**Trail 3**			
20	10.6	10.7	9.60	10.3	79.4±1.0	3.97±0.6
40	1.20	1.356	1.30	1.30	97.4±0.1	4.87±0.008
60	1.49	0.955	1.19	1.20	97.6±0.5	4.88±0.03
80	1.27	1.134	1.10	1.20	97.7±0.2	4.88±0.009
100	1.16	0.937	1.30	1.10	97.7±0.4	4.89±0.02
120	1.40	0.861	1.13	1.10	97.7±0.5	4.89±0.03
140	1.10	0.864	1.15	1.00	97.9±0.3	4.90±0.02
160	1.01	0.868	1.15	1.00	97.9±0.2	4.90±0.01

180	0.987	0.873	1.16	1.00	97.9±0.2	4.90±0.01
200	1.12	0.711	1.16	1.00	98.0±0.4	4.90±0.02
Removal of Cd(II) (V = 50 mL, initial concentration = 50 mg/L, pH = 6, beads dosage= 0.5 g, temp. =30 ºC, time = 200 min, wavelength = 228.802 nm)						
Time (min)	**CdII) Concentrations (mg/L)**			**Cd (II) Average Concentration (mg/L)**	**% Removal ± SD**	**Q_e ± SD (mg/g)**
	Trail 1	**Trail 2**	**Trail 3**			
20	1.44	1.33	1.19	1.32	97.4±0.1	4.87±0.1
40	1.40	1.29	1.12	1.27	97.5±0.1	4.87±0.1
60	1.38	1.29	1.04	1.24	97.5±0.1	4.88±0.1
80	1.13	1.15	0.882	1.05	97.9±0.1	4.89±0.1
100	0.873	1.11	0.764	0.916	98.2±0.2	4.91±0.1
120	0.749	0.892	0.709	0.783	98.4±0.09	4.92±0.08
140	0.809	0.777	0.696	0.761	98.5±0.06	4.92±0.04
160	0.648	0.83	0.678	0.719	98.6±0.09	4.93±0.08

180	0.642	0.584	0.683	0.636	98.7±0.05	4.94±0.04
200	0.660	0.529	0.605	0.598	98.80±0.07	4.940±0.05
Removal of Co(II) (V = 50 mL, initial concentration = 50 m/gL, pH = 8, beads dosage= 0.5 g, temp. =30 ºC, time = 200 min, wavelength = 228.61nm)						
Time (min)	**Co(II) Concentrations (mg/L)**			**Co(II) Average Concentration (mg/L)**	**% Removal ± SD**	**Q_e ± SD (mg/g)**
	Trail 1	**Trail 2**	**Trail 3**			
20	21.2	17.7	9.67	16.2	67.6±11.0	3.38±0.6
40	13.0	21.8	9.50	14.8	70.4±12.0	3.52±0.6
60	18.3	13.6	8.80	13.6	72.8±9.0	3.64±0.5
80	12.9	14.9	8.74	12.2	75.6±6.0	3.78±0.3
100	17.5	11.2	7.72	12.1	75.7±10.0	3.78±0.5
120	17.5	10.9	7.71	12.0	75.8±10.0	3.79±0.5
140	10.04	11.7	10.25	10.6	78.7±1.0	3.93±0.09
160	7.59	11.6	9.47	9.58	80.8±4.0	4.04±0.2
180	8.70	10.8	7.97	9.16	81.7±3.0	4.08±0.2

200	8.08	9.31	7.92	8.44	83.1±1.0	4.16±0.08
Removal of Zn(II) (V = 50 mL, initial concentration = 50 mg/L, pH = 8, beads dosage= 0.5 g, temp. =30 ºC, time = 200 min, wavelength = 206.200 nm)						
Time (min)	**Zn(II) Concentrations (mg/L)**			**Zn(II) Average Concentration (mg/L)**	**%Removal ± SD**	**Q_e ± SD (mg/g)**
	Trail 1	**Trail 2**	**Trail 3**			
20	0.166	0.064	0.058	0.0960	99.8±0.1	4.99±0.006
40	0.108	0.070	0.036	0.0713	99.9±0.07	4.99±0.004
60	0.212	0.213	0.162	0.196	99.6±0.06	4.98±0.003
80	0.100	0.105	0.087	0.0973	99.8±0.02	4.99±0.0009
100	0.149	0.058	0.055	0.0873	99.8±0.1	4.99±0.005
120	0.130	0.127	0.065	0.107	99.8±0.07	4.99±0.004
140	0.183	0.108	0.058	0.116	99.8±0.01	4.99±0.006
160	0.128	0.121	0.036	0.0950	99.8±0.1	4.99±0.005
180	0.101	0.103	0.030	0.0780	99.8±0.08	4.99±0.004
200	0.111	0.078	0.043	0.0773	99.8±0.07	4.99±0.003

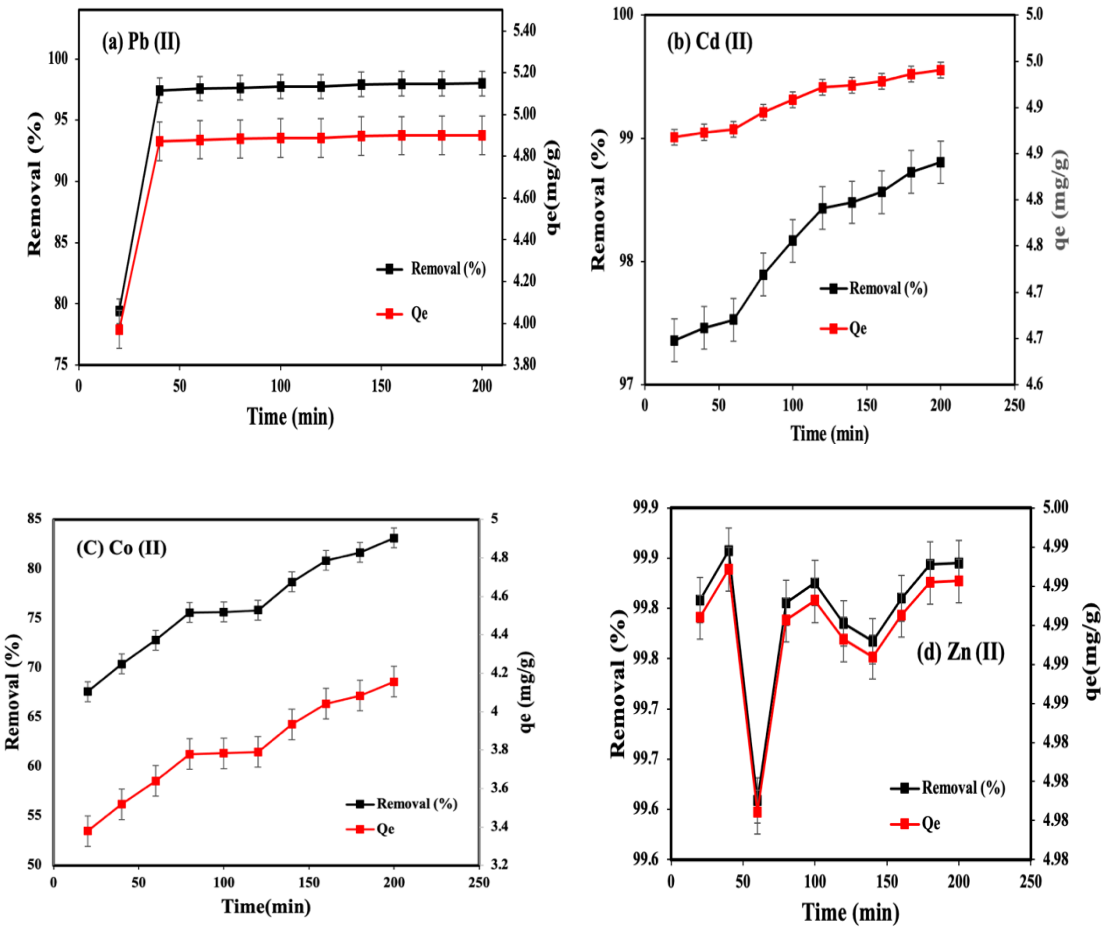


Fig. 4. 37: Effect of contact time on the adsorption capacity and removal percentage of HMIs onto the semi-IPN PVA- CHTS-CLS nanocomposite hydrogel beads. (a) Pb(II) (b) Cd(II), (c) Co(II) and (d) Zn(II) (C0[Metals] = 50 mg/L, V = 50 mL, beads dosage = 0.5 g, pH = 6 (Pb & Cd), 8 (Co &Zn) , t = 200 min, T = 30 °C).

4.2.4.3. Effect of Initial HMIs Concentration

Concerning the removal metal ions from industrial wastewater, the initial concentration of metallic ions is critical and important factor to evaluate the adsorption capacity of the adsorbent nanocomposites' beads (Zulfiqar et al., 2020). Table 4.20 and Fig. 4.38 demonstrate the effect of initial concentration on the adsorption capacity and the removal percentage of Pb (II), Cd (II), Co (II) and Zn(II) ions on PVA-CHTS-CLS nanocomposites beads. The results showed that by increasing the

concentration of the adsorbate ions, the adsorption capacity increased and the removal efficiency decreased. At high concentration of the adsorbate ions, more collision of ions with the adsorbent surface is occurred which enhances the binding between the active sites of the adsorbents and the metals ions resulting in high surface coverage and saturation of sites (R. Ahmad & Mirza, 2018a; Fahim Chyad et al., 2021). As a results the available adsorption sites becomes fewer and the ratio of the initial concentration to the available surface area is high.

Table (4. 20): Effect of initial concentrations on the adsorption capacity and removal percentage of HMIs onto the PVA-CHTS-CLS nanocomposite hydrogel beads.

Removal of Pb(II) (V = 50 mL, initial concentration = 50-200 mg/L, pH =6, beads dosage= 0.5 g, temp. =30 ºC, time = 200 min, wavelength = 220.353 nm)							
Initial Pb(II) conc. (ppm)	**Time (min)**	**Pb (II) concentartion (mg/L)**			**Pb (II) Average conc. (mg/L)**	**% Removal ±SD**	**Q_e ± SD (mg/g)**
		Trail 1	**Trail 2**	**Trail 3**			
50 ppm	20	10.6	10.7	9.60	10.3	79.4±1.0	3.97±0.6
	40	1.20	1.356	1.30	1.30	97.4±0.1	4.87±0.007
	60	1.49	0.955	1.19	1.20	97.6±0.5	4.88±0.02
	80	1.27	1.134	1.10	1.20	97.7±0.1	4.88±0.009
	100	1.16	0.937	1.30	1.10	97.7±0.3	4.89±0.01
	120	1.40	0.861	1.13	1.10	97.7±0.5	4.89±0.03
	140	1.10	0.864	1.15	1.00	97.9±0.3	4.90±0.01
	160	1.01	0.868	1.157	1.00	97.9±0.3	4.90±0.01

	180	0.987	0.873	1.161	1.00	97.9±0.3	4.90±0.01
	200	1.12	0.711	1.16	1.00	98.0±0.5	4.90±0.02
100 ppm	20	24.00	27.00	25.00	25.33	74.2±1.0	7.42±0.1
	40	2.83	2.85	2.59	2.76	97.2±0.1	9.72±0.01
	60	2.66	2.70	2.56	2.64	97.4±0.07	9.74±0.007
	80	2.66	2.70	2.56	2.50	97.4±0.07	9.74±0.007
	100	2.45	2.64	2.40	2.49	97.5±0.1	9.75±0.013
	120	2.63	2.40	2.45	2.48	97.5±0.1	9.75±0.01
	140	2.47	2.42	2.56	2.45	97.5±0.07	9.75±0.007
	160	2.82	2.02	2.10	2.31	97.7±0.4	9.77±0.04
	180	1.95	2.72	2.20	2.29	97.7±0.4	9.77±0.03
	200	2.01	1.95	2.19	2.05	97.9±0.1	9.79±0.01
150 ppm	20	51.0	54.0	47.0	50.6	66.2±2.0	9.93±0.3
	40	29.2	27.0	25.0	27.1	81.9±1.0	12.29±0.2
	60	19.0	18.0	19.4	18.8	87.4±0.5	13.1±0.07
	80	10.1	5.88	3.34	6.47	95.6±2.0	14.3±0.3

	100	7.60	4.20	4.55	5.45	96.3±1.0	14.4±0.2
	120	6.69	2.70	4.57	4.66	96.9±1.0	14.53±0.2
	140	7.13	3.45	4.43	5.01	96.6±1.0	14.5±0.2
	160	6.98	3.31	4.40	4.90	96.7±1.0	14.5±0.2
	180	6.48	3.30	4.10	4.63	96.9±1.0	14.5±0.2
	200	6.61	3.20	4.00	4.60	96.9±1.0	14.5±0.2
200 ppm	20	103	98.7	131	111	44.3±8.0	8.88±1.0
	40	55.9	50.9	36.8	47.8	76.0±4.0	15.21±0.9
	60	7.90	7.30	7.00	7.40	96.3±0.2	19.26±0.05
	80	7.80	7.00	7.70	7.50	96.2±0.2	19.25±0.04
	100	7.50	6.70	7.70	7.30	96.3±0.2	19.2±0.05
	120	7.10	6.30	7.60	7.00	96.5±0.3	19.3±0.07
	140	6.80	6.10	7.80	7.00	96.5±0.4	19.3±0.09
	160	6.80	6.50	7.64	6.98	96.5±0.3	19.3±0.06
	180	7.20	6.70	7.07	6.99	96.5±0.3	19.3±0.03
	200	6.00	6.50	7.90	6.80	96.6±0.5	19.3±0.1

Removal of Cd(II) (V = 50 mL, initial concentration = 50-200 mg/L, pH =6, beads dosage= 0.5 g, temp. =30 ºC, time = 200 min, wavelength = 228.802 nm)							
Initial Cd (II) conc. (ppm)	**Time (min)**	**Cd(II) concentration (mg/L)**			**Cd (II) Average conc. (mg/L)**	**% Removal ± SD**	**Q_e ± SD (mg/g)**
		Trail 1	**Trail 2**	**Trail 3**			
50 ppm	20	1.44	1.33	1.19	1.32	97.4±0.1	4.87±0.1
	40	1.40	1.29	1.12	1.27	97.5±0.1	4.87±0.1
	60	1.38	1.29	1.04	1.24	97.5±0.1	4.88±0.1
	80	1.13	1.15	0.882	1.05	97.9±0.1	4.89±0.1
	100	0.873	1.11	0.764	0.916	98.2±0.1	4.91±0.1
	120	0.749	0.892	0.709	0.783	98.4±0.09	4.92±0.07
	140	0.809	0.777	0.696	0.761	98.5±0.05	4.92±0.04
	160	0.648	0.83	0.678	0.719	98.6±0.09	4.93±0.08
	180	0.642	0.584	0.683	0.636	98.7±0.05	4.94±0.04

	200	0.660	0.529	0.605	0.598	98.8±0.06	4.94±0.05
100 ppm	20	49.0	47.8	48.1	48.3	51.7±0.6	5.17±0.06
	40	48.4	46.0	44.2	46.2	53.8±2.0	5.38±0.2
	60	45.0	40.6	40.6	42.1	57.9±2.0	5.79±0.2
	80	43.1	38.9	36.1	39.4	60.6±3.0	6.06±0.3
	100	36.3	35.8	35.5	35.9	64.1±0.4	6.41±0.04
	120	33.7	32.7	31.9	32.8	67.2±0.9	6.72±0.09
	140	20.6	28.0	29.6	26.1	73.9±4.0	7.39±0.4
	160	14.8	24.1	24.1	21.0	79.0±5.0	7.90±0.3
	180	8.88	10.4	10.4	9.9	90.1±0.8	9.01±0.08
	200	7.91	4.386	5.6	6.0	94.0±1.0	9.40±0.1
150 ppm	20	94.3	99.3	94.7	96.1	35.9±1.0	5.39±0.2
	40	93.2	88.4	83.1	88.2	41.1±3.0	6.18±0.5
	60	89.7	86.5	81.6	85.9	42.7±2.0	6.41±0.5
	80	81.8	79.5	76.2	79.2	47.2±1.0	7.08±0.2
	100	51.3	61.7	60.8	57.9	61.3±3.0	9.21±0.5

	120	47.3	43.2	48.9	46.5	69.0±1.0	10.3±0.2
	140	34.9	37.1	38.6	36.9	75.42±1.0	11.3±0.1
	160	16.6	17.9	19.1	17.9	88.0±0.8	13.2±0.1
	180	14.0	13.7	15.1	14.3	90.4±0.0.4	13.5±0.07
	200	13.1	13.4	2.427	13.7	90.8±0.5	13.63±0.08
200 ppm	20	130.0	138.0	120	129.3	35.3±4.51	7.07±0.9
	40	92.8	109.1	110	104.0	48.0±4.84	9.60±0.9
	60	87.6	81.9	80.2	83.2	58.4±1.94	11.6±0.3
	80	77.9	74.2	73.4	75.2	62.4±1.20	12.4±0.2
	100	40.0	46.9	45.4	44.1	78.0±1.81	15.5±0.3
	120	39.3	45.9	43.2	42.8	78.6±1.66	15.7±0.3
	140	36.0	43.7	39.8	39.8	80.1±1.92	16.0±0.3
	160	26.5	33.8	30.7	30.3	84.8±2.0	16.9±0.3
	180	24.4	31.9	29.8	28.7	85.6±2.0	17.1±0.3
	200	22.0	27.5	21.8	23.8	88.1±1.0	17.62±0.3

Removal of Co(II) (V = 50 mL, initial concentration = 50-200 mg/L, pH =6, beads dosage= 0.5 g, temp. =30 ºC, time = 200 min, wavelength = 228.61 nm)							
Initial Co(II) conc. (ppm)	**Time (min)**	**Co(II) concentration (ppm)**			**Co(II) Average conc. (ppm)**	**% Removal ± SD**	**Q_e ± SD (mg/g)**
		Trail 1	**Trail 2**	**Trail 3**			
50 ppm	20	21.2	17.7	9.67	16.2	67.6±11.0	3.38±0.6
	40	13.0	21.8	9.50	14.8	70.4±12.0	3.52±0.6
	60	18.3	13.6	8.80	13.6	72.8±9.0	3.64±0.4
	80	12.9	14.9	8.74	12.2	75.6±6.0	3.78±0.3
	100	17.5	11.2	7.72	12.1	75.7±10.0	3.78±0.5
	120	17.5	10.9	7.71	12.0	75.8±10.0	3.79±0.5
	140	10.04	11.7	10.25	10.6	78.7±2.0	3.93±0.09
	160	7.59	11.6	9.47	9.58	80.8±4.0	4.04±0.2
	180	8.70	10.8	7.97	9.16	81.7±3.0	4.08±0.1
	200	8.08	9.31	7.92	8.44	83.1±2.0	4.16±0.08

100 ppm	20	41.9	42.6	40.8	41.8	58.2±0.9	5.82±0.09
	40	35.9	37.1	38.2	37.1	62.9±1.0	6.29±0.1
	60	31.3	31.8	32.8	31.9	68.1±0.7	6.81±0.08
	80	30.2	31.0	30.5	30.6	69.4±0.4	6.94±0.04
	100	27.1	28.4	27.1	27.5	72.5±0.7	7.25±0.08
	120	27.0	26.3	26.0	26.4	73.6±0.5	7.36±0.05
	140	23.8	24.6	24.6	24.3	75.7±0.5	7.57±0.05
	160	18.4	21.5	23.2	21.0	79.0±2.0	7.90±0.2
	180	20.9	20.2	21.6	20.9	79.1±0.7	7.91±0.07
	200	20.2	19.3	20.8	20.1	79.9±0.7	7.99±0.08
150 ppm	20	81.9	79.6	85.1	82.2	45.2±2.0	6.8±0.28
	40	76.1	73.0	78.8	76.0	49.4±2.0	7.40±0.2
	60	65.1	69.1	67.3	67.2	55.2±1.0	8.30±0.2
	80	64.1	65.2	66.6	65.3	56.5±0.8	8.500±0.1
	100	51.9	60.2	61.3	57.8	61.5±3.0	9.2±0.5
	120	48.3	49.8	46.2	48.1	67.9±1.0	10.2±0.1

	140	41.3	47.8	42.2	43.7	70.8±2.0	10.6±0.3
	160	39.2	42.3	41.3	40.9	72.7±1.0	10.9±0.1
	180	38.5	41.3	40.3	40.0	73.3±0.9	11.0±0.1
	200	38.2	41.2	40.2	39.8	73.4±1.0	11.0±0.1
200 ppm	20	100.4	95.3	92.8	96.2	51.9±2.0	10.4±0.4
	40	92.9	90.2	87.2	90.1	55.0±1.0	11.0±0.3
	60	87.7	89.2	85.7	87.5	56.3±0.9	11.3±0.2
	80	84.2	86.7	83.1	84.7	57.7±0.9	11.5±0.2
	100	81.3	83.1	82.8	82.4	58.8±0.4	11.8±0.
	120	78.9	81.9	80.6	80.5	59.8±0.	12.0±0.1
	140	74.2	79.6	78.6	77.5	61.3±1.0	12.3±0.1
	160	70.1	78.0	77.6	75.2	62.4±2.0	12.5±0.4
	180	68.5	77.2	76.2	74.0	63.0±2.0	12.6±0.4
	200	64.5	76.8	75.9	72.4	63.8±3.0	12.8±0.6
Removal of Zn(II) (V = 50 mL, initial concentration = 50-200 mg/L, pH =6, beads dosage= 0.5 g, temp. =30 ºC, time = 200 min, wavelength = 206.200 nm)							

Initial Zn(II) conc. (ppm)	Time (min)	Zn (II) concentration (ppm)			Zn (II) Average conc. (ppm)	% Removal ± SD	Q_e ± SD (mg/g)
		Trail 1	Trail 2	Trail 3			
50 ppm	20	0.212	0.213	0.1620	0.196	99.6±0.06	4.98±0.002
	40	0.183	0.108	0.0580	0.116	99.8±0.1	4.99±0.006
	60	0.130	0.127	0.0650	0.107	99.8±0.07	4.99±0.003
	80	0.100	0.105	0.0870	0.097	99.8±0.02	4.99±0.0009
	100	0.166	0.064	0.0580	0.096	99.8±0.1	4.99±0.006
	120	0.128	0.121	0.0360	0.095	99.8±0.1	4.99±0.005
	140	0.149	0.058	0.0550	0.087	99.8±0.1	4.99±0.005
	160	0.101	0.103	0.0300	0.078	99.8±0.08	4.99±0.004
	180	0.111	0.078	0.0430	0.077	99.8±0.07	4.99±0.003
	200	0.108	0.070	0.0360	0.071	99.9±0.07	4.99±0.004
100 ppm	20	1.52	1.54	1.32	1.46	98.5±0.1	9.85±0.01
	40	1.48	1.39	1.56	1.48	98.5±0.09	9.85±0.009

	60	1.42	1.34	1.52	1.42	98.6±0.09	9.86±0.009
	80	1.25	1.27	1.45	1.32	98.7±0.1	9.87±0.01
	100	1.21	1.31	1.41	1.31	98.7±0.1	9.87±0.01
	120	1.21	1.21	1.39	1.27	98.7±0.1	9.87±0.0102
	140	1.28	1.22	1.31	1.27	98.7±0.04	9.87±0.00440
	160	1.26	1.19	1.28	1.25	98.8±0.05	9.88±0.00470
	180	1.29	1.44	1.26	1.33	98.7±0.09	9.87±0.009
	200	1.23	1.53	1.33	1.36	98.6±0.1	9.86±0.01
150 ppm	20	5.80	5.82	6.88	6.17	95.9±0.4	14.4±0.06
	40	5.72	5.80	6.42	5.98	96.0±0.2	14.4±0.04
	60	4.91	5.61	5.78	5.43	96.4±0.3	14.5±0.04
	80	4.67	4.33	5.23	4.75	96.8±0.3	14.5±0.04
	100	4.28	4.29	3.15	3.91	97.4±0.4	14.6±0.07
	120	4.18	3.82	3.86	3.95	97.4±0.1	14.6±0.02
	140	4.10	3.15	3.50	3.58	97.6±0.3	14.6±0.04
	160	3.68	3.15	3.62	3.48	97.7±0.2	14.7±0.03

	180	3.51	2.97	3.24	3.24	97.8±0.2	14.7±0.03
	200	3.47	2.76	3.15	3.13	97.9±0.2	14.7±0.04
200 ppm	20	10.19	11.81	8.90	10.30	94.9±0.7	19.0±0.1
	40	9.67	11.56	8.28	9.84	95.1±0.8	19.0±0.17
	60	9.18	10.78	8.11	9.36	95.3±0.7	19.1±0.1
	80	8.22	7.60	8.90	8.24	95.9±0.3	19.2±0.06
	100	7.93	7.21	8.28	7.81	96.1±0.3	19.2±0.05
	120	7.22	6.56	8.11	7.30	96.4±0.4	19.3±0.07
	140	7.18	6.30	7.90	7.13	96.4±0.4	19.3±0.08
	160	6.96	5.84	7.77	6.86	96.6±0.5	19.3±0.09
	180	6.62	5.68	7.12	6.47	96.8±0.3	19.4±0.07
	200	6.34	5.33	6.61	6.09	97.0±0.3	19.4±0.07

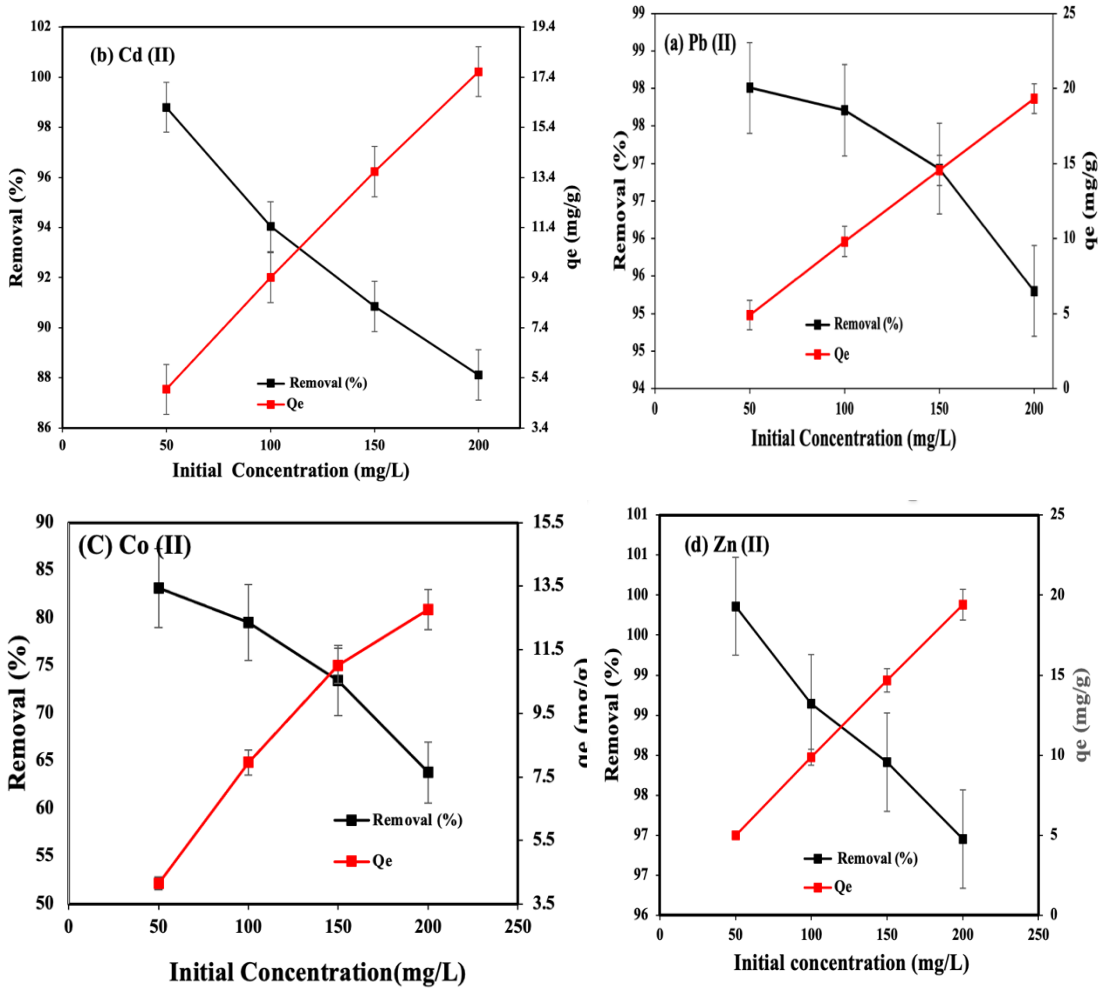


Fig. 4. 38: Effect of initial HMIs concentration on the adsorption capacity and removal percentage onto the semi-IPN PVA- CHTS-CLS nanocomposite hydrogel beads. (a) Pb^{2+}, (b) Cd^{2+}, (c) Co^{2+} and (d) Zn^{2+} (C_0[Metals] = 50 mg/L, V = 50 mL, beads dosage = 0.5 g, pH = 6 (Pb and Cd), 8 (Co &Zn), t = 200 min, T = 30 °C

4.2.4.4. Effect of Adsorbent Dosage on the removal of HMIs

To study the effect of adsorbent dosage on the removal efficiency of the metal ions, different quantities of adsorbent (0.1, 0.3 and 0.5 g) were added to aqueous solution of 50 ppm initial concentration of metal ions Pb (II),

Cd (II), Co (II) and Zn(II). The results are illustrated in Table 4.21 and Fig. 4.39. At constant adsorbate concentration, an increase in the percentage removal on HMIs was observed as the adsorbent dosage increased until saturation point is reached (Sheth et al., 2021). In case of Pb (II) and Cd (II) the removal efficiency nearly remains constant as the adsorbent mass increased above 0.1 g. In case of Co (II) and Zn (II) the removal efficiency increased as the adsorbent dosage increased from 0.1 g to 0.5 g. In case of Co (II) the removal percentage increased from 45% to 84 % and for Zn (II) the removal percentage increased from 50 % to 99.8 %. This increase in the removal efficiency can be related to the increase of active adsorption sites when the adsorbent mass increases. Additionally, the adsorption capacity decreased at higher dosage of adsorbent because of the increase in the unoccupied adsorption site (Khayyun & Mseer, 2019; Sheth et al., 2021). Similar results have been reported by(Esrafili et al., 2019).

Table (4. 21): Effect of adsorbent's dosage on the adsorption capacity and removal percentage of HMIs onto the PVA-CHTS-CLS nanocomposite hydrogel beads.

Removal of Pb(II) (V = 50 mL, initial concentration = 50mg/L, pH =6, beads dosage= 0.1-0.5 g, temp. =30 ºC, time = 200 min, wavelength = 220.353 nm)						
Beads Dosage (g)	**Pb (II) Concentrations (mg/L)**			**Pb(II) Average Concentration (mg/L)**	**% Removal ± SD**	**Q_e ± SD (mg/g)**
	Trail 1	**Trail 2**	**Trail 3**			
0.1	0.864	0.116	1.81	0.900	98.1±1.0	24.5±0.4
0.3	1.07	1.81	1.66	1.50	96.9±0.8	8.08±0.07
0.5	1.12	0.711	1.16	1.00	98.0±0.5	4.90±0.02
Removal of Cd(II) (V = 50 mL, initial concentration = 50mg/L, pH =6, beads dosage= 0.1-0.5 g, temp. =30 ºC, time = 200 min, wavelength = 228.802 nm)						
Beads Dosage (g)	**Cd(II) Concentrations (mg/L)**			**Cd(II) average Concentration (mg/L)**	**% Removal ± SD**	**Q_e ± SD (mg/g)**
	Trail 1	**Trail**	**Trail**			

		2	3			
0.1	1.16	1.19	1.47	1.28	97.51±0.3	24.4±0.08
0.3	1.28	0.867	0.87	1.006	98.1±0.5	8.16±0.04
0.5	0.660	0.529	0.605	0.598	98.8±0.07	4.940±0.05

Removal of Co(II) (V = 50 mL, initial concentration = 50 mg/L, pH =8, beads dosage= 0.1-0.5 g, temp. =30 ºC, time = 200 min, wavelength = 228.61 nm)

Beads Dosage (g)	Co(II) Concentrations (mg/L)			Co(II) Average Concentration (mg/L)	%Removal ± SD	Q_e ± SD (mg/g)
	Trail 1	Trail 2	Trail 3			
0.1	22.4	27.9	29.0	26.5	47.1±7.0	11.8±2.0
0.2	26.2	20.9	19.6	22.3	55.5±7.0	6.94±0.8
0.3	19.8	15.9	20.3	18.7	62.7±5.0	5.22±0.4
0.4	16.4	14.9	14.6	15.3	69.4±2.0	4.34±0.1
0.5	8.08	9.31	7.92	8.44	83.1±2.0	4.16±0.07

Removal of Zn(II) (V = 50 mL, initial concentration = 50mg/L, pH =8, beads dosage= 0.1-0.5 g, temp. =30 ºC, time = 200 min, wavelength = 206.200 nm)						
Beads Dosage (g)	**Zn(II) Concentrations (mg/L)**			**Zn (II) Average Concentration (mg/L)**	**% Removal ± SD**	**Q_e ± SD (mg/g)**
	Trail 1	**Trail 2**	**Trail 3**			
0.1	27.6	21.5	25.8	24.9	50.1±6.00	12.5±2.0
0.2	8.19	8.93	8.51	8.54	82.9±0.7	10.4±0.09
0.3	6.73	6.03	5.93	6.23	87.5±0.9	7.29±0.07
0.4	1.27	1.90	1.98	1.72	96.6±0.8	6.04±0.05
0.5	0.111	0.078	0.043	0.080	99.9±0.07	4.99±0.003

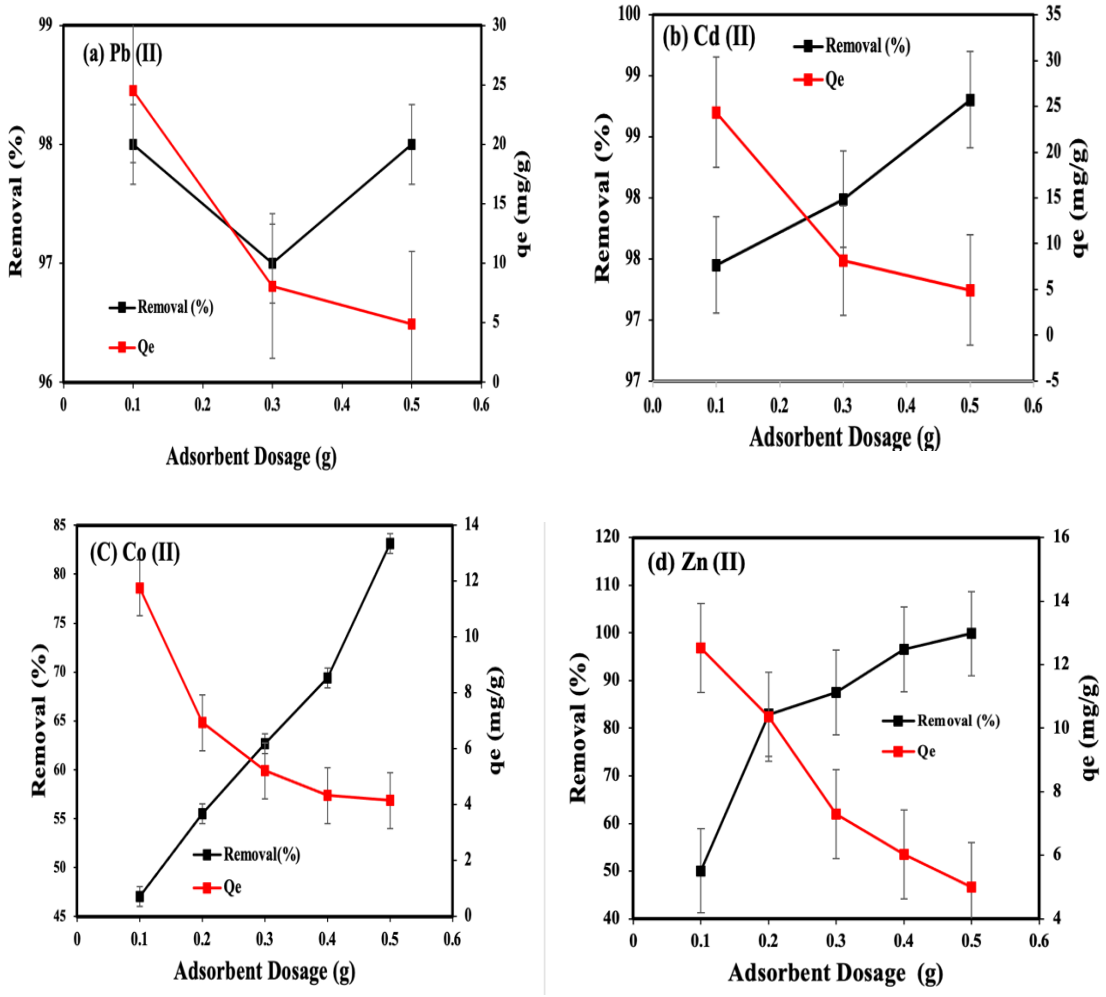


Fig. 4. 39: Effect of adsorbent dosages (PVA- CHTS-CLS nanocomposite hydrogel beads) on the adsorption capacity and removal percentage of HMIs: (a) Pb (II), (b) Cd (II), (c) Co (II) and (d) Zn (II) (C_0[Metals] = 50 mg/L, V = 50 mL, beads dosage = 0.1-0.5 g, pH = 6 (Pb and Cd), 8 (Co &Zn), t = 200 min, T = 30 °C).

4.2.4.5. Effect of Temperature on the removal of HMIs

The effect of solution temperature on the removal of heavy metal ions by PVA-CHTS-CLS from aqueous solution was investigated and the results are presented in Table 4.22 and Fig. 4.40. The adsorption efficiency increased with increasing the temperature of the solution from 20 to 30 °C for all metal ions because of the increase in the rate of diffusion and

mobility of the ions toward adsorption sites (Alhogbi et al., 2019; Sarkar et al., 2020). However, the percentage removal of Pb (II), Cd (II), Co (II) and Zn(II) ions decreased as the temperature increased to 40°C, this is because the metal ions adsorbed on the surface of the hydrogel may be expelled into the water solution as the saturation point of heated solution decreases due to ion desorption from the gel surface (Kubilay et al., 2007). The decrease of ions removal with increasing temperature indicated that the adsorption process is an exothermic in nature and favored at low temperatures. Our results are in agreement with previous studies (Alhogbi et al., 2019; Hayrunnisa Nadaroglu, 2012; Kubilay et al., 2007) .

Table (4. 22): Effect of temperature on the adsorption capacity and removal percentage of HMIs onto the PVA-CHTS-CLS nanocomposite hydrogel beads.

Removal of Pb(II) (V = 50 mL, initial concentration = 50mg/L, pH =6, beads dosage= 0.1-0.5 g, temp. =30 ºC, time = 200 min, wavelength = 220.353 nm)							
Temp. (ºC)	**Time (min)**	**Pb (II) Conc. (mg/L)**			**Pb (II) Average Conc. (mg/L)**	**% Removal ± SD**	**Q_e ± SD (mg/g)**
		Trail 1	**Trail 2**	**Trail 3**			
20 ºC	20	11.5	10.0	11.4	11.0	78.4±1.0	3.92±0.07
	40	5.00	4.20	3.70	4.30	91.4±1.0	4.57±0.06
	60	2.10	5.60	3.80	3.80	92.3±3.0	4.62±0.2
	80	2.30	5.50	3.80	3.80	92.3±3.0	4.62±0.2
	100	2.40	4.80	3.70	3.70	92.6±2.0	4.63±0.1
	120	2.00	4.90	3.90	3.60	92.9±3.0	4.64±0.1
	140	2.10	4.40	3.0	3.50	93.0±3.0	4.65±0.1
	160	2.20	4.00	3.900	3.40	93.2±2.0	4.66±0.09
	180	2.00	3.60	4.00	3.20	93.6±2.06	4.68±0.1

	200	2.40	3.00	3.10	2.80	94.4±0.8	4.72±0.04
30 ºC	20	10.6	10.7	9.60	10.3	79.4±1.0	3.97±0.6
	40	1.20	1.356	1.30	1.30	97.4±0.1	4.87±0.008
	60	1.49	0.955	1.19	1.20	97.6±0.5	4.88±0.03
	80	1.27	1.134	1.10	1.20	97.7±0.2	4.88±0.009
	100	1.16	0.937	1.30	1.10	97.7±0.4	4.89±0.02
	120	1.40	0.861	1.13	1.10	97.7±0.5	4.89±0.03
	140	1.10	0.864	1.15	1.00	97.9±0.3	4.90±0.02
	200	1.01	0.868	1.157	1.00	97.9±0.3	4.90±0.01
	180	0.987	0.873	1.161	1.00	97.9±0.3	4.90±0.01
	200	1.12	0.711	1.16	1.00	98.0±0.5	4.90±0.02
40 ºC	20	14.7	6.90	7.90	9.80	80.3±8.0	4.02±0.4
	40	13.1	10.3	2.80	8.70	82.5±10.0	4.13±0.5
	60	12.5	7.00	5.20	8.20	83.6±7.0	4.18±0.4
	80	6.30	4.100	4.00	8.00	90.4±3.0	4.52±0.1
	100	6.70	11.3	5.10	7.70	84.6±6.0	4.23±0.3

	120	8. 0	5.70	4.90	6.400	87.2±4.0	4.36±0.2
	140	7. 0	4.30	7.50	6.40	87.1±4.0	4.30±0.2
	200	6.40	5.90	4.10	5.40	89.1±2.0	4.46±0.1
	180	5.10	7.30	3.50	5.30	89.4±4.0	4.47±0.2
	200	6.30	4.10	4.00	4.80	90.4±3.0	4.52±0.1
Removal of Cd(II) (V = 50 mL, initial concentration = 50mg/L, pH =6, beads dosage= 0.1-0.5 g, temp. =30 ºC, time = 200 min, wavelength = 228.802 nm)							
Temp. (ºC)	**Time (min)**	**Cd(II) Concentration (mg/L)**			**Cd(II) Average Concentration (mg/L)**	**% Removal ± SD**	**Q_e ± SD (mg/g)**
		Trail 1	**Trail 2**	**Trail 3**			
20 ºC	20	17.3	18.1	19.2	18.2	63.6±0.9	15.9±0.7
	40	16.1	17.3	18.5	17.3	65.4±1.0	16.3±0.9
	60	14.1	15.5	17.2	15.6	68.8±1.0	17.2±1.0
	80	14.5	14.8	16.5	15.3	69.4±1.0	17.4±0.9
	100	13.7	13.7	14.1	13.9	72.3±0.2	18.1±0.2

	120	9.5	10.8	12.6	10.9	78.1±1.0	19.5±1.0
	140	5.7	9.1	9.8	8.20	83.6±2.0	20.9±2.0
	160	5.2	7.5	7.3	6.66	86.7±1.0	21.7±1.0
	180	4.6	6.9	6.2	5.91	88.2±1.0	22.0±0.9
	200	3.4	6.2	5.9	5.18	89.6±1.0	22.4±1.0
30 ºC	20	1.44	1.33	1.19	1.32	97.4±0.1	4.87±0.1
	40	1.40	1.29	1.12	1.27	97.5±0.1	4.87±0.1
	60	1.38	1.29	1.04	1.24	97.5±0.1	4.88±0.1
	80	1.13	1.15	0.882	1.05	97.9±0.1	4.89±0.1
	100	0.873	1.11	0.764	0.916	98.2±0.2	4.91±0.1
	120	0.749	0.892	0.709	0.783	98.4±0.1	4.92±0.08
	140	0.809	0.777	0.696	0.761	98.5±0.06	4.92±0.05
	160	0.648	0.83	0.678	0.719	98.6±0.09	4.93±0.08
	180	0.642	0.584	0.683	0.636	98.7±0.05	4.94±0.04
	200	0.660	0.529	0.605	0.598	98.8±0.07	4.94±0.05
40 ºC	20	5.90	6.06	5.72	4.35	91.3±0.4	22.8±0.3

	40	5.65	5.97	5.12	3.93	92.1±0.3	23.0±0.3
	60	5.06	5.93	4.96	3.67	92.7±0.5	23.2±0.4
	80	3.84	4.93	4.34	3.25	93.5±0.5	23.4±0.5
	100	3.83	4.12	3.57	2.58	94.8±0.4	23.7±0.3
	120	3.20	3.71	3.32	2.26	95.5±0.4	23.9±0.3
	140	3.16	3.31	3.17	1.83	96.3±0.1	24.1±0.1
	160	2.92	2.96	2.78	1.65	96.7±0.02	24.2±0.01
	180	2.28	1.33	1.78	1.35	97.3±0.2	24.3±0.1
	200	2.14	1.18	1.36	1.28	97.5±0.2	24.4±0.1

Removal of Co (II) (V = 50 mL, initial concentration = 50mg/L, pH =8, beads dosage= 0.1-0.5 g, temp. =30 ºC, time = 200 min, wavelength = 228.61 nm)

Temp. (ºC)	**Time (min)**	**Co (II) Concentration (mg/L)**			**Co (II) Average Concentration, (mg/L)**	**% Removal ± SD**	**Q_e ± SD (mg/g)**
		Trail 1	**Trail 2**	**Trail 3**			
20ºC	20	23.3	23.1	21.1	22.1	55.7±2.9	13.9±0.1

	40	22.8	19.9	18.2	20.3	59.4±4.0	14.8±0.2
	60	21.5	17.	17.3	18.9	62.2±4.0	15.6±0.2
	80	18.4	17.	16.7	17.5	65.1±2.0	16.3±0.08
	100	18.2	16.4	16.1	16.9	66.2±2.0	16.6±0.1
	120	15.1	14.3	15.16	14.9	70.3±0.9	17.6±0.04
	140	11.67	12.0	14.19	12.6	74.4±2.0	18.7±0.1
	160	11.17	10.8	13.6	11.8	76.3±3.0	19.1±0.1
	180	9.81	10.7	13.0	11.3	77.4±4.0	19.4±0.2
	200	9.53	10.1	12.9	10.9	78.3±3.0	19.6±0.2
30ºC	20	21.2	17.7	9.67	16.2	67.6±11.0	3.38±0.6
	40	13.0	21.8	9.50	14.8	70.4±12.0	3.52±0.6
	60	18.3	13.6	8.80	13.6	72.8±10.0	3.64±0.5
	80	12.9	14.9	8.74	12.2	75.6±6.0	3.78±0.32
	100	17.5	11.2	7.72	12.1	75.7±10.0	3.78±0.5
	120	17.5	10.9	7.71	12.0	75.8±10.0	3.79±0.5
	140	10.04	11.7	10.25	10.6	78.7±2.0	3.93±0.09

	160	7.59	11.6	9.47	9.58	80.8±4.0	4.04±0.2
	180	8.70	10.8	7.97	9.16	81.7±3.0	4.08±0.2
	20	21.2	17.7	9.67	16.2	67.6±11.0	3.38±0.6
40ºC	20	24.5	27.9	24.2	25.5	24.5±4.0	2.43±0.2
	40	22.4	26.3	22.6	23.8	22.4±4.0	2.62±0.2
	60	18.6	22.7	21.5	20.9	18.6±4.0	2.91±0.2
	80	17.3	19.8	19.2	18.7	17.3±2.0	3.12±0.1
	100	17.1	18.1	19.5	18.2	17.1±2.0	3.18±0.1
	120	13.6	14.4	19.3	15.8	13.6±6.0	3.42±0.3
	140	12.6	13.7	18.9	15.1	12.0 ±7.0	3.49±0.3
	160	12.9	12.3	17.2	14.1	12.94±5.0	3.59±0.2
	180	12.2	11.4	16.8	13.5	12.2±6.0	3.65±0.3
	200	11.9	9.4	15.5	12.3	11.9±6.0	3.77±0.3
Removal of Zn(II) (V = 50 mL, initial concentration = 50mg/L, pH =8, beads dosage= 0.1-0.5 g, temp. =30 ºC, time = 200 min, wavelength = 206.200 nm)							
	Time	**Zn(II) Concentration**		**Zn(II) average Concentration**		**% Removal**	**Q_e ± SD**

Temp. (ºC)	(min)	(mg/L)			(mg/L)	± SD	(mg/g)
		Trail 1	Trail 2	Trail 3			
20 º C	20	1.989	1.83	1.721	1.85	96.3±0.2	4.82±0.01
	40	1.776	1.85	1.762	1.80	96.4±0.09	4.82±0.004
	60	1.804	1.14	1.671	1.54	96.9±0.7	4.85±0.03
	80	1.399	1.13	1.719	1.42	97.2±0.6	4.86±0.03
	100	1.276	1.15	1.692	1.37	97.3±0.6	4.86±0.03
	120	1.004	1.15	1.528	1.23	97.5±0.5	4.88±0.03
	140	0.766	1.65	1.160	1.19	97.6±0.9	4.88±0.04
	160	0.892	0.74	0.991	0.87	98.3±0.3	4.91±0.01
	180	0.735	0.94	0.912	0.86	98.3±0.2	4.91±0.01
	200	0.655	0.634	0.911	0.73	98.5±0.3	4.93±0.02
30º C	20	0.166	0.064	0.058	0.0960	99.8±0.1	4.99±0.006
	40	0.108	0.07	0.036	0.0713	99.9±0.07	4.99±0.003
	60	0.212	0.213	0.162	0.196	99.6±0.6	4.98±0.003
	80	0.100	0.105	0.087	0.0973	99.6±0.02	4.99±0.0009

	100	0.149	0.058	0.055	0.087	99.8±0.1	4.99±0.005
	120	0.13	0.127	0.0650	0.107	99.8±0.07	4.99±0.004
	140	0.183	0.108	0.0580	0.116	99.8±0.1	4.99±0.006
	160	0.128	0.121	0.0360	0.0950	99.8±0.1	4.99±0.005
	180	0.101	0.103	0.0300	0.0780	99.8±0.08	4.99±0.004
	200	0.111	0.0780	0.0430	0.0773	99.8±0.07	4.99±0.003
40º C	20	0.801	0.527	0.972	0.767	98.5±0.4	4.92±0.02
	40	0.743	0.534	0.87	0.716	98.6±0.3	4.93±0.02
	60	0.828	0.697	0.725	0.750	98.5±0.1	4.93±0.007
	80	0.617	0.827	0.728	0.724	98.6±0.2	4.93±0.01
	100	0.584	0.913	0.917	0.805	98.4±0.4	4.92±0.02
	120	0.607	0.599	0.874	0.693	98.6±0.3	4.93±0.02
	140	0.88	0.916	0.921	0.906	98.2±0.04	4.91±0.002
	160	0.536	0.797	0.931	0.755	98.5±0.4	4.92±0.02
	180	0.679	0.646	0.983	0.769	98.5±0.4	4.92±0.02
	200	0.708	0.544	0.893	0.715	98.6±0.3	4.93±0.02

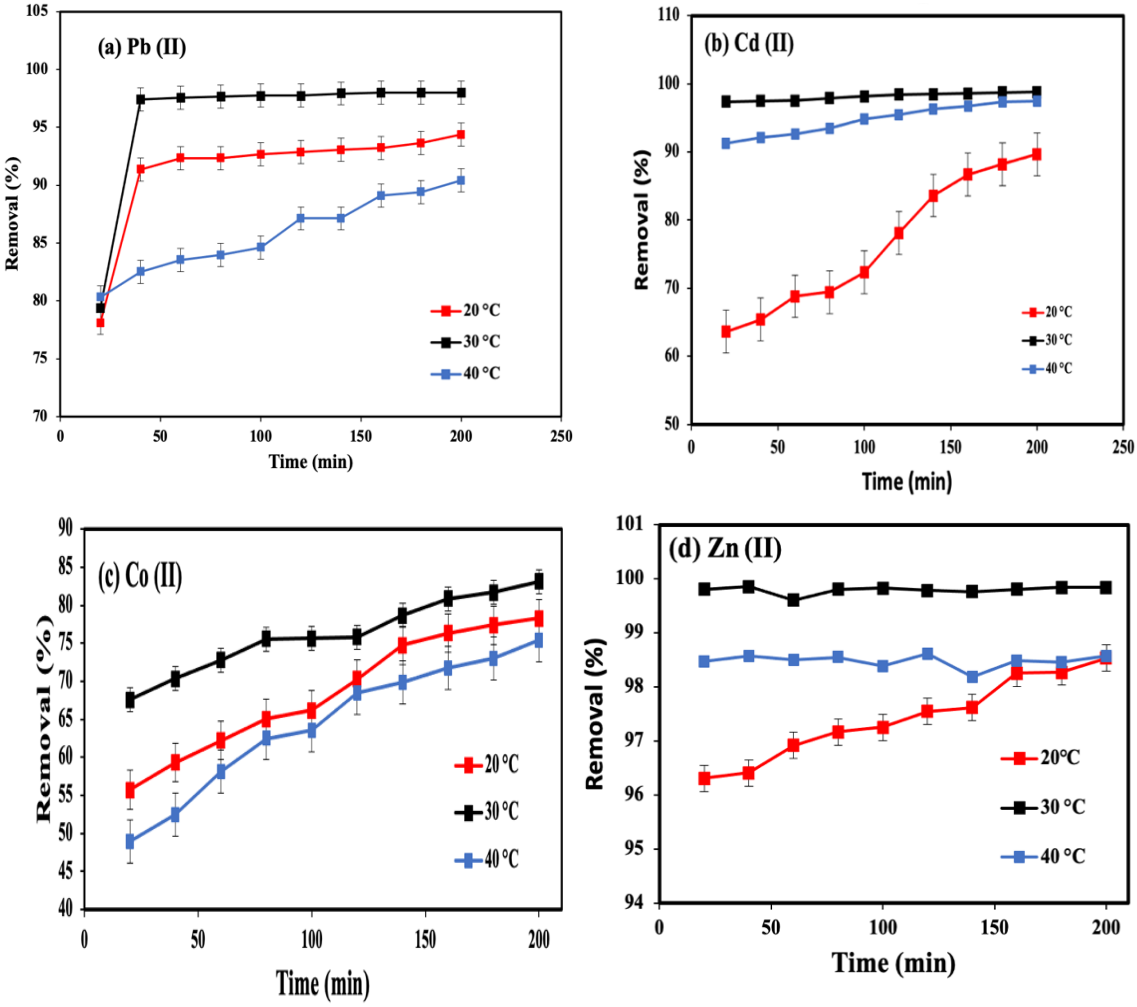


Fig. 4. 40: Effect of temperature on the adsorption capacity and removal percentage of HMIs: (a) Pb (II), (b) Cd (II), (c) Co (II) and (d) Zn (II) ((C_0[Metals] = 50 mg/L, V = 50 mL, beads dosage = 0.1-0.5 g, pH = 6 (Pb and Cd), 8 (Co &Zn), t = 200 min, T = 20-40 °C)

4.2.5. Adsorbent Reusability Test for HMIs adsorption

To remove the adsorbed metals ions from the adsorbent surface and make the adsorbent more economical and applicable to use several times, the adsorption ability of the nanocomposites was tested for five successive desorption cycles. First, the adsorbent beads were washed by acid (HCl)

for 15 minutes, thereafter the adsorbent beads were filtered and dried. The collected adsorbent beads were utilized for the removal of metal ions Pb (II), Cd (II), Co (II) and Zn (II) for five consequence experiments and the recovery experiment was repeated for each cycle of adsorption. The findings of the reusability test are displayed in Table 4.23 and Fig. 4.41, after the fifth adsorption process the adsorbent could remove up to 80.0% of heavy metal ions. The % reuse efficiency for HMIS were found to be 93 % for both Pb^{2+} and Cd (II), Cd (II)96 % for Co (II) and 94 % for Zn (II) . This might be driven by the fact that under acidic conditions repulsion between protonated amine groups and metal ions take place which accelerates desorption process (R. Ahmad & Mirza, 2018b). Thus, the as-prepared hydrogel beads were reusable for several cycles of adsorptions and considered as potential adsorbent for the adsorption of heavy metals ion.

Table (4. 23): Reusability study onto the PVA-CHTS-CLS nanocomposite hydrogel beads for the removal of HMIs

Pb (II) (V = 50 mL, initial concentration = 50mg/L, pH =6, beads dosage= 0.1-0.5 g, temp. =30 ºC, time = 200 min, wavelength = 220.353 nm)						
Number of cycles	**Pb (II) Concentration (mg/L)**			**Pb (II) Average Concentration (mg/L)**	**Pb (II) % Removal**	**Q_e ± SD (mg/g)**
	Trail 1	**Trail 2**	**Trail 3**			
I	1.12	0.711	1.16	0.997	98.0±0.5	4.90±0.02
II	1.52	2.34	1.79	1.88	96.2±0.8	4.81±0.04
III	1.52	2.81	1.79	2.04	95.9±1.0	4.80±0.07
IV	1.11	2.84	2.67	2.21	95.6±2.0	4.78±0.09
V	1.99	7.83	2.19	4.00	91.9±6.0	4.60±0.3
Cd (II) (V = 50 mL, initial concentration = 50mg/L, pH =6, beads dosage= 0.1-0.5 g, temp. =30 ºC, time = 200 min, wavelength = 228.802 nm)						
	Cd (II) Concentration.				**% Removal**	**Q_e ± SD**

Number of cycles	(mg/L)			Cd (II) Average Concentration. (mg/L)	± SD	(mg/g)
	Trail 1	Trail 2	Trail 3			
I	0.660	0.53	0.60	0.598	98.8±0.1	4.94±0.007
II	0.194	0.986	1.83	1.00	98.0±1.0	4.90±0.08
III	1.15	1.98	2.90	2.14	95.7±1.0	4.79±0.07
IV	3.19	4.23	3.13	3.51	93.0±1.0	4.65±0.06
V	3.19	3.98	3.81	3.66	92.7±0.8	4.63±0.04
Co(II) (V = 50 mL, intial concentration = 50mg/L, pH =8, beads dosage= 0.1-0.5 g, temp. =30 ºC, time = 200 min, wavelength = 228.61 nm)						
Number of cycles	**Cd (II) Concentration. (mg/L)**			**Co(II) Average Concentration. (m/gL)**	**% Removal ± SD**	**Q_e ± SD (mg/g)**
	Trail 1	**Trail 2**	**Trail 3**			
I	8.081	9.312	7.915	8.426	83.128±1.0	4.156±0.07
II	8.67	8.32	8.90	8.63	82.7±0.5	4.14±0.02

III	7.44	9.77	10.2	9.14	81.7±3.0	4.09±0.1
IV	6.13	11.0	11.1	9.42	81.1±5.0	4.06±0.2
V	8.79	10.9	9.67	9.79	80.4±2.13	4.02±0.106

Zn(II) (V = 50 mL, initial concentration = 50mg/L, pH =8, beads dosage= 0.1-0.5 g, temp. =30 ºC, time = 200 min, wavelength = 206.200 nm)						
Number of cycles	**Zn (II) Concentration. (m/gL)**			**Zn (II) Average Concentration. (mg/L)**	**% Removal ± SD**	**Q_e ± SD (mg/g)**
	Trail 1	**Trail 2**	**Trail 3**			
I	0.111	0.0780	0.0430	0.077	99.8±0.7	4.99±0.003
II	0.633	0.361	0.514	0.503	99.0±0.3	4.95±0.01
III	2.19	2.76	1.98	2.31	95.4±0.8	4.77±0.04
IV	2.99	2.31	2.72	2.68	94.6±0.7	4.73±0.03
V	3.17	2.00	3.89	3.02	94.0±2.0	4.70±0.09

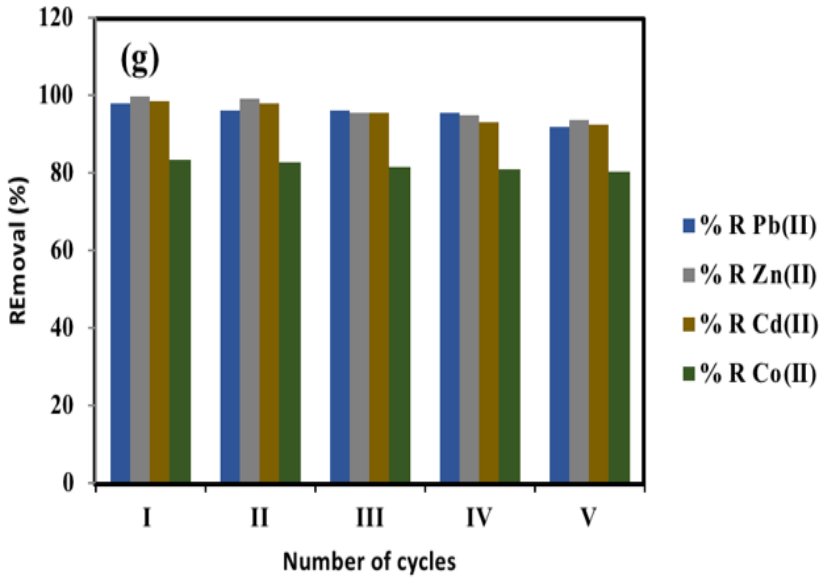


Fig. 4. 41: Reusability test for the removal of HMIs on PVA-CHTS-CLS (C_0[Metals] = 50 mg/L, V = 50 mL, pH = 6 (Pb &Cd) and pH = 8 (Co &Zn)), beads dosage = 0.5 g, t = 200 min, T = 30 °C).

4.2.6. Adsorption Isotherm Study for the adsorption of HMIs

In order to describe the adsorption behaviors of the studied heavy metal ions in an aqueous solution, sorption data was determined using isotherm equations. The equations take into consideration the surface property and affinity of the adsorbent, of which the theoretical Langmuir and Freundlich models were produced to derive the adsorption isotherms. The Langmuir isotherm model is used to describe the adsorption behavior associated with monolayer adsorption on the surface of an adsorbent, while the Freundlich model describes the adsorption behavior on heterogeneous adsorbent surfaces, assuming the formation of a multilayer adsorption on the surface (Dandil et al., 2019). The fitting parameters for Langmuir and Freundlich isotherms for the adsorption of Pb(II), Cd(II), Co(II), and Zn(II)

onto PVA-CS/CE adsorbent beads are represented in Table 4.24. The linear relationships between qe and Ce of the Langmuir and Freundlich correlations of each metal ion are presented in Figure 4.42 and 4.43, respectively.

The plot of Ce/qe vs Ce gives a straight line with high correlation coefficients. Accordingly, the adsorptions of HMIs were likely to comprise monolayer adsorption on homogeneous surface. The Langmuir constants q_m and K_L are obtained from the slop and the intercept of the linear plot. The results showed that, R_L values lay between ($0 < RL < 1$), which represent a favorable adsorption based on monolayer coverage of dyes molecules over a homogenous surface of adsorbent. This indicates that the adsorption sites of the adsorbent have equal adsorption energies and the whole process can be explained via chemisorption mechanism(Kang et al., 2017) .

Additionally, the equilibrium results were fitted also using Freundlich linear equation by plotting ln qe vs ln Ce. The high correlation coefficient of Pb (II), Cd (II), Co (II), and Zn (II) adsorption suggests the agreement of Freundlich isotherm. Examining parameters related to the Freundlich isotherm i.e., k_F and 1/n, large k_F value indicated a good adsorption capacity to the metal ions. In addition, the 1/n value in the range of 0.1–1.0 indicated a good adsorption process (Kang et al., 2017). A comparison of q_m value for the removal of heavy metals by PVA-CHTS-CLS nanocomposite hydrogel beads with that of other adsorbents that are published in literature is listed in Table (4.25), which clearly indicates the excellent adsorption capacity of the designed beads.

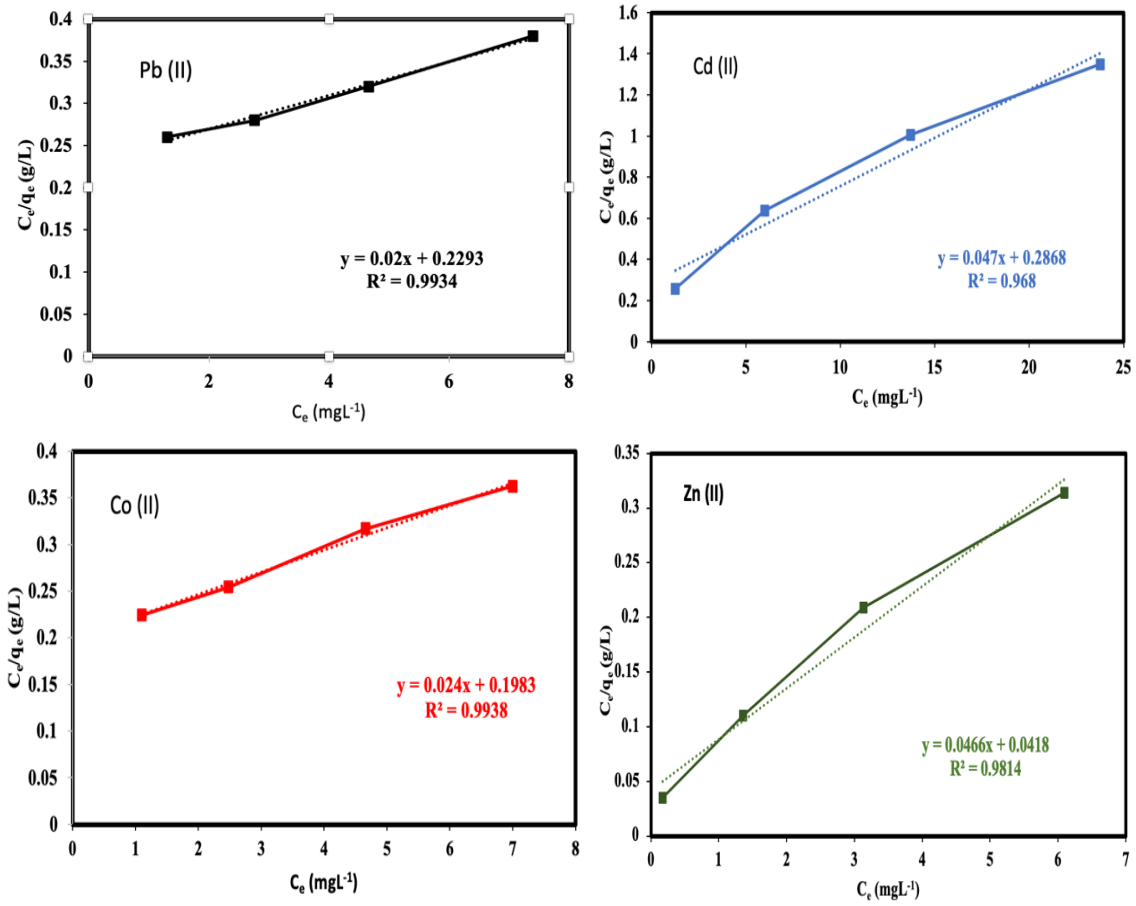


Fig. 4. 42: (a) The Langmuir adsorption isotherm models for the adsorption of Pb (II), Cd (II), Co (II) and Zn(II) onto the semi-IPN PVA-CHTS-CLS composite hydrogel beads

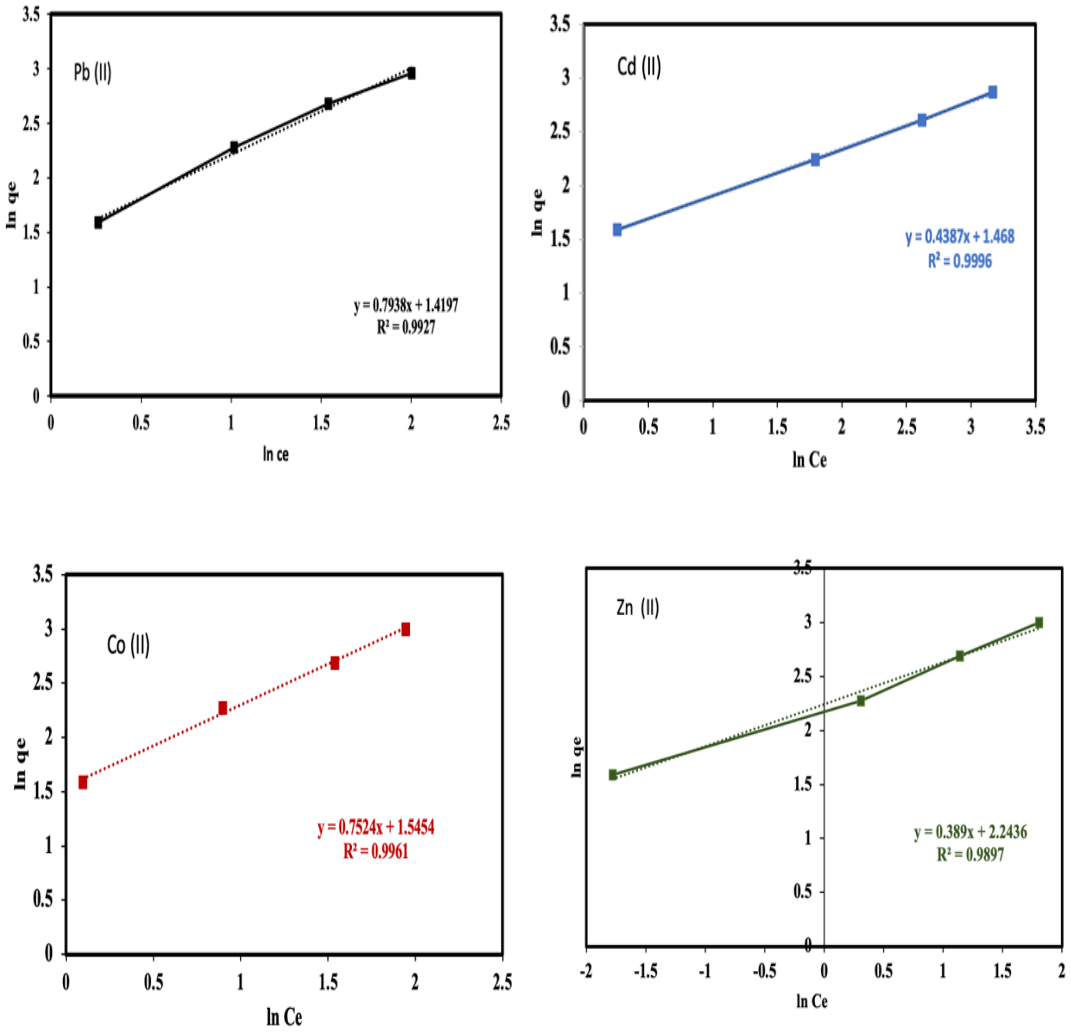


Fig. 4. 43: Freundlich adsorption isotherm models for the adsorption of Pb (II), Cd (II), Co (II) and Zn(II) onto the semi-IPN PVA-CHTS-CLS composite hydrogel beads.

Table (4. 24): Adsorption isotherm parameters of Pb (II), Cd (II), Co (II) and Zn(II) on to PVA-CHTS-CLS

Model	Parameter	Pb (II)	Cd (II)	Co (II)	Zn (II)
Langmuir isotherm	q_m (mg/g)	50	21.27	41.66	21.45
	R_L	0.054-0.187	0.029-0.109	0.04-0.141	0.0048-0.0176
	R^2	0.993	0.968	0.994	0.981
	K_L	0.0872	0.163	0.121	1.11
Freundlich Isotherm	K_F (L/mg)	4.13	4.135	4.69	9.42
	1/n	0.7932	0.438	0.752	0.389
	R^2	0.993	0.999	0.996	0.989

Table (4. 25): Adsorption capacity of some adsorbents for Pb (II), Cd (II), Co (II) and Zn(II)

Adsorbent	Q_m (mg/g)				References
	Pb (II)	Cd (II)	Co (II)	Zn (II)	
sulfhydryl attapulgite (SH-ATP)		22.7			(C. Fu et al., 2021)
Activated carbon–calcium alginate composite	15.7				(Cataldo et al., 2016)
Silica modified calcium alginate–xanthan gum hybrid bead composite	18.9				(S. Zhang et al., 2013)
Natural zeolite				13.02	(Katsou et al., 2011)
bentonite			7.3		(Al-Shahrani, 2014)
Cellulose derived from corn stalk		21.38			(Zheng et al., 2012)
Nano-TiO_2	7.41				(Poursani et al., 2016)
PVA-CHTS-CLA	24.0	24.0	11.76	12.5	This study

4.2.7. Adsorption Kinetics Study for the adsorption of HMIs

The adsorption of Pb (II), Cd (II), Co (II) and Zn (II) onto PVA-CHTS-CLS stimulates the formation of metal-adsorbent complex by coordinating theses cationic ions with the lone electrons of nitrogen and oxygen atoms (Esrafili et al., 2019). The transferring of metal ions to the surface of the adsorbents defines the rate of adsorption process (Aslani et al., 2018). In this study, adsorption kinetic analysis of those metallic ions was studied using both PFO and PSO kinetic models. Fig. 4.44 a &b showed the linear plots for PFO and PSO kinetic models, respectively. All time dependent adsorption kinetics parameters are shown in Table 4.26. Regression coefficient (R^2) suggests that the adsorption of HMIs on to PVA-CHTS-CLS was found to obey PSO model. Moreover, the calculated q_e obtained from PSO is closer to the experimental qe of all HMIs. Therefore, the pseudo second order kinetic model is more adapted for PVA-CHTS-CLS.

Table (4. 26): Kinetics parameters for the sorption metal ions on a batch adsorption system

HMIS	Kinetic models	q_{exp} (mg/g)	q_e (mg/g)	K	R^2
Pb (II)	PFO	4.9	0.404	K_1= 0.0353 (1/min)	0.843
	PSO		4.97	K_2= 0.0932 (g/mg.min)	0.999
Cd (II)	PFO	4.94	0.147	K_1= 0.0173 (1/min)	0.909

HMIS	Kinetic models	q_{exp} (mg/g)	q_e (mg/g)	K	R^2
	PSO		4.95	K_2= 0.274 (g/mg.min)	1.00
Co (II)	PFO	4.16	0.833	K_1= 0.0136 (1/min)	0.903
	PSP		4.27	K_2= 0.0240 (g/mg.min)	0.997
Zn (II)	PFO	4.99	0.528	K_1= 0.0584 (1/min)	0.5026
	PSO		4.99	K_2=4.06 (g/mg.min)	1.00

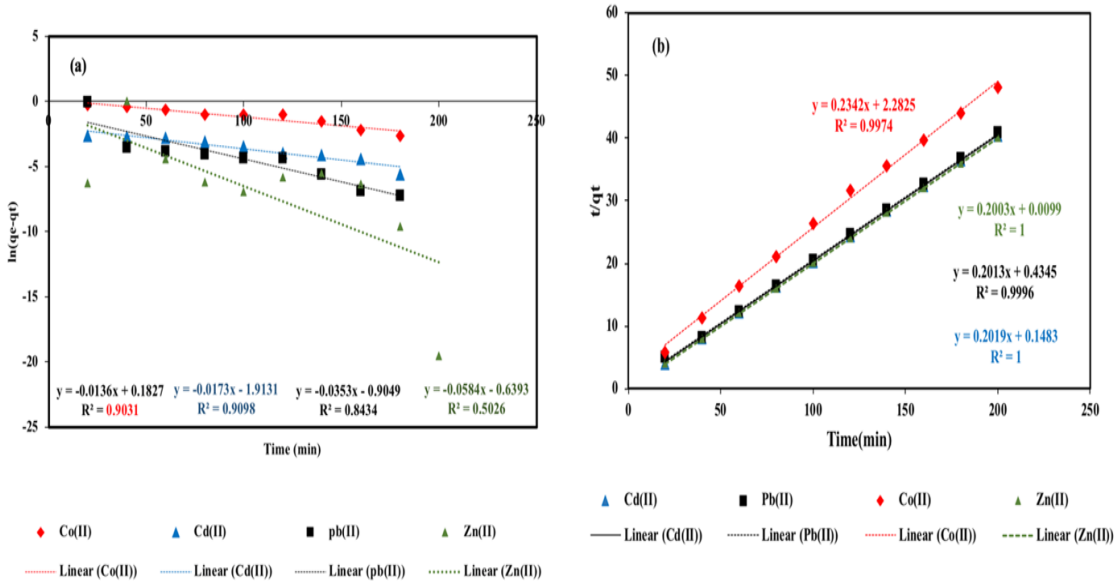


Fig. 4. 44: (a) The (PFO) and (b) (PSO) kinetic models for the adsorption of Pb (II), Cd (II), Co (II) and Zn (II) onto the semi-IPN PVA-CHTS-CLS nanocomposite hydrogel beads.

4.2.8. Selectivity adsorption of HMIs

Type of HMIS is an important parameter in its adsorption selectivity on the surface of the adsorbent. Fig. 4.45 shows the selective adsorption of the studied HMIs on PVA-CHTS-CLS. The results showed that Pb has the highest adsorption affinity, followed by Cd, than Zn and Co has the least adsorption affinity. Each heavy metal has a different degree of adsorption, and this variation may be connected to various parameters including the ionic radius. The affinity of adsorption by PVA-CS/EC was found to decrease in the order: Pb(II) > Cd(II) > Zn(II) > Co(II). The reason for these observations is the hydrated metal ion radius effect (Osińska, 2017) . Metal ions in an aqueous medium form hydrates with water molecules, and the ionic radii of Pb(II), Cd(II), Zn(II), and Co(II) are 1.19, 0.96, 0.74, and 0.74 Å, respectively. When the ionic radius of a metal ion is large, it is easy to react with water molecules and induces a quick saturation of adsorption sites, because of steric overcrowding on the surface(Osińska, 2017) . As PVA-CHTS-CLS is a hydrophilic material, metal ions in the surrounding are easily brought onto the adsorbent in the form of hydrated ions, resulting in attractive interactions between cationic contaminants and the anionic adsorbent surface(Zhou et al., 2012). Since Pb(II) has the highest ionic radius among the four heavy metal ions and has reached the highest adsorption rate. It seems that the difference in removal efficiency order and adsorption capacity may be related not only to metal ions' properties but also to physical-chemical properties of the adsorbent such as morphology, surface area, and pores distribution.

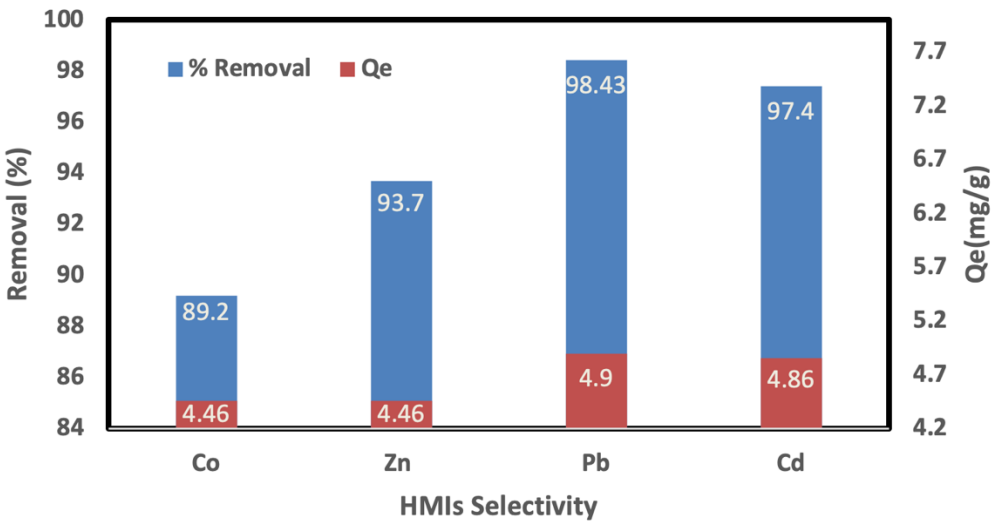


Fig. 4. 45: Adsorption selectivity of HMIs. (C_0[HMIS] = 50mg/L, V = 50 mL, pH =6, t =120 min, T = 30 ºC).

4.2.9. Adsorption Mechanism of PVA-CHTS-CLS and HMI

The mechanism of HMIs adsorption can be explained by physisorption and chemisorption mechanisms. In fact, its theorized that physisorption and chemisorption occur simultaneously (Shi et al., 2022). As mentioned in the literature, the physical adsorption can be explained by Van dar Waal forces, hydrogen bond, polarity, dipole-dipole interaction, and hydrophilicity. Moreover, physisorption has the properties of single or multi adsorption layers, no change in the structure of the adsorbed compounds, reversibility and no formation of the new chemical bonds. In contract, chemisorption is regarded as a single molecular adsorption and can be described by Langmuir isotherm. Fig. 4.45 displays an illustrative scheme for the proposed adsorption mechanism of HMIs on the designed beads. As mentioned before, when the pH is above the pH_{PZC} values, the negative surface charge of the PVA-CHTS-CLS nanocomposite hydrogel gel adsorbent is dominant due to the deprotonation of OH group to (O^-). The suggested mechanisms of metal removal are by both electrostatic

interaction between the positive charges of the HMIs and the abundant negative charges of the nanocomposite adsorbent and the formation of coordination interactions between the metal cations and lone pairs of heteroatoms (N and O) (Ragab et al., 2017).

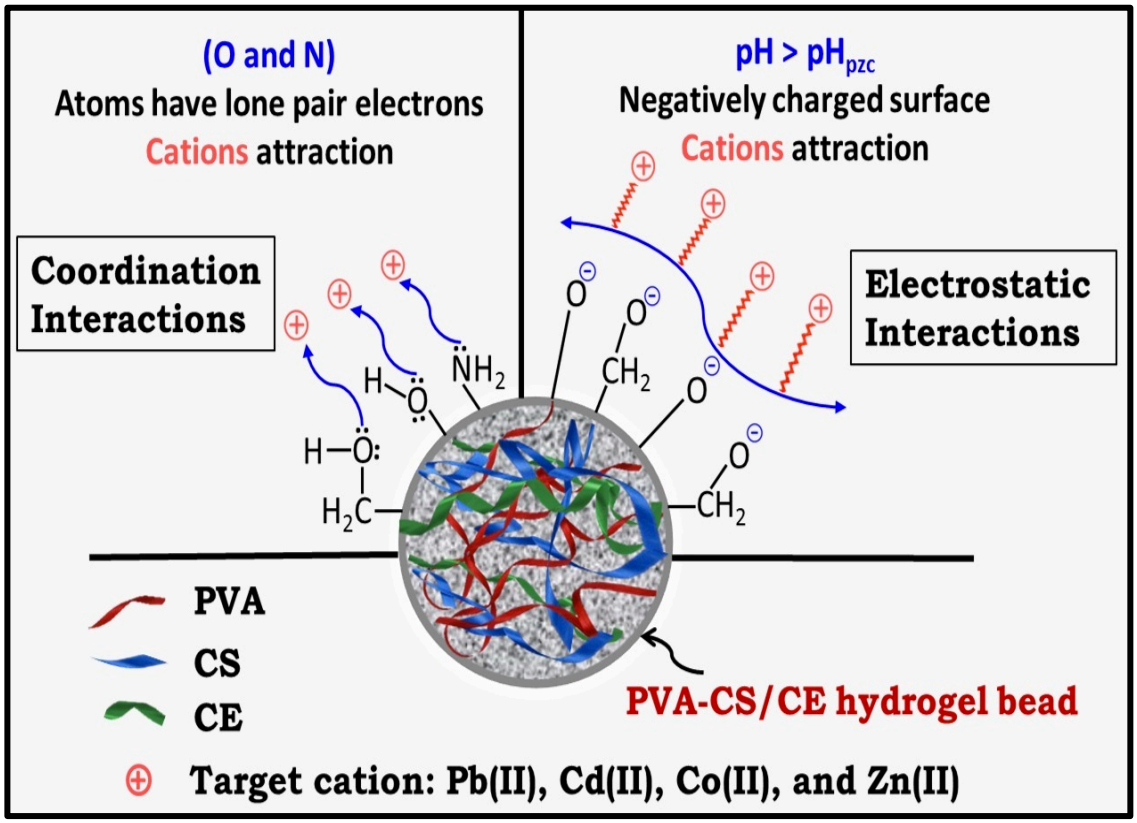


Fig. 4. 46: Proposed scheme indicating the possible interaction mechanism of the HMIs onto the PVA-CHTS-CLS nanocomposite hydrogel beads. Adapted from REF:(Kong et al., 2018)

4.2.10. Application in real samples:

Table 4.27 gathers the initial concentrations of HMIs in three samples collected from three locations nearby the industrial locations in the kingdom of Bahrain. The results showed that that Bahrain's sea comprises low levels of HMIs (0.02-0.1 ppm), the results agreed to that

obtained by (Bersuder et al., 2020) which is mentioned in section 2.2.1. However, after applying the adsorption experiments on the real samples, the results showed that the % removal of HMIS decreased. The decrease in % removal can be explained because of the salinity of sea water. The high salinity of solution can slow the adsorption time and thus decreases both the adsorption capacity of the adsorbent and the % removal of HMIs. The presence of high concentration of ions increases the interaction and the competition for the adsorption sites on the adsorbent's surface (Barus et al., 2021).

Table (4. 27): Levels of HMIs in real sample in Kingdom of Bahrain

Locations	**Average conc. of Pb (ppm)**	**Average conc. of Cd (ppm)**	**Average conc. of Co (ppm)**	**Average conc. of Zn (ppm)**
Location 1	0.063	0.059	0.066	0.053
Location 2	0.053	0.058	0.045	0.071
Location 3	0.024	0.043	0.053	0.111



Fig. 4. 47: Locations of samples in kingdom of Bahrain

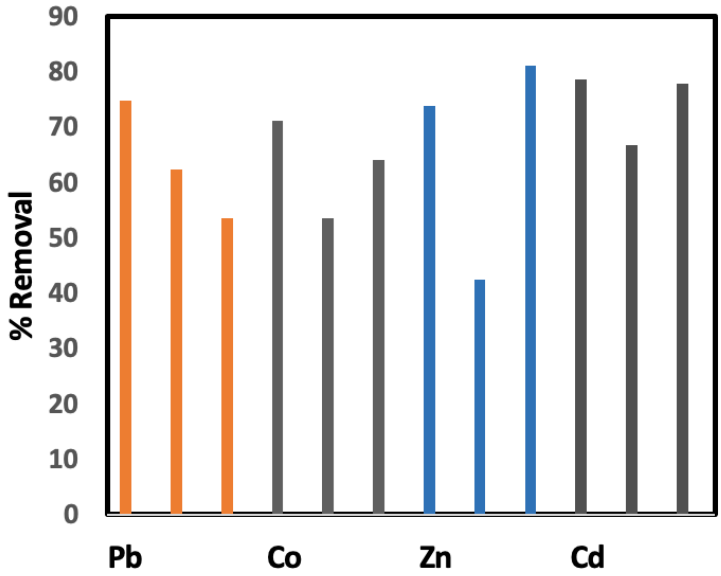


Fig. 4. 48: The % removal of HMIS on the surface of PVA-CHTS-CLS in three locations of real sea water samples.

4.3. Conclusion

In this study, two environmentally friendly nanocomposites adsorbents (PVA-ALG-BENT and PVA-CHTS-CLS) had been designed and used as recyclable adsorbents for the removal of pollutants from synthetic wastewater solution. The hydrogels composites beads were synthesized by physical crosslinking reaction. PVA-ALG-BENT was evaluated towards the removal of MB, CR dyes and PVA-CHTS-CLS was used to test its removal capacity towards HMIs. Hydrogels' characterizations were done by using SEM, XRD, and EDX analysis. The designed adsorbent beads possess a porous structure, high specific surface area and provide many channels for the rapid adsorption of organic dyes and HMIs. Based on the experimental results the following points can be concluded:

1. The adsorption results showed that the incorporating of BENT and CLS particles in the matrix of PVA-ALG and PVA-CHTS enhanced the adsorption capacity of both polymers.
2. The percentage removal and adsorption capacity are dependent on the type of surface functional groups. The more the adsorption binding sites the higher the adsorption capacity of hydrogels. Moreover, the adsorption process depends on several adsorption parameters such as initial pH, adsorbate's concentration, adsorbent dosage, contact time and initial temperature. The adsorption capacity of PVA-ALG-BENT for the removal of MB and CR dyes were found to be 51.27, 16.19 mg/g of the adsorbent respectively. While the maximum adsorption capacities of PVA-CHTS-CLS for Pb (II), Cd (II), Co (II) and Zn (II) ions were 24.0, 24.0, 11.76, and 12.5 mg/g respectively.

For MB, the findings showed that the optimum removal efficiency of 90.2% was obtained at optimal pH of 8, adsorbent dosage of 1.5 g, initial concentration of 200 ppm and a temperature at 30 °C. While for CR, the results showed that the optimum removal efficiency of 75.0% was obtained at optimal pH of 3, adsorbent dosage of 1.5 g, initial concentration of 100 ppm at 30 °C. For Pb and Cd the findings showed that the optimum removal efficiencies of 98.0% for both metals were obtained at optimal pH of 6, adsorbent dosage 0.5 g, initial concentration of 50 ppm and temperature at 30 °C. For Co and Zn the findings showed that the optimum removal efficiencies of 83.0 % and 99.8 % for Co and Zn respectively were obtained at optimal pH of 8, adsorbent dosage 0.5 g, initial concentration of 50 ppm at 30 °C.

3. Although results have been reliable, the adsorption mechanism depends on the functional groups on the surface of the adsorbent, electrostatic interaction has been the main adsorption mechanism for hydrogels containing R-NH_2 and R-COO^- functional groups
4. With time spent in contact, adsorption generally increases because more adsorbate is adsorbed over time, thus fewer free sites are available for adsorption until saturation is attained. The ideal contact time for equilibrium were found to be between 120 mins for HMIs and 300 mins for organic dyes.
5. pH plays an important factor for adsorption process. For positively charged adsorbate such as MB and HMIs the adsorbent's removal effectiveness rises as pH increased. While for a negatively charged adsorbate such as CR, the adsorption increases as pH decreased.

6. The number of adsorption sites increases by increasing the adsorbent dosage. For HMIs removal, the ideal adsorbent dosage was 0.5 g and for organic dyes the optimum adsorbent dosage was 1.5 g. The increase in adsorption is relatively small when the adsorbent dosage increased over the optimal level, and it becomes economically useless.
7. There is a decrease in adsorption with an increase in the adsorbate's initial concentration because at high concentration the adsorption sites becomes fewer and the ratio between the initial number of adsorbate to the available adsorption sites is high.
8. Increasing temperature is known to increase adsorption capacity. Adsorbate's ions have high kinetic energy at higher temperatures, where molecules have enough energy to engage with the adsorption sites.
9. The studies revealed that the adsorbent beads had a good stability and reusability after five repeated cycles of adsorption and desorption.
10. Based on the kinetics study, the pseudo-second-order model truly reflects the adsorption data with R^2 almost 0.99 for all adsorption studies.
11. Although both the Freundlich and Langmuir isotherm modes are suited to fit the experimental data, the data is fitted best to Langmuir isotherm.

In conclusion, both PVA-ALG-BENT and PVA-CHTS-CLS have significant potential in organic dyes and metal ions removal, respectively due to their strong regeneration ability, green bio adsorbent, low cost

environmentally friendly and remarkable adsorption capacity. Therefore, they could be suitable for the wastewater remediation.

4.4. Recommendation:

Based on the findings and conclusions of the study, the following suggestions can be drawn:

1. One effective method for enhancing the adsorption capabilities of adsorbents is to dominate suitable functional groups (including nitrogen and oxygen) on the adsorbent's surface. The performance of the adsorbent will be significantly enhanced by increasing the layer and number of functional groups in the adsorbent. Therefore, the research can be expanded by incorporating additional material composite to the adsorbent beads to enhance the adsorption performance
2. It is advised to conduct more research to determine the stability of the reused adsorbents.
3. Investigations of the adsorbent cost analysis are recommended especially in large scale studies to increase the applicability of the adsorption process in industrial level.
4. The existing technologies for wastewater treatment are expensive and energy consuming, thus there is a critical need for new research to develop sustainable methods to remediate water at low cost, ~~use~~ less energy, and considerably have limited impact on the environment.

5.0 References:

A. D. fergusont, & P. Taylor. (2020). *Anon Standard Methods for the Determination of the Color Fastness of Textiles and Leather*. https://www.researchgate.net/publication/244636293_Anon_Standard_Methods_for_the_Determination_of_the_Color_Fastness_of_Textiles_and_Leather

A. Haug, B. L. (1966). A study of the constitution of alginic acid by partial acid hydrolysis. *Acta Chem. Scand.*, *20*, 183–190. https://doi.org/10.1007/978-0-387-30160-0_400

Abdul Khalil, H. P. S., Saurabh, C. K., Adnan, A. S., Nurul Fazita, M. R., Syakir, M. I., Davoudpour, Y., Rafatullah, M., Abdullah, C. K., Haafiz, M. K. M., & Dungani, R. (2016). A review on chitosan-cellulose blends and nanocellulose reinforced chitosan biocomposites: Properties and their applications. *Carbohydrate Polymers*, *150*, 216–226. https://doi.org/10.1016/j.carbpol.2016.05.028

Abin-Bazaine, A., Campos Trujillo, A., & Olmos-Marquez, M. (2022). Adsorption Isotherms: Enlightenment of the Phenomenon of Adsorption. In *Wastewater Treatment [Working Title]*. IntechOpen. https://doi.org/10.5772/intechopen.104260

Achparaki, M., Thessalonikeos, E., Tsoukali, H., Mastrogianni, O., Zaggelidou, E., Chatzinikolaou, F., Vasilliades, N., Raikos, N., Isabirye, M., Raju, D. V. N., Kitutu, M., Yemeline, V., Deckers, J., & J. Poesen Additional. (2012). Solubility of Chitin: Solvents, Solution Behaviors and Their Related Mechanisms Jagadish. *Intech*, 13.

Afrin, S., & Karim, Z. (2021). Polysaccharides. *Polysaccharide-Based Nanocomposites for Gene Delivery and Tissue Engineering*, 1–14. https://doi.org/10.1016/B978-0-12-821230-1.00010-4

Ahmad, A., Rafatullah, M., Sulaiman, O., Ibrahim, M. H., Chii, Y. Y., & Siddique, B. M. (2009). Removal of Cu(II) and Pb(II) ions from aqueous solutions by adsorption on sawdust of Meranti wood. *Desalination*, *247*(1–3), 636–646. https://doi.org/10.1016/j.desal.2009.01.007

Ahmad, R., & Mirza, A. (2018a). Facile one pot green synthesis of Chitosan-Iron oxide (CS-Fe2O3) nanocomposite: Removal of Pb(II) and Cd(II) from synthetic

and industrial wastewater. *Journal of Cleaner Production*, *186*, 342–352. https://doi.org/10.1016/j.jclepro.2018.03.075

Ahmad, R., & Mirza, A. (2018b). Facile one pot green synthesis of Chitosan-Iron oxide (CS-Fe2O3) nanocomposite: Removal of Pb(II) and Cd(II) from synthetic and industrial wastewater. *Journal of Cleaner Production*, *186*, 342–352. https://doi.org/10.1016/j.jclepro.2018.03.075

Ahmed, E. M. (2015a). Hydrogel : Preparation , characterization , and applications : A review. *Journal of Advanced Research*, *6*(2), 105–121.

Ahmed, E. M. (2015b). Hydrogel: Preparation, characterization, and applications: A review. In *Journal of Advanced Research* (Vol. 6, Issue 2, pp. 105–121). Elsevier B.V. https://doi.org/10.1016/j.jare.2013.07.006

Ahmed, M. J., Hameed, B. H., & Hummadi, E. H. (2020). Review on recent progress in chitosan/chitin-carbonaceous material composites for the adsorption of water pollutants. *Carbohydrate Polymers*, *247*(June), 116690. https://doi.org/10.1016/j.carbpol.2020.116690

Akpor, O. B. (2014). Heavy Metal Pollutants in Wastewater Effluents: Sources, Effects and Remediation. *Advances in Bioscience and Bioengineering*, *2*(4), 37. https://doi.org/10.11648/j.abb.20140204.11

Al-Ansari, M. S. (2013). The water demand management in the Kingdom of Bahrain. *International Journal of Engineering and Advanced Technology (IJEAT)*, *2*(5), 544–554.

Alasadi, A. M., Khaili, F. I., & Awwad, A. M. (2019). *Adsorption of Cu (II), Ni (II) and Zn (II) ions by nano kaolinite : Thermodynamics and kinetics studies*. 258–268.

Aleisa, E., & Al-Zubari, W. (2017). Wastewater reuse in the countries of the Gulf Cooperation Council (GCC): the lost opportunity. *Environmental Monitoring and Assessment*, *189*(11). https://doi.org/10.1007/s10661-017-6269-8

Al-Ghouti, M. A., & Al-Degs, Y. S. (2011). New adsorbents based on microemulsion modified diatomite and activated carbon for removing organic and inorganic pollutants from waste lubricants. *Chemical Engineering Journal*, *173*(1), 115–128. https://doi.org/10.1016/j.cej.2011.07.047

Alhogbi, B. G., Salam, M. A., & Ibrahim, O. (2019). Environmental remediation of toxic lead ions from aqueous solution using palm tree waste fibers biosorbent.

Desalination and Water Treatment, *145*(January), 179–188. https://doi.org/10.5004/dwt.2019.23507

Ali, A., & Ahmed, S. (2018). Recent Advances in Edible Polymer Based Hydrogels as a Sustainable Alternative to Conventional Polymers [Review-article]. *Journal of Agricultural and Food Chemistry*, *66*(27), 6940–6967. https://doi.org/10.1021/acs.jafc.8b01052

AlJaberi, F. Y., & Mohammed, W. T. (2018). The Most Practical Treatment Methods for Wastewaters: A Systematic Review. *Mesopotamia Environmental Journal*, *5*(1), 1–28. www.bumej.com

Aljar, M. A. A., Rashdan, S., & El-fattah, A. A. (2021). *Environmentally Friendly Polyvinyl Alcohol Alginate / Bentonite Semi-Interpenetrating Polymer Network Nanocomposite Hydrogel Beads as An Efficient Adsorbent for the Removal of Methylene Blue from Aqueous Solution*. 1–19.

Almomani, F., Bhosale, R., Khraisheh, M., kumar, A., & Almomani, T. (2020). Heavy metal ions removal from industrial wastewater using magnetic nanoparticles (MNP). *Applied Surface Science*, *506*(October 2019), 144924. https://doi.org/10.1016/j.apsusc.2019.144924

Al-Najar, B., Peters, C. D., Albuflasa, H., & Hankins, N. P. (2020). Pressure and osmotically driven membrane processes: A review of the benefits and production of nano-enhanced membranes for desalination. *Desalination*, *479*(January). https://doi.org/10.1016/j.desal.2020.114323

Al-Noaimi, M. A. (2005). *Water Use and Management in Bahrain: An Overview*. *September*, 25. http://niadbh.com/wp-content/uploads/2018/08/Water-Use-and-Management-in-Bahrain.pdf

Al-Obaidi, M. A., Ruiz-García, A., Hassan, G., Li, J. P., Kara-Zaïtri, C., Nuez, I., & Mujtaba, I. M. (2021). Model based simulation and genetic algorithm based optimisation of spiral wound membrane ro process for improved dimethylphenol rejection from wastewater. *Membranes*, *11*(8), 1–19. https://doi.org/10.3390/membranes11080595

Alsamhary, K., Al-Enazi, N. M., Alhomaidi, E., & Alwakeel, S. (2021). Spirulina platensis mediated biosynthesis of Cuo Nps and photocatalytic degradation of toxic azo dye Congo red and kinetic studies. *Environmental Research*, *October*, 112172. https://doi.org/10.1016/j.envres.2021.112172

ALSamman, M. T., & Sánchez, J. (2021). Recent advances on hydrogels based on chitosan and alginate for the adsorption of dyes and metal ions from water. *Arabian Journal of Chemistry*, *14*(12). https://doi.org/10.1016/j.arabjc.2021.103455

Al-Shahrani, S. S. (2014). Treatment of wastewater contaminated with cobalt using Saudi activated bentonite. *Alexandria Engineering Journal*, *53*(1), 205–211. https://doi.org/10.1016/J.AEJ.2013.10.006

Al-Zubari, W. K., El-Sadek, A. A., Al-Aradi, M. J., & Al-Mahal, H. A. (2018a). Impacts of climate change on the municipal water management system in the Kingdom of Bahrain: Vulnerability assessment and adaptation options. *Climate Risk Management*, *20*(February), 95–110. https://doi.org/10.1016/j.crm.2018.02.002

Al-Zubari, W. K., El-Sadek, A. A., Al-Aradi, M. J., & Al-Mahal, H. A. (2018b). Impacts of climate change on the municipal water management system in the Kingdom of Bahrain: Vulnerability assessment and adaptation options. *Climate Risk Management*, *20*(February), 95–110. https://doi.org/10.1016/j.crm.2018.02.002

Al-Zubari, W. K., El-Sadek, A. A., Al-Aradi, M. J., & Al-Mahal, H. A. (2018c). Impacts of climate change on the municipal water management system in the Kingdom of Bahrain: Vulnerability assessment and adaptation options. *Climate Risk Management*, *20*(August 2017), 95–110. https://doi.org/10.1016/j.crm.2018.02.002

Amri, N., Ghemati, D., Bouguettaya, N., & Aliouche, D. (2019). Swelling kinetics and rheological behavior of chitosan-PVA/montmorillonite hybrid polymers. *Periodica Polytechnica Chemical Engineering*, *63*(1), 179–189. https://doi.org/10.3311/PPch.12227

Annaduzzaman, M. (2015). *Chitosan biopolymer as an adsorbent for drinking water treatment Investigation on Arsenic and Uranium* (Issue June).

Ansari, T. M., Marr, I. L., & Tariq, N. (2003). Heavy Metals in Marine Pollution Perspective–A Mini Review. *Journal of Applied Sciences*, *4*(1), 1–20. https://doi.org/10.3923/jas.2004.1.20

Ardean, C., Davidescu, C. M., Nemeş, N. S., Negrea, A., Ciopec, M., Duteanu, N., Negrea, P., Duda-seiman, D., & Musta, V. (2021). Factors influencing the antibacterial activity of chitosan and chitosan modified by functionalization. In

International Journal of Molecular Sciences (Vol. 22, Issue 14). MDPI AG. https://doi.org/10.3390/ijms22147449

Asadi, S., Eris, S., & Azizian, S. (2018). Alginate-Based Hydrogel Beads as a Biocompatible and E ffi cient Adsorbent for Dye Removal from Aqueous Solutions. *ACS Omega*, *3*, 15140–15148. https://doi.org/10.1021/acsomega.8b02498

Ashbolt, N. J. (2004). Microbial contamination of drinking water and disease outcomes in developing regions. *Toxicology*, *198*(1), 229. https://doi.org/10.1016/J.TOX.2004.01.030

Aslani, H., Ebrahimi Kosari, T., Naseri, S., Nabizadeh, R., & Khazaei, M. (2018). Hexavalent chromium removal from aqueous solution using functionalized chitosan as a novel nano-adsorbent: modeling and optimization, kinetic, isotherm, and thermodynamic studies, and toxicity testing. *Environmental Science and Pollution Research*, *25*(20), 20154–20168. https://doi.org/10.1007/s11356-018-2023-1

Atta, S., Khaliq, S., Islam, A., Javeria, I., Jamil, T., Athar, M. M., Shafiq, M. I., & Ghaffar, A. (2015). Injectable biopolymer based hydrogels for drug delivery applications. *International Journal of Biological Macromolecules*, *80*, 240–245. https://doi.org/10.1016/j.ijbiomac.2015.06.044

Azizian, S., & Eris, S. (2021). Adsorption isotherms and kinetics. *Interface Science and Technology*, *33*, 445–509. https://doi.org/10.1016/B978-0-12-818805-7.00011-4

Azzam, E. M. S., Eshaq, G., Rabie, A. M., Bakr, A. A., Abd-Elaal, A. A., El Metwally, A. E., & Tawfik, S. M. (2016). Preparation and characterization of chitosan-clay nanocomposites for the removal of Cu(II) from aqueous solution. *International Journal of Biological Macromolecules*, *89*(Ii), 507–517. https://doi.org/10.1016/j.ijbiomac.2016.05.004

Bahrain Renewable water resources per capita, 1958-2021 - knoema.com. (n.d.). Retrieved November 6, 2022, from https://knoema.com/atlas/Bahrain/topics/Water/Total-Renewable-Water-Resources/Renewable-water-resources-per-capita

Baigorria, E., Cano, L. A., Sanchez, L. M., Alvarez, V. A., & Ollier, R. P. (2020a). Bentonite-composite polyvinyl alcohol/alginate hydrogel beads: Preparation, characterization and their use as arsenic removal devices. *Environmental*

Nanotechnology, Monitoring and Management, *14*(April), 1–8. https://doi.org/10.1016/j.enmm.2020.100364

Baigorria, E., Cano, L. A., Sanchez, L. M., Alvarez, V. A., & Ollier, R. P. (2020b). Bentonite-composite polyvinyl alcohol/alginate hydrogel beads: Preparation, characterization and their use as arsenic removal devices. *Environmental Nanotechnology, Monitoring and Management*, *14*(September), 100364. https://doi.org/10.1016/j.enmm.2020.100364

Baker, J. R., McCluskey, A., & Russell, C. C. (2022). 1,3-Thiazines and Their Benzo Derivatives. *Comprehensive Heterocyclic Chemistry IV*, 583–634. https://doi.org/10.1016/B978-0-12-818655-8.00104-9

Banerjee, S., & Chattopadhyaya, M. C. (2017a). Adsorption characteristics for the removal of a toxic dye, tartrazine from aqueous solutions by a low cost agricultural by-product. *Arabian Journal of Chemistry*, *10*, S1629–S1638. https://doi.org/10.1016/j.arabjc.2013.06.005

Banerjee, S., & Chattopadhyaya, M. C. (2017b). Adsorption characteristics for the removal of a toxic dye, tartrazine from aqueous solutions by a low cost agricultural by-product. *Arabian Journal of Chemistry*, *10*, S1629–S1638. https://doi.org/10.1016/j.arabjc.2013.06.005

Barclay, T. G., Day, C. M., Petrovsky, N., & Garg, S. (2019). Review of polysaccharide particle-based functional drug delivery. *Carbohydrate Polymers*, *221*, 94–112. https://doi.org/10.1016/j.carbpol.2019.05.067

Barus, B. S., Chen, K., Cai, M., Li, R., Chen, H., Li, C., Wang, J., & Cheng, S. Y. (2021). Heavy Metal Adsorption and Release on Polystyrene Particles at Various Salinities. *Frontiers in Marine Science*, *8*. https://doi.org/10.3389/fmars.2021.671802

Bavya, M. C., George, L., Srivastava, R., & Vimal Rohan, K. (2021). Natural and Synthetic Materials in Regenerative Medicine: Progress Over the Past Five Years: Hydrogels: An Insight. *Encyclopedia of Smart Materials*, 113–144. https://doi.org/10.1016/B978-0-12-803581-8.11361-X

Belhouchat, N., Zaghouane-Boudiaf, H., & Viseras, C. (2017a). Removal of anionic and cationic dyes from aqueous solution with activated organo-bentonite/sodium alginate encapsulated beads. *Applied Clay Science*, *135*, 9–15. https://doi.org/10.1016/j.clay.2016.08.031

Belhouchat, N., Zaghouane-Boudiaf, H., & Viseras, C. (2017b). Removal of anionic and cationic dyes from aqueous solution with activated organo-bentonite/sodium alginate encapsulated beads. *Applied Clay Science*, *135*, 9–15. https://doi.org/10.1016/j.clay.2016.08.031

Belyadi, H., Fathi, E., & Belyadi, F. (2019). Hydraulic fracturing chemical selection and design. *Hydraulic Fracturing in Unconventional Reservoirs*, 107–120. https://doi.org/10.1016/B978-0-12-817665-8.00008-4

Benkhaya, S., M' rabet, S., & el Harfi, A. (2020). A review on classifications, recent synthesis and applications of textile dyes. In *Inorganic Chemistry Communications* (Vol. 115). Elsevier B.V. https://doi.org/10.1016/j.inoche.2020.107891

Benkhaya, S., M'rabet, S., & el Harfi, A. (2020). Classifications, properties, recent synthesis and applications of azo dyes. *Heliyon*, *6*(1). https://doi.org/10.1016/j.heliyon.2020.e03271

Bersuder, P., Smith, A. J., Hynes, C., Warford, L., Barber, J. L., Losada, S., Limpenny, C., Khamis, A. S., Abdulla, K. H., Le Quesne, W. J. F., & Lyons, B. P. (2020). Baseline survey of marine sediments collected from the Kingdom of Bahrain: PAHs, PCBs, organochlorine pesticides, perfluoroalkyl substances, dioxins, brominated flame retardants and metal contamination. *Marine Pollution Bulletin*, *161*(August), 111734. https://doi.org/10.1016/j.marpolbul.2020.111734

Beyene, H. D., Hailegebrial, T. D., & Direrssa, W. B. (2016). Investigation of Coagulation Activity of Cactus Powder in Water Treatment. *Journal of Applied Chemistry*, *2016*, 1–9. https://doi.org/10.1155/2016/7815903

Bhatti, H. N., Safa, Y., Yakout, S. M., Shair, O. H., Iqbal, M., & Nazir, A. (2020). *International Journal of Biological Macromolecules Ef fi cient removal of dyes using carboxymethyl cellulose / alginate / polyvinyl alcohol / rice husk composite : Adsorption / desorption , kinetics and recycling studies*. *150*, 861–870.

Bläker, C., Muthmann, J., Pasel, C., & Bathen, D. (2019). Characterization of Activated Carbon Adsorbents – State of the Art and Novel Approaches. *ChemBioEng Reviews*, *6*(4), 119–138. https://doi.org/10.1002/cben.201900008

Burakov, A. E., Galunin, E. V., Burakova, I. V., Kucherova, A. E., Agarwal, S., Tkachev, A. G., & Gupta, V. K. (2018). Adsorption of heavy metals on conventional and nanostructured materials for wastewater treatment purposes: A

review. *Ecotoxicology and Environmental Safety*, *148*(August 2017), 702–712. https://doi.org/10.1016/j.ecoenv.2017.11.034

Capanema, N. S. V., Mansur, A. A. P., Mansur, H. S., de Jesus, A. C., Carvalho, S. M., Chagas, P., & de Oliveira, L. C. (2018). Eco-friendly and biocompatible cross-linked carboxymethylcellulose hydrogels as adsorbents for the removal of organic dye pollutants for environmental applications. *Environmental Technology (United Kingdom)*, *39*(22), 2856–2872. https://doi.org/10.1080/09593330.2017.1367845

Cataldo, S., Gianguzza, A., Milea, D., Muratore, N., & Pettignano, A. (2016). Pb(II) adsorption by a novel activated carbon - alginate composite material. A kinetic and equilibrium study. *International Journal of Biological Macromolecules*, *92*, 769–778. https://doi.org/10.1016/J.IJBIOMAC.2016.07.099

Chopra, A. K., Kumar Sharma, A., & Kumar, V. (2011). Overview of Electrolytic treatment: An alternative technology for purification of wastewater. *Archives of Applied Science Research Arch. Appl. Sci. Res*, *3*(35).

Chuang, J. J., Huang, Y. Y., Lo, S. H., Hsu, T. F., Huang, W. Y., Huang, S. L., & Lin, Y. S. (2017). Effects of pH on the Shape of Alginate Particles and Its Release Behavior. *International Journal of Polymer Science*, *2017*. https://doi.org/10.1155/2017/3902704

Çınar, S., Kaynar, Ü. H., Aydemir, T., Çam Kaynar, S., & Ayvacıklı, M. (2017). An efficient removal of RB5 from aqueous solution by adsorption onto nano-ZnO/Chitosan composite beads. *International Journal of Biological Macromolecules*, *96*, 459–465. https://doi.org/10.1016/j.ijbiomac.2016.12.021

Crini, G. (2005). Recent developments in polysaccharide-based materials used as adsorbents in wastewater treatment. *Progress in Polymer Science (Oxford)*, *30*(1), 38–70. https://doi.org/10.1016/j.progpolymsci.2004.11.002

Crini, G., Lichtfouse, E., Wilson, L. D., & Morin-Crini, N. (2018). *Adsorption-Oriented Processes Using Conventional and Non-conventional Adsorbents for Wastewater Treatment* (pp. 23–71). https://doi.org/10.1007/978-3-319-92111-2_2

Crini, G., Lichtfouse, E., Wilson, L., Morin-crini, N., Crini, G., Lichtfouse, E., Wilson, L., Adsorption-oriented, N. M., Crini, G., Lichtfouse, E., Wilson, L. D., & Morin-crini, N. (2019). Adsorption-oriented processes using conventional and non-conventional adsorbents for wastewater treatment To cite this version : HAL

Id : hal-02065600 Adsorption-Oriented Processes Using Conventional and Non-conventional Adsorbents for Wastewater Treatmen. In *Environmental Chemistry for a Sustainable World.* (Vol. 18).

Crini, G., Torri, G., Lichtfouse, E., Kyzas, G. Z., Wilson, L. D., & Morin-Crini, N. (2019). Dye removal by biosorption using cross-linked chitosan-based hydrogels. *Environmental Chemistry Letters*, *17*(4), 1645–1666. https://doi.org/10.1007/s10311-019-00903-y

da Silva Alves, D. C., Healy, B., Pinto, L. A. de A., Cadaval, T. R. S., & Breslin, C. B. (2021). Recent developments in Chitosan-based adsorbents for the removal of pollutants from aqueous environments. In *Molecules* (Vol. 26, Issue 3). MDPI AG. https://doi.org/10.3390/molecules26030594

Dandil, S., Akin Sahbaz, D., & Acikgoz, C. (2019). Adsorption of Cu(II) ions onto crosslinked chitosan/Waste Active Sludge Char (WASC) beads: Kinetic, equilibrium, and thermodynamic study. *International Journal of Biological Macromolecules*, *136*, 668–675. https://doi.org/10.1016/j.ijbiomac.2019.06.063

Darban, Z., Shahabuddin, S., Gaur, R., Ahmad, I., & Sridewi, N. (2022). Hydrogel-Based Adsorbent Material for the Effective Removal of Heavy Metals from Wastewater: A Comprehensive Review. In *Gels* (Vol. 8, Issue 5). https://doi.org/10.3390/gels8050263

Das, L., Das, P., Bhowal, A., & Bhattachariee, C. (2020). Synthesis of hybrid hydrogel nano-polymer composite using Graphene oxide, Chitosan and PVA and its application in waste water treatment. *Environmental Technology and Innovation*, *18*, 100664. https://doi.org/10.1016/j.eti.2020.100664

David, E. (2015). Mechanical strength and reliability of the porous materials used as adsorbents/ catalysts and the new development trends. *Archives of Materials Science and Engineering*, *73*(1), 5–17.

De Carvalho Gomes, S., Zhou, J. L., Li, W., & Long, G. (2019). Progress in manufacture and properties of construction materials incorporating water treatment sludge: A review. *Resources, Conservation and Recycling*, *145*(December 2018), 148–159. https://doi.org/10.1016/j.resconrec.2019.02.032

de Castro, M. L. F. A., Abad, M. L. B., Sumalinog, D. A. G., Abarca, R. R. M., Paoprasert, P., & de Luna, M. D. G. (2018). Adsorption of Methylene Blue dye and Cu(II) ions on EDTA-modified bentonite: Isotherm, kinetic and

thermodynamic studies. *Sustainable Environment Research*, *28*(5), 197–205. https://doi.org/10.1016/j.serj.2018.04.001

de la Guardia, M., & Armenta, S. (2011). Multianalyte determination versus one-at-a-time methodologies. *Comprehensive Analytical Chemistry*, *57*, 121–156. https://doi.org/10.1016/B978-0-444-53709-6.00006-9

Demey, H., Vincent, T., & Guibal, E. (2018). A novel algal-based sorbent for heavy metal removal. *Chemical Engineering Journal*, *332*(September), 582–595. https://doi.org/10.1016/j.cej.2017.09.083

Deng, F., Luo, X. B., Ding, L., & Luo, S. L. (2018). Application of Nanomaterials and Nanotechnology in the Reutilization of Metal Ion From Wastewater. *Nanomaterials for the Removal of Pollutants and Resource Reutilization*, 149–178. https://doi.org/10.1016/B978-0-12-814837-2.00005-6

Dhall, R. K., & Alam, M. S. (2020). Biodegradable Packaging. *Encyclopedia of Renewable and Sustainable Materials*, 26–43. https://doi.org/10.1016/B978-0-12-803581-8.11516-4

Donkadokula, N. Y., Kola, A. K., Naz, I., & Saroj, D. (2020). A review on advanced physico-chemical and biological textile dye wastewater treatment techniques. *Reviews in Environmental Science and Biotechnology*, *19*(3), 543–560. https://doi.org/10.1007/s11157-020-09543-z

Dragan, E. S. (2014). Design and applications of interpenetrating polymer network hydrogels. A review. *Chemical Engineering Journal*, *243*, 572–590. https://doi.org/10.1016/j.cej.2014.01.065

Dutta, S., Gupta, B., Srivastava, S. K., & Gupta, A. K. (2021). Recent advances on the removal of dyes from wastewater using various adsorbents: A critical review. *Materials Advances*, *2*(14), 4497–4531. https://doi.org/10.1039/d1ma00354b

Elanchezhiyan, S. S., Karthikeyan, P., Rathinam, K., Hasmath Farzana, M., & Park, C. M. (2021). Magnetic kaolinite immobilized chitosan beads for the removal of Pb(II) and Cd(II) ions from an aqueous environment. *Carbohydrate Polymers*, *261*(March), 117892. https://doi.org/10.1016/j.carbpol.2021.117892

El-Hefian, E. A., Nasef, M. M., & Yahaya, A. H. (2014). Chitosan-based polymer blends: Current status and applications. *Journal of the Chemical Society of Pakistan*, *36*(1), 11–27.

El-Naas, M. H., & Alhaija, M. A. (2013). Modelling of adsorption processes. *Mathematical Modelling*, *May*, 579–600.

El-sayed, M. E. A. (2020). Nanoadsorbents for water and wastewater remediation. *Science of The Total Environment*, *739*, 139903. https://doi.org/10.1016/j.scitotenv.2020.139903

Eltaweil, A. S., Mamdouh, I. M., Abd El-Monaem, E. M., & El-Subruiti, G. M. (2021). Highly Efficient Removal for Methylene Blue and Cu2+onto UiO-66 Metal-Organic Framework/Carboxylated Graphene Oxide-Incorporated Sodium Alginate Beads. *ACS Omega*. https://doi.org/10.1021/acsomega.1c03479

Esrafili, A., Bagheri, S., Kermani, M., Gholami, M., & Moslemzadeh, M. (2019). Simultaneous adsorption of heavy metal ions (Cu2+ and Cd2+) from aqueous solutions by magnetic silica nanoparticles (Fe3O4@SiO2) modified using edta. *Desalination and Water Treatment*, *158*, 207–215. https://doi.org/10.5004/dwt.2019.24274

Fahim Chyad, T., Fahim Chyad Al-Hamadani, R., Ageel Hammood, Z., & Abd Ali, G. (2021). Removal of Zinc (II) ions from industrial wastewater by adsorption on to activated carbon produced from pine cone. *Materials Today: Proceedings*, *xxxx*. https://doi.org/10.1016/j.matpr.2021.07.016

Farooq, U., Kozinski, J. A., Khan, M. A., & Athar, M. (2010). Biosorption of heavy metal ions using wheat based biosorbents - A review of the recent literature. *Bioresource Technology*, *101*(14), 5043–5053. https://doi.org/10.1016/j.biortech.2010.02.030

Fennell, E., & Huyghe, J. M. (2019). Chemically responsive hydrogel deformation mechanics: A review. *Molecules*, *24*(19), 1–22. https://doi.org/10.3390/molecules24193521

Fernandes, S., Regina, M., Moura, D., Glenn, G. M., & Ahmad, F. (2018). Thermal , microstructural , and spectroscopic analysis of Ca 2+ alginate / clay nanocomposite hydrogel beads. *Journal of Molecular Liquids*, *265*, 327–336. https://doi.org/10.1016/j.molliq.2018.06.005

Frachini, E. C. G., & Petri, D. F. S. (2019). Magneto-responsive hydrogels: Preparation, characterization, biotechnological and environmental applications. *Journal of the Brazilian Chemical Society*, *30*(10), 2010–2028. https://doi.org/10.21577/0103-5053.20190074

Fu, C., Zhu, X., Dong, X., Zhao, P., & Wang, Z. (2021). Study of adsorption property and mechanism of lead(II) and cadmium(II) onto sulfhydryl modified attapulgite.

Arabian Journal of Chemistry, *14*(2), 102960. https://doi.org/10.1016/J.ARABJC.2020.102960

Fu, F., & Wang, Q. (2011). Removal of heavy metal ions from wastewaters: A review. *Journal of Environmental Management*, *92*(3), 407–418. https://doi.org/10.1016/j.jenvman.2010.11.011

Fytianos, G., Tziolas, E., Papastergiadis, E., & Samaras, P. (2020). Least cost analysis for biocorrosion mitigation strategies in concrete sewers. *Sustainability (Switzerland)*, *12*(11), 1–13. https://doi.org/10.3390/su12114578

Gallego-Valero, L., Moral-Parajes, E., & Román-Sánchez, I. M. (2021). Wastewater treatment costs: A research overview through bibliometric analysis. *Sustainability (Switzerland)*, *13*(9), 1–14. https://doi.org/10.3390/su13095066

Garnica-Palafox, I. M., & Sánchez-Arévalo, F. M. (2016). Influence of natural and synthetic crosslinking reagents on the structural and mechanical properties of chitosan-based hybrid hydrogels. *Carbohydrate Polymers*, *151*, 1073–1081. https://doi.org/10.1016/j.carbpol.2016.06.036

Garrido-Cardenas, J. A., Esteban-García, B., Agüera, A., Sánchez-Pérez, J. A., & Manzano-Agugliaro, F. (2020). Wastewater treatment by advanced oxidation process and their worldwide research trends. *International Journal of Environmental Research and Public Health*, *17*(1). https://doi.org/10.3390/ijerph17010170

Goh, P. S., Ng, B. C., Lau, W. J., & Ismail, A. F. (2015). Inorganic nanomaterials in polymeric ultrafiltration membranes for water treatment. *Separation and Purification Reviews*, *44*(3), 216–249. https://doi.org/10.1080/15422119.2014.926274

Gomez-Maldonado, D., Erramuspe, I. B. V., & Peresin, M. S. (2019). Natural polymers as alternative adsorbents and treatment agents for water remediation. *BioResources*, *14*(4), 10093–10160. https://doi.org/10.15376/biores.14.4.10093-10160

Gupta, K., Joshi, P., Gusain, R., & Khatri, O. P. (2021). Recent advances in adsorptive removal of heavy metal and metalloid ions by metal oxide-based nanomaterials. *Coordination Chemistry Reviews*, *445*. https://doi.org/10.1016/j.ccr.2021.214100

Gupta, V. K., Ali, I., Saleh, T. A., Nayak, A., & Agarwal, S. (2012). Chemical treatment technologies for waste-water recycling - An overview. *RSC Advances*, *2*(16), 6380–6388. https://doi.org/10.1039/c2ra20340e

Gyles, D. A., Castro, L. D., Silva, J. O. C., & Ribeiro-Costa, R. M. (2017). A review of the designs and prominent biomedical advances of natural and synthetic hydrogel formulations. *European Polymer Journal*, *88*(01), 373–392. https://doi.org/10.1016/j.eurpolymj.2017.01.027

Habiba, U., Joo, T. C., Siddique, T. A., Salleh, A., Ang, B. C., & Afifi, A. M. (2017). Effect of degree of deacetylation of chitosan on adsorption capacity and reusability of chitosan/polyvinyl alcohol/TiO2 nano composite. *International Journal of Biological Macromolecules*, *104*, 1133–1142. https://doi.org/10.1016/j.ijbiomac.2017.07.007

Habiba, U., Siddique, T. A., Joo, T. C., Salleh, A., Ang, B. C., & Afifi, A. M. (2017a). Synthesis of chitosan/polyvinyl alcohol/zeolite composite for removal of methyl orange, Congo red and chromium(VI) by flocculation/adsorption. *Carbohydrate Polymers*, *157*, 1568–1576. https://doi.org/10.1016/j.carbpol.2016.11.037

Habiba, U., Siddique, T. A., Joo, T. C., Salleh, A., Ang, B. C., & Afifi, A. M. (2017b). Synthesis of chitosan/polyvinyl alcohol/zeolite composite for removal of methyl orange, Congo red and chromium(VI) by flocculation/adsorption. *Carbohydrate Polymers*, *157*(Vi), 1568–1576. https://doi.org/10.1016/j.carbpol.2016.11.037

Hamad, M. T. M. H., & Saied, M. S. S. (2021a). Kinetic studies of Congo red dye adsorption by immobilized Aspergillus niger on alginate. *Applied Water Science*, *11*(2), 1–12. https://doi.org/10.1007/s13201-021-01362-z

Hamad, M. T. M. H., & Saied, M. S. S. (2021b). Kinetic studies of Congo red dye adsorption by immobilized Aspergillus niger on alginate. *Applied Water Science*, *11*(2). https://doi.org/10.1007/s13201-021-01362-z

Hamedi, H., Moradi, S., Hudson, S. M., & Tonelli, A. E. (2018). Chitosan based hydrogels and their applications for drug delivery in wound dressings: A review. *Carbohydrate Polymers*, *199*(June), 445–460. https://doi.org/10.1016/j.carbpol.2018.06.114

Hasan, M. M., Habib, M. L., Anwaruzzaman, M., Kamruzzaman, M., Khan, M. N., & Rahman, M. M. (2020). Processing techniques of chitosan-based interpenetrating

polymer networks, gels, blends, composites and nanocomposites. *Handbook of Chitin and Chitosan: Volume 2: Composites and Nanocomposites from Chitin and Chitosan, Manufacturing and Characterisations*, 61–93. https://doi.org/10.1016/B978-0-12-817968-0.00003-2

Hasanpour, M., & Hatami, M. (2020). Application of three dimensional porous aerogels as adsorbent for removal of heavy metal ions from water/wastewater: A review study. *Advances in Colloid and Interface Science*, *284*, 102247. https://doi.org/10.1016/j.cis.2020.102247

Hashem, M. S., & Qi, X. bin. (2021). Treated wastewater irrigation-a review. *Water (Switzerland)*, *13*(11). https://doi.org/10.3390/w13111527

Hayrunnisa Nadaroglu. (2012). Removal of cobalt (II) ions from aqueous solution by using alternative adsorbent industrial red mud waste material. *International Journal of the Physical Sciences*, *7*(9). https://doi.org/10.5897/ijps11.1748

Ho, T.-C., Chang, C.-C., Chan, H.-P., Chung, T.-W., Shu, C.-W., Chuang, K.-P., Duh, T.-H., Yang, M.-H., & Tyan, Y.-C. (2022). Hydrogels: Properties and Applications in Biomedicine. *Molecules*, *27*(9), 2902. https://doi.org/10.3390/molecules27092902

Ho, Y. S., & McKay, G. (1999). Pseudo-second order model for sorption processes. *Process Biochemistry*, *34*(5), 451–465. https://doi.org/10.1016/S0032-9592(98)00112-5

Hong, G. B., Yu, T. J., Lee, H. C., & Ma, C. M. (2021). Using rice bran hydrogel beads to remove dye from aqueous solutions. *Sustainability*, *13*(10), 5640. https://doi.org/10.3390/su13105640

Hossain, A. K. M. N. U., Sela, S. K., Saha, S., Das, A., Iqbal, S. F., & Hassan, M. N. (2018). Treatment of textile waste water using natural catalyst (chitosan and microorganism). *Journal of Textile Engineering & Fashion Technology*, *4*(5), 320–325. https://doi.org/10.15406/jteft.2018.04.00159

Hou, J., Aydemir, B. E., & Dumanli, A. G. (2021). Understanding the structural diversity of chitins as a versatile biomaterial. In *Philosophical Transactions of the Royal Society A: Mathematical, Physical and Engineering Sciences* (Vol. 379, Issue 2206). https://doi.org/10.1098/rsta.2020.0331

Hou, N., Wang, R., Wang, F., Bai, J., Zhou, J., Zhang, L., Hu, J., Liu, S., & Jiao, T. (2020a). Fabrication of Hydrogels via Host-Guest Polymers as Highly Efficient

Organic Dye Adsorbents for Wastewater Treatment. *ACS Applied Materials and Interfaces*. https://doi.org/10.1021/acsomega.0c00076

Hou, N., Wang, R., Wang, F., Bai, J., Zhou, J., Zhang, L., Hu, J., Liu, S., & Jiao, T. (2020b). Fabrication of Hydrogels via Host-Guest Polymers as Highly Efficient Organic Dye Adsorbents for Wastewater Treatment. *ACS Omega*, *5*, 5470–5479. https://doi.org/10.1021/acsomega.0c00076

Hou, N., Wang, R., Wang, F., Bai, J., Zhou, J., Zhang, L., Hu, J., Liu, S., & Jiao, T. (2020c). Fabrication of Hydrogels via Host-Guest Polymers as Highly Efficient Organic Dye Adsorbents for Wastewater Treatment. *ACS Applied Materials and Interfaces*. https://doi.org/10.1021/acsomega.0c00076

Hu, T., Liu, Q., Gao, T., Dong, K., Wei, G., & Yao, J. (2018). Facile Preparation of Tannic Acid-Poly(vinyl alcohol)/Sodium Alginate Hydrogel Beads for Methylene Blue Removal from Simulated Solution. *ACS Omega*, *3*(7), 7523–7531. https://doi.org/10.1021/acsomega.8b00577

Igberase, E., Osifo, P., & Ofomaja, A. (2014). The adsorption of copper (II) ions by polyaniline graft chitosan beads from aqueous solution: Equilibrium, kinetic and desorption studies. *Journal of Environmental Chemical Engineering*, *2*(1), 362–369. https://doi.org/10.1016/j.jece.2014.01.008

Int, C. (2019). *Chemical precipitation method for chromium removal and its recovery from tannery wastewater in Ethiopia*. *May*. https://doi.org/10.31221/osf.io/m7h5k

Int, C., & Iqbal, M. (2019). *Bioassays based on higher plants as excellent dosimeters for ecotoxicity monitoring: A review*. *April*. https://doi.org/10.31221/osf.io/z2ynm

Jain, P., Sahoo, K., Mahiya, L., Ojha, H., Trivedi, H., Parmar, A. S., & Kumar, M. (2021). Color removal from model dye effluent using PVA-GA hydrogel beads. *Journal of Environmental Management*, *281*(July 2020). https://doi.org/10.1016/j.jenvman.2020.111797

Jana, S., Ray, J., Mondal, B., & Tripathy, T. (2019). Efficient and selective removal of cationic organic dyes from their aqueous solutions by a nanocomposite hydrogel, katira gum-cl-poly(acrylic acid-co-N, N-dimethylacrylamide)@bentonite. *Applied Clay Science*, *173*, 46–64. https://doi.org/10.1016/j.clay.2019.03.009

Jawad, A. H., Abdulhameed, A. S., & Mastuli, M. S. (2020). Mesoporous Crosslinked Chitosan-Activated Charcoal Composite for the Removal of Thionine Cationic Dye: Comprehensive Adsorption and Mechanism Study. *Journal of Polymers and the Environment*, *28*(3), 1095–1105. https://doi.org/10.1007/s10924-020-01671-5

Jayakumar, A., Radoor, S., Radhakrishnan, E. K., Nair, I. C., Siengchin, S., & Parameswaranpillai, J. (2021). Soy protein-based polymer blends and composites. *Biodegradable Polymers, Blends and Composites*, 39–57. https://doi.org/10.1016/B978-0-12-823791-5.00012-0

J.Fernandes, A.Rodrigues, R.Menezes, & G.Neves. (2020). Adsorption of Anionic Dye on the Acid-Functionalized Bentonite. *Materials*, *13*, 3600.

Jiménez-Gómez, C. P., & Cecilia, J. A. (2020a). Chitosan: A Natural Biopolymer with a Wide and Varied Range of Applications. *Molecules*, *25*(17). https://doi.org/10.3390/molecules25173981

Jiménez-Gómez, C. P., & Cecilia, J. A. (2020b). Chitosan: A Natural Biopolymer with a Wide and Varied Range of Applications. In *Molecules* (Vol. 25, Issue 17, p. 3981). MDPI AG. https://doi.org/10.3390/molecules25173981

Jiménez-Miramontes, J. A., Domínguez-Arvizu, J. L., Salinas-Gutiérrez, J. M., Meléndez-Zaragoza, M. J., López-Ortiz, A., & Collins-Martínez, V. (2017). Synthesis, characterization and photocatalytic evaluation of strontium ferrites towards H2 production by water splitting under visible light irradiation. *International Journal of Hydrogen Energy*, *42*(51), 30257–30266. https://doi.org/10.1016/j.ijhydene.2017.09.162

Jing, G., Wang, L., Yu, H., Amer, W. A., & Zhang, L. (2013). Recent progress on study of hybrid hydrogels for water treatment. *Colloids and Surfaces A: Physicochemical and Engineering Aspects*, *416*(1), 86–94. https://doi.org/10.1016/j.colsurfa.2012.09.043

Jintakosol, T., & Nitayaphat, W. (2016). Adsorption of Silver (I) from Aqueous Solution Using Chitosan/Montmorillonite Composite Beads. *Materials Research*, *19*(5), 1114–1121. https://doi.org/10.1590/1980-5373-MR-2015-0738

Kang, D., Yu, X., Ge, M., Xiao, F., & Xu, H. (2017). Novel Al-doped carbon nanotubes with adsorption and coagulation promotion for organic pollutant removal. *Journal of Environmental Sciences (China)*, *54*, 1–12. https://doi.org/10.1016/j.jes.2016.04.022

Karim, M. R., Aijaz, M. O., Alharth, N. H., Alharbi, H. F., Al-Mubaddel, F. S., & Awual, M. R. (2019). Composite nanofibers membranes of poly(vinyl alcohol)/chitosan for selective lead(II) and cadmium(II) ions removal from wastewater. *Ecotoxicology and Environmental Safety*, *169*(July 2018), 479–486. https://doi.org/10.1016/j.ecoenv.2018.11.049

Katsou, E., Malamis, S., Tzanoudaki, M., Haralambous, K. J., & Loizidou, M. (2011). Regeneration of natural zeolite polluted by lead and zinc in wastewater treatment systems. *Journal of Hazardous Materials*, *189*(3), 773–786. https://doi.org/10.1016/J.JHAZMAT.2010.12.061

Kaur, G., Kumar, V., Saruchi, Mishra, A. K., & Mishra, S. (2022). Toxicological effect of biopolymers and their applications. *Bio-Based Nanomaterials: Synthesis Protocols, Mechanisms and Applications*, 265–284. https://doi.org/10.1016/B978-0-323-85148-0.00002-6

Kausar, A., Rehman, S. U., Khalid, F., Bonilla-Petriciolet, A., Mendoza-Castillo, D. I., Bhatti, H. N., Ibrahim, S. M., & Iqbal, M. (2022). Cellulose, clay and sodium alginate composites for the removal of methylene blue dye: Experimental and DFT studies. *International Journal of Biological Macromolecules*, *209*(November 2021), 576–585. https://doi.org/10.1016/j.ijbiomac.2022.04.044

Kemp, K. C., Seema, H., Saleh, M., Le, N. H., Mahesh, K., Chandra, V., & Kim, K. S. (2013). Environmental applications using graphene composites: Water remediation and gas adsorption. *Nanoscale*, *5*(8), 3149–3171. https://doi.org/10.1039/c3nr33708a

Khan, F. S. A., Mubarak, N. M., Khalid, M., Walvekar, R., Abdullah, E. C., Mazari, S. A., Nizamuddin, S., & Karri, R. R. (2020). Magnetic nanoadsorbents' potential route for heavy metals removal—a review. *Environmental Science and Pollution Research*, *27*(19), 24342–24356. https://doi.org/10.1007/s11356-020-08711-6

Khan, S. R., Sharma, B., Chawla, P. A., & Bhatia, R. (2022). Inductively Coupled Plasma Optical Emission Spectrometry (ICP-OES): a Powerful Analytical Technique for Elemental Analysis. *Food Analytical Methods*, *15*(3), 666–688. https://doi.org/10.1007/S12161-021-02148-4/METRICS

Khapre, M. A., Pandey, S., & Jugade, R. M. (2021). Glutaraldehyde-cross-linked chitosan–alginate composite for organic dyes removal from aqueous solutions.

International Journal of Biological Macromolecules, *190*(September), 862–875. https://doi.org/10.1016/j.ijbiomac.2021.09.026

Khayyun, T. S., & Mseer, A. H. (2019). Comparison of the experimental results with the Langmuir and Freundlich models for copper removal on limestone adsorbent. *Applied Water Science*, *9*(8), 1–8. https://doi.org/10.1007/s13201-019-1061-2

Kim, J. J., Kim, Y. S., & Kumar, V. (2019). Heavy metal toxicity: An update of chelating therapeutic strategies. In *Journal of Trace Elements in Medicine and Biology* (Vol. 54, pp. 226–231). Elsevier GmbH. https://doi.org/10.1016/j.jtemb.2019.05.003

Kim, W. Y., Yun, C. Y., Son, D. J., Chang, D., Kim, D. G., & Hong, K. H. (2017). Electrolyte addition for enhanced wastewater treatment by electrolysis using Cu electrode. *Journal of Electrochemical Science and Technology*, *8*(1), 35–42. https://doi.org/10.5229/JECST.2017.8.1.35

Kinuthia, G. K., Ngure, V., Beti, D., Lugalia, R., Wangila, A., & Kamau, L. (2020). Levels of heavy metals in wastewater and soil samples from open drainage channels in Nairobi, Kenya: community health implication. *Scientific Reports*, *10*(1), 1–13. https://doi.org/10.1038/s41598-020-65359-5

Kluczka, J., Gnus, M., Kazek-Kęsik, A., & Dudek, G. (2018). Zirconium-chitosan hydrogel beads for removal of boron from aqueous solutions. *Polymer*, *150*, 109–118. https://doi.org/10.1016/j.polymer.2018.07.010

Kong, A., Ji, Y., Ma, H., Song, Y., He, B., & Li, J. (2018). A novel route for the removal of Cu(II) and Ni(II) ions via homogeneous adsorption by chitosan solution. *Journal of Cleaner Production*, *192*, 801–808. https://doi.org/10.1016/j.jclepro.2018.04.271

Koumanova, B., & Allen, S. J. (2005). Decolourisation of Water / Wastewater Using Adsorption (Review). *Journal of the University of Chemical Technology and Metallurgy*, *40*, 175–192.

Kubilay, Ş., Gürkan, R., Savran, A., & Şahan, T. (2007). Removal of Cu(II), Zn(II) and Co(II) ions from aqueous solutions by adsorption onto natural bentonite. *Adsorption*, *13*(1), 41–51. https://doi.org/10.1007/s10450-007-9003-y

Kumar, A., Sood, A., & Han, S. S. (2022). Poly (vinyl alcohol)-alginate as potential matrix for various applications: A focused review. *Carbohydrate Polymers*, *277*(October 2021), 118881. https://doi.org/10.1016/j.carbpol.2021.118881

Kumar, M., Seth, A., Singh, A. K., Rajput, M. S., & Sikandar, M. (2021). Remediation strategies for heavy metals contaminated ecosystem: A review. *Environmental and Sustainability Indicators*, *12*, 100155. https://doi.org/10.1016/J.INDIC.2021.100155

Kumar, M., Tripathi, B. P., & Shahi, V. K. (2009). Crosslinked chitosan/polyvinyl alcohol blend beads for removal and recovery of Cd(II) from wastewater. *Journal of Hazardous Materials*, *172*(2–3), 1041–1048. https://doi.org/10.1016/j.jhazmat.2009.07.108

Kumari, P., Alam, M., & Siddiqi, W. A. (2019). Usage of nanoparticles as adsorbents for waste water treatment: An emerging trend. *Sustainable Materials and Technologies*, *22*, e00128. https://doi.org/10.1016/j.susmat.2019.e00128

Laaz, I., Stébé, M. J., Benhamou, A., Zoubir, D., & Blin, J. L. (2016). Influence of porosity and surface modification on the adsorption of both cationic and anionic dyes. *Colloids and Surfaces A: Physicochemical and Engineering Aspects*, *490*, 30–40. https://doi.org/10.1016/j.colsurfa.2015.11.024

Langmuir, I. (1917). The constitution and fundamental properties of solids and liquids. Part II.-Liquids. *Journal of the Franklin Institute*, *184*(5), 721. https://doi.org/10.1016/s0016-0032(17)90088-2

Lau, Y. Y., Wong, Y. S., Teng, T. T., Morad, N., Rafatullah, M., & Ong, S. A. (2014). Coagulation-flocculation of azo dye acid orange 7 with green refined laterite soil. *Chemical Engineering Journal*, *246*, 383–390. https://doi.org/10.1016/j.cej.2014.02.100

Lee, K. Y., & Mooney, D. J. (2012). Alginate: Properties and biomedical applications. In *Progress in Polymer Science (Oxford)* (Vol. 37, Issue 1, pp. 106–126). Elsevier Ltd. https://doi.org/10.1016/j.progpolymsci.2011.06.003

Lellis, B., Fávaro-Polonio, C. Z., Pamphile, J. A., & Polonio, J. C. (2019). Effects of textile dyes on health and the environment and bioremediation potential of living organisms. *Biotechnology Research and Innovation*, *3*(2), 275–290. https://doi.org/10.1016/j.biori.2019.09.001

Lemma, S. M., Bossard, F., & Rinaudo, M. (2016). Preparation of pure and stable chitosan nanofibers by electrospinning in the presence of poly(ethylene oxide). In *International Journal of Molecular Sciences* (Vol. 17, Issue 11). https://doi.org/10.3390/ijms17111790

Lewandowska, K., Sionkowska, A., Kaczmarek, B., & Furtos, G. (2014). Characterization of chitosan composites with various clays. *International Journal of Biological Macromolecules*, *65*, 534–541. https://doi.org/10.1016/j.ijbiomac.2014.01.069

Li, H., Kruteva, M., Dulle, M., Wang, Z., Mystek, K., Ji, W., Pettersson, T., & Wågberg, L. (2021). Understanding the Drying Behavior of Regenerated Cellulose Gel Beads: The Effects of Concentration and Nonsolvents. *ACS Nano*. https://doi.org/10.1021/acsnano.1c09338

Li, Y., Dong, X., & Zhao, L. (2021). Application of magnetic chitosan nanocomposites modified by graphene oxide and polyethyleneimine for removal of toxic heavy metals and dyes from water. *International Journal of Biological Macromolecules*, *192*(October), 118–125. https://doi.org/10.1016/j.ijbiomac.2021.09.202

Li, Y., Qiu, T., & Xu, X. (2013). Preparation of lead-ion imprinted crosslinked electro-spun chitosan nanofiber mats and application in lead ions removal from aqueous solutions. *European Polymer Journal*, *49*(6), 1487–1494. https://doi.org/10.1016/j.eurpolymj.2013.04.002

Liang, J., Wang, J., Li, S., Xu, L., Wang, R., Chen, R., & Sun, Y. (2019). The size-controllable preparation of chitosan/silver nanoparticle composite microsphere and its antimicrobial performance. *Carbohydrate Polymers*, *220*(January), 22–29. https://doi.org/10.1016/j.carbpol.2019.05.048

Lim, J. Y. C., Goh, S. S., Liow, S. S., Xue, K., & Loh, X. J. (2019). Molecular gel sorbent materials for environmental remediation and wastewater treatment. *Journal of Materials Chemistry A*, *7*(32), 18759–18791. https://doi.org/10.1039/c9ta05782j

Litefti, K., Freire, M. S., Stitou, M., & González-Álvarez, J. (2019a). Adsorption of an anionic dye (Congo red) from aqueous solutions by pine bark. *Scientific Reports*, *9*(1), 1–11. https://doi.org/10.1038/s41598-019-53046-z

Litefti, K., Freire, M. S., Stitou, M., & González-Álvarez, J. (2019b). Adsorption of an anionic dye (Congo red) from aqueous solutions by pine bark. *Scientific Reports*, *9*(1). https://doi.org/10.1038/s41598-019-53046-z

Liu, C., Omer, A. M., & Ouyang, X. kun. (2018). Adsorptive removal of cationic methylene blue dye using carboxymethyl cellulose/k-carrageenan/activated montmorillonite composite beads: Isotherm and kinetic studies. *International*

Journal of Biological Macromolecules, *106*, 823–833. https://doi.org/10.1016/j.ijbiomac.2017.08.084

Liu, J., Chen, T. W., Yang, Y. L., Bai, Z. C., Xia, L. R., Wang, M., Lv, X. L., & Li, L. (2020). Removal of heavy metal ions and anionic dyes from aqueous solutions using amide-functionalized cellulose-based adsorbents. *Carbohydrate Polymers*, *230*(October 2019). https://doi.org/10.1016/j.carbpol.2019.115619

Liu, T., Yang, X., Wang, Z. L., & Yan, X. (2013). Enhanced chitosan beads-supported Fe0-nanoparticles for removal of heavy metals from electroplating wastewater in permeable reactive barriers. *Water Research*, *47*(17), 6691–6700. https://doi.org/10.1016/j.watres.2013.09.006

Liu, W., Liu, L., Liu, C., Hao, Y., Yang, H., Yuan, B., & Jiang, J. (2016). Methylene blue enhances the anaerobic decolorization and detoxication of azo dye by Shewanella onediensis MR-1. *Biochemical Engineering Journal*, *110*, 115–124. https://doi.org/10.1016/j.bej.2016.02.012

Liu, X. J., Li, M. F., & Singh, S. K. (2021). Manganese-modified lignin biochar as adsorbent for removal of methylene blue. *Journal of Materials Research and Technology*, *12*, 1434–1445. https://doi.org/10.1016/j.jmrt.2021.03.076

Liu, Y., Hu, L., Yao, Y., Su, Z., & Hu, S. (2019). Construction of composite chitosan-glucose hydrogel for adsorption of Co2+ ions. *International Journal of Biological Macromolecules*, *139*, 213–220. https://doi.org/10.1016/j.ijbiomac.2019.07.202

Liu, Z., Haddad, M., Sauvé, S., & Barbeau, B. (2021). Alleviating the burden of ion exchange brine in water treatment: From operational strategies to brine management. *Water Research*, *205*(May). https://doi.org/10.1016/j.watres.2021.117728

Lone, S., Yoon, D. H., Lee, H., & Cheong, I. W. (2019). Gelatin-chitosan hydrogel particles for efficient removal of Hg(ii) from wastewater. *Environmental Science: Water Research and Technology*, *5*(1), 83–90. https://doi.org/10.1039/c8ew00678d

Luo, J., Fu, K., Yu, D., Hristovski, K. D., Westerhoff, P., & Crittenden, J. C. (2021). Review of Advances in Engineering Nanomaterial Adsorbents for Metal Removal and Recovery from Water: Synthesis and Microstructure Impacts. *ACS ES&T Engineering*, *1*(4), 623–661. https://doi.org/10.1021/acsestengg.0c00174

Luo, J., Yu, D., Hristovski, K. D., Fu, K., Shen, Y., Westerhoff, P., & Crittenden, J. C. (2021). Critical Review of Advances in Engineering Nanomaterial Adsorbents for Metal Removal and Recovery from Water: Mechanism Identification and Engineering Design. In *Environmental Science and Technology* (Vol. 55, Issue 8, pp. 4287–4304). American Chemical Society. https://doi.org/10.1021/acs.est.0c07936

Lv, S. H. (2016). High-performance superplasticizer based on chitosan. *Biopolymers and Biotech Admixtures for Eco-Efficient Construction Materials*, 131–150. https://doi.org/10.1016/B978-0-08-100214-8.00007-5

Ma, D., Zhu, B., Cao, B., Wang, J., & Zhang, J. (2017). Fabrication of the novel hydrogel based on waste corn stalk for removal of methylene blue dye from aqueous solution. *Applied Surface Science*, *422*, 944–952. https://doi.org/10.1016/j.apsusc.2017.06.072

Mahmoud, D. K., Salleh, M. A. M., Karim, W. A. W. A., Idris, A., & Abidin, Z. Z. (2012). Batch adsorption of basic dye using acid treated kenaf fibre char: Equilibrium, kinetic and thermodynamic studies. *Chemical Engineering Journal*, *181–182*, 449–457. https://doi.org/10.1016/j.cej.2011.11.116

Malik, P. K. (2003). Use of activated carbons prepared from sawdust and rice-husk for adsoprtion of acid dyes: A case study of acid yellow 36. *Dyes and Pigments*, *56*(3), 239–249. https://doi.org/10.1016/S0143-7208(02)00159-6

Mallakpour, S., Azadi, E., & Hussain, C. M. (2021). State-of-the-art of 3D printing technology of alginate-based hydrogels—An emerging technique for industrial applications. *Advances in Colloid and Interface Science*, *293*, 102436. https://doi.org/10.1016/j.cis.2021.102436

Mallakpour, S., & Rashidimoghadam, S. (2017). Poly(vinyl alcohol)/carbon nanotube nanocomposites. *Biodegradable and Biocompatible Polymer Composites: Processing, Properties and Applications*, 297–315. https://doi.org/10.1016/B978-0-08-100970-3.00010-9

Mandal, B., & Ray, S. K. (2013). Synthesis of interpenetrating network hydrogel from poly(acrylic acid-co-hydroxyethyl methacrylate) and sodium alginate: Modeling and kinetics study for removal of synthetic dyes from water. *Carbohydrate Polymers*, *98*(1), 257–269. https://doi.org/10.1016/j.carbpol.2013.05.093

Maquet, & Christophe. (2020). Wastewater reuse: a solution with a future. *Http://Journals.Openedition.Org/Factsreports*, *Special Issue 22*, 64–69. http://journals.openedition.org/factsreports/6341

Marcos-Hernández, M., & Villagrán, D. (2018). Mesoporous composite nanomaterials for dye removal and other applications. *Composite Nanoadsorbents*, 265–293. https://doi.org/10.1016/B978-0-12-814132-8.00012-5

Marrakchi, F., Khanday, W. A., Asif, M., & Hameed, B. H. (2016). Cross-linked chitosan/sepiolite composite for the adsorption of methylene blue and reactive orange 16. *International Journal of Biological Macromolecules*, *93*, 1231–1239. https://doi.org/10.1016/j.ijbiomac.2016.09.069

Maryanti, R., Nandiyanto, A. B. D., Manullang, T. I. B., Hufad, A., & Sunardi. (2020). Adsorption of dye on carbon microparticles: Physicochemical properties during adsorption, adsorption isotherm and education for students with special needs. *Sains Malaysiana*, *49*(12), 2977–2988. https://doi.org/10.17576/jsm-2020-4912-09

Masindi, V., & Africa, S. (2016). *for degree of Doctor of Philosophy in Environmental Science . Promoter :* (Issue December 2015). https://doi.org/10.13140/RG.2.1.4488.3442

Meneses, M., Pasqualino, J. C., & Castells, F. (2010). Environmental assessment of urban wastewater reuse: Treatment alternatives and applications. *Chemosphere*, *81*(2), 266–272. https://doi.org/10.1016/j.chemosphere.2010.05.053

Merakchi, A., Bettayeb, S., Drouiche, N., & Adour, L. (2019). Cross - linking and modification of sodium alginate biopolymer for dye removal in aqueous solution. *Polymer Bulletin*, *76*(7), 3535–3554. https://doi.org/10.1007/s00289-018-2557-x

Mitra, S., Chakraborty, A. J., Tareq, A. M., Emran, T. bin, Nainu, F., Khusro, A., Idris, A. M., Khandaker, M. U., Osman, H., Alhumaydhi, F. A., & Simal-Gandara, J. (2022). Impact of heavy metals on the environment and human health: Novel therapeutic insights to counter the toxicity. *Journal of King Saud University - Science*, *34*(3). https://doi.org/10.1016/J.JKSUS.2022.101865

Mohammadzadeh Pakdel, P., & Peighambardoust, S. J. (2018a). A review on acrylic based hydrogels and their applications in wastewater treatment. *Journal of Environmental Management*, *217*, 123–143. https://doi.org/10.1016/j.jenvman.2018.03.076

Mohammadzadeh Pakdel, P., & Peighambardoust, S. J. (2018b). Review on recent progress in chitosan-based hydrogels for wastewater treatment application. *Carbohydrate Polymers*, *201*(June), 264–279. https://doi.org/10.1016/j.carbpol.2018.08.070

Mohammadzadeh Pakdel, P., & Peighambardoust, S. J. (2018c). Review on recent progress in chitosan-based hydrogels for wastewater treatment application. *Carbohydrate Polymers*, *201*(August), 264–279. https://doi.org/10.1016/j.carbpol.2018.08.070

Mok, C. F., Ching, Y. C., Muhamad, F., Abu Osman, N. A., Hai, N. D., & Che Hassan, C. R. (2020). Adsorption of Dyes Using Poly(vinyl alcohol) (PVA) and PVA-Based Polymer Composite Adsorbents: A Review. *Journal of Polymers and the Environment*, *28*(3), 775–793. https://doi.org/10.1007/s10924-020-01656-4

Mokhtar, A., Abdelkrim, S., Djelad, A., Sardi, A., Boukoussa, B., Sassi, M., & Bengueddach, A. (2020). Adsorption behavior of cationic and anionic dyes on magadiite-chitosan composite beads. *Carbohydrate Polymers*, *229*(October 2019), 115399. https://doi.org/10.1016/j.carbpol.2019.115399

Moreira, V. R., Lebron, Y. A. R., Couto, C. F., Maia, A., Moravia, W. G., & Amaral, M. C. S. (2021). Process development for textile wastewater treatment towards zero liquid discharge: Integrating membrane separation process and advanced oxidation techniques. *Process Safety and Environmental Protection*, *xxxx*. https://doi.org/10.1016/j.psep.2021.10.037

Morote, Á. F., & Hernández, M. (2016). Urban sprawl and its effects on water demand: A case study of Alicante, Spain. *Land Use Policy*, *50*, 352–362. https://doi.org/10.1016/j.landusepol.2015.06.032

Mu, R., Liu, B., Chen, X., Wang, N., & Yang, J. (2020a). Adsorption of Cu (II)and Co (II) from aqueous solution using lignosulfonate/chitosan adsorbent. *International Journal of Biological Macromolecules*, *163*, 120–127. https://doi.org/10.1016/j.ijbiomac.2020.06.260

Mu, R., Liu, B., Chen, X., Wang, N., & Yang, J. (2020b). Hydrogel adsorbent in industrial wastewater treatment and ecological environment protection. *Environmental Technology and Innovation*, *20*. https://doi.org/10.1016/j.eti.2020.101107

Munagapati, V. S., & Kim, D. S. (2017). Equilibrium isotherms, kinetics, and thermodynamics studies for congo red adsorption using calcium alginate beads impregnated with nano-goethite. *Ecotoxicology and Environmental Safety*, *141*(March), 226–234. https://doi.org/10.1016/j.ecoenv.2017.03.036

Naseeruteen, F., Hamid, N. S. A., Suah, F. B. M., Ngah, W. S. W., & Mehamod, F. S. (2018). Adsorption of malachite green from aqueous solution by using novel chitosan ionic liquid beads. *International Journal of Biological Macromolecules*, *107*(PartA), 1270–1277. https://doi.org/10.1016/j.ijbiomac.2017.09.111

Nasrollahzadeh, M., Sajjadi, M., Iravani, S., & Varma, R. S. (2021). Starch, cellulose, pectin, gum, alginate, chitin and chitosan derived (nano)materials for sustainable water treatment: A review. *Carbohydrate Polymers*, *251*(August 2020), 116986. https://doi.org/10.1016/j.carbpol.2020.116986

Nechita, P. (2017). Applications of Chitosan in Wastewater Treatment. *Biological Activities and Application of Marine Polysaccharides*, *1*, 209–228.

Nemr, A. El, Abdelwahab, O., El-Sikaily, A., & Khaled, A. (2009). Removal of direct blue-86 from aqueous solution by new activated carbon developed from orange peel. *Journal of Hazardous Materials*, *161*(1), 102–110. https://doi.org/10.1016/j.jhazmat.2008.03.060

Nicolaus, E. E. M., Maxwell, D. L., Khamis, A. S., Abdulla, K. H., Harrod, R. P., Devlin, M. J., & Lyons, B. P. (2022). Spatial and temporal analysis of the risks posed by metal contamination in coastal and marine sediments of Bahrain. *Environmental Monitoring and Assessment*, *194*(2), 1–11. https://doi.org/10.1007/s10661-021-09722-7

Nisar, S., Pandit, A. H., Wang, L. F., & Rattan, S. (2020). Strategy to design a smart photocleavable and pH sensitive chitosan based hydrogel through a novel crosslinker: A potential vehicle for controlled drug delivery. *RSC Advances*, *10*(25), 14694–14704. https://doi.org/10.1039/c9ra10333c

Olusegun, S. J., Freitas, E. T. F., Lara, L. R. S., & Mohallem, N. D. S. (2021). Synergistic effect of a spinel ferrite on the adsorption capacity of nano bio-silica for the removal of methylene blue. *Environmental Technology (United Kingdom)*, *42*(14), 2163–2176. https://doi.org/10.1080/09593330.2019.1694083

Osińska, M. (2017). Removal of lead(II), copper(II), cobalt(II) and nickel(II) ions from aqueous solutions using carbon gels. *Journal of Sol-Gel Science and Technology*, *81*(3), 678–692. https://doi.org/10.1007/s10971-016-4256-0

Østberg, T., Lund, E. M., & Graffner, C. (1994). Calcium alginate matrices for oral multiple unit administration: IV. Release characteristics in different media. *International Journal of Pharmaceutics*, *112*(3), 241–248. https://doi.org/10.1016/0378-5173(94)90360-3

Oussalah, A., & Boukerroui, A. (2020). Alginate - bentonite beads for efficient adsorption of methylene blue dye. *Euro-Mediterranean Journal for Environmental Integration*, *5*, 1–10. https://doi.org/10.1007/s41207-020-00165-z

P., A., K., V., M., S., T., G., K., R., P.N., S., & Sukumaran, A. (2017). Removal of toxic heavy metal lead (II) using chitosan oligosaccharide-graft-maleic anhydride/polyvinyl alcohol/silk fibroin composite. *International Journal of Biological Macromolecules*, *104*(February 2018), 1469–1482. https://doi.org/10.1016/j.ijbiomac.2017.05.111

Paredes Juárez, G. A., Spasojevic, M., Faas, M. M., & de Vos, P. (2014). Immunological and technical considerations in application of alginate-based microencapsulation systems. *Frontiers in Bioengineering and Biotechnology*, *2*(AUG), 1–15. https://doi.org/10.3389/fbioe.2014.00026

Patel, P., & Thareja, P. (2022). Hydrogels differentiated by length scales: A review of biopolymer-based hydrogel preparation methods, characterization techniques, and targeted applications. *European Polymer Journal*, *163*(August 2021). https://doi.org/10.1016/j.eurpolymj.2021.110935

Petrova, V. A., Elokhovskiy, V. Y., Raik, S. V., Poshina, D. N., Romanov, D. P., & Skorik, Y. A. (2019). Alginate gel reinforcement with chitin nanowhiskers modulates rheological properties and drug release profile. *Biomolecules*, *9*(7). https://doi.org/10.3390/biom9070291

Pita-López, M. L., Fletes-Vargas, G., Espinosa-Andrews, H., & Rodríguez-Rodríguez, R. (2021). Physically cross-linked chitosan-based hydrogels for tissue engineering applications: A state-of-the-art review. *European Polymer Journal*, *145*(November 2020). https://doi.org/10.1016/j.eurpolymj.2020.110176

Poerio, T., Piacentini, E., & Mazzei, R. (2019). Membrane processes for microplastic removal. *Molecules*, *24*(22). https://doi.org/10.3390/molecules24224148

Pooresmaeil, M., & Namazi, H. (2019). Application of polysaccharide-based hydrogels for water treatments. *Hydrogels Based on Natural Polymers*, 411–455. https://doi.org/10.1016/B978-0-12-816421-1.00014-8

Pourhakkak, P., Taghizadeh, A., Taghizadeh, M., Ghaedi, M., & Haghdoust, S. (2021). Fundamentals of adsorption technology. *Interface Science and Technology*, *33*, 1–70. https://doi.org/10.1016/B978-0-12-818805-7.00001-1

Poursani, A. S., Nilchi, A., Hassani, A., Shariat, S. M., Nouri, J., Poursani, A. S., Nilchi, A., Hassani, A., Shariat, S. M., & Nouri, J. (2016). The Synthesis of Nano TiO2 and Its Use for Removal of Lead Ions from Aqueous Solution. *Journal of Water Resource and Protection*, *8*(4), 438–448. https://doi.org/10.4236/JWARP.2016.84037

Purkait, M. K., DasGupta, S., & De, S. (2005). Adsorption of eosin dye on activated carbon and its surfactant based desorption. *Journal of Environmental Management*, *76*(2), 135–142. https://doi.org/10.1016/j.jenvman.2005.01.012

Purkait, M. K., Maiti, A., DasGupta, S., & De, S. (2007). Removal of congo red using activated carbon and its regeneration. *Journal of Hazardous Materials*, *145*(1–2), 287–295. https://doi.org/10.1016/j.jhazmat.2006.11.021

Qi, X., Tong, X., Pan, W., Zeng, Q., You, S., & Shen, J. (2021). Recent advances in polysaccharide-based adsorbents for wastewater treatment. *Journal of Cleaner Production*, *315*(July), 128221. https://doi.org/10.1016/j.jclepro.2021.128221

Qi, X., Wu, L., Su, T., Zhang, J., & Dong, W. (2018). Polysaccharide-based cationic hydrogels for dye adsorption. *Colloids and Surfaces B: Biointerfaces*, *170*(June), 364–372. https://doi.org/10.1016/j.colsurfb.2018.06.036

Qin, Y. (2016). Applications of advanced technologies in the development of functional medical textile materials. *Medical Textile Materials*, 55–70. https://doi.org/10.1016/B978-0-08-100618-4.00005-4

Radoor, S., Karayil, J., Parameswaranpillai, J., & Siengchin, S. (2020a). Removal of anionic dye Congo red from aqueous environment using polyvinyl alcohol/sodium alginate/ZSM-5 zeolite membrane. *Scientific Reports*, *10*(1), 1–15. https://doi.org/10.1038/s41598-020-72398-5

Radoor, S., Karayil, J., Parameswaranpillai, J., & Siengchin, S. (2020b). Adsorption of methylene blue dye from aqueous solution by a novel PVA/CMC/halloysite nanoclay bio composite: Characterization, kinetics, isotherm and antibacterial properties. *Journal of Environmental Health Science and Engineering*, *18*(2), 1311–1327. https://doi.org/10.1007/s40201-020-00549-x

Ragab, M. A. A., Korany, M. A., Ibrahim, H. Z., Abdel-Kawi, M. A., & Sayed, A. E. A. A. A. (2017). Adsorption behavior of some metal ions on nanoparticles used

in pharmaceutical matrices: Application to laboratory made drug formulation. *Bulletin of Faculty of Pharmacy, Cairo University*, *55*(1), 155–162. https://doi.org/10.1016/j.bfopcu.2017.01.002

Ragadhita, R., & Nandiyanto, A. B. D. (2021). How to calculate adsorption isotherms of particles using two-parameter monolayer adsorption models and equations. *Indonesian Journal of Science and Technology*, *6*(1), 205–234. https://doi.org/10.17509/ijost.v6i1.32354

Rahmi, Fathurrahmi, Lelifajri, Purnamawati, F., & Sembiring, R. (2019). Preparation of Magnetic Chitosan Beads for Heavy Metal Ions Removal from Water. *IOP Conference Series: Earth and Environmental Science*, *276*(1). https://doi.org/10.1088/1755-1315/276/1/012004

RAVI, & Pandey, L. M. (2019). Enhanced adsorption capacity of designed bentonite and alginate beads for the e ff ective removal of methylene blue. *Applied Clay Science*, *169*(December 2018), 102–111. https://doi.org/10.1016/j.clay.2018.12.019

Rey, C., Combes, C., Drouet, C., Grossin, D., Bertrand, G., & Soulié, J. (2017). Bioactive calcium phosphate compounds: Physical chemistry. *Comprehensive Biomaterials II*, 244–290. https://doi.org/10.1016/B978-0-12-803581-8.10171-7

Rouhani, F., & Morsali, A. (2018). Fast and Selective Heavy Metal Removal by a Novel Metal-Organic Framework Designed with In-Situ Ligand Building Block Fabrication Bearing Free Nitrogen. *Chemistry - A European Journal*, *24*(21), 5529–5537. https://doi.org/10.1002/chem.201706016

Salah, D., Hamd, A., Soliman, N. K., Elzanaty, A. M., Alanazi, A. M., Shaban, M., El-Sayed, R., & Ahmed, S. A. (2022). Polyaniline/Glauconite Nanocomposite Adsorbent for Congo Red Dye from Textile Wastewater. *Separations*, *9*(11), 384. https://doi.org/10.3390/separations9110384

Samsami, S., Mohamadi, M., Sarrafzadeh, M. H., Rene, E. R., & Firoozbahr, M. (2020). Recent advances in the treatment of dye-containing wastewater from textile industries: Overview and perspectives. In *Process Safety and Environmental Protection* (Vol. 143, pp. 138–163). Institution of Chemical Engineers. https://doi.org/10.1016/j.psep.2020.05.034

Sanchez, L. M., Ollier, R. P., & Alvarez, V. A. (2019a). Sorption behavior of polyvinyl alcohol/bentonite hydrogels for dyes removal. *Journal of Polymer Research*, *26*(6). https://doi.org/10.1007/s10965-019-1807-4

Sanchez, L. M., Ollier, R. P., & Alvarez, V. A. (2019b). Sorption behavior of polyvinyl alcohol/bentonite hydrogels for dyes removal. *Journal of Polymer Research*, *26*(6). https://doi.org/10.1007/s10965-019-1807-4

Sanchez, L. M., Shuttleworth, P. S., Waiman, C., Zanini, G., Alvarez, V. A., & Ollier, R. P. (2020). Physically-crosslinked polyvinyl alcohol composite hydrogels containing clays, carbonaceous materials and magnetic nanoparticles as fillers. *Journal of Environmental Chemical Engineering*, *8*(3). https://doi.org/10.1016/j.jece.2020.103795

Sarkar, N., Sahoo, G., & Swain, S. K. (2020). Graphene quantum dot decorated magnetic graphene oxide filled polyvinyl alcohol hybrid hydrogel for removal of dye pollutants. *Journal of Molecular Liquids*, *302*. https://doi.org/10.1016/j.molliq.2020.112591

Sazali, N., Harun, Z., & Sazali, N. (2020). A review on batch and column adsorption of various adsorbent towards the removal of heavy metal. *Journal of Advanced Research in Fluid Mechanics and Thermal Sciences*, *67*(2), 66–88.

Shen, Y., Ni, W. X., & Li, B. (2021). Porous Organic Polymer Synthesized by Green Diazo-Coupling Reaction for Adsorptive Removal of Methylene Blue. *ACS Omega*, *6*(4), 3202–3208. https://doi.org/10.1021/acsomega.0c05634

Sheth, Y., Dharaskar, S., Khalid, M., & Sonawane, S. (2021). An environment friendly approach for heavy metal removal from industrial wastewater using chitosan based biosorbent: A review. *Sustainable Energy Technologies and Assessments*, *43*(August 2020). https://doi.org/10.1016/j.seta.2020.100951

Shi, R. J., Wang, T., Lang, J. Q., Zhou, N., & Ma, M. G. (2022). Multifunctional Cellulose and Cellulose-Based (Nano) Composite Adsorbents. In *Frontiers in Bioengineering and Biotechnology* (Vol. 10). Frontiers Media S.A. https://doi.org/10.3389/fbioe.2022.891034

Shojaeipoor, F., Elhamifar, D., Masoumi, B., Elhamifar, D., & Barazesh, B. (2019). Ionic liquid based nanoporous organosilica supported propylamine as highly efficient adsorbent for removal of congo red from aqueous solution. *Arabian Journal of Chemistry*, *12*(8), 4171–4181. https://doi.org/10.1016/j.arabjc.2016.05.001

Shon, H. K., Vigneswaran, S., & Snyder, S. A. (2006). Effluent organic matter (EfOM) in wastewater: Constituents, effects, and treatment. *Critical Reviews in*

Environmental Science and Technology, *36*(4), 327–374. https://doi.org/10.1080/10643380600580011

Silvestri, S., Stefanello, N., Sulkovski, A. A., & Foletto, E. L. (2020). Preparation of TiO2 supported on MDF biochar for simultaneous removal of methylene blue by adsorption and photocatalysis. *Journal of Chemical Technology and Biotechnology*, *95*(10), 2723–2729. https://doi.org/10.1002/jctb.6279

Singh, R., Gautam, S., Sharma, B., Jain, P., & Chauhan, K. D. (2021). Biopolymers and their classifications. *Biopolymers and Their Industrial Applications*, 21–44. https://doi.org/10.1016/B978-0-12-819240-5.00002-X

Sivarajasekar, N. (2015). Agriculture waste biomass valorisation for cationic dyes sequestration: A concise review Reverse micelles View project Biomolecules View project. In *Article in Journal of Chemical and Pharmaceutical Research*. www.jocpr.com

Sobhanardakani, S., Zandipak, R., & Sahraei, R. (2013). Removal of Janus Green dye from aqueous solutions using oxidized multi-walled carbon nanotubes. *Toxicological and Environmental Chemistry*, *95*(6), 909–918. https://doi.org/10.1080/02772248.2013.840379

Soliman, N. K., & Moustafa, A. F. (2020). Industrial solid waste for heavy metals adsorption features and challenges; a review. *Journal of Materials Research and Technology*, *9*(5), 10235–10253. https://doi.org/10.1016/j.jmrt.2020.07.045

Son, D. J., Kim, W. Y., Jung, B. R., Chang, D., & Hong, K. H. (2020). Pilot-scale anoxic/aerobic biofilter system combined with chemical precipitation for tertiary treatment of wastewater. *Journal of Water Process Engineering*, *35*(January). https://doi.org/10.1016/j.jwpe.2020.101224

Song, N., Wu, X. L., Zhong, S., Lin, H., & Chen, J. R. (2015). Biocompatible G-Fe3O4/CA nanocomposites for the removal of Methylene Blue. *Journal of Molecular Liquids*, *212*, 63–69. https://doi.org/10.1016/j.molliq.2015.08.059

Sonone, S. S., Jadhav, S. v, Sankhla, M. S., & Kumar, R. (2021). Water Contamination by Heavy Metals and their Toxic Effect on Aquaculture and Human Health through Food Chain. *Letters in Applied NanoBioScience*, *10*(2), 2148–2166. https://doi.org/10.33263/lianbs102.21482166

Sonune, A., & Ghate, R. (2004). Developments in wastewater treatment methods. *Desalination*, *167*(1–3), 55–63. https://doi.org/10.1016/j.desal.2004.06.113

Srivastava, V., & Choubey, A. K. (2021). Investigation of adsorption of organic dyes present in wastewater using chitosan beads immobilized with biofabricated CuO nanoparticles. *Journal of Molecular Structure*, *1242*, 130749. https://doi.org/10.1016/j.molstruc.2021.130749

Su, T., Wu, L., Pan, X., Zhang, C., Shi, M., Gao, R., Qi, X., & Dong, W. (2019). Pullulan-derived nanocomposite hydrogels for wastewater remediation: Synthesis and characterization. *Journal of Colloid and Interface Science*, *542*, 253–262. https://doi.org/10.1016/j.jcis.2019.02.025

Sumanjit, Seema, Mahajan, R. K., & Gupta, V. K. (2015). Modification of surface behaviour of Eichhornia crassipes using surface active agent: An adsorption study. *Journal of Industrial and Engineering Chemistry*, *21*, 189–197. https://doi.org/10.1016/j.jiec.2014.02.024

Sun, Y., Liu, X., Lv, X., Wang, T., & Xue, B. (2021). Synthesis of novel lignosulfonate-modified graphene hydrogel for ultrahigh adsorption capacity of Cr(VI) from wastewater. *Journal of Cleaner Production*, *295*. https://doi.org/10.1016/j.jclepro.2021.126406

Supreme Council For Environment. (2020). Bahrain ' s Third National Communication. *Unfccc*, *July*.

Sutirman, Z. A., Sanagi, M. M., & Wan Aini, W. I. (2021). Alginate-based adsorbents for removal of metal ions and radionuclides from aqueous solutions: A review. *International Journal of Biological Macromolecules*, *174*, 216–228. https://doi.org/10.1016/j.ijbiomac.2021.01.150

Tan, K. B., Vakili, M., Horri, B. A., Poh, P. E., Abdullah, A. Z., & Salamatinia, B. (2015). Adsorption of dyes by nanomaterials: Recent developments and adsorption mechanisms. In *Separation and Purification Technology* (Vol. 150, pp. 229–242). Elsevier B.V. https://doi.org/10.1016/j.seppur.2015.07.009

Tanan, W., Panichpakdee, J., & Saengsuwan, S. (2019). Novel biodegradable hydrogel based on natural polymers: Synthesis, characterization, swelling/reswelling and biodegradability. *European Polymer Journal*, *112*(September 2018), 678–687. https://doi.org/10.1016/j.eurpolymj.2018.10.033

Tang, S., Yang, J., Lin, L., Peng, K., Chen, Y., Jin, S., & Yao, W. (2020a). Construction of physically crosslinked chitosan/sodium alginate/calcium ion double-network hydrogel and its application to heavy metal ions removal.

Chemical Engineering Journal, *393*(January). https://doi.org/10.1016/j.cej.2020.124728

Tang, S., Yang, J., Lin, L., Peng, K., Chen, Y., Jin, S., & Yao, W. (2020b). Construction of physically crosslinked chitosan/sodium alginate/calcium ion double-network hydrogel and its application to heavy metal ions removal. *Chemical Engineering Journal*, *393*(January), 124728. https://doi.org/10.1016/j.cej.2020.124728

Tanhaei, B., Ayati, A., Lahtinen, M., & Sillanpää, M. (2015). Preparation and characterization of a novel chitosan/Al2O3/magnetite nanoparticles composite adsorbent for kinetic, thermodynamic and isotherm studies of Methyl Orange adsorption. *Chemical Engineering Journal*, *259*, 1–10. https://doi.org/10.1016/j.cej.2014.07.109

Teh, C. Y., Budiman, P. M., Shak, K. P. Y., & Wu, T. Y. (2016). Recent Advancement of Coagulation-Flocculation and Its Application in Wastewater Treatment. In *Industrial and Engineering Chemistry Research* (Vol. 55, Issue 16, pp. 4363–4389). American Chemical Society. https://doi.org/10.1021/acs.iecr.5b04703

The Kingdom of Bahrain's First Voluntary National Review (2018) on the implementation of the 2030 Agenda for Sustainable Development and the Sustainable Development Goals. (2018).

Tran, H. V., Tran, L. D., & Nguyen, T. N. (2010). Preparation of chitosan/magnetite composite beads and their application for removal of Pb(II) and Ni(II) from aqueous solution. *Materials Science and Engineering C*, *30*(2), 304–310. https://doi.org/10.1016/j.msec.2009.11.008

Tran, H. v., Bui, L. T., Dinh, T. T., Le, D. H., Huynh, C. D., & Trinh, A. X. (2017). Graphene oxide/Fe3O4/chitosan nanocomposite: A recoverable and recyclable adsorbent for organic dyes removal. Application to methylene blue. *Materials Research Express*, *4*(3). https://doi.org/10.1088/2053-1591/aa6096

Ullah, F., Othman, M. B. H., Javed, F., Ahmad, Z., & Akil, H. M. (2015). Classification, processing and application of hydrogels: A review. *Materials Science and Engineering C*, *57*, 414–433. https://doi.org/10.1016/j.msec.2015.07.053

Umoren, S. A., Etim, U. J., & Israel, A. U. (2013). Adsorption of methylene blue from industrial effluent using poly (vinyl alcohol). *J. Mater. Environ. Sci*, *4*(1), 75–86.

UN. (2019). Uncertainty in forecasts of long-run economic growth. *Department of Economic and Social Affairs*, *115*(21), 5409–5414. https://doi.org/10.1073/pnas.1713628115

UNWWDR. (2003). Water for people, water for life. *The World Water Development Report*, 36.

Upadhyay, U., Sreedhar, I., Singh, S. A., Patel, C. M., & Anitha, K. L. (2021). Recent advances in heavy metal removal by chitosan based adsorbents. *Carbohydrate Polymers*, *251*(May 2020), 117000. https://doi.org/10.1016/j.carbpol.2020.117000

Urbanova, M., Pavelkova, M., Czernek, J., Kubova, K., Vyslouzil, J., Pechova, A., Molinkova, D., Vyslouzil, J., Vetchy, D., & Brus, J. (2019). Interaction Pathways and Structure-Chemical Transformations of Alginate Gels in Physiological Environments. *Biomacromolecules*, *20*(11), 4158–4170. https://doi.org/10.1021/acs.biomac.9b01052

Vakili, M., Deng, S., Liu, D., Li, T., & Yu, G. (2019). Preparation of aminated cross-linked chitosan beads for efficient adsorption of hexavalent chromium. *International Journal of Biological Macromolecules*, *139*, 352–360. https://doi.org/10.1016/j.ijbiomac.2019.07.207

Vakili, M., Rafatullah, M., Salamatinia, B., Abdullah, A. Z., Ibrahim, M. H., Tan, K. B., Gholami, Z., & Amouzgar, P. (2014). Application of chitosan and its derivatives as adsorbents for dye removal from water and wastewater: A review. *Carbohydrate Polymers*, *113*, 115–130. https://doi.org/10.1016/j.carbpol.2014.07.007

Valdés, A., Ramos, M., García-Serna, E., Carmen Garrigós, M. del, & Jiménez, A. (2016). Polymers Extracted from Biomass. *Reference Module in Food Science*. https://doi.org/10.1016/B978-0-08-100596-5.03207-8

Varaprasad, K., Karthikeyan, C., Yallapu, M. M., & Sadiku, R. (2022). The significance of biomacromolecule alginate for the 3D printing of hydrogels for biomedical applications. *International Journal of Biological Macromolecules*, *212*(March), 561–578. https://doi.org/10.1016/j.ijbiomac.2022.05.157

Vázquez, V. L., Rodríguez, G., Daddi, T., de Giacomo, M. R., Polders, C., & Dils, E. (2015). Policy challenges in transferring the integrated pollution Prevention and control approach to Southern Mediterranean countries: A case study. *Journal of Cleaner Production*, *107*(November 2010), 486–497. https://doi.org/10.1016/j.jclepro.2014.06.090

Velasco-Garduño, O., Martínez, M. E., Gimeno, M., Tecante, A., Beristain-Cardoso, R., & Shirai, K. (2020). Copper removal from wastewater by a chitosan-based biodegradable composite. *Environmental Science and Pollution Research*, *27*(23), 28527–28535. https://doi.org/10.1007/s11356-019-07560-2

Vidal, R. R. L., & Moraes, J. S. (2019). Removal of organic pollutants from wastewater using chitosan: a literature review. *International Journal of Environmental Science and Technology*, *16*(3), 1741–1754. https://doi.org/10.1007/s13762-018-2061-8

Vimonses, V., Lei, S., Jin, B., Chow, C. W. K., & Saint, C. (2009). Kinetic study and equilibrium isotherm analysis of Congo Red adsorption by clay materials. *Chemical Engineering Journal*, *148*(2–3), 354–364. https://doi.org/10.1016/j.cej.2008.09.009

Vinardell, S., Astals, S., Mata-Alvarez, J., & Dosta, J. (2020). Techno-economic analysis of combining forward osmosis-reverse osmosis and anaerobic membrane bioreactor technologies for municipal wastewater treatment and water production. *Bioresource Technology*, *297*, 122395. https://doi.org/10.1016/j.biortech.2019.122395

Vinchhi, P., Rawal, S. U., & Patel, M. M. (2021). Biodegradable hydrogels. *Drug Delivery Devices and Therapeutic Systems*, 395–419. https://doi.org/10.1016/B978-0-12-819838-4.00012-2

Wabnitz, C.C., Lam, et. al. (2018). Climate change impacts on marine biodiversity, sheries and society in the Arabian Gulf. *PLoS ONE*, 1–26.

Wallmersperger, T., Kröplin, B., & Gülch, R. W. (2004). Coupled chemo-electro-mechanical formulation for ionic polymer gels - Numerical and experimental investigations. *Mechanics of Materials*, *36*(5–6), 411–420. https://doi.org/10.1016/S0167-6636(03)00068-1

Wang, D., Cheng, W., Yue, Y., Xuan, L., Ni, X., & Han, G. (2018). Electrospun cellulose nanocrystals/chitosan/polyvinyl alcohol nanofibrous films and their

exploration to metal ions adsorption. *Polymers*, *10*(10). https://doi.org/10.3390/polym10101046

Wang, J., & Guo, X. (2020a). Adsorption isotherm models: Classification, physical meaning, application and solving method. *Chemosphere*, *258*. https://doi.org/10.1016/j.chemosphere.2020.127279

Wang, J., & Guo, X. (2020b). Adsorption kinetic models: Physical meanings, applications, and solving methods. *Journal of Hazardous Materials*, *390*(January), 122156. https://doi.org/10.1016/j.jhazmat.2020.122156

Wang, J., & Zhuang, S. (2022). *Chitosan-based materials : Preparation , modification and application*. *355*(April).

Wang, S., Boyjoo, Y., Choueib, A., & Zhu, Z. H. (2005). Removal of dyes from aqueous solution using fly ash and red mud. *Water Research*, *39*(1), 129–138. https://doi.org/10.1016/j.watres.2004.09.011

Wang, S., Liu, Y., Yang, A., Zhu, Q., Sun, H., Sun, P., Yao, B., Zang, Y., Du, X., & Dong, L. (2022). *Xanthate-Modified Magnetic Fe 3 O 4 @SiO 2-Based Polyvinyl Alcohol/Chitosan Composite Material for Efficient Removal of Heavy Metal Ions from Water*. https://doi.org/10.3390/polym14061107

Wang, W., Fan, M., Ni, J., Peng, W., Cao, Y., Li, H., Huang, Y., Fan, G., Zhao, Y., & Song, S. (2022). Efficient dye removal using fixed-bed process based on porous montmorillonite nanosheet/poly(acrylamide-co-acrylic acid)/sodium alginate hydrogel beads. *Applied Clay Science*, *219*(February). https://doi.org/10.1016/j.clay.2022.106443

Wang, W., Zhao, Y., Bai, H., Zhang, T., & Ibarra-galvan, V. (2018). Methylene blue removal from water using the hydrogel beads of poly (vinyl alcohol) -sodium alginate-chitosan-montmorillonite. *Carbohydrate Polymers*, *198*(June), 518–528. https://doi.org/10.1016/j.carbpol.2018.06.124

Wang, W., Zhao, Y., Bai, H., Zhang, T., Ibarra-Galvan, V., & Song, S. (2018a). Methylene blue removal from water using the hydrogel beads of poly(vinyl alcohol)-sodium alginate-chitosan-montmorillonite. *Carbohydrate Polymers*, *198*(March), 518–528. https://doi.org/10.1016/j.carbpol.2018.06.124

Wang, W., Zhao, Y., Bai, H., Zhang, T., Ibarra-Galvan, V., & Song, S. (2018b). Methylene blue removal from water using the hydrogel beads of poly(vinyl alcohol)-sodium alginate-chitosan-montmorillonite. *Carbohydrate Polymers*, *198*(June), 518–528. https://doi.org/10.1016/j.carbpol.2018.06.124

Wang, X., Jiang, C., Hou, B., Wang, Y., Hao, C., & Wu, J. (2018). Chemosphere Carbon composite lignin-based adsorbents for the adsorption of dyes. *Chemosphere*, *206*, 587–596. https://doi.org/10.1016/j.chemosphere.2018.04.183

Water Scarcity in Bahrain, 2022. (n.d.). Retrieved September 30, 2022, from https://www.ecomena.org/water-scarcity-in-bahrain/

Watkinson, A. J., Murby, E. J., & Costanzo, S. D. (2007). Removal of antibiotics in conventional and advanced wastewater treatment: Implications for environmental discharge and wastewater recycling. *Water Research*, *41*(18), 4164–4176. https://doi.org/10.1016/j.watres.2007.04.005

Weijiang, Z., Yace, Z., Yuvaraja, G., & Jiao, X. (2017a). Adsorption of Pb(II) ions from aqueous environment using eco-friendly chitosan schiff's base@Fe3O4 (CSB@Fe3O4) as an adsorbent; kinetics, isotherm and thermodynamic studies. *International Journal of Biological Macromolecules*, *105*(Ii), 422–430. https://doi.org/10.1016/j.ijbiomac.2017.07.063

Weijiang, Z., Yace, Z., Yuvaraja, G., & Jiao, X. (2017b). Adsorption of Pb(II) ions from aqueous environment using eco-friendly chitosan schiff's base@Fe3O4 (CSB@Fe3O4) as an adsorbent; kinetics, isotherm and thermodynamic studies. *International Journal of Biological Macromolecules*, *105*, 422–430. https://doi.org/10.1016/j.ijbiomac.2017.07.063

Wintgens, T., Li, Y., & Kazner, C. (2013). Water Resources and Industry. *Water Resources and Industry*, *1–2*(October), 29–36. https://doi.org/10.1016/j.wri.2013.08.001

Wu, N., Niu, F., Lang, W., & Xia, M. (2019). Highly efficient flame-retardant and low-smoke-toxicity poly (vinyl alcohol)/ alginate / montmorillonite composite aerogels by two-step crosslinking strategy. *Carbohydrate Polymers*, *221*(June), 221–230. https://doi.org/10.1016/j.carbpol.2019.06.007

WWAP. (2017). The United Nations World Water Development Report 2017: Wastewater the untapped resource. *United Nations World Water Assessment Programme*, *5*(October), 1–49.

Xie, M., Zeng, L., Zhang, Q., Kang, Y., Xiao, H., Peng, Y., Chen, X., & Luo, J. (2015). Synthesis and adsorption behavior of magnetic microspheres based on chitosan/organic rectorite for low-concentration heavy metal removal. *Journal of Alloys and Compounds*, *647*, 892–905. https://doi.org/10.1016/j.jallcom.2015.06.065

Yadav, S., Asthana, A., Chakraborty, R., & Jain, B. (2020). Cationic Dye Removal Using Novel Magnetic / Activated Charcoal / β - Cyclodextrin / Alginate Polymer Nanocomposite. *Nanomaterials*, *10*, 170.

Yan, J., Yuan, W., Liu, J., Ye, W., Lin, J., Xie, J., Huang, X., Gao, S., Xie, J., Liu, S., Chen, W., & Zhang, H. (2019). An integrated process of chemical precipitation and sulfate reduction for treatment of flue gas desulphurization wastewater from coal-fired power plant. *Journal of Cleaner Production*, *228*, 63–72. https://doi.org/10.1016/j.jclepro.2019.04.227

Yang, L., Chu, J. S., & Fix, J. A. (2002). Colon-specific drug delivery: New approaches and in vitro/in vivo evaluation. *International Journal of Pharmaceutics*, *235*(1–2), 1–15. https://doi.org/10.1016/S0378-5173(02)00004-2

Yang, L. W., Peng, Y. Q., Qian, C. F., Xing, G. H., He, J. J., Zhao, C. L., & Lai, B. (2021). Enhanced adsorption/photocatalytic removal of Cu(II) from wastewater by a novel magnetic chitosan@ bismuth tungstate coated by silver (MCTS-Ag/Bi2WO6) composite. *Chemosphere*, *263*, 128120. https://doi.org/10.1016/j.chemosphere.2020.128120

Yi, X., Sun, F., Han, Z., Han, F., He, J., Ou, M., Gu, J., & Xu, X. (2018). Graphene oxide encapsulated polyvinyl alcohol/sodium alginate hydrogel microspheres for Cu (II) and U (VI) removal. *Ecotoxicology and Environmental Safety*, *158*(April), 309–318. https://doi.org/10.1016/j.ecoenv.2018.04.039

Younis, A. M., Aly-Eldeen, M. A., & Elkady, E. M. (2019). Effect of different molecular weights of chitosan on the removal efficiencies of heavy metals from contaminated water. *Egyptian Journal of Aquatic Biology and Fisheries*, *23*(4), 149–158. https://doi.org/10.21608/ejabf.2019.52591

Yu, D., Wang, Y., Wu, M., Zhang, L., Wang, L., & Ni, H. (2019). Surface functionalization of cellulose with hyperbranched polyamide for efficient adsorption of organic dyes and heavy metals. *Journal of Cleaner Production*, *232*, 774–783. https://doi.org/10.1016/j.jclepro.2019.06.024

Zahir, A., Aslam, Z., Kamal, M. S., Ahmad, W., Abbas, A., & Shawabkeh, R. A. (2017). Development of novel cross-linked chitosan for the removal of anionic Congo red dye. *Journal of Molecular Liquids*, *244*, 211–218. https://doi.org/10.1016/j.molliq.2017.09.006

Zhang, J., Zhou, Q., & Ou, L. (2012). Kinetic, isotherm, and thermodynamic studies of the adsorption of methyl orange from aqueous solution by chitosan/alumina

composite. *Journal of Chemical and Engineering Data*, *57*(2), 412–419. https://doi.org/10.1021/je2009945

Zhang, L., Gao, Y., Yue, Q., Zhang, P., Wang, Y., & Gao, B. (2020). Prepartion and application of novel blast furnace dust based catalytic-ceramic-filler in electrolysis assisted catalytic micro-electrolysis system for ciprofloxacin wastewater treatment. *Journal of Hazardous Materials*, *383*(September 2019), 121215. https://doi.org/10.1016/j.jhazmat.2019.121215

Zhang, S., Xu, F., Wang, Y., Zhang, W., Peng, X., & Pepe, F. (2013). Silica modified calcium alginate-xanthan gum hybrid bead composites for the removal and recovery of Pb(II) from aqueous solution. *Chemical Engineering Journal*, *234*, 33–42. https://doi.org/10.1016/J.CEJ.2013.08.102

Zhang, W., Deng, Q., He, Q., Song, J., Zhang, S., Wang, H., Zhou, J., & Zhang, H. (2018a). A facile synthesis of core-shell/bead-like poly (vinyl alcohol)/alginate@PAM with good adsorption capacity, high adaptability and stability towards Cu(II) removal. *Chemical Engineering Journal*, *351*(March), 462–472. https://doi.org/10.1016/j.cej.2018.06.129

Zhang, W., Deng, Q., He, Q., Song, J., Zhang, S., Wang, H., Zhou, J., & Zhang, H. (2018b). A facile synthesis of core-shell/bead-like poly (vinyl alcohol)/alginate@PAM with good adsorption capacity, high adaptability and stability towards Cu(II) removal. *Chemical Engineering Journal*, *351*(March), 462–472. https://doi.org/10.1016/j.cej.2018.06.129

Zhang, X. (2022). Selective separation membranes for fractionating organics and salts for industrial wastewater treatment: Design strategies and process assessment. *Journal of Membrane Science*, *643*(November 2021). https://doi.org/10.1016/j.memsci.2021.120052

Zhang, Z. H., Xu, J. Y., & Yang, X. L. (2021a). MXene/sodium alginate gel beads for adsorption of methylene blue. *Materials Chemistry and Physics*, *260*(November 2020), 124123. https://doi.org/10.1016/j.matchemphys.2020.124123

Zhang, Z. H., Xu, J. Y., & Yang, X. L. (2021b). MXene/sodium alginate gel beads for adsorption of methylene blue. *Materials Chemistry and Physics*, *260*. https://doi.org/10.1016/j.matchemphys.2020.124123

Zhao, C., Zhou, J., Yan, Y., Yang, L., Xing, G., Li, H., Wu, P., Wang, M., & Zheng, H. (2021). Application of coagulation/flocculation in oily wastewater treatment:

A review. *Science of the Total Environment*, *765*. https://doi.org/10.1016/j.scitotenv.2020.142795

Zheng, L., Zhu, C., Dang, Z., Zhang, H., Yi, X., & Liu, C. (2012). Preparation of cellulose derived from corn stalk and its application for cadmium ion adsorption from aqueous solution. *Carbohydrate Polymers*, *90*(2), 1008–1015. https://doi.org/10.1016/J.CARBPOL.2012.06.035

Zhou, Y., Zhang, L., Fu, S., Zheng, L., & Zhan, H. (2012). *ADSORPTION BEHAVIOR OF Cd 2+ , Pb 2+ , AND Ni 2+ FROM AQUEOUS SOLUTIONS ON CELLULOSE-BASED HYDROGELS*.

Zou, Z., Zhang, B., Nie, X., Cheng, Y., Hu, Z., Liao, M., & Li, S. (2020a). A sodium alginate-based sustained-release IPN hydrogel and its applications. *RSC Advances*, *10*(65), 39722–39730. https://doi.org/10.1039/d0ra04316h

Zou, Z., Zhang, B., Nie, X., Cheng, Y., Hu, Z., Liao, M., & Li, S. (2020b). A sodium alginate-based sustained-release IPN hydrogel and its applications. *RSC Advances*, *10*(65), 39722–39730. https://doi.org/10.1039/d0ra04316h

Zubari, W. (2005). Spatial and Temporal Trends in Groundwater Resources in Bahrain, 1992-2002. *Emirates Journal for Engineering Research*, *10*(1), 57–67. http://eclsun.uaeu.ac.ae/ejer/issues/v10/pdf_iss1_10/p7_Zubari.pdf

Zubari, W. K., & Lori, I. J. (2006). Management and sustainability of groundwater resources in Bahrain. *Water Policy*, *8*(2), 127–145. https://doi.org/10.2166/wp.2006.029

Zulfiqar, M., Lee, S. Y., Mafize, A. A., Kahar, N. A. M. A., Johari, K., & Rabat, N. E. (2020). Ecient removal of Pb(II) from aqueous solutions by using oil palm bio-waste/MWCNTs reinforced pva hydrogel composites: Kinetic, isotherm and thermodynamic modeling. *Polymers*, *12*(2), 1–29. https://doi.org/10.3390/polym12020430

جامعة البحرين

كلية العلوم **برنامج البيئة والتنمية المستدام**

تطوير أنظمة هيدروجيل بوليمرية كنهج بديل لمعالجة مياه الصرف في مملكة البحرين

أطروحة مقدمة استكمالًا لمتطلبات درجة الدكتوراه في البيئة والتنمية المستدام

مقدمة من

الباحثة منى عبدالعزيز الجار

19951462

إشراف

د. أحمد عبدالفتاح حسين

(أستاذ مشارك)

جامعة البحرين

المشرف المشارك

د. سعاد أحمد رشدان

(أستاذ مساعد)

جامعة البحرين

مملكة البحرين

مايو 2023

ملخص الرسالة

تهدف هذه الدراسة الي تحضير هيدروجيل البوليمر كمواد مازه مستدامة وصديقة للبيئة لإزالة الأصباغ العضوية: (Methylene Blue and Congo red)، وأيونات المعادن الثقيلة مثل (الرصاص (Pb) والكادميوم (Cd) ، الكوبلت (Co) والزنك (Zn)) من المحاليل المائية الاصطناعية.

تم استخدام نظام مستدام وآمن باستخدام أنواع مختلفة من البوليمرات (الطبيعية والصناعية) جنبًا إلى جنب مع الجسيمات النانوية المضافة. تم تحضير مادتين لتنقيه المياه؛ الأول يتكون من (polyvinyl alcohol, sodium alginate and Bentonite clay) لإزالة الأصباغ العضوية، والثاني يتكون من (polyvinyl alcohol, chitosan and cellulose) لإزالة المعادن الثقيلة. كما تم دراسة التركيب الكيميائي للمواد المحضرة باستخدام تقنيات طيفية مختلفة مثل الأشعة تحت الحمراء، والميكروسكوب الماسح الإلكتروني المقترن بتحليل الأشعة السينية. ثم تم فحص قدرة المواد المحضرة في إزالة الملوثات العضوية والغير عضويه من المحلول المائي باستخدام خاصيه الامتزاز الكيميائي.

أظهرت النتائج إمكانيه الهيدروجيل الأول (Polyvinyl alcohol-Alginate--Bentonite) في إزالة الأصباغ العضوية بكفاءة عالية تصل (90%) لل (Methylene Blue) و (75.5%) لل (Congo red) .كما اثبتت النتائج بقدره الهيدروجيل الثاني (Polyvinyl alcohol-chitosan-cellulose) في إزالة أيونات المعادن الثقيلة من أنظمة المياه الاصطناعية بكفاءة عالية تصل الي (98.8%) لعنصر الرصاص، و (98.8%) لعنصر الكوبالت، و(83.13%) لعنصر الكادميوم و(99.85%) لعنصر الزنك .

تشير النتائج التجريبية إلى أن إضافة الجسيمات النانونية (Bentonite and cellulose) في تركيبة المركبات الهيدرولوجية المحضرة يحافظ على البنية المسامية ويحافظ على امتصاص الماء ويزيد من إزالة الأصباغ والمعادن الثقيلة شديده السمية. والجدير بالذكر بأن عند تحقيق توازن امتصاص المادة السائلة(adsorbate) والمادة المازه (adsorbent) تم العثور على أقصى سعة امتصاص لنظام الامتزاز الكيميائي(Qe, mg/g) تصل ال (51.34) لل (Methylene Blue) و (16.19) لل (Congo red) و (24) لعنصر الرصاص و (24) لعنصر الكوبالت و(11.76) لعنصر الكادميوم و (12.5) لعنصر الزنك.

كما اثبتت النتائج بأن من خلال نوع وطبيعة الترابط على سطح المادة المازه يمكن تصنيف عمليه الامتزاز الي نوعين: الامتزاز الفيزيائي (Vander Waal forces) والامتزاز الكيميائي (ترابط تساهمي). كما يمكن الاستثمار في هذا المجال للحصول على مواد مازة اقتصادية قليلة التكلفة ومتوفرة بالطبيعة بكثرة.